

# **BODIPY based Small Molecules and Polymers for Organic Field Effect Transistors**

Thesis Submitted to AcSIR for the Award of the  
Degree of

DOCTOR OF PHILOSOPHY  
In Chemical Sciences



*By*

**Saumya Singh**

Registration Number: 10CC11J26040

Under the Guidance of

**Dr. Kothandam Krishnamoorthy**

Polymer Science and Engineering Division

CSIR-NATIONAL CHEMICAL LABORATORY

PUNE – 411008, INDIA

**August 2016**



सीएसआईआर - राष्ट्रीय रासायनिक प्रयोगशाला

(वैज्ञानिक तथा औद्योगिक अनुसंधान परिषद)

डॉ. होमी भाभा मार्ग, पुणे - 411 008. भारत



**CSIR - NATIONAL CHEMICAL LABORATORY**

(Council of Scientific & Industrial Research)

Dr. Homi Bhabha Road, Pune - 411 008. India

### CERTIFICATE

This is to certify that the work incorporated in this Ph.D. thesis entitled “**BODIPY based Small Molecules and Polymers for Organic Field Effect Transistors**” submitted by **Ms. Saumya Singh** to Academy of Scientific and Innovative Research (AcSIR) in fulfillment of the requirements for the award of the Degree of **Doctor of Philosophy in Chemical Sciences**, embodies original research work under my supervision. I further certify that this work has not been submitted to any other University or Institution in part or full for the award of any degree or diploma. Research material obtained from other sources has been duly acknowledged in the thesis. Any text, illustration, table etc., used in the thesis from other sources, have been duly cited and acknowledged.

*Saumya Singh*  
Research Student

**Ms. Saumya Singh**

*Dr. Kothandam Krishnamoorthy*

Research Guide

**Dr. Kothandam Krishnamoorthy**

Senior Scientist

Communication  
Channels

+91 - 20 - 2590 2380  
+91 - 20 - 2590 2663  
+91 - 20 - 2590 2690 (Stores)



FAX  
+91 - 20 - 2590 2664

E-MAIL  
sspo@ncl.res.in

WEBSITE  
www.ncl-india.org

## DECLARATION

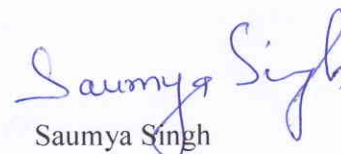
I, hereby declare that the research work in this thesis entitled, "**BODIPY based Small Molecules and Polymers for Organic Field Effect Transistors**" submitted for the degree of **Doctor of Philosophy in Chemical Sciences** to the Academy of Scientific & Innovative Research (AcSIR), has been carried out at the Polymer Science and Engineering Division of CSIR-National Chemical Laboratory, Pune, India under the guidance of **Dr. Kothandam Krishnamoorthy**. Research material obtained from other sources has been duly cited and acknowledged in the thesis. The work is original and has not been submitted in part or full by me for any other degree or diploma to other University.

Date: 09-08-2016

Polymer Science and Engineering Division

CSIR-National Chemical Laboratory,

Pune - 411008, India.



Saumya Singh

Research Student

*I dedicate this thesis to my family who has always stood  
by me. Thank you for all your love, support, and  
encouragement.*

## Acknowledgements

*I would like to express my sincere appreciation and gratitude to all those who helped and supported me during the period of my thesis work. Firstly, I would like to thank my research adviser, Dr. Kothandam Krishnamoorthy for his guidance throughout my Ph.D. research work. I wish to express my sincere gratitude to him for sharing his scientific knowledge and experience with me. I would also like to thank Dr. Jayaraj Nithyanandhan for the helpful discussions and suggestions on scientific problems during our weekly research review meetings. I further extend my gratitude to my Doctoral Advisory Committee (DAC) members, Dr. Ashootosh V. Ambade and Dr. P. R. Rajamohanan, who encouraged me with their valuable suggestions, advice, and constructive criticism during my work presentations.*

*I sincerely thank the University Grants Commission (UGC) for my Ph.D. fellowship. I would also like to thank Director, CSIR-National Chemical Laboratory and Head of Polymer Science and Engineering Division, for providing the infrastructure and advanced facilities for research.*

*I would like to thank Dr. Rahul Banerjee, Dr. Pankaj Poddar, and Dr. M. Jayakannan (IISER, Pune) for their helpful discussions and for providing instrumental facilities. I am also thankful to Mr. Narsimha Karnati (IISER, Pune) for helping me with polarized light microscopy related experiments.*

*I want to acknowledge the support of all the members of the CSIR-NCL instrumental facilities, NMR, Mass, SEM, and XRD. I wish to thank Mrs. Pooja Mudellu for AFM analysis and Mr. Shyamal Menon for GPC analysis. I sincerely thank the Student Academic Office staff, library staff, members of Glassblowing, Workshop, Accounts and Bill section and other office staffs for their timely help.*

*I wish to thank my fellow labmates, Dr. Manik Bhosale, Mrinmoy Chini, Dr. Bhanprakash Jain, Chayanika Das, Anup Singh, Kumar S, Gunvant Deshmukh, Chithira Vel, Sudhakar Nesan, Raja P, and Vijay Venugopalan for all their help and support: from opening solvent drums to scholarly interactions. I am also thankful to Dr. J. Nithyanandhan's group members, M K Munavvar Fairoos, Kubandiran Kolanji, Alagumalai Ananthan, Rajesh Bisht, Manik shil, Neeta Karjule, Punith Arasu, and Amresh Singh for providing all the required help.*

*I wish to appreciate and acknowledge my colleagues, Dr. Kaushlendra Kumar, Dr. Rekha Narayan, Dr. Nagesh Kolhe, Dr. Nisha Kumari, Dr. Chinmay Nardele, Dr. Shyambo Chatterjee, Dr. Pradip Pachfule, Dr. Tamas Panda, Dr. Arijit Mallick, Dr. Tanay Kundu, Dr. Munmun Ghosh, Dr. Nagendra Kalva, Prajitha K. P, Saibal Bhaumik, Shekhar Shinde, Swapnil Sonawane, Sandeep Kumar Sharma, Sarabjot kaur, Naganath Patil, Kavita Garg, Vikas Garg, Soumen Das and Puneet Khandelwal for providing all the necessary help and scholarly interactions.*

*I would like to express my gratitude towards all my teachers who laid a strong base for my personal development from the beginning of my formal education. I sincerely thank my professors from Banaras Hindu University for their encouragements and guidance.*

*I would like to express my special appreciation to my friends in NCL and IISER from Banaras Hindu University, Agni (Late), Arpan, Smita, Anshu, Shubhodeep, Sumit, Laxman and Bijoy for their care and support when I was new in NCL.*

*My time at NCL was enjoyable and memorable largely because of my friends, Anshu, Pushpa, Jaya, Roshna, and Bhawana. I thankfully remember my friends, Roopshikha and Shweta from Banaras Hindu University for all their help. I am forever grateful to all of you and thank you so much for your friendship, care, advice and constructive criticism.*

*Lastly, I would like to express my gratitude to my family for supporting me from all aspects, especially my mummy and papa for all their unconditional love, blessings, and sacrifices. I shall forever remain indebted to you for your constant moral support and encouragement which helped me to face all difficult challenges during my research work. Thank you for everything.*

*Saumya Singh  
CSIR-NCL, Pune  
August 2016*

# Table of Contents

Abbreviations.....	i
General Remarks .....	iv

Abstract .....	1
----------------	---

## Chapter 1

### Introduction

1.1 Organic Electronics: Introduction to Organic Field Effect Transistors .....	5
1.2 Basics of Organic Field-Effect Transistors .....	6
1.2.1 Device Geometry.....	6
1.2.2 Working Principle of OFETs .....	7
1.2.3 Current-Voltage Characteristics .....	8
1.3 Organic Semiconductors (Polymers and Small Molecules) for OFETs .....	9
1.3.1 <i>p</i> -Type Organic Semiconductors.....	9
1.3.2 <i>n</i> -Type Organic Semiconductors.....	12
1.3.3 Ambipolar Organic Semiconductors .....	15
1.4 Organic Semiconductors based on Dyes and Pigments.....	17
1.5 Boron–Dipyrromethene (BODIPY) Dyes .....	18
1.5.1 Synthetic Routes towards the BODIPY Core .....	19
1.5.2 Functionalization of the BODIPY Core .....	21
1.6 BODIPY based Conjugated Systems for OFETs .....	23
1.7 Scope and Objectives of the Present Work.....	25
1.8 References.....	26

## Chapter 2

### Oligoethylene Glycol Substituted BODIPY based Conjugated Small Molecules with Improved Hole Mobility

2.1 Introduction.....	34
2.2. Experimental Section .....	36

2.2.1 Materials .....	36
2.2.2 Instrumentation Details .....	36
2.2.3 Device Fabrication (OFET).....	36
2.2.4 Synthetic Procedures and Characterization Data .....	37
2.3 Results and Discussion .....	40
2.3.1 Synthesis and Thermal Characterization.....	40
2.3.2 Optical and Electrochemical Properties .....	42
2.3.3 Electronic Structure Calculations from DFT .....	43
2.3.4 Impedance Spectroscopy .....	44
2.3.5 Crystallinity and Thin Film Morphology .....	45
2.3.6 Characterization of Organic Field Effect Transistor Devices .....	47
2.4 Summary .....	51
2.5 References.....	51

### **Chapter 3**

#### Tuning the Frontier Molecular Orbital Energy Levels of BODIPY based Small Molecules by Side Chain Variation at Meso Position

3.1 Introduction.....	57
3.2. Experimental Section .....	58
3.2.1 Materials .....	58
3.2.2 Instrumentation Details .....	59
3.2.3 Device Fabrication (OFET).....	59
3.2.4 Synthetic Procedures and Characterization Data .....	59
3.3 Results and Discussion .....	63
3.3.1 Synthesis and Thermal Characterization.....	63
3.3.2 Molecular Geometry and Electronic Structure Calculations from DFT .....	65
3.3.3 Optical and Electrochemical Properties .....	67
3.3.4 Crystallinity and Thin Film Morphology .....	70
3.3.5 Characterization of Organic Field Effect Transistor Devices .....	71
3.4 Summary .....	73
3.5 References.....	74



## Chapter 4

### BODIPY in Conjugation with Diketopyrrolopyrrole (DPP) Core for Solution-Processable Small Molecule Organic Field Effect Transistors

4.1 Introduction.....	77
4.2. Experimental Section.....	79
4.2.1 Materials .....	79
4.2.2 Instrumentation Details .....	79
4.2.3 Device Fabrication (OFET).....	80
4.2.4 Synthetic Procedures and Characterization Data .....	80
4.3 Results and Discussion .....	84
4.3.1 Synthesis and Thermal Characterization.....	84
4.3.2 Molecular Geometry and Electronic Structure Calculations from DFT .....	86
4.3.3 Optical and Electrochemical Properties .....	88
4.3.4 Thin Film Morphology.....	90
4.3.5 Characterization of Organic Field Effect Transistor Devices .....	91
4.4 Summary.....	94
4.5 References.....	94

## Chapter 5

### BODIPY based Copolymers as p- Channel and Ambipolar Semiconductors for Organic Field Effect Transistors

5.1 Introduction.....	98
5.2. Experimental Section.....	100
5.2.1 Materials .....	100
5.2.2 Instrumentation Details .....	100
5.2.3 Device Fabrication (OFET).....	100
5.2.4 Synthetic Procedures and Characterization Data .....	101
5.3 Results and Discussion: p(BODIPY- <i>alt</i> -Isoindigo).....	108
5.3.1 Synthesis and Thermal Characterization.....	108
5.3.2 Molecular Geometry and Electronic Structure Calculations from DFT .....	110
5.3.3 Optical and Electrochemical Properties .....	111

5.3.4 Characterization of Organic Field Effect Transistor Devices .....	112
5.4 Results and Discussion: p(BODIPY- <i>alt</i> -DPP).....	112
5.4.1 Synthesis and Thermal Characterization.....	113
5.4.2 Molecular Geometry and Electronic Structure Calculations from DFT .....	116
5.4.3 Optical and Electrochemical Properties .....	118
5.4.4 Thin Film Morphology.....	120
5.4.5 Characterization of Organic Field Effect Transistor Devices .....	121
5.5 Results and Discussion: p(BODIPY- <i>alt</i> -BDT).....	126
5.5.1 Synthesis and Thermal Characterization.....	126
5.5.2 Molecular Geometry and Electronic Structure Calculations from DFT .....	129
5.5.3 Optical and Electrochemical Properties .....	130
5.5.4 Characterization of Organic Field Effect Transistor Devices .....	131
5.6 Summary.....	133
5.7 References.....	133

## Chapter 6

### Summary and Future Directions

6.1 Summary.....	139
6.2 Future Directions .....	141
6.3 References.....	141

## Appendix

Appendix I .....	142
Appendix II .....	151
Appendix III .....	158
Appendix IV .....	163
<b>List of publications .....</b>	<b>171</b>

## Abbreviations

Abbreviation	Expansion
BODIPY	Boron-dipyrromethene
DPP	Diketopyrrolopyrrole
BDT	Benzodithiophenedione
FET	Field effect transistor
OFET	Organic field effect transistor
DFT	Density functional theory
FMO	Frontier molecular orbital
HOMO	Highest occupied molecular orbital
LUMO	Lowest unoccupied molecular orbital
$E_g$	Energy band gap
UV-vis	Ultraviolet-visible
NMR	Nuclear magnetic resonance
MALDI-TOF	Matrix-assisted laser desorption ionization-time of flight
GPC	Gel permeation chromatography
$M_n$	Number average molecular weight
$M_w$	Weight average molecular weight
PDI	Polydispersity index
PLM	Polarized light microscope
RI	Refractive index

HMDS	Hexamethyldisilazane
OTS	Octadecyltrichlorosilane
TMS	Tetramethylsilane
DCM	Dichloromethane
DMF	N,N-Dimethylformamide
EtOAc	Ethyl acetate
THF	Tetrahydrofuran
BF <sub>3</sub> .OEt <sub>2</sub>	Boron trifluoride diethyl etherate
DDQ	2,3-Dichloro-5,6-dicyano-p-benzoquinone
TFA	Trifluoroacetic acid
dppf	1,1'-Ferrocenediyl-bis(diphenylphosphine)
DSC	Differential scanning calorimetry
TGA	Thermogravimetric analysis
T <sub>m</sub>	Melting temperature
T <sub>g</sub>	Glass transition temperature
T <sub>c</sub>	Crystallization temperature
T <sub>d</sub>	Decomposition temperature
mmol	Millimole
MHz	Megahertz
ppm	Parts per million
Å	Angstrom

$\lambda$	Wavelength
eV	Electron volt
°C	Degree Celsius
min	Minute(s)
h	Hour (s)
br	Broad
PXRD	Powder X-ray diffraction
TTF	Tetrathiafulvalene
CuPc	Copper phthalocyanine
ZnPc	Zinc phthalocyanine
BBL	Poly(benzobisimidazobenzophenanthroline)
PPV	Poly(pphenylenevinylene)
NDI	Naphthalene diimide
OEG	Oligoethylene glycol
CSMs	Conjugated small molecules

## General Remarks

Unless otherwise stated, all the chemicals and reagents were obtained commercially. Dry solvents were prepared by the standard procedures. Air and moisture sensitive reactions were performed using oven-dried glasswares and under an inert atmosphere. Analytical Thin Layer Chromatography was done on precoated silica gel plates (Kieselgel 60F<sub>254</sub>, Merck). Column chromatographic purifications were done with 60-120, 100-200 and 230-400 mesh silica gels. NMR spectra were recorded in CDCl<sub>3</sub> on AV 200 MHz, AV 400 MHz and AV 500 MHz Bruker NMR spectrometers. All chemical shifts are reported in  $\delta$  ppm downfield to TMS and peak multiplicities are referred as singlet (s), doublet (d), triplet (t), quartet (q), pentet (p), and multiplet (m). MALDI-TOF/TOF mass spectra were obtained from ABSCIEX TOF/TOF<sup>TM</sup> 5800 mass spectrometer using dithranol as matrix. Average molecular weights ( $M_w$ ,  $M_n$ ) of polymers were determined by Gel permeation chromatography (GPC) against polystyrene standards. CHCl<sub>3</sub> and THF were used as eluent with a flow rate of 1ml/min.

UV-vis absorption spectra were recorded on SPECORD<sup>®</sup> 210/PLUS, UV-visible spectrophotometer. Cyclic voltammetry experiments were performed on BioLogic Science Instruments. Thermogravimetric analysis (TGA) was done under nitrogen on a SDT model Q600 of TA Instruments thermogravimetric analyzer at a heating rate of 10 °C min<sup>-1</sup>. Differential scanning calorimetry (DSC) was conducted on a TA Instruments Q10 DSC, under nitrogen at a heating/cooling rate of 10 °C/min. Powder X-ray diffraction (PXRD) patterns were recorded on a PANalytical X'PERT PRO instrument using iron-filtered Cu K $\alpha$  radiation ( $\lambda = 1.5406 \text{ \AA}$ ). Atomic-force microscopy (AFM) experiments were performed on Veeco metrology Multimode<sup>TM</sup> Atomic-force microscope, using tapping mode method.

Bottom-gate bottom-contact field-effect transistors substrates were purchased from Fraunhofer IPMS (interdigitated S/D electrodes), with channel lengths (L) 2.5, 5, 10 and 20  $\mu\text{m}$  and channel width (W) of 10  $\mu\text{m}$ . OFET measurements were performed on Agilent 4156C semiconductor probe analyzer and semi probe station.

## Abstract

Organic semiconductors have several advantages over inorganic semiconductors, such as they are lighter in weight, can be solution processed, flexible devices can be fabricated using them, and hence they are futuristic materials for the development of the next generation of electronics. One of the applications of organic semiconductors is organic field effect transistor (OFET). OFET is a three terminal device, consists of an organic semiconducting layer, Source, Drain, and Gate electrodes, and a dielectric material on top of the gate electrode. They can be deposited at low temperature and their applications include electronic paper displays, sensors, low-cost radio-frequency identifications (RFIDs), etc.

In the past few years, organic dyes and pigments, i.e. phthalocyanines, perylene (PDI) and naphthalene (NDI) diimides, diketopyrrolopyrroles (DPP), isoindigos, squaraines, and merocyanines are being explored as building blocks of organic semiconducting materials. Another promising dye is BODIPY dye which is commonly used in biological studies. BODIPY (4, 4-difluoro-4-bora-3a, 4a-diaza-*s*-indacene) dyes are known for their remarkable thermal/photochemical stability, intense absorption/emission profiles, negligible triplet-state formation, and small Stokes shifts. Because of the excellent optical properties, BODIPY based small molecules and polymers have been widely explored in different areas for a variety of applications, such as sensors, biological labeling, photodynamic therapy, etc. By bringing a structural variation on dipyrromethene core, fine tuning of molecular orbital energy levels can be achieved which is an important parameter for designing any organic semiconducting material. There are few reports of BODIPY based systems for OFET applications, and charge carrier mobility values have been modest so far. In this connection, the thesis entitled, "BODIPY based small molecules and polymers for organic field effect transistors" attempts the design and synthesis of conjugated systems incorporating BODIPY dyes and their application in organic field effect transistors. The broad objective of the work is directed towards the structural variations on BODIPY core and understanding their impact on charge transport properties.

Conjugated small molecules and polymers, incorporating BODIPY are synthesized from Pd catalyzed Suzuki coupling reactions, and their structural, molecular, and electronic properties are measured. All small molecules and polymers are characterized by techniques like  $^1\text{H}$  NMR,  $^{13}\text{C}$  NMR, MALDI, GPC to confirm purity, and UV-vis absorption spectra, cyclic voltammetry experiments, TGA, DSC, AFM, and powder XRD to measure electronic

and physical properties. OFET experiments are performed to calculate charge carrier mobility values.

**Chapter 1** reviews the importance of organic semiconductors, working principle and applications of organic field effect transistors (OFETs), significance and synthesis of BODIPY dyes, and BODIPY based systems reported for OFETs. It begins with the general description of the topics mentioned above and narrows down towards the thesis work. This chapter concludes with the overview of scope and objectives of the thesis.

**Chapter 2** deals with the impact of side chains on the charge transport properties. Side chains are substituted to make conjugated systems soluble in common organic solvents but they also affect solid state packing depending on their nature. In this work, we have substituted alkyl and diethylene glycol side chain on the TPA BODIPY TPA small molecule. Since side chains are on the phenyl ring which is not in the conjugation with the conjugated backbone, they have no impact on electronic properties which is evident from the same absorption profile of all the four molecules. Physical properties of these molecules are different. OEG side chain containing CSM forms smooth and ordered film and shows least interplanar spacing among all CSMs. Also, the OEG side chain comprising CSM showed higher hole carrier mobility compared to all the other derivatives.

**Chapter 3** describes the impact of side chain on both electronic and physical properties of the conjugated small molecules. In this work, side chain is connected at the meso position of the BODIPY core. Meso position is sensitive to variations since there is a large molecular orbital coefficient at meso in the lowest unoccupied molecular orbital (LUMO) energy level. Both alkyl and triethylene glycol side chains are chosen due to their different electronic and physical nature. BODIPY core is also varied by removing methyl groups at  $\beta'$  that brings a reduction in steric hindrance in the conjugated system. It also results in deeper HOMO and LUMO energy levels. CSMs with triethylene glycol are found to have deeper LUMO than molecules with alkyl side chain. CSM with dimethyl BODIPY core and triethylene glycol side is found to have lowest energy bandgap among all CSMs. CSMs substituted with triethylene glycol show higher hole mobility on unmodified FET substrates than alkyl chain substituted CSMs. After silane modification, hole carrier mobilities improve slightly for alkyl chain substituted CSMs, but a decrease in one order for triethylene glycol substituted CSMs was observed.

In **chapter 4**, unlike first two chapters where BODIPY is in the center, terminal BODIPY cores are connected to a central DPP unit. Here, a steric hindrance on the BODIPY



core is systematically removed and their impact on electronic and physical properties is studied. Molecule **3**, containing dimethyl BODIPY core, has least twisted structure and is lowest bandgap material among all three, as calculated from the theoretical, electrochemical and optical studies. Hole mobility for **3** was found to be  $1.1 \times 10^{-2} \text{ cm}^2/\text{Vs}$  from OFET studies and it is highest amongst CSMs (**1** – **3**).

**Chapter 5** deals with BODIPY based copolymers, where BODIPY is connected to isoindigo, BDT, and DPP dyes. Polymer p(BODIPY-alt-isoindigo) did not show any charge transport property and p(BODIPY-alt-BDT) copolymers have shown low mobility values. Three p(BODIPY-alt-DPP) polymers are synthesized with a variation on the BODIPY core and it is found that polymer **P3** has lowest and polymer **P2** has highest energy bandgap among all three. All three polymers are thermally stable upto 300 °C, hence they are suitable for device fabrication at a higher temperature. These polymers show ambipolar charge transport. **P3** shows highest, and **P2** shows the lowest hole and electron mobilities. Hole and electron mobilities of **P3** were calculated as  $3.0 \times 10^{-2} \text{ cm}^2/\text{Vs}$  and  $1.5 \times 10^{-2} \text{ cm}^2/\text{Vs}$  respectively from OFET studies.

**Chapter 6** summarizes important results from all chapters with respect to design, synthesis, and transport property studies of conjugated systems incorporating BODIPY dyes. It also includes the future perspective of the findings reported in the thesis work.

# Chapter 1

## Introduction

## 1.1 Organic Electronics: Introduction to Organic Field Effect Transistors (OFETs)

Devices in which flow of electrons can be regulated are the basic unit of all the electronic circuits. Earlier, before the emergence of solid state semiconductors, such devices were mostly based on vacuum tubes/ valves which were bulky, high power consuming, and had limited life. The first transistor was invented by John Bardeen, William Shockley, and Walter Brattain in 1947 and since then a vast majority of modern semiconductor electronics are based on inorganic semiconductors, and in particular, on silicon.<sup>1</sup> Silicon-based electronics has solved many of the challenges associated with our increased use of electronics and has created affordable and high-performing devices. However, there are technological limitations associated with the use of inorganic semiconductors, such as high processing temperature, expensive manufacturing, and low flexibility, and that led to the emergence of organic semiconductors based devices. Such devices could be exploited in flexible displays<sup>2</sup>, (RFID) tags<sup>3</sup>, solar cells<sup>4</sup>, light emitting diodes<sup>5</sup>, etc.

Organic semiconductors are carbon-rich  $\pi$ -conjugated systems and can be broadly categorized as small molecules and polymers based on their molecular weight. Chemical synthesis can tailor their electronic properties by incorporating functionality in molecular design. Like inorganic semiconductors, they absorb light, conduct electricity, and emit light, but they differ from inorganic semiconductors regarding mechanical flexibility, reduced weight, and low-temperature processing. Organic materials can be solution processed and hence they can be applied for fabricating large area devices by printing techniques. Main focus areas of organic semiconductors are displays, transistors, and solar cells. In addition to these applications, they also demonstrate sensors and biological applications.<sup>6</sup> However, moderate charge transport properties, stability issues associated with organic semiconductors, and the lack of knowledge about structure-property relationships limit the rapid growth of organic electronics.

Field-effect transistors (FETs) are the main logic units in electronic circuits and are commonly used either a switch or an amplifier. A FET can be described as a three terminal device, consisting of a semiconducting layer, Source, Drain, and Gate electrodes, and a dielectric material on top of the gate electrode.<sup>1,7</sup> It operates as a parallel plate capacitor in which one plate is a conducting channel between two ohmic contacts, the source and drain electrodes, and charges are induced at the interface of the dielectric and semiconductor by applying a voltage to the second plate of the capacitor, the gate electrode. Organic Field Effect Transistors (OFETs) are based on based on organic semiconducting materials. The

first report of OFET came in 1986 by Koezuka and coworkers and was based on a film of electrochemically grown polythiophene.<sup>8</sup> Over the past 25 years, a tremendous amount of work has been done in this area, and performance of OFETs have improved enormously, and charge carrier mobility values of the same order as amorphous silicon ( $0.1\text{-}1.0\text{ cm}^2\text{ V}^{-1}\text{ S}^{-1}$ ) have been achieved.<sup>9</sup> Major advantages of working with OFET are light and flexible nature of devices, easier processing as OFET devices can be fabricated at or near room temperature. In the beginning, device fabrication methods were mainly based on evaporation of the organic materials. With versatility of synthesis processes, and modifications in molecular designs, the solubility of organic semiconductors in common organic solvents has improved a lot and they can be easily deposited by cost effective solution based methods such as spin coating or printing techniques for large area devices.<sup>10</sup> The improvements in performance of organic materials have facilitated impressive applications such as high-resolution, flexible displays, “e-paper”, and integrated circuits.<sup>2a, 11</sup> Also, significant advancements have been made in industrial manufacturing technology over the time.

## 1.2 Basics of Organic Field-Effect Transistors

### 1.2.1 Device Geometry

Device configuration plays a critical role in the device performance. The most common device configurations (with respect to the substrate) (Figure 1.1) are the bottom contact/top gate (BC/TG, Figure 1.1a), bottom contact/bottom gate (BC/BG, Figure 1.1b), and top contact/bottom gate (TC/BG, Figure 1.1c).

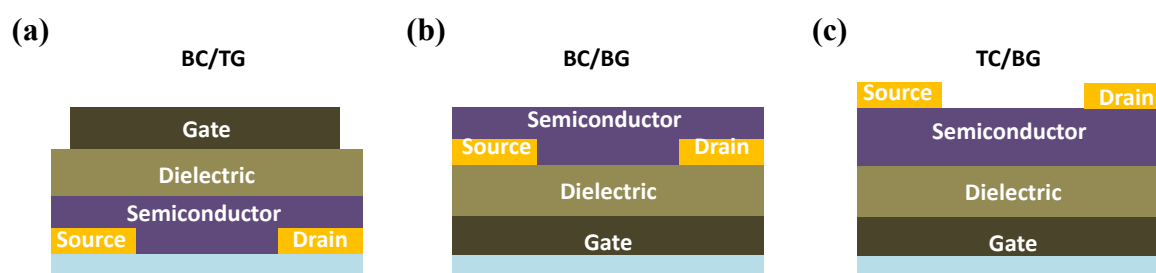


**Figure 1.1** Schematic of (a) bottom contact/top gate (BC/TG), (b) bottom contact/bottom gate (BC/BG), and (c) top contact/bottom gate (TC/BG) Organic Field-Effect Transistor device

Despite same components, transistor performance can vary with variation in device geometry. The position of the injecting electrodes with respect to the gate is one of the major differences between these device geometries. In the case of bottom contact/bottom gate (BC/BG) configuration, charges are directly injected into the channel at the semiconductor-

dielectric interface. In other two configurations, bottom contact/top gate (BC/TG) and top contact/bottom gate (TC/BG), the source/drain electrodes are separated from the channel by the semiconducting material. Here, charges are injected not only from the edge of the electrode but also from the overlapping area with the gate electrode.<sup>1,7,12</sup> In addition to device configuration, properties of the interface between the semiconductor and the electrodes and between the semiconductor and the dielectric play a crucial role towards the device performance.

### 1.2.2 Working Principle of OFETs

Operating principle of OFET is demonstrated in the simplified electronic energy level diagrams shown in figure 1.2. Figure 1.2a shows the positions of the HOMO (highest occupied molecular orbital) and the LUMO (lowest unoccupied molecular orbital) orbitals of the organic semiconductors relative to the Fermi level of the source and drain metal electrodes when there is no gate voltage applied.

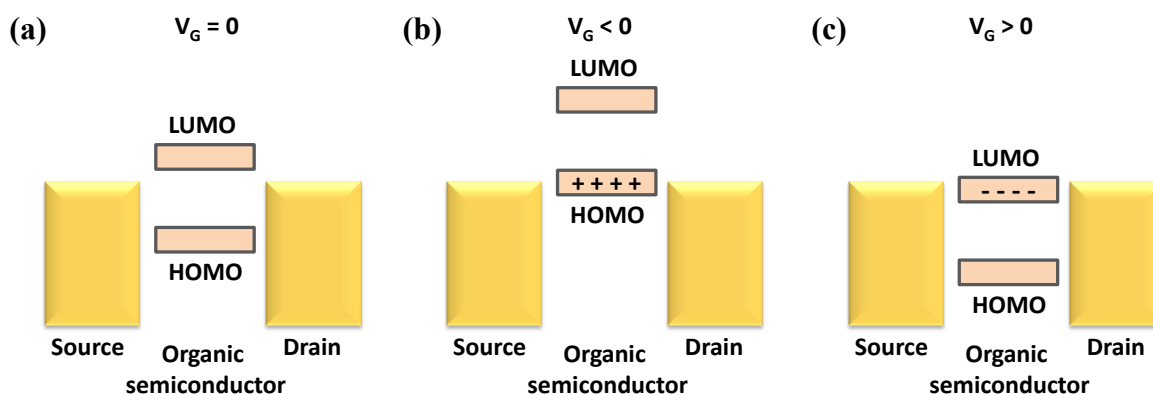


**Figure 1.2** Illustration of working principle of an OFET device (a) at  $V_G = 0$  (b) when a negative voltage is applied to the gate ( $V_G < 0$ ), and (c) when a positive voltage is applied to the gate ( $V_G > 0$ ).

The organic semiconductor which is intrinsically undoped is not conducting at zero gate bias. Application of a negative gate voltage causes large electric field at the semiconductor/ dielectric interface, and HOMO and LUMO energy levels shift up with respect to the Fermi level of the metal electrodes (Figure 1.2b). If the HOMO becomes resonant with the Fermi level of the metal, then electrons from the HOMO of semiconductors will flow into the metal contact leaving the positively charged holes. These positively charged holes accumulated at the semiconductor/ dielectric interface are mobile, and upon application of a drain voltage results in electric current between the source and drain. In this case, the semiconductor will behave as a hole conducting p-type semiconductor.<sup>13</sup> The Same

principle applies when a positive gate voltage is applied. On positive bias, HOMO and LUMO energy levels shift down such that the Fermi level of the metal resonant with the LUMO of the semiconductor, and electrons from metal contact flow into the LUMO, result in the accumulation of electrons at the semiconductor/ dielectric interface (Figure 1.2c). Here, semiconductor will behave as an electron transporting n-type semiconductor.<sup>13</sup>

### 1.2.3 Current-Voltage Characteristics

FETs are typically characterized in two ways. Figure 1.3a shows a typical source–drain current versus source–drain voltage ( $I_D$ - $V_D$ ) plot at different constant gate voltage  $V_G$ , commonly referred as output characteristic curves. There are two regimes in the output characteristic curves, the linear regime where the current is described by a parabola and increases linearly with applied gate voltage, and the saturation regime, where the  $I_D$  is independent of the  $V_D$ . Figure 1.3b shows the source–drain current versus gate voltage ( $I_D$ - $V_G$ ) plot at constant  $V_D$  or the transfer characteristic curves.

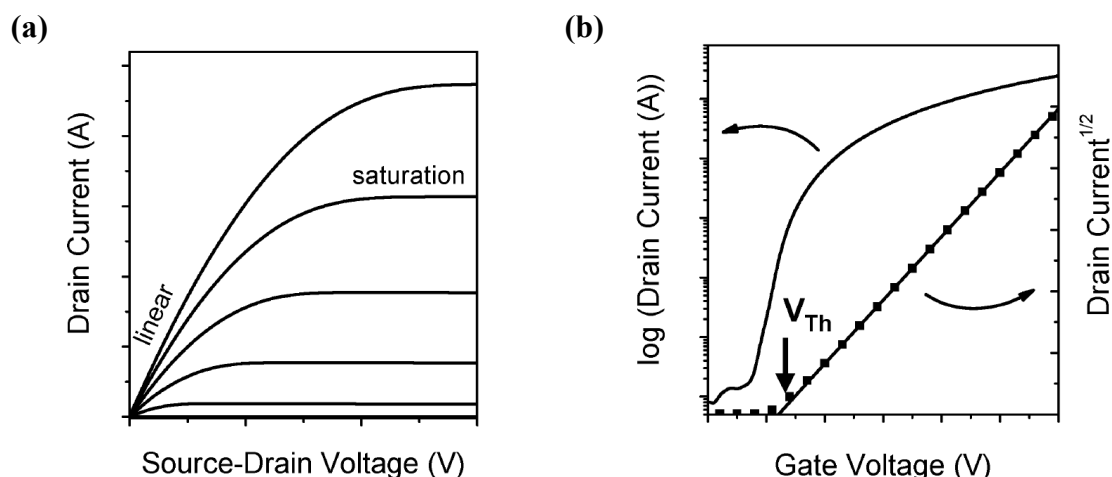


**Figure 1.3** Representative current-voltage characteristics of an OFET device: (a) output characteristics indicating the linear and saturation regimes and (b) transfer characteristics curves (Adapted from Ref 7a).

OFET performance is mainly determined by the charge carrier mobility ( $\mu$ ) that is a measure of the charge carrier drift velocity per unit of electric field. Other relevant parameters are the  $I_{on}/I_{off}$  ratio, and the threshold voltage ( $V_T$ ), that is, the gate voltage from which the conduction channel starts to form.<sup>7a</sup> The high  $I_{on}/I_{off}$  ratio helps in good switching behaviour of OFETs.

In linear regime,  $I_D$  increases linearly with  $V_D$ , and is determined according to the following equation:

$$I_D = \frac{W}{L} \mu_{\text{in}} C_i (V_G - V_T) V_D \quad (1)$$

In the equation (1),  $W$  is the channel width,  $L$  is the channel length,  $C_i$  is the capacitance per unit area of the dielectric layer,  $V_T$  is the threshold voltage, and  $\mu$  is the charge carrier mobility.

When  $V_D = V_G - V_T$ , the channel is pinched off, and the current  $I_D$  tends to saturate. The saturation current can be obtained by the following equation:

$$I_{D,\text{sat}} = \frac{W}{2L} \mu_{\text{sat}} C_i (V_G - V_T)^2 \quad (2)$$

The threshold voltage ( $V_T$ ) can be calculated from the graph of  $(\sqrt{I_D - V_G})$  which is shown in Figure 1.3b.

### 1.3 Organic Semiconductors (Polymers and Small Molecules) for OFET

There are two essential features required in organic semiconductors for their application in printed electronics.<sup>14</sup> The first feature is a  $\pi$ -conjugated backbone for achieving the characteristic optical and charge-transport properties.<sup>15</sup> Second feature is the substitution of solubilizing groups which is required for inexpensive solution processing manufacture and also for enhancing solid-state packing.<sup>9a,16</sup> Organic semiconductors are classified according to the nature of the charge carrier. These materials are extrinsic in nature, and charges are generally injected from the source electrode into the semiconducting material and transported toward the drain electrode. Organic materials with the electron-donating property are p-type organic semiconductors and that those with electron -accepting properties are n-type organic semiconductors, and form p- and n-channels, respectively, in OFETs. Organic semiconductor materials which allow injection of both hole and electron from the source electrode efficiently show ambipolar nature.

#### 1.3.1 p-Type Organic Semiconductors

The most explored organic semiconductors for OFET are p-type small molecules and polymers.<sup>17,18</sup> They are hole-transporting materials. Usually, materials with low ionization potentials and low electron affinities function as p-Type organic semiconductors. The basic design strategy for these molecules is to have a balanced HOMO energy level that should lie somewhere in between 5.0 - 5.5 eV.<sup>19,20</sup> If the HOMO energy level is too high (low ionization potential), easy oxidation by air is possible and leads to poor OFET stability under ambient conditions. If HOMO energy level is too low, high  $I_{\text{on/off}}$  and good mobilities can be achieved,

but such devices typically show large threshold voltages. Design strategy and development of both small molecules and polymers are discussed here.

### a) Polymers

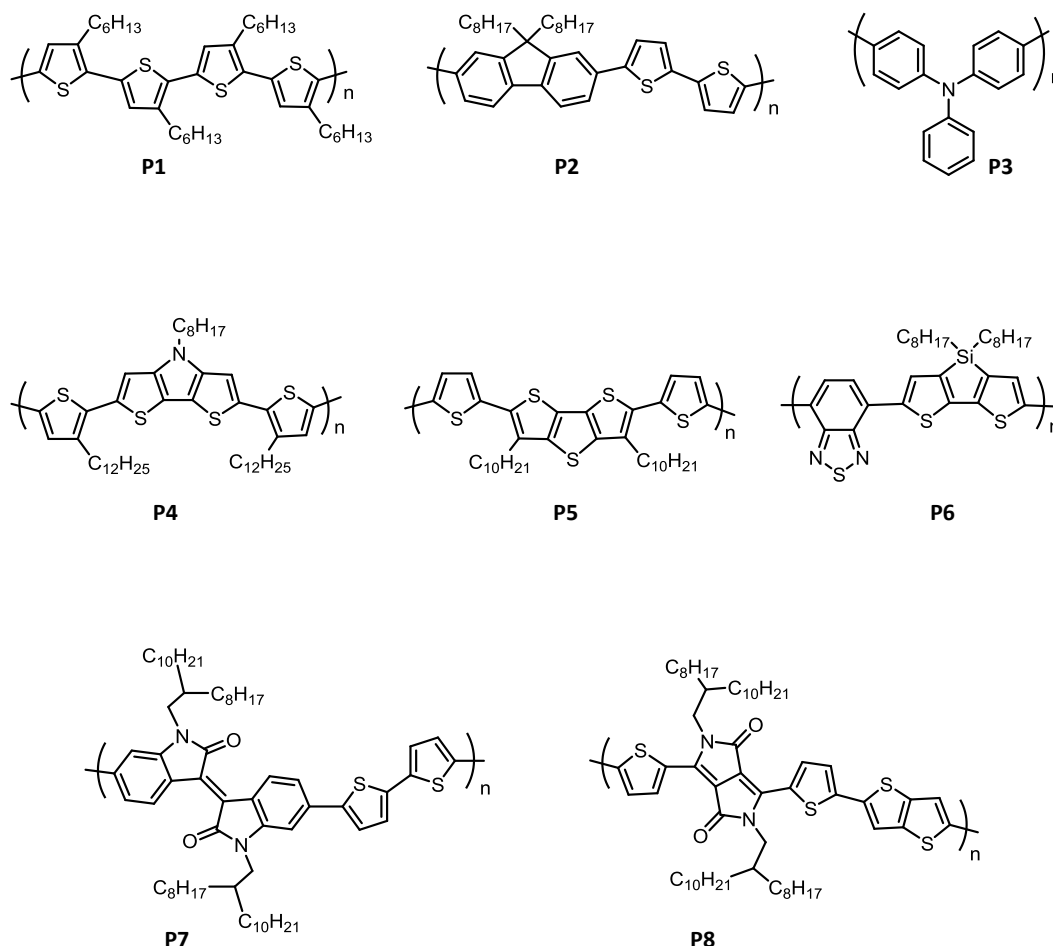


**Chart 1.1** Chemical structures of p-type polymer semiconductors reported for OFET.

There are several advantages in using polymeric material over small molecules. They generally form uniform and smooth thin films which is a desired property for roll-to-roll fabrication on flexible substrates. The first polymer OFET was developed using electrochemically grown polythiophene, and the device showed poor performance.<sup>8</sup> Since then a great amount of work has been done to develop polymeric material for OFET. Chart 1.1 shows the chemical structures of some of the common p-type polymer semiconductors that have been used in the OFETs. The thiophene ring has been one of the most widely used building blocks in polymer design and poly(3-substitutedthiophene)s one of the most studied polymer families so far. The performance of poly(3-hexylthiophene) (P3HT) (P1) based OFET has been investigated by various groups considering the effects of the molecular



weight, film morphology, film thickness, and fabrication process.<sup>21–24</sup> Other important first-generation polymeric semiconductor families are those based on 9,9-dialkylfluorene-alt-bithiophene (P2)<sup>25,26</sup>, triarylamine (P3)<sup>27</sup>, and carbazole<sup>28</sup>. A series of polymers based on fused unit N-alkyldithieno[3,2-b:2',3'-d]pyrrole (DTP) was synthesized by McCullough et al. resulting in better p-channel OFET performances. The highest maximum and average mobilities were obtained for P4 (0.21 and 0.13 cm<sup>2</sup>V<sup>-1</sup>s<sup>-1</sup>, respectively).<sup>29</sup> He, Malliaras, and coworkers reported series of fused-ring thiophene copolymers. Devices made from the polymer P5 shows hole mobility of 0.0017 cm<sup>2</sup>V<sup>-1</sup>s<sup>-1</sup>.<sup>30</sup> Following the donor–acceptor concept Reynolds reported silole based systems, copolymer P6 of dithienosilole with BTB.<sup>31</sup> The first air-stable polymer for OFETs with high performance was reported by Pei et al. P7, a copolymer of isoindigo unit with bithiophene shows hole mobilities of up to 0.79 cm<sup>2</sup>V<sup>-1</sup>s<sup>-1</sup>.<sup>32</sup> Polymers based on Diketopyrrolopyrrole (DPP) are among the high-performing materials. Ong and coworkers reported Polymer P8<sup>33</sup> which has an unsubstituted planar thienothiophene moiety to reduce conformational energy, and it shows an extremely high hole mobility of 10.5 cm<sup>2</sup>V<sup>-1</sup>s<sup>-1</sup>.

## b) Small Molecules

Small molecule semiconductors are easy to purify and easily form crystalline films for the device fabrication. Chart 1.2 shows the chemical structures of some of the common p-type small molecule semiconductors that have been used in the OFETs. Many of the highest-performing small molecules OFETs are based on acenes, fused heteroacene and oligothiophene materials. OFETs based on pentacene (M1) have shown mobility upto 1.5 cm<sup>2</sup>V<sup>-1</sup>s<sup>-1</sup> and could approach to 5.0 cm<sup>2</sup>V<sup>-1</sup>s<sup>-1</sup> when polycrystalline films were used.<sup>34</sup> Rubrene, a tetracene derivative with substituents in the peripositions, shows remarkably high mobility of 15.4 cm<sup>2</sup>V<sup>-1</sup>s<sup>-1</sup> for single crystal.<sup>35</sup> Sexithiophene has been the most studied oligothiophene and exhibits a field-effect mobility of ~0.03 cm<sup>2</sup>V<sup>-1</sup>s<sup>-1</sup>.<sup>36</sup> Fused-thiophene ring containing M4 derivatives with aromatic substituents have shown mobilities higher than 0.1 cm<sup>2</sup>V<sup>-1</sup>s<sup>-1</sup> with ideal solubility and environmental stability.<sup>37</sup> Tetrathiafulvalene (TTF, M5) and its derivatives have been widely studied as organic semiconductors.<sup>38</sup> Phthalocyanines Copper phthalocyanine (CuPc), Zinc phthalocyanine (ZnPc) are the nitrogen-containing heterocyclic semiconductor, and they are widely studied for applications in OFETs. OFET based on M6 show mobility of 10<sup>-3</sup> cm<sup>2</sup>V<sup>-1</sup>s<sup>-1</sup>.<sup>39</sup> Materials based on donor-acceptor design are attractive for use in OFETs because of tunable electronic properties. Oligomer containing thiophene and thiazole (M7) shows mobility of 0.02 cm<sup>2</sup>V<sup>-1</sup>s<sup>-1</sup>.<sup>40</sup>

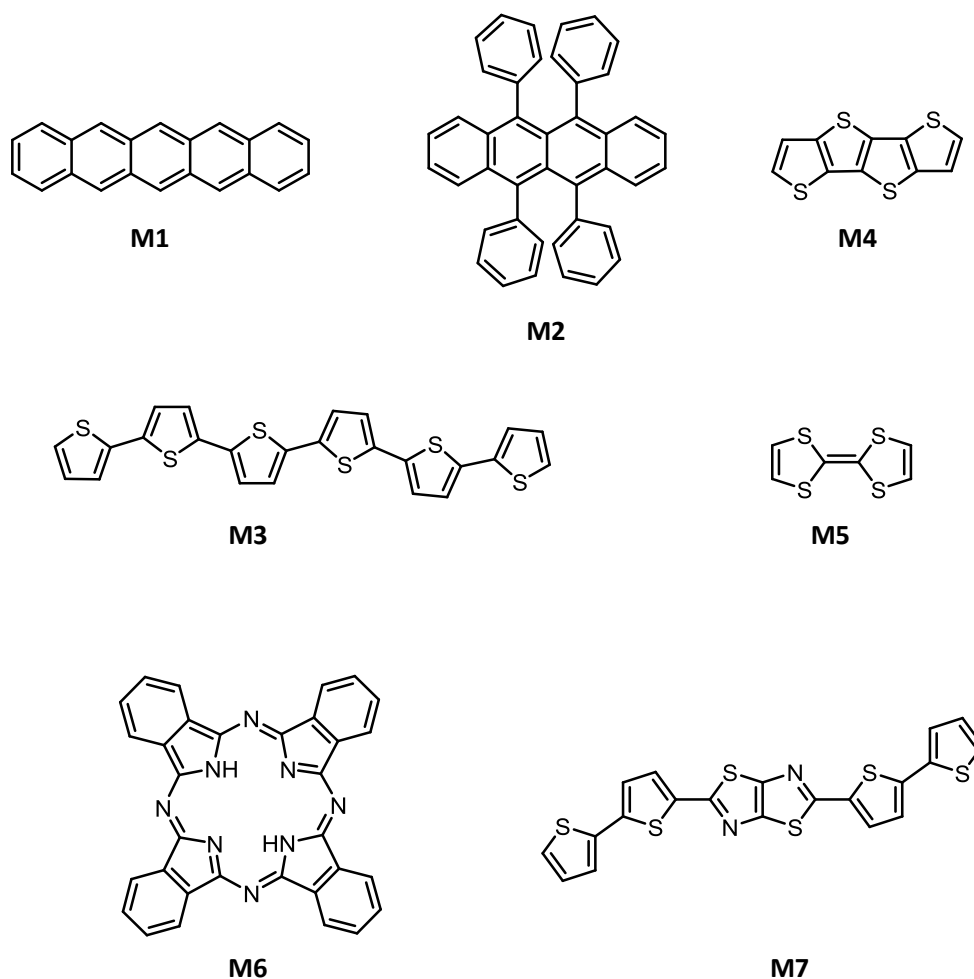


**Chart 1.2** Chemical structures of p-type small molecule semiconductors reported for OFET.

### 1.3.2 n-Type Organic Semiconductors

n-type small molecules and polymers are electron conducting materials. They are relatively less explored than p-type materials. Factors on which performance of n-channel OFET depends are as follows: (i) Gate dielectric.  $\text{SiO}_2$  is the commonly used gate dielectric which efficiently traps electrons on the surface. (ii) Creation of large energy barrier for electron injection in case of high work function metals like Au, which is commonly used for source and drain electrodes. (iii) Ambient atmosphere composition. It is known that  $\text{O}_2$  and  $\text{H}_2\text{O}$  can inhibit electron transport and affect the device performance. To control these issues several measures have been taken, for example, use of polymeric dielectric materials to avoid electron trap, and use of low work function metal contacts for efficient electron injection.

#### a) Polymers

Chart 1.3 shows the chemical structures of some of the common n-type polymer semiconductors that have been used in the OFETs. The first report of an n-type polymer for

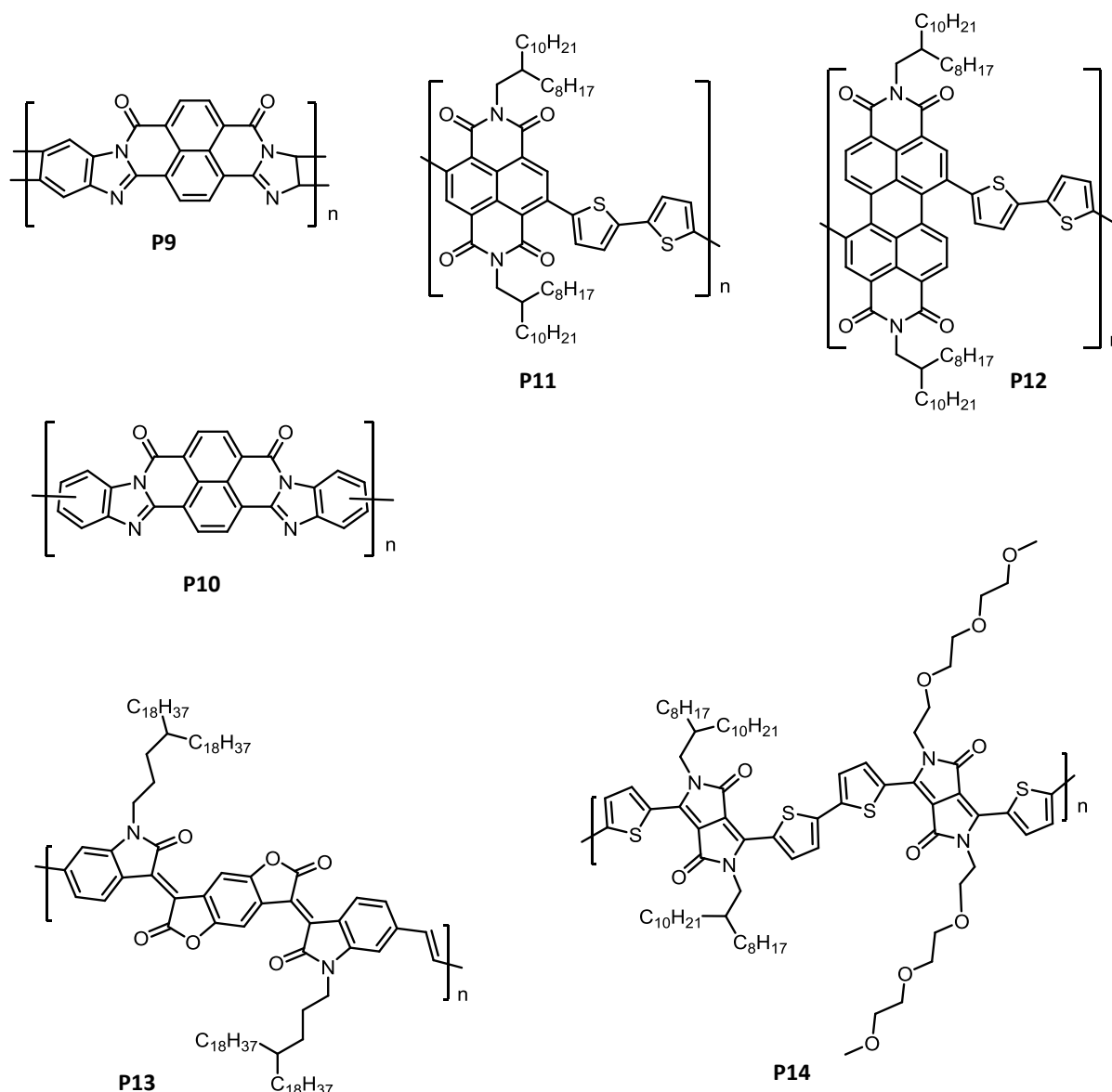


**Chart 1.3** Chemical structures of n-type polymer semiconductors reported for OFET.

OFET was poly(benzobisimidazobenzophenanthroline) (BBL, P9) and its analogue poly(benzobisimidazobenzophenanthroline) (BBB, P10). BBL exhibits a much higher performance with an electron mobility  $0.1 \text{ cm}^2\text{V}^{-1}\text{s}^{-1}$  in comparison to that of BBB ( $10^{-6} \text{ cm}^2\text{V}^{-1}\text{s}^{-1}$ ).<sup>41</sup> Facchetti's group developed both perylenedicarboximide-(P11) and naphthalenedicarboximide- bithiophene (P12) based copolymers.<sup>42</sup>

The naphthalenedicarboximide-based copolymer exhibits a high mobility ( $0.06 \text{ cm}^2\text{V}^{-1}\text{s}^{-1}$ ) and good stability, whereas the perylenedicarboximide-based copolymer exhibits a lower mobility ( $0.002 \text{ cm}^2\text{V}^{-1}\text{s}^{-1}$ ) and poor stability. A novel highly electron-deficient poly(p-phenylenevinylene) (PPV) derivative, benzodifurandione-based PPV (P13) was reported by Pei and coworkers.<sup>43</sup> TG-BC OFET device based on P13 shows electron mobilities as high as

$1.1 \text{ cm}^2\text{V}^{-1}\text{s}^{-1}$  under ambient conditions, and this is one of the highest mobilities achieved for n-channel polymer OFETs. Patil et al. reported a DPP–DPP based copolymer (P14) with alternating alkyl and triethylene glycol side chains which shows electron mobilities up to  $3 \text{ cm}^2\text{V}^{-1}\text{s}^{-1}$  for unipolar n-channel OFET devices.<sup>44</sup>

### b) Small Molecules

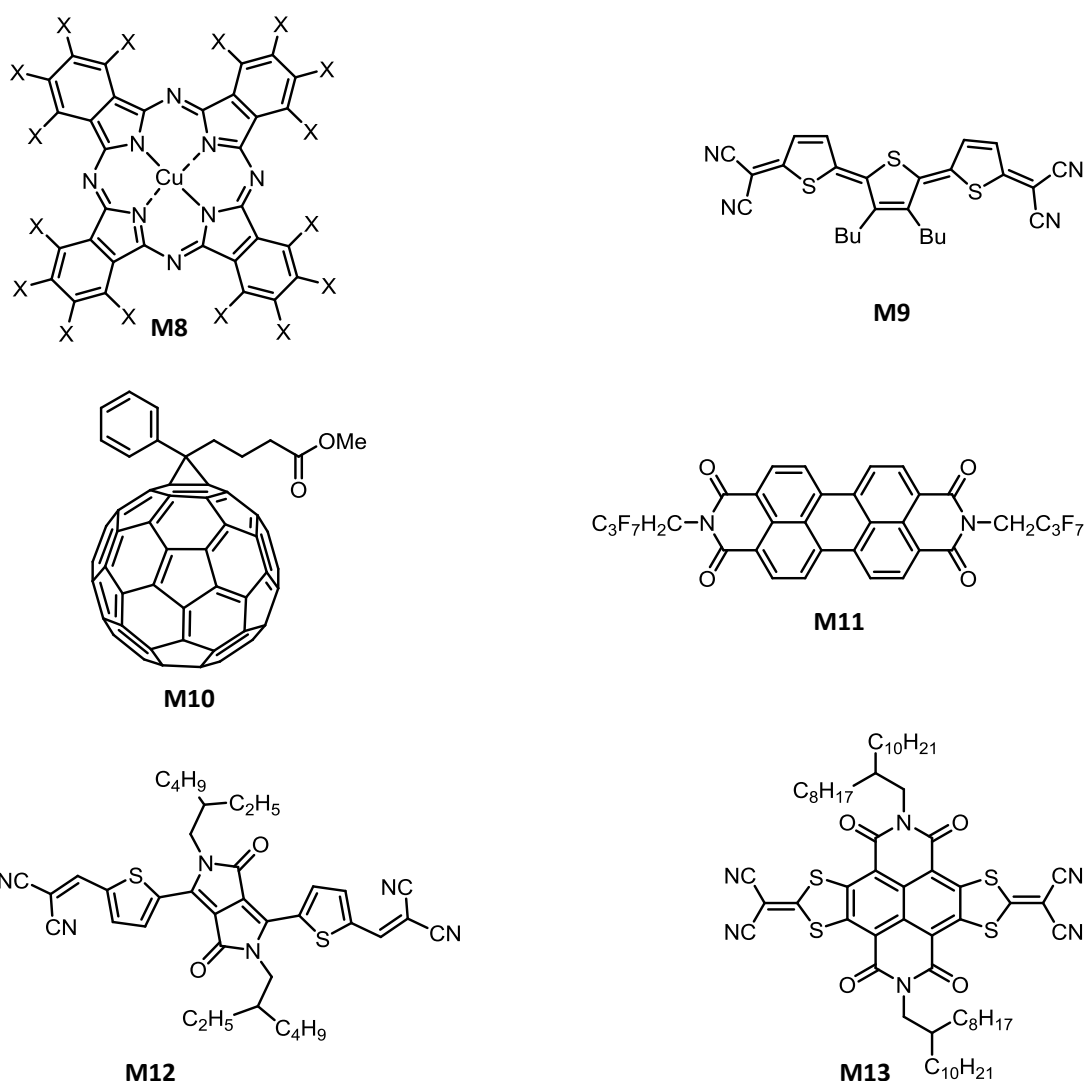


**Chart 1.4** Chemical structures of n-type small molecule organic semiconductors reported for OFET.

Chemical structures of some of the common n-type small molecule semiconductors that have been used in the OFETs are given in the Chart 1.4. Bao et al. demonstrated the first air-stable vacuum-deposited perfluorinated phthalocyanines (M8) n-channel OTFTs that exhibited maximum electron mobilities of  $\sim 0.03 \text{ cm}^2\text{V}^{-1}\text{s}^{-1}$ .<sup>45</sup> Molecule quinomethane terthiophene (M9) reported by Frisbie et al. shows electron mobility of  $0.002\text{--}0.5 \text{ cm}^2\text{V}^{-1}\text{s}^{-1}$ .<sup>46</sup>

Functionalized fullerenes are explored for solution-processed n-channel OTFTs. OFET based on [6,6]-phenyl-C61-butyric acid methyl ester (M10) show electron mobility of  $0.21 \text{ cm}^2 \text{ V}^{-1} \text{ s}^{-1}$ .<sup>47</sup> Bao, Würthner, and coworkers reported that OFETs based on PDI (M11) exhibit electron mobility of  $0.72 \text{ cm}^2 \text{ V}^{-1} \text{ s}^{-1}$  which decrease slightly after air exposure and remain stable for more than 50 days.<sup>48</sup> A dicyanovinyl-substituted DPP-based molecule (M12) was developed by Park et al and electron mobilities up to  $0.96 \text{ cm}^2 \text{ V}^{-1} \text{ s}^{-1}$  were obtained from solution-processed single-crystal OFET devices.<sup>49</sup> Rylene imide based small molecule (M13) was reported by Zhu et al. shows electron mobility upto  $0.46 \text{ cm}^2 \text{ V}^{-1} \text{ s}^{-1}$  for OFET fabricated by inkjet printing.<sup>50</sup>

### 1.3.3 Ambipolar Organic Semiconductors

Ambipolar semiconductors transport both electron and hole, and fabrication of complementary-like logic circuits can be achieved by using a single-component solution process. They are in general lower bandgap (<2 eV) in comparison to corresponding unipolar semiconductors.<sup>7a,51</sup>

#### a) Polymers

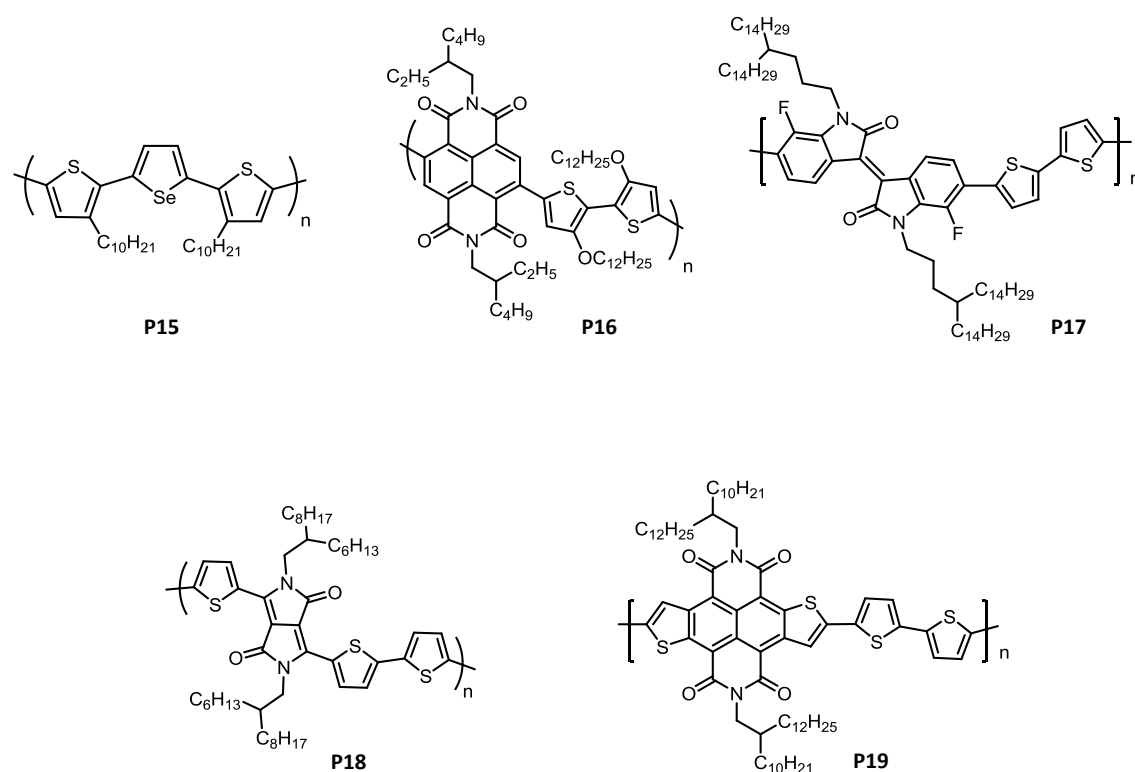


**Chart 1.5** Chemical structures of ambipolar polymer semiconductors reported for OFET.

Chart 1.5 shows the chemical structures of some of the common ambipolar polymer semiconductors that have been used in the OFETs. Sirringhaus et al. observed ambipolar charge transport in a series of regioregular polyselenophenes. Polymer P15 shows ambipolar charge transport with balanced hole and electron mobilities of  $>0.01 \text{ cm}^2 \text{ V}^{-1} \text{ s}^{-1}$ .<sup>52</sup> Ambipolar polymer P16 with electron-donating dialkoxybithiophene and electron-accepting naphthalene bisimide reported by Watson and Jenekhe et al. exhibits electron and hole mobilities in the range of 0.04 and  $0.003 \text{ cm}^2 \text{ V}^{-1} \text{ s}^{-1}$  respectively.<sup>53</sup> Pei et al. developed isoindigo-based donor-acceptor  $\pi$ -conjugated polymers with alternating fluorinated isoindigo and bithiophene units (P17) which shows electron and hole mobilities of 0.43 and  $1.85 \text{ cm}^2 \text{ V}^{-1} \text{ s}^{-1}$  respectively in ambient conditions.<sup>54</sup> Low-bandgap DPP-based polymer, P18, reported by Janssen et al. exhibits balanced ambipolar transport with hole and electron mobilities in the range of  $\sim 0.01 \text{ cm}^2 \text{ V}^{-1} \text{ s}^{-1}$ .<sup>55</sup> Polymer P19 based on thiophene-fused, core-extended NDI unit shows electron and hole mobilities of 0.30 and  $0.10 \text{ cm}^2 \text{ V}^{-1} \text{ s}^{-1}$  respectively.<sup>56</sup>

### b) Small Molecules

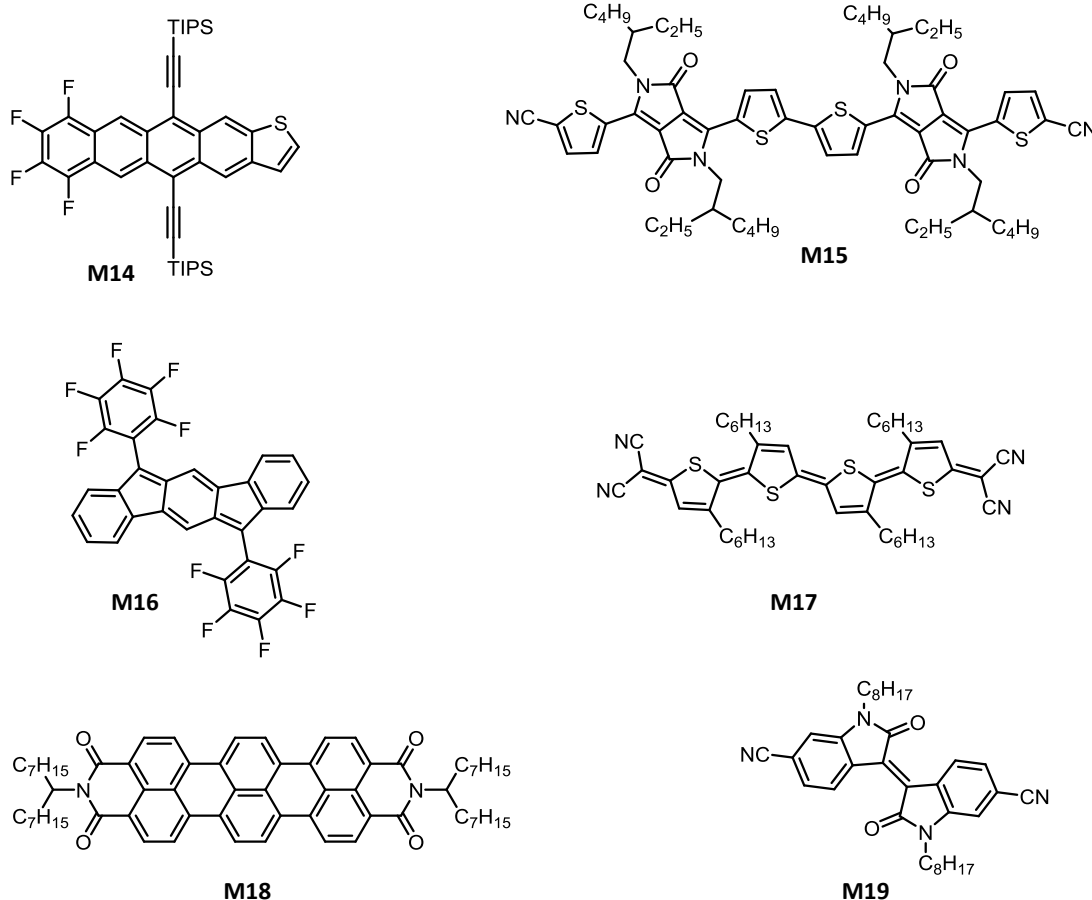


**Chart 1.6** Chemical structures of ambipolar small molecule organic semiconductors.

Chart 1.6 shows the chemical structures of some of the common ambipolar small molecule semiconductors that have been used in the OFETs. Acene-based semiconductor (M14) reported by Bao et al. exhibits ambipolar charge transport with a hole mobility of  $\sim 0.1 \text{ cm}^2 \text{ V}^{-1} \text{ s}^{-1}$  and electron mobility of  $0.133 \text{ cm}^2 \text{ V}^{-1} \text{ s}^{-1}$ .<sup>57</sup> Bottom-gate/top-contact OFETs fabricated under ambient conditions for a DPP-based oligomer M15 with cyano terminal groups, developed by Wang and coworkers, shows hole and electron mobilities of 0.07 and  $0.03 \text{ cm}^2 \text{ V}^{-1} \text{ s}^{-1}$ , respectively.<sup>58</sup> OFET devices fabricated with an antiaromatic, small-molecule M16, developed by Haley and coworkers yields ambipolar charge transport with hole and electron mobilities of  $7.0 \times 10^{-4}$  and  $3.0 \times 10^{-3} \text{ cm}^2 \text{ V}^{-1} \text{ s}^{-1}$ , respectively.<sup>59</sup> Quinoidal oligothiophene derivative based small molecule (M17) ambipolar OFETs reported by Aoyama et al. shows hole and electron mobilities of 0.1 and  $0.006 \text{ cm}^2 \text{ V}^{-1} \text{ s}^{-1}$ , respectively.<sup>60</sup> Müllen and Sirringhaus et al. reported a solution-processable, rylene diimide-based Semiconductor M18, which shows ambipolar charge transport with hole and electron mobilities of  $2.2 \times 10^{-3}$  and  $7.2 \times 10^{-3} \text{ cm}^2 \text{ V}^{-1} \text{ s}^{-1}$ , respectively for TG-BC OFET structure.<sup>61</sup> Würthner and coworkers reported a new core-cyanated isoindigo derivative M19 with ambipolar charge transport where electron and hole mobilities are 0.11 and  $0.045 \text{ cm}^2 \text{ V}^{-1} \text{ s}^{-1}$  respectively.<sup>62</sup>

#### 1.4 Organic Semiconductors based on Dyes and Pigments

Organic dyes and pigments, i.e., phthalocyanines, perylene (PDI) and naphthalene (NDI) diimides, diketopyrrolopyrroles (DPP), isoindigos, squaraines, and merocyanines are widely used as building blocks of organic semiconducting materials. Chart 1.7 shows the chemical structures of some of the common organic dyes that have been used as building blocks of organic semiconductors for OTFTs. For these dyes, charge-carrier mobilities exceeding  $1 \text{ cm}^2 \text{ V}^{-1} \text{ s}^{-1}$  have been achieved. Due to their n-channel operation, PDI and NDI are most widely investigated molecules among these dyes, for which charge-carrier mobilities values close to  $10 \text{ cm}^2 \text{ V}^{-1} \text{ s}^{-1}$  have been demonstrated.<sup>42</sup> Other dyes such as quadrupolar DPP<sup>33,44,49</sup> and isoindigo<sup>54,62</sup> dyes also constitute a major class of high performing organic semiconductors, both as small molecule and as polymers. Mostly they are used in a donor-acceptor configuration in conjugated systems. These materials have been employed for both transistors and solar cells. Another promising dye among them is the BODIPY dye which is commonly used in biological studies. It is thermally and photochemically stable and possesses structural robustness. Despite these, BODIPY based organic semiconductors are rare and they are moderate performers.<sup>63,64</sup>

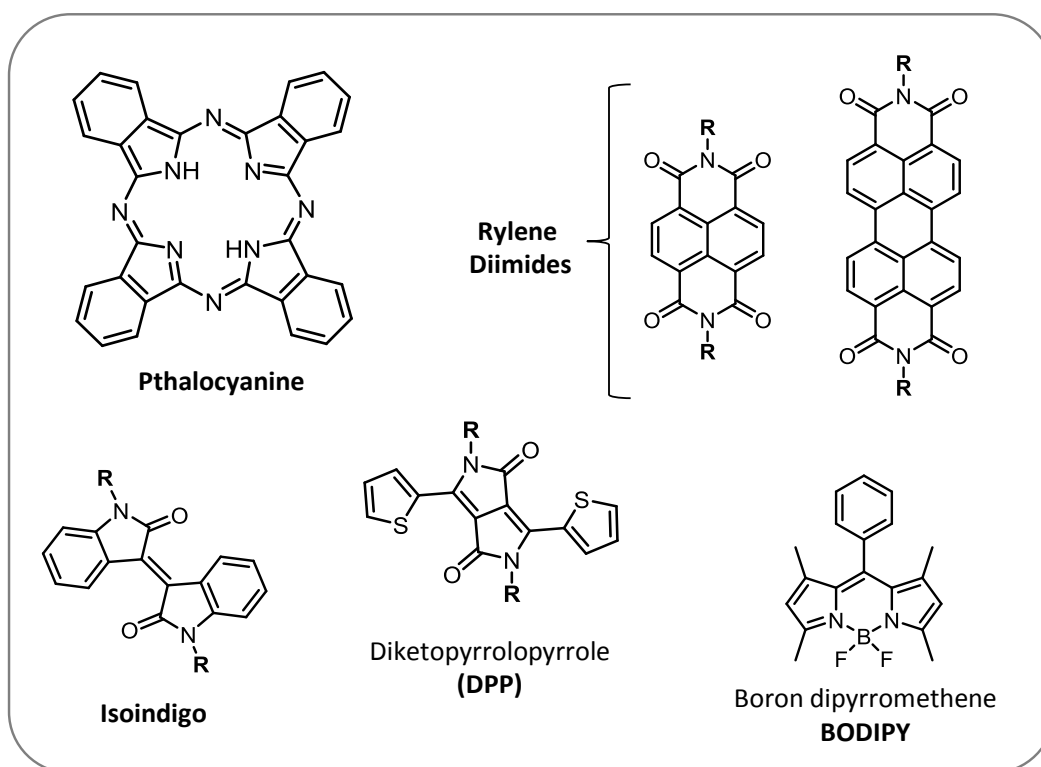


**Chart 1.7** Chemical structures of organic dyes commonly used as building blocks of organic semiconductors.

This thesis work attempts the design and synthesis of conjugated systems incorporating BODIPY dyes, and their application in organic field effect transistors. Extensive literature survey on BODIPY dyes focusing synthetic methods, post-functionalization related to semiconductor material synthesis, and BODIPY based materials reported for OFET is done and discussed in this chapter.

### 1.5 Boron–Dipyrromethene (BODIPY) Dyes

Boron–dipyrromethene or BODIPY (4,4-difluoro-4-bora-3a,4a-diaza-s-indacene) dyes are one of the most versatile fluorophores. Although the first BODIPY dye was discovered in 1968 by Treibs and Kreuzer,<sup>65</sup> their full potential was recognized only since the mid-1990s. BODIPY derivatives have sharp absorbance and emittance profiles with low Stokes shifts. These dyes are highly coloured, neutral compounds with high molar absorption coefficients ( $40,000 - 80,000 \text{ M}^{-1}\text{cm}^{-1}$ ) and high fluorescence quantum yields ( $\Phi_F > 0.60$ ).<sup>66-68</sup> They have excellent thermal and photostability, great solubility in common solvents, ease of functionalization from various positions, and their characteristics are insensitive to change in the pH and polarity of the solvents.<sup>68</sup> Due to these desirable properties and low toxicity, BODIPY derivatives have been extensively used as probes in biological systems<sup>69</sup>. Several different BODIPY dyes have been synthesized by functionalizing the BODIPY core and have



been employed in different applications such as chemosensors,<sup>70</sup> laser dyes,<sup>71</sup> light harvester,<sup>72</sup> photodynamic therapy reagents,<sup>73</sup> and for organic electronics.<sup>63,64</sup>

BODIPY core is analogous to the all-carbon tricyclic ring, s-indacene, and commonly described as a boradiazaindacene. The IUPAC numbering system for BODIPY framework is derived from indacene. The 8-position is referred as meso while the 3,5-positions and 2,6-positions are denoted as  $\alpha$  and  $\beta$  respectively.<sup>66</sup> These positions of the BODIPY core are possible sites for functionalization, and  $\pi$  conjugation along the backbone can be extended by introducing suitable groups.

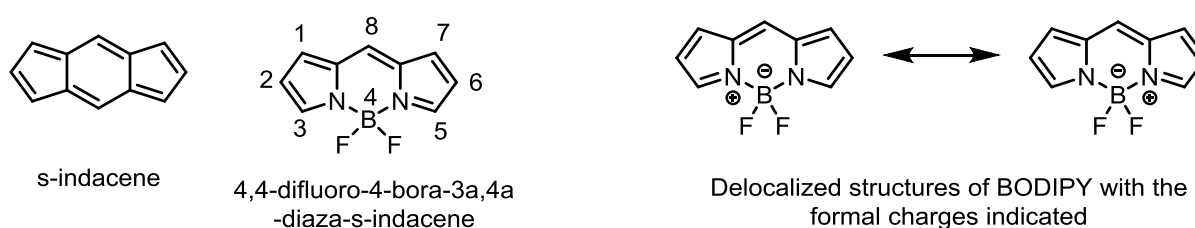


**Figure 1.4** IUPAC numbering scheme used for the BODIPY framework derived from indacene (left). The two equivalent resonance structures of BODIPY core (right).

### 1.5.1 Synthetic Routes towards the BODIPY Core

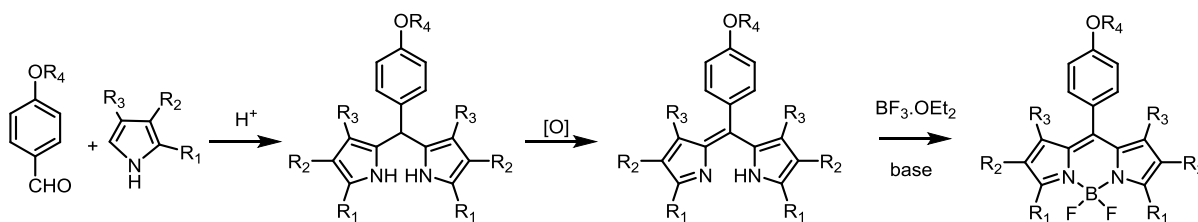
Dipyrromethene ligands are synthesized following the pyrrole condensation reaction, which after complexation with  $\text{BF}_3$ .etherate in the presence of a base, give the required BODIPY dyes.

#### a) Synthesis of Symmetric BODIPY Dyes

Meso-substituted symmetric BODIPY dyes are generally synthesized by acid-catalyzed condensation reactions of pyrroles with acid chlorides, anhydrides or aldehydes. BODIPY dyes bearing substituents at the meso-position tend to be more stable than meso-unsubstituted dyes. Pyrroles are usually substituted at the C-2 position to avoid polymerization or porphyrin formation otherwise an excess of non-substituted pyrrole is required to get the desired BODIPY.

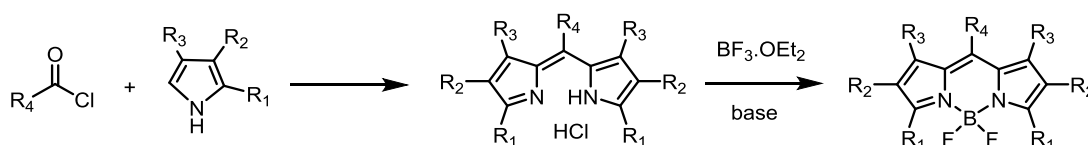
##### (i) From Pyrroles and Aldehydes

The acid catalyzed condensation reaction of pyrroles with aldehydes<sup>74</sup> gives dipyrromethanes which upon oxidation with DDQ or chloronil yields dipyrromethenes, or dipyrrens. Complexation of dipyrrens with boron trifluoride etherate ( $\text{BF}_3 \cdot \text{OEt}_2$ ) in the presence of a base, such as triethylamine, yields the desired BODIPY dyes (Scheme 1.1). These dyes can be easily purified by column chromatography.



**Scheme 1.1** Synthetic route to BODIPY from acid catalyzed condensation of aromatic aldehydes with pyrrole.

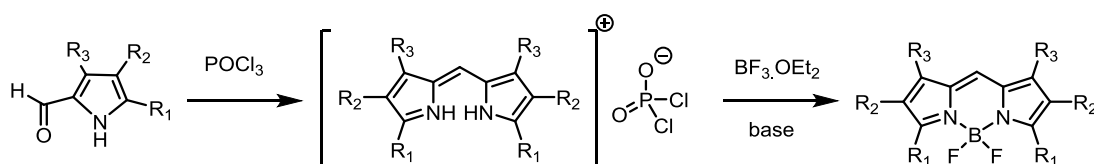
### (ii) From Pyrroles and Acid Chlorides



**Scheme 1.2** Synthetic route to BODIPY from acid chloride with pyrrole.

This route involves acid-catalyzed condensation of pyrroles with acid chlorides<sup>75,76</sup> and produces unstable dipyrromethene hydrochloride salt intermediates (Scheme 1.2). Further reaction with boron trifluoride etherate ( $\text{BF}_3 \cdot \text{OEt}_2$ ) in the presence of a base yields BODIPY dyes. Pure dyes can be obtained by using column chromatography.

### (iii) From Ketopyrroles

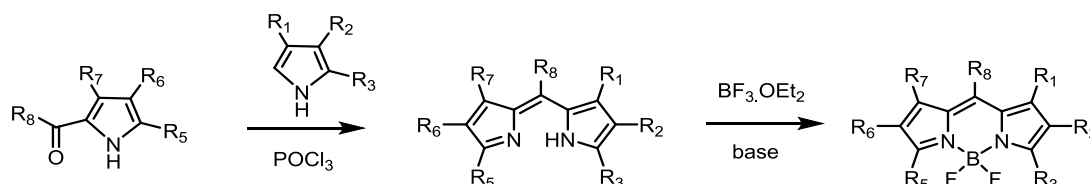


**Scheme 1.3** Synthetic route to symmetric meso-unsubstituted BODIPY dyes.

Symmetric BODIPY dyes unsubstituted at the meso-position can be obtained by self-condensation of substituted pyrrole-2-carbaldehydes in the presence of phosphorus oxychloride (Scheme 1.3).<sup>77</sup> Here, reaction of phosphorus oxychloride with pyrrole-2-carbaldehyde generates a chlorinated azafulvene, which upon reaction with second pyrrole to yield the dipyrromethenium cation and dichlorophosphate counterion. Hereafter, BODIPY dyes are routinely synthesized by complexation reaction.

## b) Synthesis of Asymmetric BODIPY Dyes

Asymmetric BODIPY dyes, substituted or unsubstituted at the *meso*-position, are obtained by condensation of a carbonyl-containing pyrrole with an  $\alpha$ -free pyrrole (Scheme 1.4).<sup>78</sup> These are generally high yield reactions, but when an electron-deficient  $\alpha$ -free pyrrole is used, self-condensation of carbonyl-containing pyrrole dominates, and yield of the desired dye reduces drastically.



**Scheme 1.4** General outline for the synthesis of asymmetric BODIPY dyes mediated by  $\text{POCl}_3$ .

### 1.5.2 Functionalization of the BODIPY core

Fine-tuning of optoelectronic properties of BODIPY dyes have been achieved by functionalization of the BODIPY core. A variety of functionalization methods is available such as substitution at the 8- (*meso*-), 2,6-, 3,5- positions, and at the boron center. Out of them, few relevant methods are briefly described here.

#### a) Electrophilic Substitution

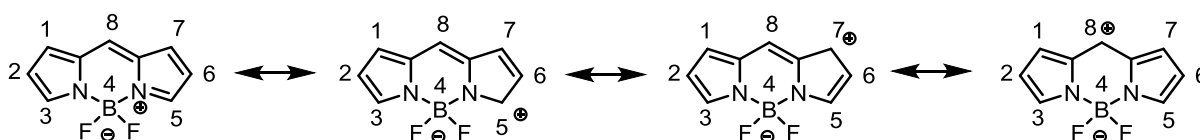
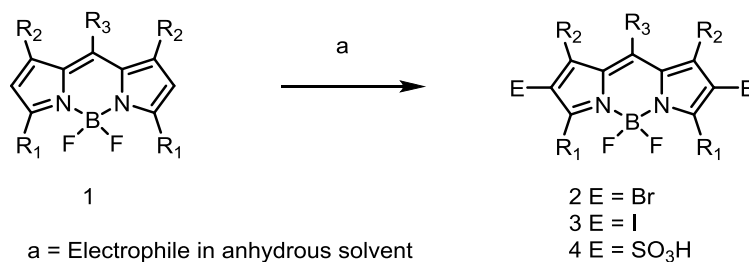


**Figure 1.5** Equivalent resonance structures of BODIPY core and susceptible positions for the electrophilic attack on 1,3,5,7-tetramethyl BODIPY dye.

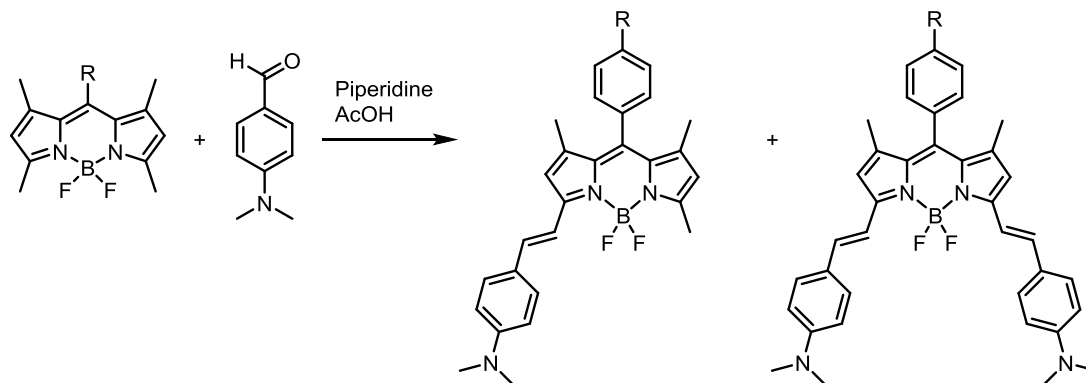
Mesomeric structures of BODIPY shown in figure 1.5 demonstrate that the 2 and/or 6-positions of the BODIPY core are most susceptible to electrophilic attack. Some examples of



**Scheme 1.5** General procedure for electrophilic substitution at the BODIPY core.

electrophilic substitution reactions on the BODIPY core are sulfonation,<sup>79</sup> nitration,<sup>80</sup> halogenation,<sup>81</sup> and formylation<sup>82</sup> reactions (Scheme 1.5).

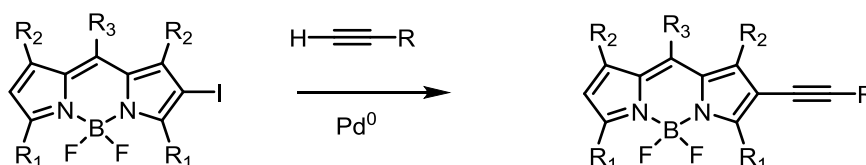
### b) Active Methyl Groups



**Scheme 1.6** Condensation reaction of 3,5-methyl substituents with aromatic aldehydes.

The 3,5-methyl groups on BODIPY dyes are relatively acidic and can perform base-catalyzed Knoevenagel-type condensations.<sup>83-85</sup> Condensation of different aromatic aldehydes with fluorophores introduces different styryl moieties at the 3- and/or 5-positions, and results in a pronounced bathochromic shift to both absorption and fluorescence spectral maxima. Such reactions require the removal of water from the reaction mixture, which can be done by azeotropic removal of the water by a Dean-Stark apparatus, or by using molecular sieves (Scheme 1.6).

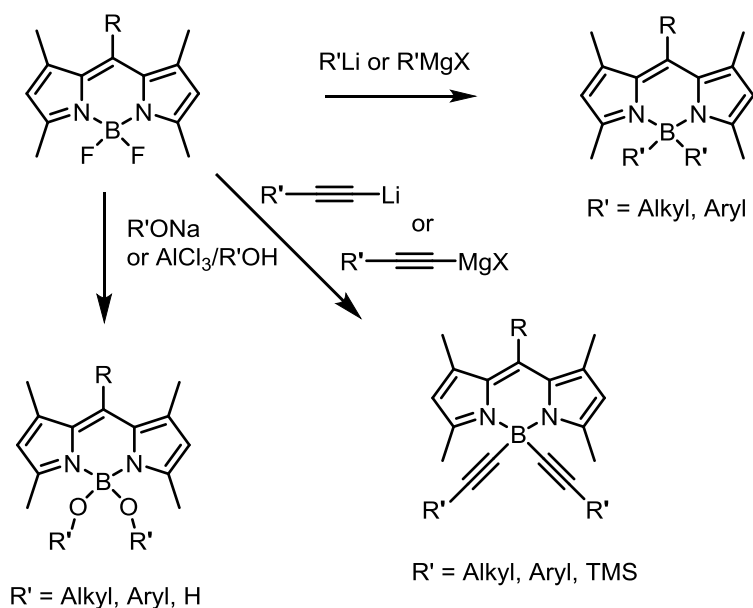
### c) Metal-Catalyzed Cross-Coupling



**Scheme 1.7** General outline for palladium-catalyzed cross-coupling reaction on the BODIPY core.

Palladium-catalyzed coupling reactions of halogenated BODIPY core (Scheme 1.7) lead to an extension of the conjugation length and fine-tuning of the optoelectronic properties. Various types of palladium-catalyzed coupling reactions, such as Suzuki, Stille, Sonogashira or Heck can be used to introduce new functionality onto the BODIPY core.<sup>74a,86,87</sup>

### d) Modifications at the Boron Center

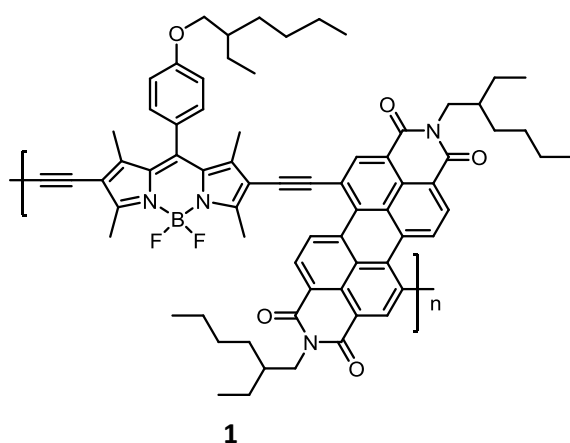


**Scheme 1.8** Selected methods for modification at the boron center. (TMS = trimethylsilyl)

Replacement of the fluorine atoms in BODIPY dyes by aryl, ethynyl, and alkoxide, groups (Scheme 1.8), generates a new family of dyes called C-BODIPY,<sup>88</sup> E-BODIPY,<sup>89-91</sup> and O-BODIPY<sup>92</sup> respectively. For C-BODIPY and E-BODIPY, organolithium or Grignard reagents are used to substitute the fluorine atoms as per nature of the BODIPY core. O-BODIPY synthesis involves displacement of the fluorine atoms with O-phenoxy groups and that can be done using sodium alkoxides or thiolates. Using this method of pi conjugation, many BODIPY scaffold-based molecular dyads, organic solar cells, energy transfer cassettes and supramolecular assemblies have been explored.<sup>93</sup>

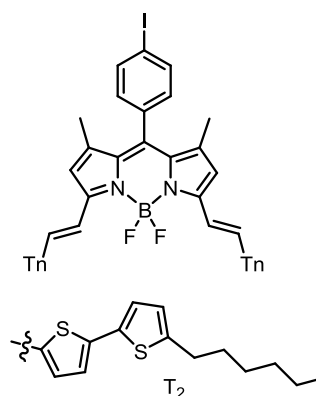
### 1.6 BODIPY based Conjugated Systems for OFETs

Considering their outstanding optical and redox properties, chemical and photochemical Stabilities and tunable optical features, conjugated small molecules and polymers based on BODIPY dyes are being explored as a material for organic electronics. BODIPY based small molecules and polymers have been applied as electron donors in bulk heterojunction (BHJ) solar cells and as a dye for Dye-sensitized solar cells. There is growing interest in BODIPY based systems for OFETs. Chemical structures of some of the BODIPY based semiconductors that have been reported for OTFTs applications are given in the Chart 1.8. Popere et al. reported four donor-acceptor  $\pi$ -conjugated copolymers and studied their charge transport properties.<sup>100</sup> In this work they incorporated BODIPY as a donor with other electron



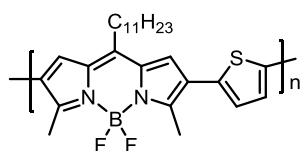
1

Popere *et al.*  
*Macromolecules* 2011, **44**, 4767



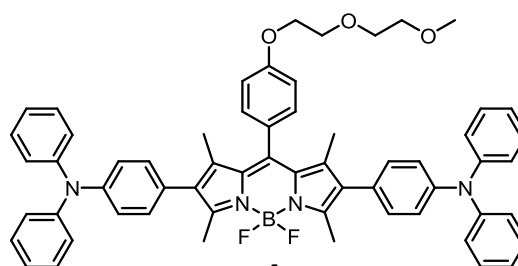
2

Bura *et al.*  
*J. Am. Chem. Soc.* 2012, **134**, 17404



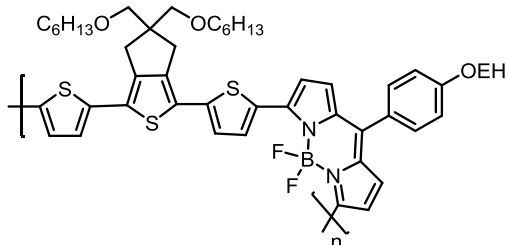
3

Usta *et al.*  
*Adv. Mater.* 2013, **25**, 4327



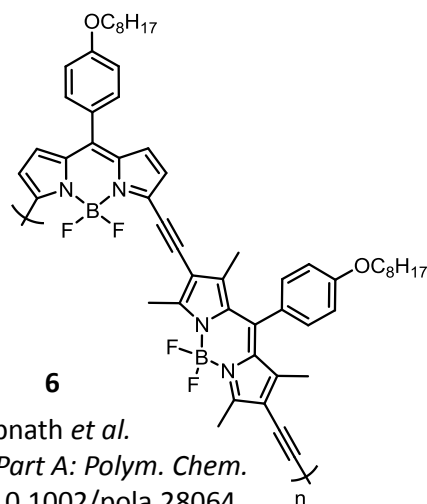
4

Singh *et al.*  
*Phys. Chem. Chem. Phys.* 2014, **16**, 13376



5

Debnath *et al.*  
*J. Phys. Chem. C*, 2015, **119**, 15859



6

Debnath *et al.*  
*J. Polym. Sci. Part A: Polym. Chem.*  
2016, DOI: 10.1002/pola.28064

**Chart 1.8** Chemical structures of BODIPY based small molecules and polymeric materials reported for OFETs.

poor moieties and found hole and electron mobilities in the range of  $10^{-9}$ - $10^{-5}$   $\text{cm}^2\text{V}^{-1}\text{s}^{-1}$ . p(BODIPY-alt-BzT), and p(BODIPY-alt-Qx) showed p-type and p(BODIPY-alt-NDI) and p(BODIPY-alt-PDI) showed n-type semiconductor behaviour. p(BODIPY-alt-PDI) exhibits best charge transport property among all with an electron mobility of  $1.4 \times 10^{-5}$   $\text{cm}^2\text{V}^{-1}\text{s}^{-1}$ .

Conjugated small molecules reported by Bura et al.<sup>101</sup> show hole transport in the range of  $10^{-3}$  -  $10^{-8}$   $\text{cm}^2\text{V}^{-1}\text{s}^{-1}$ . Molecule 2 shown in chart 1.8 gives ambipolar charge transport with hole and electron mobility in the  $1.0 \times 10^{-3}$   $\text{cm}^2\text{V}^{-1}\text{s}^{-1}$  range. Usta et al. reported BODIPY–thiophene copolymers as p-type semiconductors.<sup>102</sup> Four polymers based on two different BODIPY core give hole mobility in the range of  $4 \times 10^{-4}$  to  $0.17$   $\text{cm}^2\text{V}^{-1}\text{s}^{-1}$ . Polymer 3 given in chart 1.7 shows hole mobility of 0.17, and this is highest charge carrier mobility value for a BODIPY based system so far. Molecule 4, bearing a diethylene glycol side chain, reported by Singh et al.<sup>74a</sup>, shows hole mobility in the range of  $10^{-5}$   $\text{cm}^2\text{V}^{-1}\text{s}^{-1}$  and that is two order higher than the hole mobilities of other three molecules. Debnath et al. reported three BODIPY and Cyclopenta[c]Thiophene Containing  $\pi$ -Conjugated Copolymers.<sup>63b</sup> These polymers show hole mobility in the range of  $1 \times 10^{-2}$  to  $10^{-6}$   $\text{cm}^2\text{V}^{-1}\text{s}^{-1}$ . Polymer 5 shown here in chart 1.7 give hole mobility of  $1 \times 10^{-2}$   $\text{cm}^2\text{V}^{-1}\text{s}^{-1}$ . In another work, Debnath et al. reported a site-selective synthesis of BODIPY–acetylene copolymers.<sup>63c</sup> Out of three, two polymers display p-type, and one displays n-type semiconducting properties. Polymer 6 (chart 1.7) exhibits electron mobility of  $9.5 \times 10^{-5}$   $\text{cm}^2\text{V}^{-1}\text{s}^{-1}$ .

### 1.7 Scope and Objectives of the Present Work

The extensive literature survey given above shows the importance of organic semiconducting materials. OFET devices fabricated using these materials can be cost effective and their applications range from daily life uses to bio-medical applications. To synthesize organic materials, a variety of organic dyes have been explored as building blocks. These dyes display strong absorption, and remarkable thermal and photochemical stability. They are easy to synthesize and desired redox properties can be achieved by easy synthetic routes. Among them, BODIPY dyes are relatively least explored for OFET applications. BODIPY is a strong fluorophore and it has a structurally robust core which can undergo structural variations by easy synthetic routes. Redox properties of BODIPY based systems can be fine-tuned by changing substitution at the core. BODIPY core is rigid which facilitates solid state packing. BODIPY based small molecules and polymers are generally soluble in common organic solvents. Such characteristics displayed by BODIPY are important parameters for organic semiconducting material design. Despite these, there are few reports of BODIPY based systems in the area of Organic Field Effect Transistors, and charge carrier mobility values have been moderate so far. In this connection the thesis entitled, “BODIPY based small molecules and polymers for organic field effect transistors” attempts the design and synthesis of conjugated systems incorporating BODIPY dyes, and their application in organic field

effect transistors. The broad objective of the work is directed towards the structural variations on BODIPY core and understanding their impact on charge transport properties. The specific objectives are as follows:

- 1) To synthesize conjugated small molecules incorporating BODIPY dyes with variation in alkyl chain to understand the impact of physical properties governed by nature of side chain on charge transport properties.
- 2) To synthesize BODIPY based conjugated small molecules where nature of side chain impacts physical as well as electronic properties.
- 3) To incorporate another electron deficient moiety in conjugation with BODIPY to develop small molecules with ambipolar charge transport properties.
- 4) To synthesize the copolymers containing BODIPY and other electron deficient and electron rich moieties in donor-acceptor strategy to achieve low bandgap and high charge transport values.
- 5) To Fabricate Field Effect Transistors (OFET) using these small molecules and polymers and study their charge transport properties to establish a structure-property relationship in BODIPY based materials.

## 1.8 References

- 1) Mas-Torrent, M.; Rovira, C. *Chem. Soc. Rev.* **2008**, *37*, 827.
- 2) (a) Rogers, J. A.; Bao, Z.; Baldwin, K.; Dodabalapur, A.; Crone, B.; Raju, V. R.; Kuck, V.; Katz, H.; Amundson, K.; Ewing, J.; Drzaic, P. *Proc. Natl. Acad. Sci. U.S.A.* **2001**, *98*, 4835. (b) Gelinck, G. H.; Huitema, H. E. A.; van Veenendaal, E.; Cantatore, E.; Schrijnemakers, L.; van der Putten, J.; Geuns, T. C. T.; Beenhakkers, M.; Giesbers, J. B.; Huisman, B. H.; Meijer, E. J.; Benito, E. M.; Touwslager, F. J.; Marsman, A. W.; van Rens, B. J. E.; de Leeuw, D. M. *Nat. Mater.* **2004**, *3*, 106. (c) Zhou, L. S.; Wanga, A.; Wu, S. C.; Sun, J.; Park, S.; Jackson, T. N. *Appl. Phys. Lett.* **2006**, *88*, 083502.
- 3) (a) Rotzoll, R.; Mohapatra, S.; Olariu, V.; Wenz, R.; Grigas, M.; Dimmler, K.; Shchekin, O.; Dodabalapur, A. *Appl. Phys. Lett.* **2006**, *88*, 123502. (b) Baude, P. F.; Ender, D. A.; Haase, M. A.; Kelley, T. W.; Muyres, D. V.; Theiss, S. D. *Appl. Phys. Lett.* **2003**, *82*, 3964.



- 4) (a) Pron, A.; Gawrys, P.; Zagorska, M.; Djurado, D.; Demadrille, R. *Chem. Sov. Rev.* **2010**, *39*, 2577. (b) Huo, L.; Hou, J.; Chen, H.-Y.; Zhang, S.; Jiang, Y.; Chen, T. L.; Yang, Y. *Macromolecules* **2009**, *42*, 6564.
- 5) Muccini, M. *Nat. Mater.* **2006**, *5*, 605.
- 6) Sokolov, A. N.; Roberts, M. E.; Bao, Z. *Mater. Today* **2009**, *12*, 12.
- 7) (a) Zaumseil, J.; Sirringhaus, H. *Chem. Rev.* **2007**, *107*, 1296. (b) Wang, C.; Dong, H.; Hu, W.; Liu, Y.; Zhu, D. *Chem. Rev.* **2012**, *112*, 2208. (c) Horowitz, G. *Adv. Mater.* **1998**, *10*, 365.
- 8) Tsumura, A.; Koezuka, H.; Ando, T. *Appl. Phys. Lett.* **1986**, *49*, 1210.
- 9) (a) Katz, H. E. *Chem. Mater.* **2004**, *16*, 4748. (b) Dimitrakopoulos, C. D.; Malenfant, P. R. L. *Adv. Mater.* **2002**, *14*, 99.
- 10) (a) Afzali, A.; Dimitrakopoulos, C. D.; Breen, T. L. *J. Am. Chem. Soc.* **2002**, *124*, 8812. (b) Afzali, A.; Kagan, C. R.; Traub, G. P. *Synth. Met.* **2005**, *155*, 490. (c) Anthony, J. E.; Brooks, J. S.; Eaton, D. L.; Parkin, S. R. *J. Am. Chem. Soc.* **2001**, *123*, 9482.
- 11) Comiskey, B.; Albert, J. D.; Yoshizawa, H.; Jacobson, J. *Nature* **1998**, *394*, 253.
- 12) Daniele Braga, G. H. *Adv. Mater.* **2009**, *21*, 1473
- 13) Newman, C. R.; Frisbie, C. D.; da Silva, D. A.; Bredas, J. L.; Ewbank, P. C.; Mann, K. R. *Chem. Mater.* **2004**, *16*, 4436.
- 14) Karl, N. *Synth. Met.* **2003**, *649*, 133.
- 15) (a) Sirringhaus, H. *Nat. Mater.* **2003**, *2*, 641. (b) Horowitz, G. *Adv. Mater.* **1990**, *2*, 287.
- 16) Allard, S.; Forster, M.; Souharce, B.; Thiem, H.; Scherf, U. *Angew. Chem. Int. Ed.* **2008**, *47*, 4070.
- 17) (a) Schön, J. H.; Kloc, C.; Batlogg, B. *Organic Electronics* **2000**, *1*, 57. (b) Wu, W.; Liu, Y.; Zhu, D. *Chem. Soc. Rev.* **2010**, *39*, 1489. (c) Kelley, T. W.; Boardman, L. D.; Dunbar, T. D.; Muires, D. V.; Pellerite, M. J.; Smith, T. P. *J. Phys. Chem. B* **2003**, *107*, 5877.
- 18) (a) Ong, B. S.; Wu, Y. L.; Liu, P.; Gardner, S. *J. Am. Chem. Soc.* **2004**, *126*, 3378. (b) Chang, J. F.; Sun, B. Q.; Breiby, D. W.; Nielsen, M. M.; Solling, T. I.; Giles, M.; McCulloch, I.; Sirringhaus, H. *Chem. Mat.* **2004**, *16*, 4772.
- 19) Economopoulos, S. P.; Koutentis, P. A.; Ioannidou, H. A.; Choulis, S. A. *Electrochimica Acta* **2013**, *107*, 448.
- 20) Usta, H.; Facchetti, A.; *Polymeric and Small-Molecule Semiconductors for Organic Field-Effect Transistors* Caironi, M.; Noh, Y. Y., Eds.; Wiley-VCH: Weinheim, Germany, **2015**; pp 1–99.

- 21) Kline, R.J.; McGehee, M.D.; Kadnikova, E.N.; Liu, J.; Frechet, J.M.J.; Toney, M.F. *Macromolecules*, **2005** *38*, 3312.
- 22) Chang, J.-F.; Sub, B.; Breiby, D.W.; Nielsen, M.M.; Spelling, T.I.; Giles, M.; McCulloch, I.; Sirringhaus, H. *Chem. Mater.* **2004** *16*, 4772.
- 23) Majewski, L.A.; Kingsley, J.W.; Balocco, C.; Song, A.M. *Appl. Phys. Lett.* **2008**, *88*, 222108.
- 24) Kim, D.H.; Jang, Y.; Park, Y.D.; Cho, K. *J. Phys. Chem. B* **2006**, *110*, 15763.
- 25) Hamilton, M. C.; Martin, S.; Kanicki, J. *Chem. Mater.* **2004**, *16*, 4699.
- 26) Stutzmann, N.; Friend, R. H.; Sirringhaus, H. *Science* **2003**, *299*, 188.
- 27) (a) Veres, J.; Ogier, S.; Lloyd, G.; de Leeuw, D. *Chem. Mat.* 2004, *16*, 4543. (b) Veres, J.; Ogier, S. D.; Leeming, S. W.; Cupertino, D. C.; Khaffaf, S. M. *Adv. Funct. Mater.* **2003**, *13*, 199.
- 28) Li, Y.; Wu, Y.; Ong, B. S. *Macromolecules* 2006, *39*, 6521.
- 29) Liu, J.; Zhang, R.; Sauve, G.; Kowalewski, T.; McCullough, R. D. *J. Am. Chem. Soc.* **2008**, *130*, 13167.
- 30) (a) Fong, H. H.; Pozdin, V. A.; Amassian, A.; Malliaras, G. G.; Smilgies, D.-M.; He, M.; Gasper, S.; Zhang, F.; Sorensen, M. *J. Am. Chem. Soc.* **2008**, *130*, 13202. (b) He, M.; Li, J.; Sorensen, M. L.; Zhang, F.; Hancock, R. R.; Fong, H. H.; Pozdin, V. A.; Smilgies, D.-M.; Malliaras, G. G. *J. Am. Chem. Soc.* **2009**, *131*, 11930.
- 31) Beaujuge, P. M.; Tsao, H. N.; Hansen, M. R.; Amb, C. M.; Risko, C.; Subbiah, J.; Choudhury, K. R.; Mavrinskiy, A.; Pisula, W.; Brédas, J.-L.; So, F.; Müllen, K.; Reynolds, J. R., *J. Am. Chem. Soc.* **2012**, *134*, 8944-8957.
- 32) Lei, T.; Cao, Y.; Fan, Y.; Liu, C.-J.; Yuan, S.-C.; Pei, J. *J. Am. Chem. Soc.* **2011**, *133*, 6099.
- 33) Li, J.; Zhao, Y.; Tan, H. S.; Guo, Y.; Di, C.-A.; Yu, G.; Liu, Y.; Lin, M.; Lim, S. H.; Zhou, Y.; Su, H.; Ong, B. S. *Sci. Rep.* **2012**, *2*, 754.
- 34) Lin, Y. Y.; Gundlach, D. J.; Nelson, S. F.; Jackson, T. N. *IEEE Electron Device Lett.* **1997**, *18*, 606.
- 35) (a) Zeis, R.; Besnard, C.; Siegrist, T.; Schlockermann, C.; Chi, X. L.; Kloc, C. *Chem. Mater.* **2006**, *18*, 244. (b) Briseno, A. L.; Tseng, R. J.; Ling, M. M.; Talcao, E. H. L.; Yang, Y.; Wudl, F.; Bao, Z. N. *Adv. Mater.* **2006**, *18*, 2320.
- 36) (a) Katz, H. E.; Torsi, L.; Dodabalapur, A. *Chem. Mater.* **1995**, *7*, 2235. (b) Dodabalapur, A.; Torsi, L.; Katz, H. E. *Science* **1995**, *268*, 270.

- 37) Liu, Y.; Wang, Y.; Wu, W. P.; Liu, Y. Q.; Xi, H. X.; Wang, L. M.; Qiu, W. F.; Lu, K.; Du, C. Y.; Yu, G. *Adv. Funct. Mater.* **2009**, *19*, 772.
- 38) Jiang, H.; Yang, X.; Cui, Z.; Liu, Y.; Li, H.; Hu, W.; Liu, Y.; Zhu, D. *Appl. Phys. Lett.* **2007**, *91*, 123505.
- 39) Bao, Z. N.; Lovinger, A. J.; Dodabalapur, A. *Adv. Mater.* **1997**, *9*, 42.
- 40) (a) Ando, S.; Nishida, J.; Inoue, Y.; Tokito, S.; Yamashita, Y. *J. Mater. Chem.* **2004**, *14*, 1787. (b) Moon, H.; Jahng, W. S.; Curtis, M. D. *J. Mater. Chem.* **2008**, *18*, 4856.
- 41) (a) Babel, A.; Jenekhe, S. A. *Adv. Mater.* **2002**, *14*, 371. (b) Babel, A.; Jenekhe, S. A. *J. Am. Chem. Soc.* **2003**, *125*, 13656. (c) Chen, X. L.; Bao, Z. N.; Schon, J. H.; Lovinger, A. J.; Lin, Y. Y.; Crone, B.; Dodabalapur, A.; Batlogg, B. *Appl. Phys. Lett.* **2001**, *78*, 228.
- 42) Chen, Z. C.; Zheng, Y.; Yan, H.; Facchetti, A. *J. Am. Chem. Soc.* **2009**, *131*, 8.
- 43) Lei, T.; Dou, J.-H.; Cao, X.-Y.; Wang, J.-Y.; Pei, J. *J. Am. Chem. Soc.* **2013**, *135*, 12168.
- 44) Kanimozhi, C.; Yaacobi-Gross, N.; Chou, K. W.; Amassian, A.; Anthopoulos, T. D.; Patil, S. *J. Am. Chem. Soc.* **2012**, *134*, 16532.
- 45) Bao, Z. A.; Lovinger, A. J.; Brown, J. *J. Am. Chem. Soc.* **1998**, *120*, 207.
- 46) Pappenfus, T. M.; Chesterfield, R. J.; Frisbie, C. D.; Mann, K. R.; Casado, J.; Raff, J. D.; Miller, L. L. *J. Am. Chem. Soc.* **2002**, *124*, 4184.
- 47) Chikamatsu, M.; Itakura, A.; Yoshida, Y.; Azumi, R.; Yase, K. *Chem. Mater.* **2008**, *20*, 7365.
- 48) Oh, J. H.; Liu, S.; Bao, Z.; Schmidt, R.; Wurthner, F. *Appl. Phys. Lett.* **2007**, *91*, 212107.
- 49) Yoon, W. S.; Park, S. K.; Cho, I.; Oh, J.-A.; Kim, J. H.; Park, S. Y. *Adv. Funct. Mater.* **2013**, *23*, 3519.
- 50) Gao, X.; Di, C.-a.; Hu, Y.; Yang, X.; Fan, H.; Zhang, F.; Liu, Y.; Li, H.; Zhu, D. *J. Am. Chem. Soc.* **2010**, *132*, 3697.
- 51) Dou, L.; Liu, Y.; Hong, Z.; Li, G.; Yang, Y. *Chem. Rev.* **2015**, *115*, 12633.
- 52) Chen, Z.; Lemke, H.; Albert-Seifried, S.; Caironi, M.; Nielsen, M. M.; Heeney, M.; Zhang, W.; McCulloch, I.; Sirringhaus, H. *Adv. Mater.* **2010**, *22*, 2371.
- 53) Kim, F. S.; Guo, X.; Watson, M. D.; Jenekhe, S. A. *Adv. Mater.* **2010**, *22*, 478.
- 54) Lei, T.; Dou, J. H.; Ma, Z. J.; Yao, C. H.; Liu, C. J.; Wang, J. Y.; Pei, J. *J. Am. Chem. Soc.* **2012**, *134*, 20025.
- 55) Bijleveld, J. C.; Zoombelt, A. P.; Mathijssen, S. G.; Wienk, M. M.; Turbiez, M.; de Leeuw, D. M.; Janssen, R. *J. Am. Chem. Soc.* **2009**, *131*, 16616.

- 56) Fukutomi, Y.; Nakano, M.; Hu, J.-Y.; Osaka, I.; Takimiya, K. *J. Am. Chem. Soc.* **2013**, *135*, 11445.
- 57) Tang, M. L.; Reichardt, A. D.; Miyaki, N.; Stoltenberg, R. M.; Bao, Z. *J. Am. Chem. Soc.* **2008**, *130*, 6064.
- 58) Wang, L.; Zhang, X. J.; Tian, H. K.; Lu, Y. F.; Geng, Y. H.; Wang, F. S. *Chem. Commun.* **2013**, *49*, 11272.
- 59) Chase, D. T.; Fix, A. G.; Kang, S. J.; Rose, B. D.; Weber, C. D.; Zhong, Y.; Zakharov, L. N.; Lonergan, M. C.; Nuckolls, C.; Haley, M. M. *J. Am. Chem. Soc.* **2012**, *134*, 10349.
- 60) Ribierre, J. C.; Watanabe, S.; Matsumoto, M.; Muto, T.; Aoyama, T. *Appl. Phys. Lett.* **2010**, *96*, 083303.
- 61) Liu, C.; Liu, Z.; Lemke, H. T.; Tsao, H. N.; Naber, R. C. G.; Li, Y.; Banger, K.; Müllen, K.; Nielsen, M. M.; Sirringhaus, H. *Chem. Mater.* **2010**, *22*, 2120
- 62) Yue, W.; He, T.; Stolte, M.; Gsanger, M.; Wurthner, F. *Chem. Commun.* **2014**, *50*, 545.
- 63) (a) Yoshii, R.; Yamane, H.; Nagai, A.; Tanaka, K.; Taka, H.; Kita, H.; Chujo, Y. *Macromolecules* **2014**, *47*, 2316–2323. (b) Debnath, S.; Singh, S.; Bedi, A.; Krishnamoorthy, K.; Zade, S. S. *J. Phys. Chem. C* **2015**, *119*, 15859–15867. (c) Debnath, S.; Singh, S.; Bedi, A.; Krishnamoorthy, K.; Zade, S. S. *J. Polym. Sci. A: Polym. Chem.* **2016**, *54*, 1978–1986.
- 64) Usta, H.; Yilmaz, M. D.; Avestro, A.-J.; Boudinet, D.; Denti, M.; Zhao, W.; Stoddart, J. F.; Facchetti, A. *Adv. Mater.* **2013**, *25*, 4327–4334.
- 65) Treibs, A.; Kreuzer, F. H. *Justus Liebigs Ann. Chem.* **1968**, *718*, 208.
- 66) Ulrich, G.; Ziessel, R.; Harriman, A. The Chemistry of Fluorescent Bodipy Dyes: Versatility Unsurpassed. *Angew. Chem., Int. Ed.* **2008**, *47*, 1184–1201.
- 67) Boens, N.; Leen, V.; Dehaen, W. Fluorescent Indicators Based on BODIPY. *Chem. Soc. Rev.* **2012**, *41*, 1130–1172.
- 68) Loudet, A.; Burgess, K. *Chem. Rev.* **2007**, *107*, 4891.
- 69) (a) Karolin, J.; Johansson, L. B.-A.; Strandberg, L.; Ny, T. *J. Am. Chem. Soc.* **1994**, *116*, 7801. (b) Tan, K.; Jaquinod, L.; Paolesse, R.; Nardis, S.; Di Natale, C.; Di Carlo, A.; Prodi, L.; Montalti, M.; Zaccheroni, N.; Smith, K. M. *Tetrahedron* **2004**, *60*, 1099. (c) Yee, M.-c.; Fas, S. C.; Stohlmeyer, M. M.; Wandless, T. J.; Cimprich, K. A. *J. Biol. Chem.* **2005**, *280*, 29053.
- 70) (a) Turfan, B.; Akkaya, E. U. *Org. Lett.* **2002**, *4*, 2857. (b) Baki, C. N.; Akkaya, E. U. *J. Org. Chem.* **2001**, *66*, 1512.

- 71) Arbeloa, T. L.; Arbeloa, F. L.; Arbeloa, I. L.; Garcia-Moreno, I.; Costela, A.; Sastre, R.; Amat-Guerri, F. *Chem. Phys. Lett.* **1999**, *299*, 315.
- 72) Kim, B.; Ma, B.; Donuru, V. R.; Liu, H.; Fréchet, J. M. J. *Chem. Commun.* **2010**, *46*, 4148.
- 73) Gorman, A.; Killoran, J.; O'Shea, C.; Kenna, T.; Gallagher, W. M.; O'Shea, D. F. *J. Am. Chem. Soc.* **2004**, *126*, 10619.
- 74) (a) Singh, S.; Venugopalan, V.; Krishnamoorthy, K. *Phys. Chem. Chem. Phys.* **2014**, *16*, 13376. (b) Wagner, R. W.; Lindsey, J. S. *Pure Appl. Chem.* **1996**, *68*, 1373.
- 75) Shah, M.; Thangaraj, K.; Soong, M.-L.; Wolford, L. T.; Boyer, J. H.; Politzer, I. R.; Pavlopoulos, T. G. *Heteroat. Chem.* **1990**, *1*, 389.
- 76) Boyer, J. H.; Haag, A. M.; Sathyamoorthi, G.; Soong, M. L.; Thangaraj, K.; Pavlopoulos, T. G. *Heteroat. Chem.* **1993**, *4*, 39.
- 77) Nicolaou, K. C.; Claremon, D. A.; Papahatjis, D. P. *Tetrahedron Lett.* **1981**, *22*, 4647.
- 78) Wood, T. E.; Thompson, A. *Chemical Reviews* **2007**, *107*, 1831.
- 79) Worries, H. J.; Koek, J. H.; Lodder, G.; Lugtenburg, J.; Fokkens, R.; Driessen, O.; Mohn, G. R. *Recueil des Travaux Chimiques des Pays-Bas* **1985**, *104*, 288.
- 80) Pavlopoulos, T. G.; Boyer, J. H.; Shah, M.; Thangaraj, K.; Soong, M.-L. *Appl. Opt.* **1990**, *29*, 3885.
- 81) Haugland, R. P.; Kang, H. C. U.S. Patent 4,774,339, 1988.
- 82) Jiao, L.; Yu, C.; Li, J.; Wang, Z.; Wu, M.; Hao, E. *J. Org. Chem.* **2009**, *74*, 7525.
- 83) Rurack, K.; Kollmannsberger, M.; Daub, J. *New J. Chem.* **2001**, *25*, 289.
- 84) Coskun, A.; Akkaya, E. U. *Tetrahedron Lett.* **2004**, *45*, 4947.
- 85) Dost, Z.; Atilgan, S.; Akkaya, E. U. *Tetrahedron* **2006**, *62*, 8484.
- 86) Rohand, T.; Qin, W.; Boens, N.; Dehaen, W. *Eur. J. Org. Chem.* **2006**, 4658.
- 87) Móczár, I.; Huszthy, P.; Maidics, Z.; Kádár, M.; Klára, T. *Tetrahedron* **2009**, *65*, 8250.
- 88) Goze, C.; Ulrich, G.; Mallon, L. J.; Allen, B. D.; Harriman, A.; Ziessele, R. *J. Am. Chem. Soc.* **2006**, *128*, 10231.
- 89) Ulrich, G.; Goze, C.; Guardigli, M.; Roda, A.; Ziessele, R. *Angew. Chem., Int. Ed.* **2005**, *117*, 3760.
- 90) Ziessele, R.; Goze, C.; Ulrich, G. *Synthesis* **2007**, *6*, 936.
- 91) Ziessele, R.; Ulrich, G.; Harriman, A. *New J. Chem.* **2007**, *31*, 496.
- 92) Gabe, Y.; Ueno, T.; Urano, Y.; Kojima, H.; Nagano, T. *Anal. Biochem.* **2006**, *386*, 621.

- 93) (a) Harriman, A.; Izzet, G.; Ziesel, R. *J. Am. Chem. Soc.* **2006**, *128*, 10868. (b) Goze, C.; Ulrich, G.; Ziesel, R. *J. Org. Chem.* **2007**, *72*, 313.
- 94) Rousseau, T.; Cravino, A.; Bura, T.; Ulrich, G.; Ziesel, R.; Roncali, J. *Chem. Commun.* **2009**, 1673.
- 95) Rousseau, T.; Cravino, A.; Ripaud, E.; Leriche, P.; Rihn, S.; De Nicola, A.; Ziesel, R.; Roncali, J. *Chem. Commun.* **2010**, *46*, 5082.
- 96) Kim, B.; Ma, B.; Donuru, V. R.; Liu, H.; Fréchet, J. M. J. *Chem. Commun.* **2010**, *46*, 4148.
- 97) Lin, H.-Y.; Huang, W.-C.; Chen, Y.-C.; Chou, H.-H.; Hsu, C.-Y.; Lin, J. T.; Lin, H.-W. *Chem. Commun.* **2012**, *48*, 8913.
- 98) Shrestha, M.; Si, L. P.; Chang, C.-W.; He, H. S.; Sykes, A.; Lin, C.-Y.; Diao, E. W.-G. *J. Phys. Chem. C* **2012**, *116*, 10451.
- 99) Cortizo-Lacalle, D.; Howells, C. T.; Gambino, S.; Vilela, F.; Vobecka, Z.; Findlay, N. J.; Inigo, A. R.; Thomson, S. A. J.; Skabara, P. J.; Samuel, I. D. W. *J. Mater. Chem.* **2012**, *22*, 14119.
- 100) Popere, B. C.; Della Pelle, A. M.; Thayumanavan, S. *Macromolecules* **2011**, *44*, 4767.
- 101) Bura, T.; Leclerc, N.; Fall, S.; Lévêque, P.; Heiser, T.; Retailleau, P.; Rihn, S.; Mirloup, A.; Ziesel, R. *J. Am. Chem. Soc.* **2012**, *134*, 17404.
- 102) Usta, H.; Yilmaz, M. D.; Avestro, A.-J.; Boudinet, D.; Denti, M.; Zhao, W.; Stoddart, J. F.; Facchetti, A. *Adv. Mater.* **2013**, *25*, 4327.

## Chapter 2

# Oligoethylene Glycol Substituted BODIPY based Conjugated Small Molecules with Improved Hole Mobility

*This chapter is adapted from “Singh, S.; Venugopalan, V.; Krishnamoorthy, K. Phys. Chem. Chem. Phys. **2014**, 16, 13376”.*

## 2.1 Introduction

Linear and branched alkyl side chains are substituted in the majority of organic semiconductor materials, both small molecules, and polymers, to facilitate fabrication of organic electronic devices by solution processing methods.<sup>1-5</sup> Although the alkyl chains increase the solubility in common organic solvents, they impact the device efficiency due to its insulating nature.<sup>6,7</sup> Also, alkyl chains affect the solid state packing and thin film morphology of conjugated small molecules and polymers.<sup>8,9</sup> Thus, selection of suitable alkyl chain that positively impacts both solubility and device efficiency is an important factor in material design.<sup>10-12</sup> Linear and branched alkyl chains are widely used for this purpose. Branched alkyl chains bring better solubility in the conjugated systems than the linear ones. But, here the branching point also plays important role and impact the device efficiency.<sup>13-15</sup> Research works towards exploring variety of side chains for better device efficiency have been going on. In a recent report, alkyl chains with siloxane terminals have been shown to assist solid state packing in conjugated polymers with improvement in device performance.<sup>16-18</sup>

Oligoethylene glycol (OEG) side chains are widely used to synthesize water soluble polymers. However, they have been rarely used for substituting conjugated small molecules or polymers for fabricating electronic devices.<sup>19-22</sup> The possible reasons could be the poor film formation due to low glass transition temperature and hydrophilic nature of OEG substituted systems.<sup>23</sup> To address these issues amphiphilic CPs were synthesized.<sup>24-26</sup> In these studies, alkyl chains were also there in the molecules, so it was difficult to understand the impact of OEG on the device efficiency. Also, amphiphilic molecules tend to form self-assembled nanostructures which hinder the smooth film formation.<sup>27</sup> Despite all these drawbacks, recently it was found that OEG side chains facilitate better interaction between the conjugated backbones when applied for fabricating organic electronic devices.<sup>28</sup> Hence, it is clear that OEG side chains substituted molecules are preferable, provided the molecules are soluble in common organic solvents and form smooth films.

In this study, we chose to work on conjugated small molecules (CSMs), as they can be synthesized with precise molecular weight and without end group contaminations and thus better in terms of purity than polymeric materials.<sup>29-32</sup> In general, Linear and branched alkyl chains are used to solubilise CSMs in common organic solvents.<sup>33-34</sup> Triphenylamine is propeller shaped and thus it brings solubility without the presence of branched alkyl chain.<sup>35-37</sup> Triphenylamine containing *i*-indigo CSMs are soluble in common organic solvents



while substituted with short linear alkyl chain like butyl chain.<sup>35</sup> CSMs are designed following donor acceptor strategy where electron poor and electron rich moieties are connected in an alternate fashion. Here, electron rich triphenylamine is used as a component of CSMs, as it can make molecules soluble with small alkyl chains. 4,4-Difluoro-4-borata-3a-azonia-4a-aza-s-indacene (BODIPY) is selected as electron poor moiety. BODIPY dyes are strong fluorophore and stable under different reaction conditions. The core is rigid and possesses molecular dipole (3.38–4.12 Debye) that facilitates strong dipolar interactions and impact crystallinity and morphology.<sup>38</sup> Despite these properties, BODIPY based organic semiconductor materials are rare and their charge carrier mobilities have been found to vary from  $1 \times 10^{-9}$  to  $1 \times 10^{-3}$   $\text{cm}^2/\text{Vs}$ .<sup>39,40</sup> Very recently, charge carrier mobility of  $0.1 \text{ cm}^2/\text{Vs}$  have been achieved by removing the methyl groups from the  $\beta$  position.<sup>38</sup> BODIPY containing conjugated systems have been explored as donor in organic solar cells due to excellent optical properties, negligible triplet state formation, and photostability.<sup>41–49</sup> Charge carrier mobility is one of the most important factors deciding the solar cells performance. Thus an approach that can improve the charge carrier transport of BODIPY based systems would help in material design for solar cell applications.

CSMs are substituted with methyl, hexyl, 2-ethylhexyl and diethylene glycol side chains. Chemical structures of CSMs are given in Chart 2.1. To understand the effect of nature of the side chain on charge transport, field effect transistors (FET) have been fabricated using these CSMs. And because of the presence of dipoles in these molecules, the response of the CSMs as a function of alternating current (AC) is also studied.

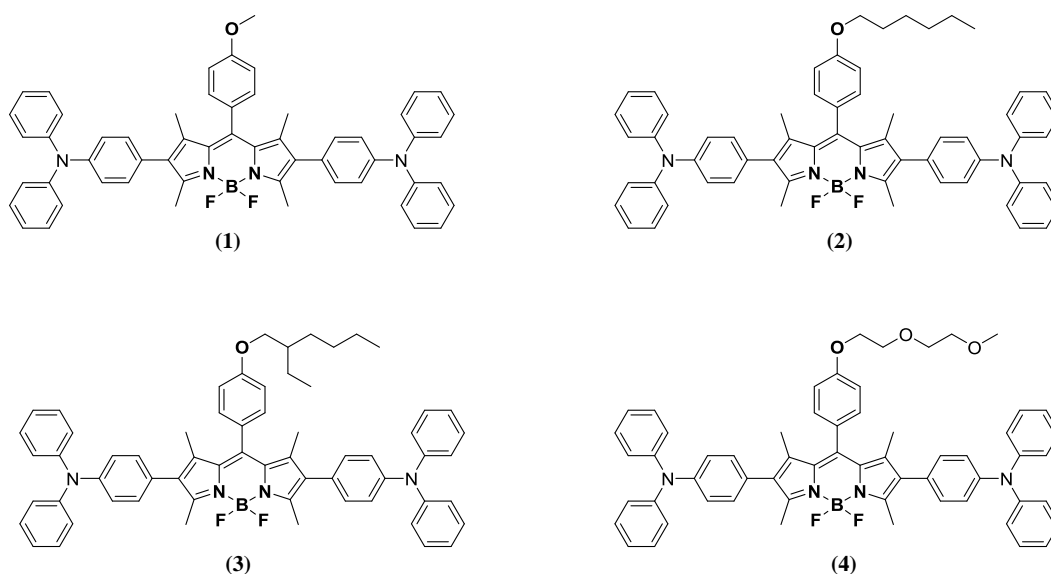


**Chart 2.1** Chemical structures of CSMs (1 – 4).

## 2.2. Experimental Section

### 2.2.1 Materials

All reagents, 2, 4-dimethylpyrrole, 4-methoxybenzaldehyde, 4-hexyloxybenzaldehyde, boron trifluoride diethyl etherate, and 4-(diphenylamino)phenylboronic acid were used directly as received from commercial sources. Compound 4-((2-ethylhexyl)oxy)benzaldehyde<sup>39</sup> and 4-(2-(2-methoxyethoxy)ethoxy)benzaldehyde<sup>78</sup> were synthesized according to the respective references.

### 2.2.2 Instrumentation Details

Cyclic voltammetry (CVs) experiments were performed on BioLogic Science Instruments. CSMs were coated on Pt wire, used as working electrode, Ag/Ag<sup>+</sup> as a reference electrode and Pt foil as counter electrode. CVs were recorded under inert condition by sweeping the working electrode potential in the anodic and cathodic segments in 0.1 M tetrabutylammonium hexafluorophosphate in dry acetonitrile at a scan rate of 100 mV/s. E<sup>ox</sup> and E<sup>red</sup> are determined from the onset potential of oxidation and reduction waves. HOMO and LUMO energy levels were calculated following the equation  $E^{\text{HOMO}} = -(E^{\text{ox}} + 4.8) \text{ eV}$  and  $E^{\text{LUMO}} = -(E^{\text{red}} - 4.8) \text{ eV}$ , and calibrated with respect to the internal standard Fc/Fc<sup>+</sup> couple. Powder X-ray diffraction (PXRD) patterns were recorded on a PANalytical X'PERT PRO instrument using iron-filtered Cu K $\alpha$  radiation ( $\lambda = 1.5406 \text{ \AA}$ ). Single crystal XRD Data was collected on a Super Nova Dual source X-ray Diffractometer system (Agilent Technologies) equipped with a CCD area detector and operated at 250 W (50 kV, 0.8 mA) to generate Mo K $\alpha$  radiation ( $\lambda = 0.71073 \text{ \AA}$ ) and Cu K $\alpha$  radiation ( $\lambda = 1.54178 \text{ \AA}$ ). The crystal was mounted on Nylon CryoLoops with Paraton-N (Hampton Research).

### 2.2.3 Device Fabrication (OFET)

Bottom-gate bottom-contact field-effect transistors substrates were purchased from Fraunhofer IPMS (interdigitated S/D electrodes, with channel lengths (L) 2.5, 5, 10 and 20  $\mu\text{m}$  and channel width (W) of 10  $\mu\text{m}$ ). OFET measurements were performed on Agilent 4156 C semiconductor probe analyzer and semi probe station. The substrates are O<sub>2</sub> plasma treated for 4 minutes with power of 30 Watts. The CSMs were spun on top of the substrates from chloroform solutions. Spin coating was done for 60 seconds, at 1000 RPM for molecules that formed a good film, and at 500RPM for non-wetting film forming conditions.

## 2.2.4 Synthetic Procedures and Characterization Data

### **BODIPY 1**

To a solution of 4-methoxybenzaldehyde (1.36 g, 10 mmol) in anhydrous dichloromethane (800 mL), 2, 4-dimethylpyrrole (1.90 g, 20 mmol) was added and the reaction mixture was purged with argon for 5 minutes. 0.2 mL of TFA was added to the solution and the reaction mixture was stirred overnight at room temperature under an argon atmosphere. The reaction mixture was then washed with 2N NaOH solution and then with water. The organic layer was dried over anhydrous Na<sub>2</sub>SO<sub>4</sub> and evaporated under reduced pressure. The residue was then dissolved in toluene (35 mL) and a solution of DDQ (2.5 g, 11 mmol) in toluene (15 mL) was added slowly to it, under argon atmosphere. After 5 minutes of stirring, triethylamine (8 mL) and borontrifluoride etherate (7 mL) were added and the reaction mixture was stirred at room temperature for 1.5 h. The reaction mixture was then diluted with diethylether and was repeatedly washed with water. The organic layer was dried over anhydrous Na<sub>2</sub>SO<sub>4</sub> and solvent was evaporated under reduced pressure. The crude product was purified by column chromatography (eluent: EtOAc/pet.ether) to furnish **BODIPY 1** (800 mg, 23%) as a bright orange solid with a metallic luster. <sup>1</sup>H NMR (200 MHz, CDCl<sub>3</sub>) δ: 7.21 (d, *J* = 8.72, 2 H), 7.04 (d, *J* = 8.72, 2 H), 5.98 (s, 2 H), 3.88 (s, 3 H), 2.56 (s, 6 H), 1.44 (s, 6 H); <sup>13</sup>C NMR (50 MHz, CDCl<sub>3</sub>) δ: 160.12, 155.25, 143.20, 141.87, 131.86, 129.20, 127.02, 121.12, 114.54, 55.33, 14.59.

### **BODIPY 2:**

Following the procedure for the compound **BODIPY 1**, using 4-(hexyloxy)benzaldehyde (2.06 g, 10 mmol), compound **BODIPY 2** (970 mg, 23%) was synthesized. <sup>1</sup>H NMR (200 MHz, CDCl<sub>3</sub>) δ: 7.18 (d, *J* = 8.59, 2 H), 7.02 (d, *J* = 8.72, 2 H), 5.98 (s, 2 H), 4.02 (t, *J* = 6.57, 2 H), 2.56 (s, 6 H), 1.84 (m, 2 H), 1.45 (s, 6 H), 1.38 (m, 6 H), 0.93 (t, *J* = 6.82, 3 H); <sup>13</sup>C NMR (50 MHz, CDCl<sub>3</sub>) δ: 159.75, 155.22, 143.22, 142.03, 131.91, 129.16, 126.83, 121.09, 115.10, 68.20, 31.64, 29.23, 25.75, 22.60, 14.57, 14.03.

### **BODIPY 3:**

Following the procedure for the compound **BODIPY 1**, using 4-((2-ethylhexyl)oxy)benzaldehyde (2.35 g, 10 mmol), compound **BODIPY 3** (1.21 g, 27%) was synthesized. <sup>1</sup>H NMR (200 MHz, CDCl<sub>3</sub>) δ: 7.18 (d, *J* = 8.72, 2 H), 7.02 (d, *J* = 8.72, 2 H), 5.98 (s, 2 H), 3.91 (d, *J* = 5.81, 2 H), 2.56 (s, 6 H), 1.77 (m, 1 H), 1.45 (s, 6 H), 1.37 (m, 6 H),

0.96 (m, 6 H);  $^{13}\text{C}$  NMR (50 MHz,  $\text{CDCl}_3$ )  $\delta$ : 160.01, 155.19, 143.21, 142.10, 131.91, 129.12, 126.75, 121.07, 115.18, 70.88, 39.44, 30.57, 29.72, 29.16, 23.90, 23.06, 23.06, 14.59, 14.10, 11.17.

#### **BODIPY 4:**

Following the procedure for the compound BODIPY 1, using 4-(2-(2-methoxyethoxy)ethoxy)benzaldehyde (2.25 g, 10 mmol), compound **BODIPY 4** (1.1 g, 25%) was synthesized.  $^1\text{H}$  NMR (200 MHz,  $\text{CDCl}_3$ )  $\delta$ : 7.18 (d,  $J = 8.84$  Hz, 2 H), 7.04 (d,  $J = 8.97$  Hz, 2 H), 5.98 (s, 2 H), 4.20 (t,  $J = 4.67$  Hz, 2 H), 3.92 (t,  $J = 4.73$  Hz, 2 H), 3.75 (m, 2 H), 3.62 (m, 2 H), 3.41 (s, 3 H), 2.55 (s, 6 H), 1.43 (s, 6 H);  $^{13}\text{C}$  NMR (50 MHz,  $\text{CDCl}_3$ )  $\delta$ : 159.37, 155.24, 143.19, 141.86, 131.84, 129.15, 127.19, 121.10, 115.20, 71.96, 70.86, 69.77, 67.48, 59.11, 14.60.

**2, 6-DiiodoBODIPY B1:** To the solution of BODIPY 1 (500 mg, 1.4 mmol) in  $\text{CH}_2\text{Cl}_2$  (15 mL), a solution of N-iodosuccinimide (760 mg, 3.46 mmol) in anhydrous and degassed DMF (5 mL) was added dropwise and the reaction mixture was stirred vigorously for 24 h at room temperature. After completion of the reaction,  $\text{CH}_2\text{Cl}_2$  was removed under reduced pressure. The residue was dissolved in diethylether and was repeatedly washed with water. Organic layer was then dried over anhydrous  $\text{Na}_2\text{SO}_4$  and was evaporated under reduced pressure. The crude product was purified by column chromatography (eluent: EtOAc/pet.ether) to furnish **B1** (590 mg, 70%) as a deep red solid.  $^1\text{H}$  NMR (400 MHz,  $\text{CDCl}_3$ )  $\delta$ : 7.16 (d,  $J = 8.70$  Hz, 2 H), 7.06 (d,  $J = 8.70$  Hz, 2 H), 3.90 (s, 3 H), 2.65 (s, 6 H), 1.45 (s, 6 H);  $^{13}\text{C}$  NMR (100 MHz,  $\text{CDCl}_3$ )  $\delta$ : 160.57, 156.59, 145.38, 141.61, 131.76, 129.12, 126.71, 114.89, 85.54, 55.42, 17.18, 16.02.

#### **2, 6-DiiodoBODIPY B2:**

Following the procedure for compound B1, using BODIPY 2 (590 mg, 1.4 mmol), Compound **B2** (660 mg, 70%) was synthesized.  $^1\text{H}$  NMR (200 MHz,  $\text{CDCl}_3$ )  $\delta$ : 7.15 (d,  $J = 8.72$  Hz, 2 H), 7.05 (d,  $J = 8.72$  Hz, 2 H), 4.03 (t,  $J = 6.57$ , 2 H), 2.65 (s, 6 H), 1.85 (m, 2 H), 1.46 (s, 6 H), 1.39 (m, 6 H), 0.94 (t,  $J = 6.82$ , 3 H);  $^{13}\text{C}$  NMR (50 MHz,  $\text{CDCl}_3$ )  $\delta$ : 160.15, 156.53, 145.41, 141.77, 131.76, 129.05, 126.45, 115.41, 85.57, 68.30, 31.65, 29.21, 25.76, 22.63, 17.22, 16.03, 14.08.

**2, 6-DiiodoBODIPY B3:**

Following the procedure for compound B1, using BODIPY 3 (630 mg, 1.4 mmol).

Compound **B3** (790 mg, 80%) was synthesized.  $^1\text{H}$  NMR(200 MHz,  $\text{CDCl}_3$ )  $\delta$ : 7.15 (d,  $J$ = 8.59 Hz, 2 H), 7.05 (d,  $J$  = 8.72 Hz, 2 H), 3.93 (d,  $J$  = 5.81, 2 H), 2.65 (s, 6 H), 1.79 (m, 1 H), 1.46 (s, 6 H), 1.38 (m, 8 H), 0.97 (m, 6 H),  $^{13}\text{C}$  NMR (50 MHz,  $\text{CDCl}_3$ )  $\delta$ : 160.42, 156.51, 145.42, 141.82, 131.81, 129.02, 126.39, 115.49, 85.55, 70.97, 39.41, 30.55, 29.16, 23.89, 23.05, 17.21, 16.04, 14.12, 11.18.

**2, 6-DiiodoBODIPY B4:**

Following the procedure for compound B1, using BODIPY 4 (620 mg, 1.4 mmol).

Compound **B4** (730 mg, 75%) was synthesized.  $^1\text{H}$  NMR (200 MHz,  $\text{CDCl}_3$ )  $\delta$ : : 7.16 (d,  $J$ = 8.84 Hz, 2 H), 7.07 (d,  $J$  = 8.97 Hz, 2 H), 4.22 (t,  $J$  = 4.67 Hz, 2 H), 3.93 (t,  $J$  = 4.73 Hz, 2 H), 3.77 (m, 2 H), 3.61 (m, 2 H), 3.42 (s, 3 H), 2.64 (s, 6 H), 1.44 (s, 6 H);  $^{13}\text{C}$  NMR (50 MHz,  $\text{CDCl}_3$ )  $\delta$ : 159.77, 156.56, 145.38, 141.57, 131.71, 129.04, 126.84, 115.51, 85.56, 71.95, 70.89, 69.74, 67.55, 59.15, 17.20, 16.03.

**CSMs (1 – 4)**

**Compound 1: B1** (182 mg, 0.3 mmol), 4-(diphenylamino)phenylboronic acid (208 mg, 0.72 mmol), Pd(dppf) $\text{Cl}_2$  (12 mg) and  $\text{Na}_2\text{CO}_3$  (315 mg, 3 mmol) were taken in a schlenk tube. The tube was evacuated and back-filled with argon three times, after which a degassed solvent mixture of toluene (30 mL), ethanol (12 mL) and water (15 mL) was transferred to the schlenk tube through a septum and the reaction was carried out at 80 °C for 6h under argon atmosphere. After completion of the reaction, solvent was removed under reduced pressure and then the residue was dissolved in ethyl acetate and washed with water. Organic layer was passed through a short pad of celite and dried over anhydrous  $\text{Na}_2\text{SO}_4$ . The filtrate was concentrated under reduced pressure and the crude product was purified by column chromatography (eluent: EtOAc/pet.ether) to furnish **1** (200 mg, 80%) as a red solid.  $^1\text{H}$  NMR (400 MHz,  $\text{CDCl}_3$ )  $\delta$ : 7.29-7.25 (m, 10 H), 7.14-7.02 (m, 22 H), 3.88 (s, 3 H), 2.59 (s, 6 H), 1.41 (s, 6 H);  $^{13}\text{C}$  NMR (100 MHz,  $\text{CDCl}_3$ )  $\delta$ : 160.18, 154.14, 147.66, 146.68, 141.84, 139.03, 133.29, 131.75, 130.89, 129.30, 127.60, 127.46, 124.55, 123.01, 114.64, 55.37, 13.53, 13.14; MALDI-TOF/TOF:  $\text{M}^+$  ( $\text{C}_{56}\text{H}_{47}\text{BF}_2\text{N}_4\text{O}$ ) calcd  $m/z$  = 840.3811, found  $m/z$  = 840.3557.

**Compound 2:** Following the procedure for 1, using **B2** (202 mg, 0.3 mmol), compound **2** (205 mg, yield 75%) was synthesized.  $^1\text{H}$  NMR (400 MHz,  $\text{CDCl}_3$ )  $\delta$ : 7.29-7.22 (m, 10 H), 7.14-7.01(m, 22 H), 4.01 (t,  $J = 6.53$  Hz, 2 H), 2.58 (s, 6 H), 1.83 (m 2 H), 1.50 (m, 2 H), 1.41 (s, 6 H), 1.37 (m, 4 H), 0.93 (t,  $J = 6.78$  Hz, 3 H);  $^{13}\text{C}$  NMR (100 MHz,  $\text{CDCl}_3$ )  $\delta$ : 159.77, 154.07, 147.67, 146.67, 141.99, 139.05, 133.25, 131.77, 130.88, 129.28, 127.50, 127.38, 124.53, 123.04, 115.21, 68.23, 31.63, 29.21, 25.73, 22.60, 14.04, 13.50, 13.13; MALDI-TOF/TOF:  $\text{M}^+$  ( $\text{C}_{61}\text{H}_{57}\text{BF}_2\text{N}_4\text{O}$ ) calcd  $m/z = 910.4593$ , found  $m/z = 910.4306$ .

**Compound 3:** Following the procedure for 1, using **B3** (211 mg, 0.3 mmol), compound **3** (220 mg, yield 80%) was synthesized.  $^1\text{H}$  NMR (500 MHz,  $\text{CDCl}_3$ )  $\delta$ : 7.28-7.23 (m, 10H), 7.14-7.02 (m, 22 H), 3.91 (d,  $J = 5.19$ , 2 H), 2.59 (s, 6 H), 1.77 (m, 1 H), 1.48 (m, 4 H), 1.42 (s, 6 H), 1.35 (m, 4 H), 0.96 (m, 6 H);  $^{13}\text{C}$  NMR (125 MHz,  $\text{CDCl}_3$ )  $\delta$ : 160.03, 154.05, 147.67, 146.66, 142.06, 139.09, 133.23, 131.79, 130.90, 129.31, 127.50, 127.30, 124.54, 123.05, 123.00, 115.29, 70.88, 39.40, 30.55, 29.15, 23.87, 23.07, 14.14, 13.53, 13.19, 11.18; MALDI-TOF/TOF:  $\text{M}^+$  ( $\text{C}_{63}\text{H}_{61}\text{BF}_2\text{N}_4\text{O}$ ) calcd  $m/z = 938.4906$ , found  $m/z = 938.4466$ .

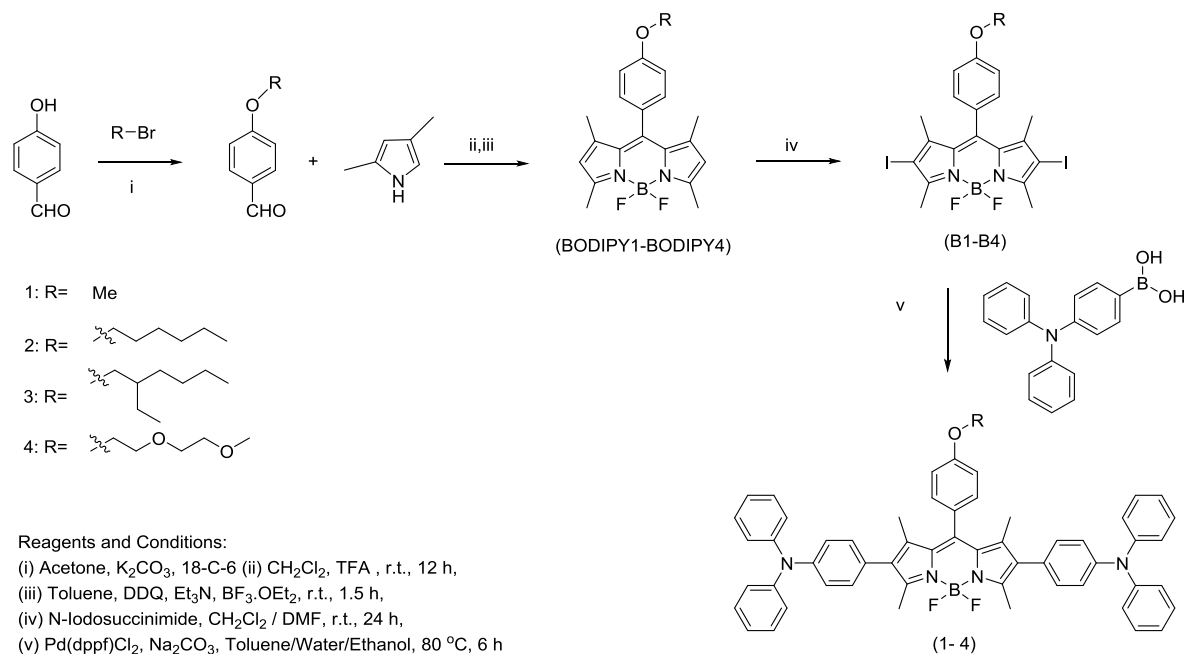
**Compound 4:** Following the procedure for 1, using **B4** (208 mg, 0.3 mmol), compound **4** (210 mg, yield 76%) was synthesized.  $^1\text{H}$  NMR (400 MHz,  $\text{CDCl}_3$ )  $\delta$ : 7.29-7.23 (m, 10 H), 7.14-7.01 (m, 22 H), 4.21 (t,  $J = 4.52$ , 2 H), 3.92 (t,  $J = 4.52$ , 2 H), 3.76 (t,  $J = 4.52$ , 2 H), 3.61 (t,  $J = 4.52$ , 2 H), 3.41 (s, 3 H), 2.58 (s, 6 H), 1.40 (s, 6 H);  $^{13}\text{C}$  NMR (100 MHz,  $\text{CDCl}_3$ )  $\delta$ : 159.40, 154.13, 147.66, 146.68, 141.81, 139.02, 133.29, 131.72, 130.88, 129.30, 127.77, 127.43, 124.55, 123.01, 115.32, 71.96, 70.88, 69.79, 67.51, 59.13, 13.52, 13.13; MALDI-TOF/TOF:  $\text{M}^+$  ( $\text{C}_{60}\text{H}_{55}\text{BF}_2\text{N}_4\text{O}_3$ ) calcd  $m/z = 928.4335$ , found  $m/z = 928.3815$ .

## 2.3 Results and Discussion

### 2.3.1 Synthesis and Thermal Characterization

BODIPY containing CSMs were synthesized by carrying out Suzuki coupling between boronic acid substituted triphenylamine and diiodoBODIPY. The diiodoBODIPY was synthesized from 4-hydroxybenzaldehydes as starting material using established protocols.<sup>50,51</sup> Acid catalysed condensation of 2,4-dimethylpyrrole and corresponding alkoxybenzaldehydes gave dipyrromethanes as shown in scheme 2.1, which upon oxidation using DDQ, generated dipyrromethene or dipyrrens. Complexation of dipyrrens with boron trifluoride etherate ( $\text{BF}_3 \cdot \text{OEt}_2$ ) in the presence of a base, such as a tertiary Amine, afforded

the desired BODIPY dyes.<sup>52–57</sup> Iodination of the BODIPY core at the 2- and 6-position using N-iodosuccinimide resulted in 2,6-diiodo BODIPY. Pd(dppf)Cl<sub>2</sub> was used as a catalyst, and Na<sub>2</sub>CO<sub>3</sub> as a base in the Suzuki coupling reaction. These reactions were carried out under an inert atmosphere.



**Scheme 2.1** Synthetic route to CSMs (1 – 4).

These molecules were characterized by <sup>1</sup>H, <sup>13</sup>C NMR spectroscopy and MALDI-TOF analysis (Appendix I).

The thermal characteristics of the CSMs were studied by thermogravimetric analysis (TGA) and differential scanning calorimetry (DSC). These CSMs are thermally stable upto 200 °C without significant weight loss (Table 2.1), and hence can be thermally annealed without degradation (Figure 2.1a). The DSC data were obtained from the second heating

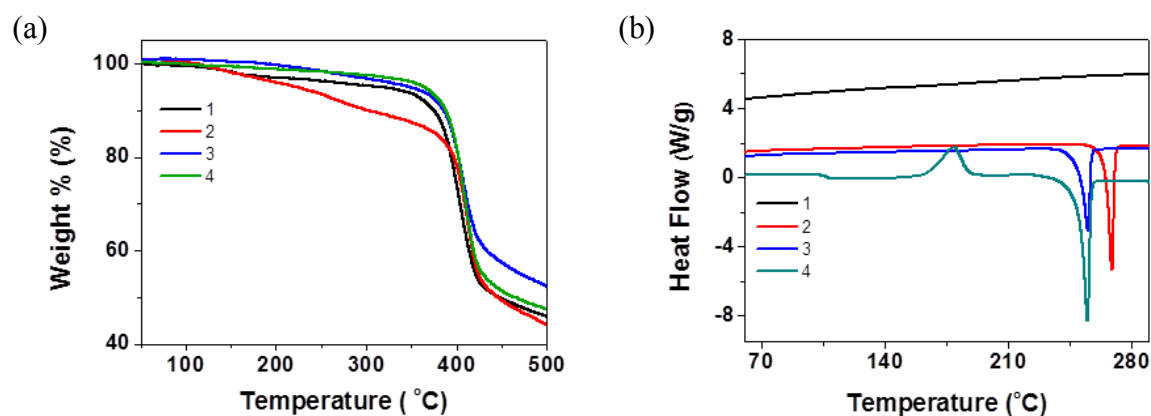


**Figure 2.1** TGA curves (a) and DSC plots (b) of CSMs (1 – 4).

cycle (Figure 2.1b). For **1**, the DSC curve was featureless. The  $T_g$  of **2** and **3** was found to be 93°C and 92°C respectively, which increased to 103 °C for **4**. Transition for crystallization was not observed for **2** and **3**. But, a well defined peak at 174 °C was observed for **4**. The increased  $T_g$  and well defined  $T_c$  observed for **4** is an indication of favourable interaction.

### 2.3.2 Optical and Electrochemical Properties

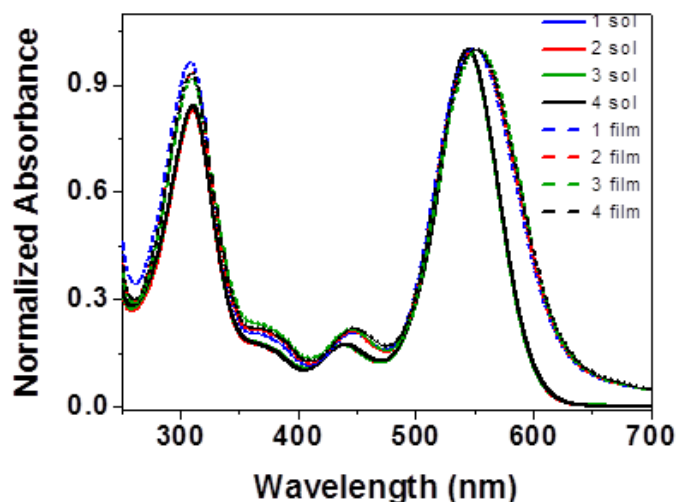


**Figure 2.2** UV-vis absorption spectra of of CSMs (**1** – **4**) in dilute chloroform solution and as thin-film on quartz substrates.

The UV-vis absorption spectra of the CSMs were recorded in chloroform as solvent and as thin films (Figure 2.2). The absorption spectra exhibit two clear peaks, a high energy peak at 310 nm and low energy peak at 545 nm. The 310 nm and 545 nm peaks arise from the triphenylamine moieties and BODIPY, respectively.<sup>58</sup> All the CSMs show identical absorption profiles indicating that the side chain has no effect on the energy levels. The energy bandgap was calculated from the onset of the low energy peak and was found to be 2 eV (Table 2.1).

Cyclic voltammetry of CSMs were recorded using CSMs coated Pt wire as working electrode, Ag/Ag<sup>+</sup> as reference electrode and Pt foil as counter electrode. The cyclic voltammograms were recorded by sweeping the working electrode potential in the anodic and cathodic segments in 0.1 M tetrabutylammonium hexafluorophosphate in dry acetonitrile (Figure 2.3). In the anodic scan, oxidation of the CSMs starts around 0.4 V vs Ag/Ag<sup>+</sup> and in the reverse scan corresponding reduction peak was observed. The  $\Delta E_p$  was found to be higher than 59 mV indicating the redox process is quasi reversible. In the cathodic sweep, the



reduction peak was observed around -1.3 V and corresponding oxidation peak was observed in the reverse scan. This redox process is also quasi reversible. The band edges with respect to vacuum level were determined by calibrating the oxidation and reduction of CSMs using ferrocene as an internal standard.<sup>59</sup> The Orbital energy level values are provided in table 2.1 The HOMO energy level of all the CSMs is around -5.2 eV, which is very close to the energy level of oxygen.<sup>60-61</sup> Cyclic voltammograms of **2**, **3**, and **4** are given in Appendix I.

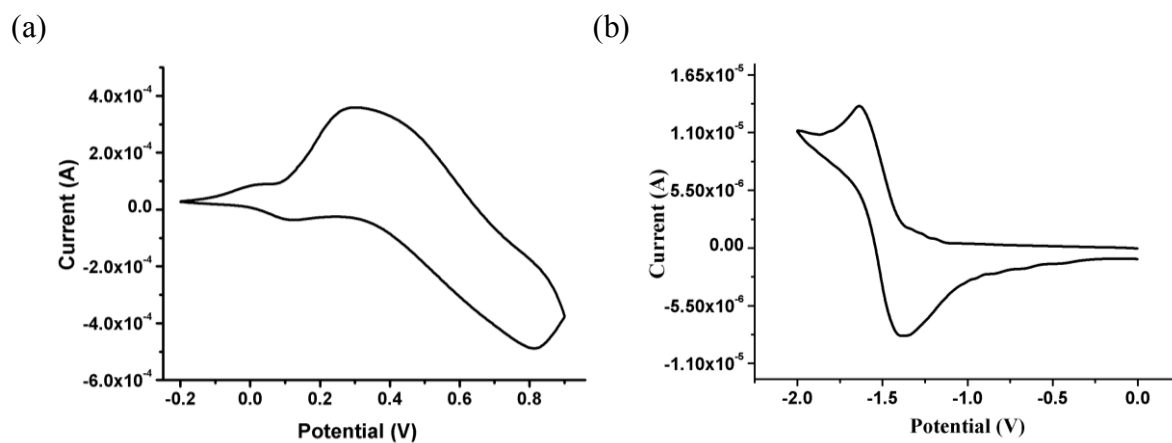


**Figure 2.3** Cyclic voltammograms of molecule **1**: (a) oxidation scan, (b) reduction scan.

### 2.3.3 Electronic Structure Calculations from Density Functional Theory (DFT)

Theoretical calculations using Density functional theory (DFT) with B3LYP functional and 6-31g\*\* basis set were carried out to understand the distribution of wave function in the CSMs.<sup>62</sup> The surface plots are shown in figure 2.4. The surface plots indicate that the HOMO wave function is distributed over the whole conjugated backbone. On the other hand, the LUMO wave function is localized on the BODIPY core. These calculations predict that these CSMs could be possible hole transporting materials.

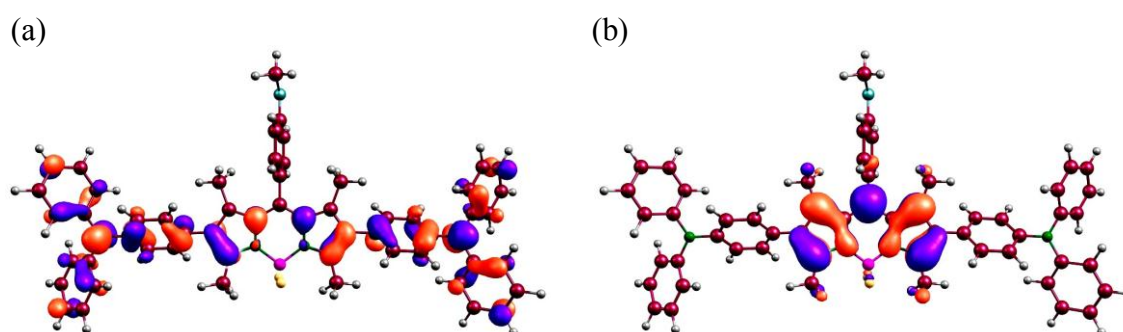


**Figure 2.4** Surface plots of **1**, HOMO (a) and LUMO (b).

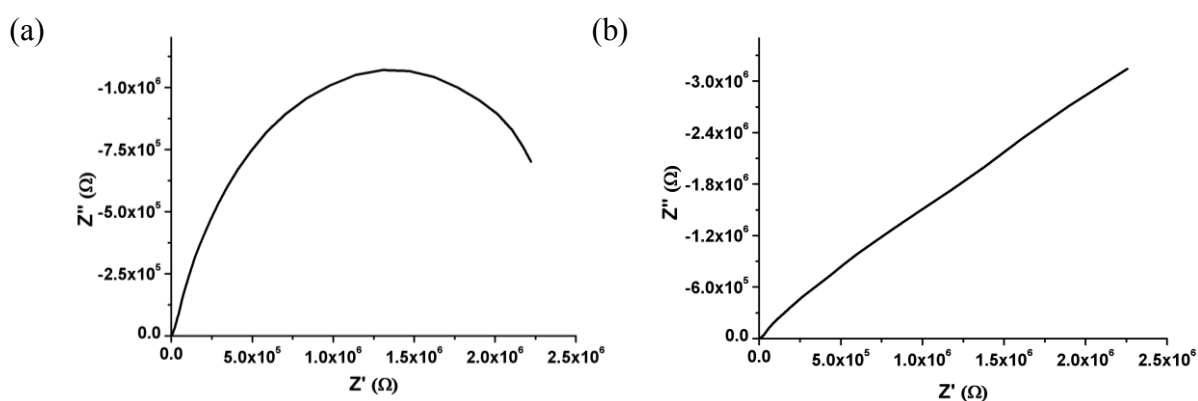
**Table 2.1:** Electrochemical, optical and thermal data for **1** – **4**.

CSM	$E^{\text{ox, onset}}$ (V)	$E^{\text{red, onset}}$ (V)	HOMO <sup>e</sup> (eV)	LUMO <sup>e</sup> (eV)	$E_g^e$ (eV)	$E_g^{\text{opt}}$ (eV)	$T_g$ (°C)	$T_c$ (°C)	$T_m$ (°C)
<b>1</b>	0.38	-1.38	-5.18	-3.42	1.76	2.07	-	-	-
<b>2</b>	0.41	-1.32	-5.21	-3.48	1.73	2.07	93	-	268
<b>3</b>	0.40	-1.34	-5.20	-3.46	1.74	2.07	92	-	254
<b>4</b>	0.39	-1.32	-5.19	-3.48	1.71	2.07	103	174	254

(e = electrochemical, opt = optical)

### 2.3.4 Impedance Spectroscopy

These CSMs has a permanent dipole, which is unique compared to other conjugated molecules, hence, their electrical characteristics were studied using AC impedance spectroscopy. These experiments were done in a conventional three electrode cell by applying potential amplitude of 5 mV and frequency range of 0.01 Hz and 100 kHz.<sup>63,64</sup> Measurements were done at 0 V and 0.6 V. In the low frequency regime, the nyquist plot is a semicircle (0 V) without linear line (Figure 2.5a), which corresponds to an equivalent circuit comprising a resistor and double layer capacitor connected in parallel. The resistance and capacitance arise from the CSMs and its interface with electrolyte and electrode. This parallel circuit is connected in series with another resistor which originates from all external resistances.<sup>65</sup> Such a nyquist plot is observed for conjugated polymers in absence of

**Figure 2.5** Impedance spectra of **4** at 0 V (a) and 0.6 V (b).

electrolyte.<sup>66</sup> When the nyquist plots were recorded at an applied potential of +0.6 V, only linear line was observed, indicating pure capacitive behaviour (Figure 2.5b). It should be noted that the conjugated polymers exhibit semicircle and linear line in presence of electrolyte.<sup>67–70</sup> Due to their response to alternating current (AC), these CSMs with the presence of dipole are likely to be suitable candidates for thin film transistors that respond to frequency.<sup>71</sup> Impedance spectra of **1**, **2**, and **3** are given in appendix I.

### 2.3.5 Crystallinity and Thin Film Morphology

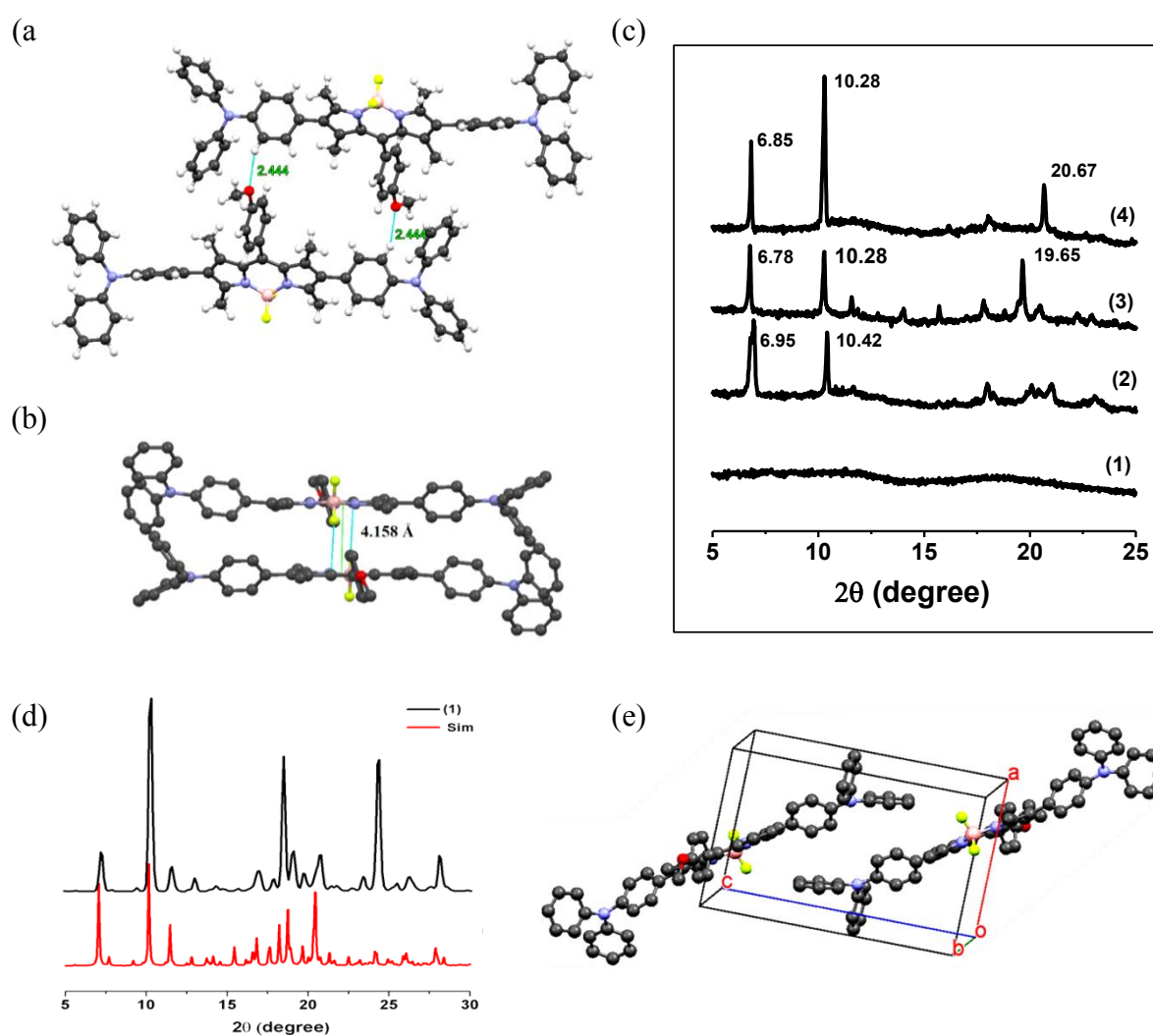


**Figure 2.6** The crystal structure showing the slip stack of **1** (a) and the inter planar distance (b). Powder XRD pattern of **1-4** (c), Comparison of the experimental PXRD pattern of recrystallized **1** with the simulated XRD patterns based on its single crystal structural data (d), and (e) Unit cell for **1**, The C, O, N, F and B atoms are shown in grey, red, cyan, yellow and pink, respectively. Hydrogen atoms are omitted for clarity.

Single crystal of **1** was grown to understand the packing pattern<sup>72–74</sup> and **1** was found to crystallize in triclinic crystal system with P-1 space group. The phenyl ring connecting the

side chain with BODIPY core is perpendicular to the plan of conjugated backbone. Similarly, the phenyl ring of the triphenylamine is twisted at an angle of  $51.1^\circ$  with respect to the plane of BODIPY. During the stacking process, the molecules slip to accommodate the twisted phenyl rings (Figure 2.6a). To calculate the interplanar distance, the least square plan was drawn connecting 26 atoms. The distance between the two backbones is found to be  $4.15 \text{ \AA}$  (Figure 2.6b). Single crystals of other molecules could not be grown large enough to be mounted on the single crystal XRD instrument. To understand solid state packing in the thin film form, thin film XRD of all the samples were recorded (Figure 2.6c). Film XRD pattern of **1** didn't show any peak indicating phase transition while preparing films. Contrary to this, sharp peaks were observed for **2**, **3**, and **4**. From the d spacing calculated for **1** and the similar structure of **2**, **3** and **4** we can assume that the interplanar spacing will be around  $4 \text{ \AA}$  for the CSMs. For **3** and **4**, sharp peaks were observed at a  $2\theta$  of  $19.6$  and  $20.6$ , which corresponds to a d spacing of  $4.51$  and  $4.30 \text{ \AA}$ , respectively. The interplanar spacing for **4** is closer to what obtained from single crystal data for **1**. Thus, the OEG side chain facilitates better interaction between CSMs than alkyl chains.

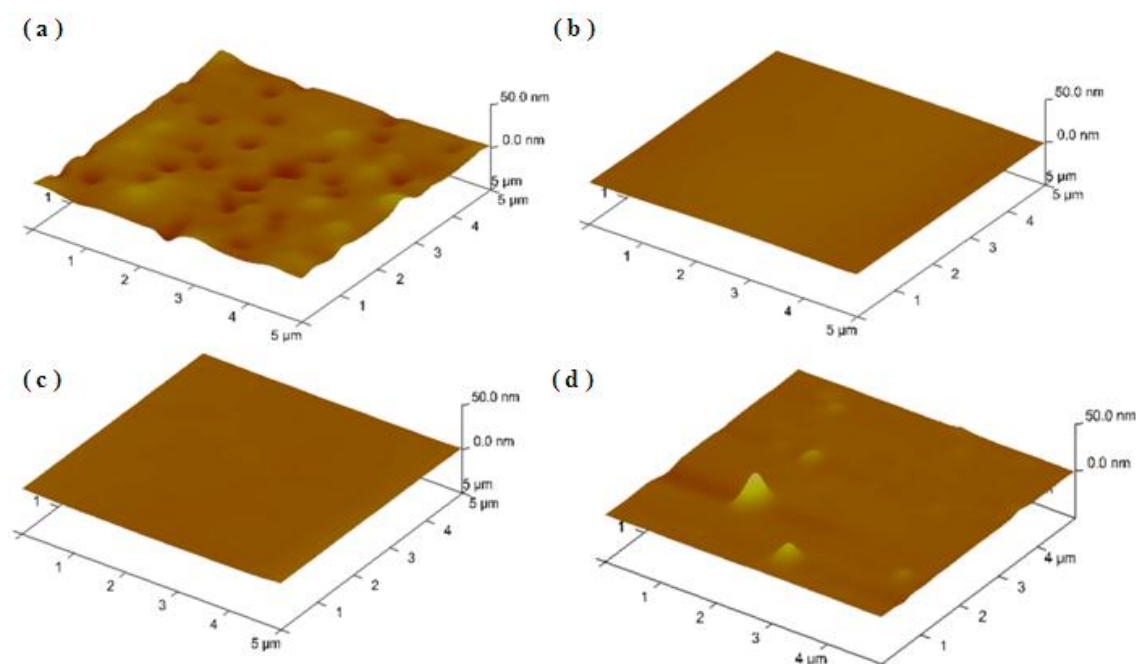


**Figure 2.7** AFM images of thin films of **1** (a), **3** (b) and **4** (c) on unmodified and **4** (d) on HMDS modified  $\text{SiO}_2$  substrate (d).

CSMs coated on plasma treated hydrophilic  $\text{SiO}_2$  surface and hexamethyldisilazane (HMDS) treated hydrophobic  $\text{SiO}_2$  surface were used for this study. These substrates were used for morphological studies because same substrates were used for the fabrication of field

effect transistors (FETs). For **1**, the films prepared on both modified and unmodified SiO<sub>2</sub> have troughs and crests indicating a rough surface (Figure 2.7a). For **2** and **3**, the films were uniform, indicating the formation of a very smooth film (Figure 2.7b). We observed different morphological features for **4**. Thin film of **4** was found to be very smooth on unmodified substrate (Figure 2.7c). Contrary to this, the morphology of **4** prepared on HMDS modified surface was rough, which is due to the incompatibility between hydrophilic OEG substituted BODIPY (**4**) and hydrophobic HMDS modified substrate (Figure 2.7d).

Because of variation in lipophilic nature of side chains, Water drop contact angle (CA) was also used to understand the surface wettability of the films. The CA was found to be 79°, 82° and 86° for **1**, **2** and **3**, respectively (Figure 2.8a, b, c). On the other hand, the CA for **4** was significantly lower (49°) (Figure 2.8d) because of the presence of hydrophilic OEG side chain. The same measurements were repeated with HMDS modified substrates. In this case, the CA for **1**, **2** and **3** was found to be 106°, 103° and 109°, respectively (Figure 2.8e, f, and g). The close CA values of these films are due to similar morphology and the surface functionalities. Here, the CA for **4** increased from 49° to 100° (Figure 2.8h). This difference is due to the change in morphology from smooth film to rough surface while modifying the base substrate from hydrophilic to hydrophobic.<sup>75-76</sup>

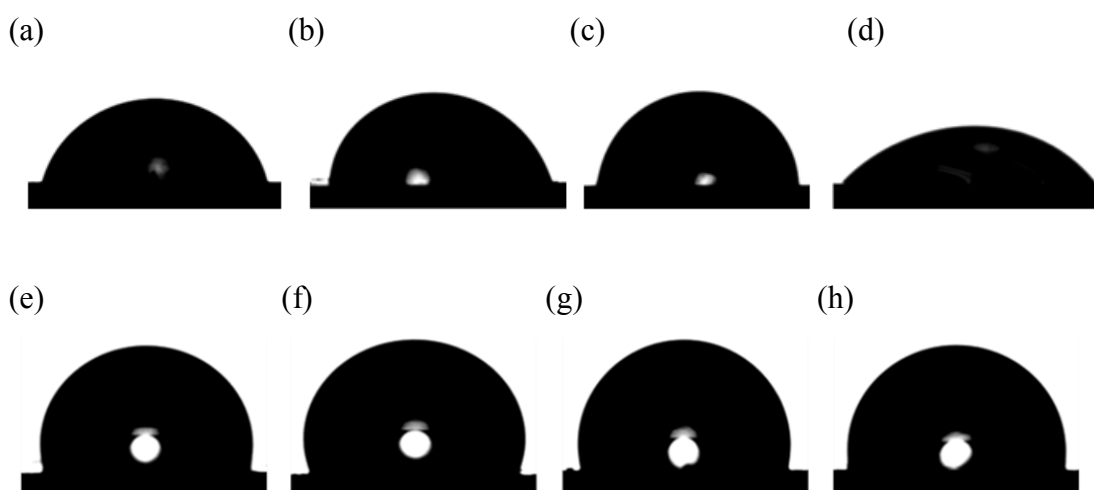


**Figure 2.8** Water drop contact angle (CA) of **1** (a), **2** (b), **3** (c) and **4** (d) coated on unmodified SiO<sub>2</sub> surface. CA of **1** (e), **2** (f), **3** (g) and **4** (h) coated on HMDS modified SiO<sub>2</sub> surface.

### 2.3.6 Characterization of Organic Field Effect Transistor Devices

Field effect transistors were fabricated using SiO<sub>2</sub> as gate dielectric, heavily n doped Si as gate and gold as source and drain electrodes. The prefabricated substrates have bottom gate,

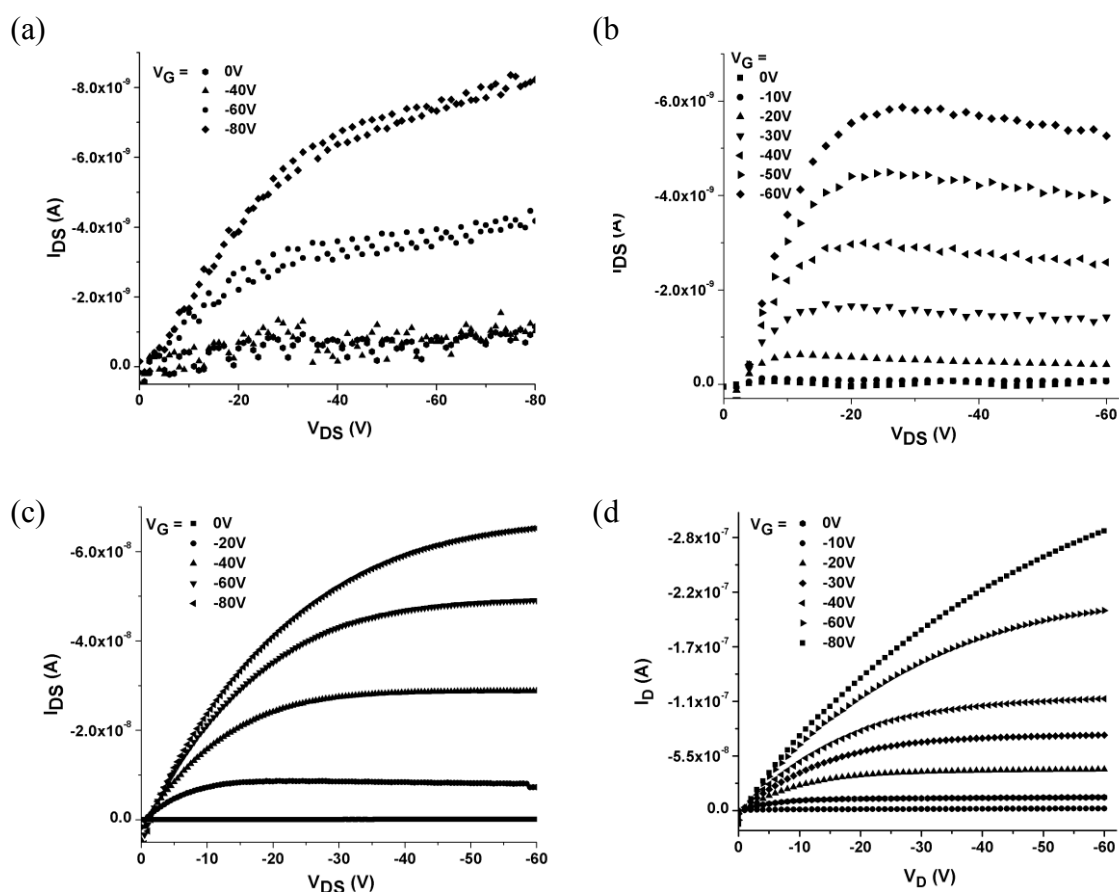


**Figure 2.9** Output characteristic curves of **1**(a), **2** (b), **3** (c), and **4** (d) on unmodified FET substrate.

bottom contact configuration. Two types of devices were fabricated (i) without silane (HMDS) modification and (ii) with silane modification. Conventionally, enhancement in hole carrier mobility has been attributed to hydrophobic silanes.<sup>77</sup> In our studies, The CSMs were spin coated on top of the substrates from chloroform solutions. The device fabrication and measurements were carried out inside argon filled glove box. Output characteristic curves were recorded while sweeping the drain voltage ( $V_D$ ) between 0 and -60V and applying a constant gate voltage ( $V_G$ ). The output characteristic curves showed standard linear and saturation regimes with a good gate modulation as a function of applied gate voltage ( $V_G$ ). The linear regime for **1**, **2** and **3** didn't start at 0V, which is likely due to contact resistance (Figure 2.9a, b, and c). Contrary to this, the linear regime for **4** started at 0 V (Figure 2.9d). Device data are given in table 2.2. The hole carrier mobility ( $\mu$ ) calculated for **4** was found to be two order higher than other CSMs. Also, the threshold voltage is -0.27 V for **4** (Figure 2.10d), which is at least an order lower than the other CSMs. All these indicate that the OEG side chain facilitates interaction with the dielectric surface and between the molecules. In the HMDS modified devices, the charge carrier mobility increased by two to nine times for **1**, **2**

and **3** (Figure 2.11) due to the favorable interaction between molecules and the surface. Contrary to this, the hole mobility is almost unaffected in the case of **4**, but the threshold voltage increased by more than an order (-8.3 V) (Figure 2.11h). And that is because of incompatibility of the hydrophobic gate dielectric surface with the hydrophilic **4**.

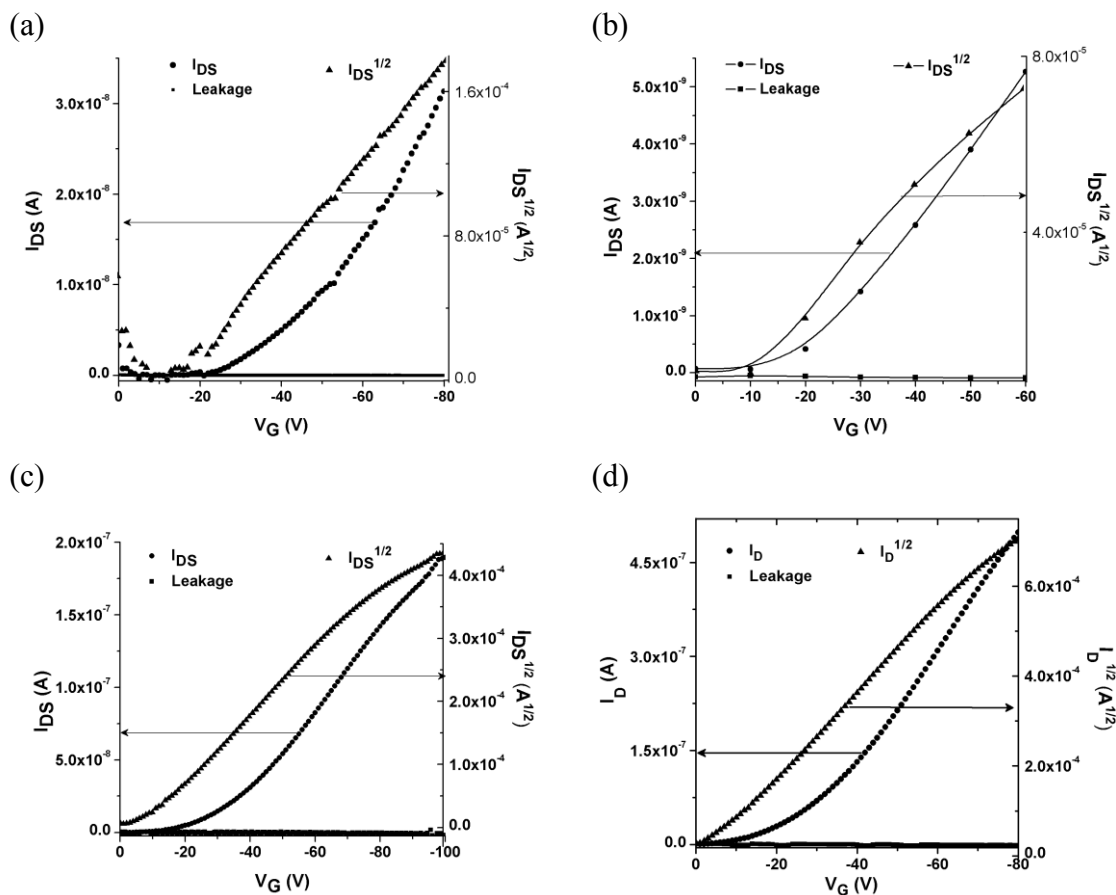


**Figure 2.10** Transfer characteristic curve of **1**(a), **2** (b), **3** (c), and **4** (d) on unmodified FET substrate.

**Table 2.2:** OFET device metrics of CSMs **1 – 4**

(a – Unmodified SiO<sub>2</sub> substrate, b – HMDS modified SiO<sub>2</sub> substrates)

CSMs	$\mu$ (cm <sup>2</sup> /Vs) <sup>a</sup>	$V_T$ (V) <sup>a</sup>	$I_{on/off}$ <sup>a</sup>	$g_m$ (nS) <sup>a</sup>	$\mu$ (cm <sup>2</sup> /Vs) <sup>b</sup>	$V_T$ (V) <sup>b</sup>	$I_{on/off}$ <sup>b</sup>	$g_m$ (nS) <sup>b</sup>
<b>1</b>	$6.80 \times 10^{-07}$	-19	$0.59 \times 10^3$	0.55	$8.16 \times 10^{-06}$	-20.3	$0.36 \times 10^3$	12.8
<b>2</b>	$3.50 \times 10^{-07}$	-6.2	$0.13 \times 10^3$	0.26	$8.57 \times 10^{-06}$	-16.3	$0.48 \times 10^3$	14
<b>3</b>	$2.91 \times 10^{-06}$	-5.5	$0.47 \times 10^3$	5.2	$8.70 \times 10^{-06}$	-19.6	$0.28 \times 10^3$	16
<b>4</b>	$1.88 \times 10^{-05}$	-0.27	$0.59 \times 10^3$	37.3	$1.41 \times 10^{-05}$	-8.33	$0.66 \times 10^3$	26.1

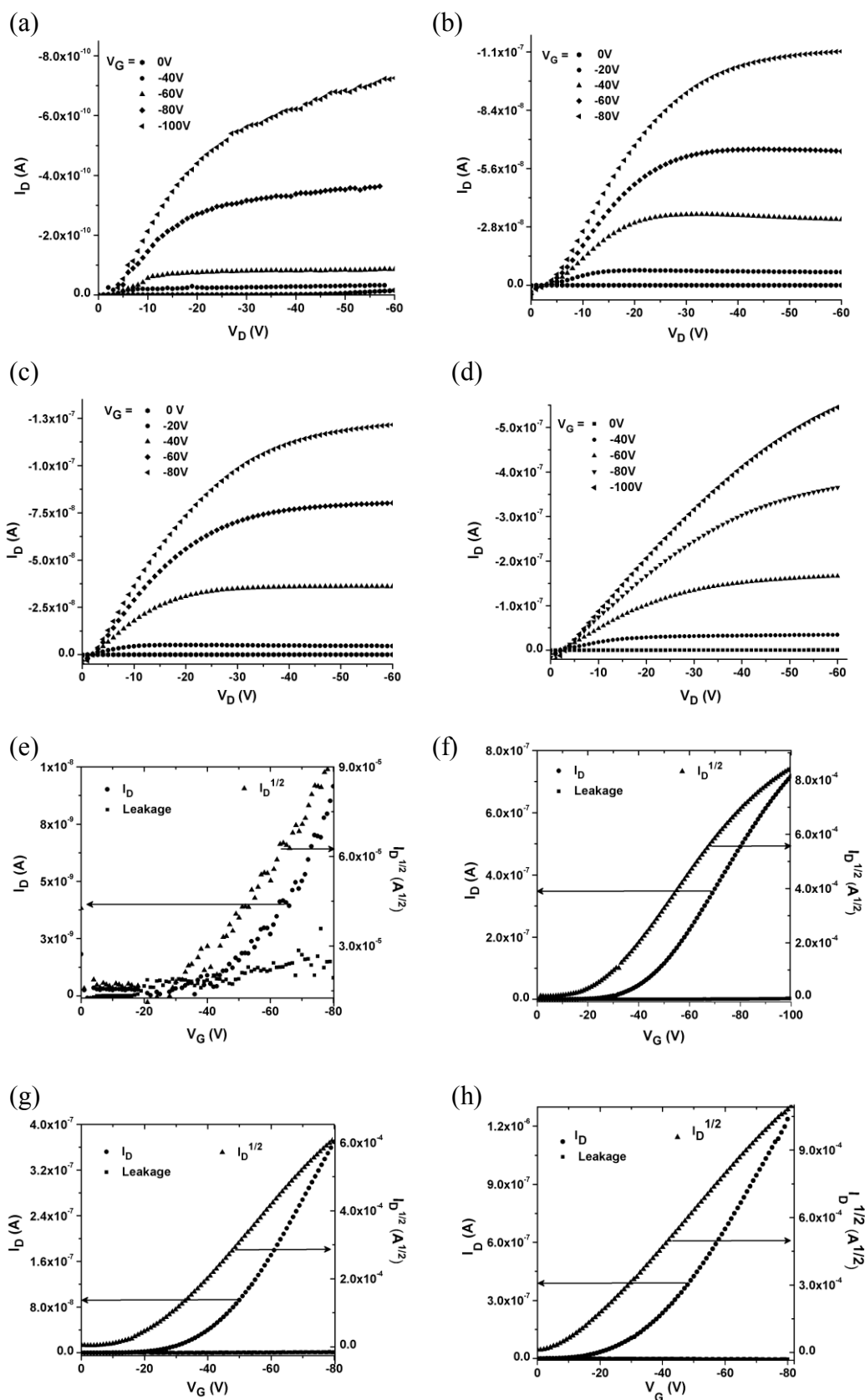


**Figure 2.11** Output characteristic curves of **1**(a), **2** (b), **3** (c), and **4** (d) on HMDS modified FET substrate. Transfer characteristic curve of **1**(e), **2** (f), **3** (g), and **4** (h) on HMDS modified FET substrate.



## 2.4 Summary

In summary, a systematic study was carried out to understand the impact of nature of side chain on the charge transport. Side chain is varied from linear and branched alkyl chain to the OEG side chain. Side chains were substituted on CSMs containing triphenylamine as donor and BODIPY as acceptor. The propeller type triphenylamine enhances the solubility of the CSMs in organic solvents. CSM with OEG side chain was found to be soluble in common organic solvents. The OEG comprising CSM exhibit high glass transition temperature and forms smooth films while processed from organic solvents. Also, it facilitates better intermolecular contact which leads to OFETs with superior device efficiencies. The threshold voltage was as small as -0.27 V and the hole carrier mobility was  $1.8 \times 10^{-5} \text{ cm}^2/\text{Vs}$ , which is comparable to regioregular polythiophene substituted with OEG side chain ( $3.5 \times 10^{-5} \text{ cm}^2/\text{Vs}$ ).<sup>23</sup> This study demonstrates that OEG side chains substituted CSMs are better than its alkyl chain analogs.

## 2.5 References

- 1) Cheng, Y.-J.; Yang, S.-H.; Hsu, C.-S. *Chem. Rev.* **2009**, *109*, 5868.
- 2) Lei, T.; Wang, J.-Y.; Pei, J. *Chem. Mater.* **2014**, *26*, 594.
- 3) Mei, J.; Bao, Z. *Chem. Mater.* **2014**, *26*, 604.
- 4) Facchetti, A. *Chem. Mater.* **2011**, *23*, 733.
- 5) Cabanetos, C.; El Labban, A.; Bartelt, J. A.; Douglas, J. D.; Mateker, W. R.; Fréchet, J. M. J.; McGehee, M. D.; Beaujuge, P. M. *J. Am. Chem. Soc.* **2013**, *135*, 4656.
- 6) Piliago, C.; Holcombe, T. W.; Douglas, J. D.; Woo, C. H.; Beaujuge, P. M.; Fréchet, J. M. J. *J. Am. Chem. Soc.* **2010**, *132*, 7595.
- 7) Zoombelt, A. P.; Leenen, M. A. M.; Fonrodona, M.; Nicolas, Y.; Wienk, M. M.; Janssen, R. A. J. *Polymer* **2009**, *50*, 4564.
- 8) Hsu, W. P.; Levon, K.; Ho, K. S.; Myerson, A. S.; Kwei, T. K. *Macromolecules* **1993**, *26*, 1318.
- 9) Keg, P.; Lohani, A.; Fichou, D.; Lam, Y. M.; Wu, Y.; Ong, B. S.; Mhaisalkar, S. G. *Macromol. Rapid Commun.* **2008**, *29*, 1197.
- 10) Beaujuge, P. M.; Fréchet, J. M. J. *J. Am. Chem. Soc.* **2011**, *133*, 20009.
- 11) Bronstein, H.; Leem, D. S.; Hamilton, R.; Woebkenberg, P.; King, S.; Zhang, W.; Ashraf, R. S.; Heeney, M.; Anthopoulos, T. D.; de Mello, J.; McCulloch, I. *Macromolecules* **2011**, *44*, 6649.

- 12) Osaka, I.; Zhang, R.; Sauv e, G.; Smilgies, D.-M.; Kowalewski, T.; McCullough, R. D. *J. Am. Chem. Soc.* **2009**, *131*, 2521.
- 13) Lei, T.; Dou, J.-H.; Pei, J. *Adv. Mater.* **2012**, *24*, 6457.
- 14) Meager, I.; Ashraf, R. S.; Mollinger, S.; Schroeder, B. C.; Bronstein, H.; Beatrup, D.; Vezie, M. S.; Kirchartz, T.; Salleo, A.; Nelson, J.; McCulloch, I. *J. Am. Chem. Soc.* **2013**, *135*, 11537.
- 15) Zhang, F.; Hu, Y.; Schuettfort, T.; Di, C.-a.; Gao, X.; McNeill, C. R.; Thomsen, L.; Mannsfeld, S. C. B.; Yuan, W.; Sirringhaus, H.; Zhu, D. *J. Am. Chem. Soc.* **2013**, *135*, 2338.
- 16) Mei, J.; Kim, D. H.; Ayzner, A. L.; Toney, M. F.; Bao, Z. *J. Am. Chem. Soc.* **2011**, *133*, 20130.
- 17) Lee, J.; Han, A.-R.; Yu, H.; Shin, T. J.; Yang, C.; Oh, J. H. *J. Am. Chem. Soc.* **2013**, *135*, 9540.
- 18) Lee, J.; Han, A.-R.; Kim, J.; Kim, Y.; Oh, J. H.; Yang, C. *J. Am. Chem. Soc.* **2012**, *134*, 20713.
- 19) Roncali, J.; Garreau, R.; Delabouglise, D.; Garnier, F.; Lemaire, M. *J. Chem. Soc., Chem. Commun.* **1989**, *0*, 679.
- 20) Roncali, J.; Shi, L. H.; Garnier, F. *J. Phys. Chem.* **1991**, *95*, 8983.
- 21) Holzer, L.; Winkler, B.; Wenzl, F. P.; Tasch, S.; Dai, L.; Mau, A. W. H.; Leising, G. *Synth. Met.* **1999**, *100*, 71.
- 22) Huang, F.; Zhang, Y.; Liu, M. S.; Jen, A. K.-Y. *Adv. Funct. Mater.* **2009**, *19*, 2457.
- 23) Shao, M.; He, Y.; Hong, K.; Rouleau, C. M.; Geohegan, D. B.; Xiao, K. *Polym. Chem.* **2013**, *4*, 5270.
- 24) Yin, J.; Zhou, Y.; Lei, T.; Pei, J. *Angew. Chem., Int. Ed.* **2011**, *50*, 6320.
- 25) Mei, J.; Graham, K. R.; Stalder, R.; Tiwari, S. P.; Cheun, H.; Shim, J.; Yoshio, M.; Nuckolls, C.; Kippelen, B.; Castellano, R. K.; Reynolds, J. R. *Chem. Mater.* **2011**, *23*, 2285.
- 26) Naik, M. A.; Venkatramaiah, N.; Kanimozhi, C.; Patil, S. *J. Phys. Chem. C* **2012**, *116*, 26128.
- 27) Bj rnholm, T.; Greve, D. R.; Reitzel, N.; Hassenkam, T.; Kjaer, K.; Howes, P. B.; Larsen, N. B.; B gelund, J.; Jayaraman, M.; Ewbank, P. C.; McCullough, R. D. *J. Am. Chem. Soc.* **1998**, *120*, 7643.

- 28) Kanimozhi, C.; Yaacobi-Gross, N.; Chou, K. W.; Amassian, A.; Anthopoulos, T. D.; Patil, S. *J. Am. Chem. Soc.* **2012**, *134*, 16532.
- 29) Roncali, J. *Acc. Chem. Res.* **2009**, *42*, 1719.
- 30) Walker, B.; Kim, C.; Nguyen, T.-Q. *Chem. Mater.* **2011**, *23*, 470.
- 31) Sun, Y.; Welch, G. C.; Leong, W. L.; Takacs, C. J.; Bazan, G. C.; Heeger, A. J. *Nat. Mater.* **2012**, *11*, 44.
- 32) Zhou, J.; Wan, X.; Liu, Y.; Zuo, Y.; Li, Z.; He, G.; Long, G.; Ni, W.; Li, C.; Su, X.; Chen, Y. *J. Am. Chem. Soc.* **2012**, *134*, 16345.
- 33) Lee, O. P.; Yiu, A. T.; Beaujuge, P. M.; Woo, C. H.; Holcombe, T. W.; Millstone, J. E.; Douglas, J. D.; Chen, M. S.; Fréchet, J. M. J. *Adv. Mater.* **2011**, *23*, 5359.
- 34) Wunsch, B. H.; Rumi, M.; Tummala, N. R.; Risko, C.; Kang, D.-Y.; Steirer, K. X.; Gantz, J.; Said, M.; Armstrong, N. R.; Brédas, J.-L.; Bucknall, D.; Marder, S. R. *J. Mater. Chem. C*, **2013**, *1*, 5250.
- 35) Dharmapurikar, S. S.; Arulkashmir, A.; Das, C.; Muddellu, P.; Krishnamoorthy, K. *ACS Appl. Mater. Interfaces*, **2013**, *5*, 7086.
- 36) Mei, J.; Graham, K. R.; Stalder, R.; Reynolds, J. R. *Org. Lett.* **2010**, *12*, 660.
- 37) Wang, E.; Ma, Z.; Zhang, Z.; Vandewal, K.; Henriksson, P.; Inganäs, O.; Zhang, F.; Andersson, M. R. *J. Am. Chem. Soc.* **2011**, *133*, 14244.
- 38) Usta, H.; Yilmaz, M. D.; Avestro, A.-J.; Boudinet, D.; Denti, M.; Zhao, W.; Stoddart, J. F.; Facchetti, A. *Adv. Mater.* **2013**, *25*, 4327.
- 39) Popere, B. C.; Della Pelle, A. M.; Thayumanavan, S. *Macromolecules* **2011**, *44*, 4767.
- 40) Bura, T.; Leclerc, N.; Fall, S.; Lévêque, P.; Heiser, T.; Retailleau, P.; Rihn, S.; Mirloup, A.; Ziessel, R. *J. Am. Chem. Soc.* **2012**, *134*, 17404.
- 41) Loudet, A.; Burgess, K. *Chem. Rev.* **2007**, *107*, 4891.
- 42) Ulrich, G.; Ziessel, R.; Harriman, A. *Angew. Chem., Int. Ed.* **2008**, *47*, 1184.
- 43) Boens, N.; Leen, V.; Dehaen, W. *Chem. Soc. Rev.* **2012**, *41*, 1130.
- 44) Rousseau, T.; Cravino, A.; Bura, T.; Ulrich, G.; Ziessel, R.; Roncali, J. *Chem. Commun.* **2009**, 1673.
- 45) Rousseau, T.; Cravino, A.; Ripaud, E.; Leriche, P.; Rihn, S.; De Nicola, A.; Ziessel, R.; Roncali, J. *Chem. Commun.* **2010**, *46*, 5082.
- 46) Kim, B.; Ma, B.; Donuru, V. R.; Liu, H.; Fréchet, J. M. J. *Chem. Commun.* **2010**, *46*, 4148.

- 47) Lin, H.-Y.; Huang, W.-C.; Chen, Y.-C.; Chou, H.-H.; Hsu, C.-Y.; Lin, J. T.; Lin, H.-W. *Chem. Commun.* **2012**, 48, 8913.
- 48) Shrestha, M.; Si, L. P.; Chang, C.-W.; He, H. S.; Sykes, A.; Lin, C.-Y.; Diao, E. W.-G. *J. Phys. Chem. C* **2012**, 116, 10451.
- 49) Cortizo-Lacalle, D.; Howells, C. T.; Gambino, S.; Vilela, F.; Vobecka, Z.; Findlay, N. J.; Inigo, A. R.; Thomson, S. A. J.; Skabara, P. J.; Samuel, I. D. W. *J. Mater. Chem.* **2012**, 22, 14119.
- 50) Zhu, S.; Dorh, N.; Zhang, J.; Vegesna, G.; Li, H.; Luo, F. -T.; Tiwari, A.; Liu, H. *J. Mater. Chem.*, **2012**, 22, 2781.
- 51) Meng, G.; Velayudham, S.; Smith, A.; Luck, R.; Liu, H. *Macromolecules* **2009**, 42, 1995.
- 52) Wood, T. E.; Thompson, A. *Chem. Rev.* **2007**, 107, 1831.
- 53) Vegesna, V. R.; Vegnesa, G. K.; Velayudham, S.; Green, S.; Liu, H. *Chem. Mater.* **2009**, 21, 2130.
- 54) Thivierge, C.; Loudet, A.; Burgess, K. *Macromolecules* **2011**, 44, 4012.
- 55) Cakmak, Y.; Akkaya, E. U. *Org. Lett.* **2009**, 11, 85.
- 56) Hayashi, Y.; Obata, N.; Tamaru, M.; Yamaguchi, S.; Matsuo, Y.; Saeki, A.; Seki, S.; Kureishi, Y.; Saito, S.; Yamaguchi, S.; Shinokubo, H. *Org. Lett.* **2012**, 14, 866.
- 57) Popere, B. C.; Della Pelle, A. M.; Poe, A.; Balaji, G.; Thayumanavan, S. *Chem. Sci.*, **2012**, 3, 3093.
- 58) Zhao, H.; Wang, B.; Liao, J.; Wang, H.; Tan, G. *Tetrahedron Lett.* **2013**, 54, 6019.
- 59) Kumar, A.; Bokria, J. G.; Buyukmumcu, Z.; Dey, T.; Sotzing, G. A. *Macromolecules*, **2008**, 41, 7098.
- 60) Thompson, B. C.; Kim, Y.-G.; Reynolds, J. R. *Macromolecules* **2005**, 38, 5359.
- 61) de Leeuw, D. M.; Simenon, M. M. J.; Brown, A. R.; Einerhand, R. E. F. *Synth. Met.* **1997**, 87, 53.
- 62) Sarkar, S. K.; Thilagar, P. *Chem. Commun.* **2013**, 49, 8558.
- 63) El-Kady, M. F.; Kaner, R. B. *Nat. Commun.*, **2013**, 4, 1-9.
- 64) Pan, L.; Yu, G.; Zhai, D.; Lee, H. R.; Zhao, W.; Liu, N.; Wang, H.; Tee, B. C.-K.; Shi, Y.; Cui, Y.; Bao, Z. *Proc. Natl. Acad. Sci. U. S. A.* **2012**, 109, 9287.
- 65) Munar, A.; Sandström, A.; Tang, S.; Edman, L. *Adv. Funct. Mater.* **2012**, 22, 1511.
- 66) Johnson, B. W.; Read, D. C.; Christensen, P.; Hamnett, A.; Armstrong, R. D. *J. Electroanal. Chem.* **1994**, 364, 103.
- 67) Meier, M.; Karg, S.; Riess, W. *J. Appl. Phys.* **1997**, 82, 1961.

- 68) Stöcker, T.; Köhler, A.; Moos, R. *J. Polym. Sci., Part B: Polym. Phys.* **2012**, *50*, 976.
- 69) Mahale, R. Y.; Arulkashmir, A.; Dutta, K.; Krishnamoorthy, K. *Phys. Chem. Chem. Phys.* **2012**, *14*, 4577.
- 70) Otero, T. F.; De Larreta, E. *J. Electroanal. Chem.* **1988**, *244*, 311.
- 71) Lenski, D. R.; Southard, A.; Fuhrer, M. S. *Appl. Phys. Lett.*, **2009**, *94*, 232103-1.
- 72) Fitzner, R.; Mena-Osteritz, E.; Mishra, A.; Schulz, G.; Reinold, E.; Weil, M.; Körner, C.; Ziehlke, H.; Elschner, C.; Leo, K.; Riede, M.; Pfeiffer, M.; Urich, C.; Bäuerle, P. *J. Am. Chem. Soc.* **2012**, *134*, 11064.
- 73) Cai, Z.; Guo, Y.; Yang, S.; Peng, Q.; Luo, H.; Liu, Z.; Zhang, G.; Liu, Y.; Zhang, D. *Chem. Mater.* **2013**, *25*, 471.
- 74) Balaji, G.; Parameswaran, M.; Jin, T. M.; Vijila, C.; Furong, Z.; Valiyaveetil, S. *J. Phys. Chem. C* **2010**, *114*, 4628.
- 75) Erbil, H. Y.; Demirel, A. L.; Avci, Y.; Mert, O. *Science* **2003**, *299*, 1377.
- 76) Jiang, L.; Zhao, Y.; Zhai, J. *Angew. Chem. Int. Ed.* **2004**, *43*, 4338.
- 77) Wen, Y.; Liu, Y.; Guo, Y.; Yu, G.; Hu, W. *Chem. Rev.* **2011**, *111*, 3358.
- 78) Lottner, C.; Bart, K.-C.; Bernhart, G.; Brunner, H. *J. Med. Chem.*, **2002**, *45*, 2079.

## Chapter 3

# Tuning the Frontier Molecular Orbital Energy Levels of BODIPY based Small Molecules by Side Chain Variation at Meso Position

### 3.1 Introduction

In chapter 1, nature of side chain was varied from hydrophobic to hydrophilic in conjugated small molecules (CSMs), and their impact on physical and electronic properties was studied.<sup>1</sup> Side chains are not only crucial for enabling solution processability in device fabrication, but also assist in solid state packing. Thus, they affect device performance either positive or in a negative manner.<sup>2,3</sup> In general, branched alkyl chains bring better solubility than the linear ones, but there are branching point issue and possibility of stereoisomers formation.<sup>4-6</sup> Conjugated systems with propeller shaped triphenylamine like those we reported in the previous work did not require really long or branched alkyl chains for solubility.<sup>7,8</sup> Also, CSM with hydrophilic Oligoethylene glycol (OEG) side chains was nicely soluble in common organic solvents.<sup>1</sup> Another moiety in the CSMs was BODIPY dye where a variety of substitutions are possible by simple synthetic methods.<sup>9-17</sup> Hence, it can be said that a CSM containing BODIPY core and triphenylamine is an ideal system to study the impact of side chains on the physical and electronic properties.

In the previous work, side chains are substituted on the phenyl ring which is not in the conjugation with the conjugated backbone. In this case, they have no impact on electronic properties and that is evident from the identical absorption profile and electrochemical properties of all four molecules. Though their physical properties like solid state packing and thermal transitions vary as per their nature. CSM with diethylene glycol side chain form smooth and ordered film, and also shows least interplanar spacing among all CSMs. It also showed an increase in mobility than other derivatives.<sup>1</sup> In this work, the impact of side chains on both electronic and physical properties of the conjugated small molecules is studied. The side chain is connected at the meso position of the BODIPY core. Since there is a large molecular orbital coefficient at meso in the lowest unoccupied molecular orbital (LUMO) energy level, nature of side chain can alter Frontier orbital energy levels.<sup>18,22</sup> The electron density at the 8 (meso) position is higher in the LUMO than in the

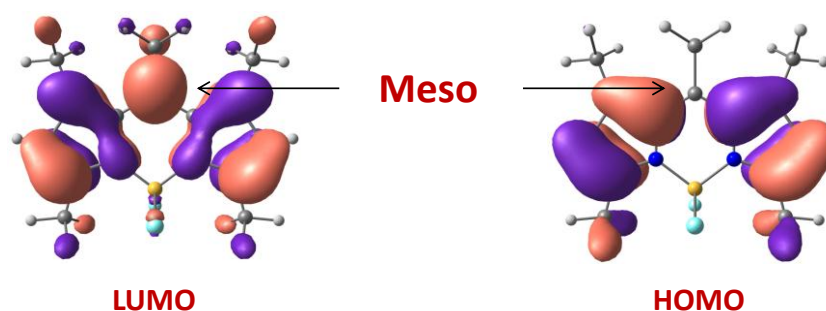


**Figure 3.1** LUMO (left) and HOMO (right) surface plots for BODIPY core.

highest occupied molecular orbital (HOMO) energy level, hence, substitution at meso will affect more extensively the LUMO than the HOMO state (Figure 3.1). Energy bandgap will also change and that, in turn, change the optical properties such as absorption and emission. Selected side chains have different physical nature and they are hydrophobic alkyl (nonyl), and hydrophilic OEG (triethylene glycol) chains. Both chains will bring different physical properties in the molecules for example thermal properties and solid state packing. Their electronic nature is also different, as OEG chain has  $-OCH_2$  group and so it will show different inductive effect than alkyl side chain.<sup>23</sup> BODIPY core is also varied by removing two methyl groups from 1 and 5 positions. Removal of two methyl groups will result in less twisting in the conjugated backbone and hence, there will be closer intermolecular packing.<sup>24</sup> To understand the effect of nature of the side chain on frontier molecular orbital energy levels, band edges have been calculated theoretically from DFT, and experimentally from UV-vis absorption spectra and cyclic voltammetry. Field effect transistors (FET) have been fabricated using these CSMs and charge carrier mobilities are measured. Chemical structures of all synthesized CSMs are given in chart 3.1.

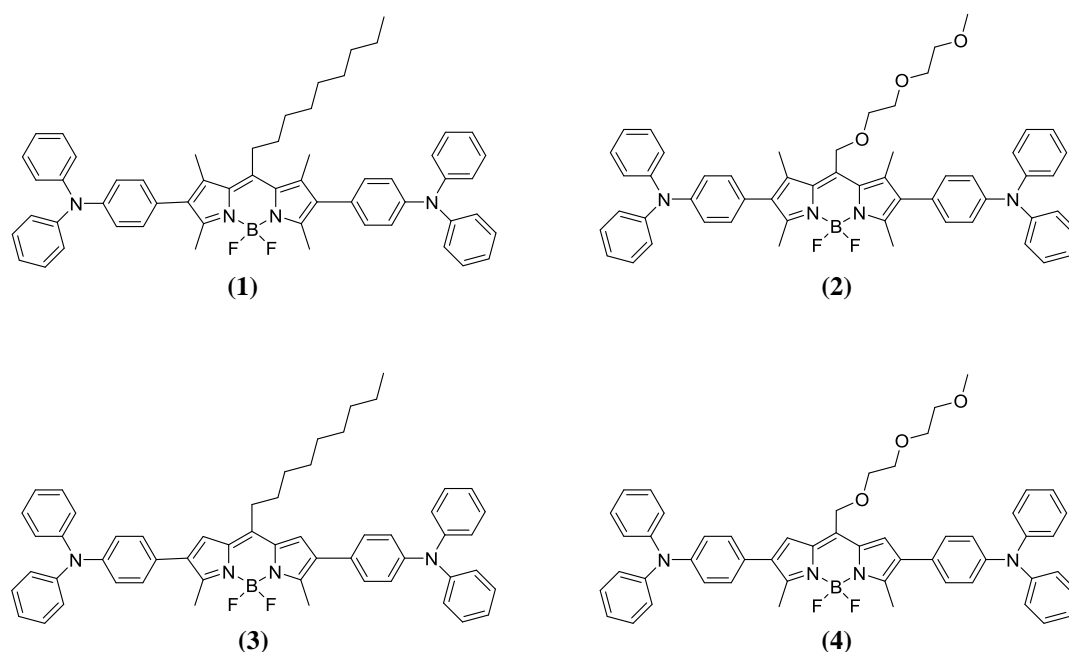


**Chart 3.1** Chemical structures of CSMs (1 – 4).

## 3.2. Experimental Section

### 3.2.1 Materials

2, 4-dimethylpyrrole, pyrrole-2-carboxaldehyde, decanoyl chloride, boron trifluoride diethyl etherate, 2-[2-(2-methoxyethoxy)ethoxy]acetic acid, 4-(diphenylamino)phenylboronic acid,



and anhydrous N,N-dimethylformamide were obtained from commercial sources and used directly as received. Dry DCM was obtained from stirring and distillation over CaH<sub>2</sub>.

### 3.2.2 Instrumentation Details

Cyclic voltammetry (CVs) experiments were performed on BioLogic Science Instruments. CSMs coated Pt wire was used as a working electrode, Ag/Ag<sup>+</sup> as a reference electrode and Pt foil as the counter electrode. CVs were recorded under inert condition in 0.1 M solution of tetrabutylammonium hexafluorophosphate in dry acetonitrile at a scan rate of 100 mV/s. E<sup>ox</sup> and E<sup>red</sup> are determined from the onset potential of oxidation and reduction waves. HOMO and LUMO energy levels were calculated following the equation  $E^{\text{HOMO}} = -(E^{\text{ox}} + 4.8)$  eV and  $E^{\text{LUMO}} = -(E^{\text{red}} - 4.8)$  eV, and calibrated with respect to the internal standard Fc/Fc<sup>+</sup> couple. Powder X-ray diffraction (PXRD) patterns were recorded on a PANalytical X'PERT PRO instrument using iron-filtered Cu K $\alpha$  radiation ( $\lambda = 1.5406 \text{ \AA}$ ).

### 3.2.3 Device Fabrication (OFET)

Bottom-gate bottom-contact field-effect transistors substrates were purchased from Fraunhofer IPMS (interdigitated S/D electrodes), with channel lengths (L) 2.5, 5, 10 and 20  $\mu\text{m}$  and channel width (W) of 10 mm. FET substrates were cleaned with acetone followed by isopropanol and dried by heat gun. The device fabrication and measurements were done inside an argon filled glove box. OFET measurements were performed on Agilent 4156C semiconductor probe analyzer and semi probe station. Substrates were modified using HMDS to make it hydrophobic. The CSMs were spun on top of the substrates from chloroform solutions. Spin coating was done for 60 seconds, at 1500 RPM.

### 3.2.4 Synthetic Procedures and Characterization Data

**2-methylpyrrole:** Pyrrole-2-carboxaldehyde (20.0 g, 0.21 mol) and KOH (40.6 g, 0.724 mol) were dissolved in ethylene glycol (300 mL). To this solution, hydrazine hydrate (27 mL, 0.87 mol) was added, and reaction mixture turned into thick yellow slurry. The reaction mixture was refluxed for 2 h and during this time the yellow solid dissolved. The reaction mixture was subjected to controlled vacuum distillation to afford water and 2-methylpyrrole (11.0 g, 64% yield; colorless liquid) in separate phases. <sup>1</sup>H NMR (400 MHz, CDCl<sub>3</sub>)  $\delta$ : 7.89 (s, 1H), 6.68 (s, 1H), 6.18 (s, 1H), 5.95 (s, 1H), 2.31 (s, 3H).

**2-(2-(2-methoxyethoxy)ethoxy)acetyl chloride:** 2-[2-(2-methoxyethoxy)ethoxy]acetic acid (5.0 g, 27.7 mmol) was dissolved in 10 mL dry DCM and the solution was kept at 0 °C for 15 min. To this solution, oxalyl chloride (5.95 mL, 69.4 mmol) was added dropwise under the inert condition and continued the stirring at the same temperature for another 30 min. The reaction was further continued at room temperature for 2 h. Unreacted oxalyl chloride and solvent were removed using high vacuum and the residue obtained was used for next step without further purification.

**BODIPY 1:** 2,4-dimethylpyrrole (2.0 g, 21 mmol) and decanoyl chloride (2.17 mL, 10.5 mmol) were dissolved in dichloromethane (200 mL) under argon atmosphere. The reaction mixture was stirred overnight at room temperature, followed by the addition of 9 mL of triethylamine and 9 mL of BF<sub>3</sub>OEt<sub>2</sub>. After 2 h, the reaction mixture was washed with H<sub>2</sub>O and organic layer was dried over anhydrous Na<sub>2</sub>SO<sub>4</sub>. After removal of solvent under reduced pressure, the crude product was purified by silica gel column chromatography (eluent: EtOAc/pet.ether) to furnish orange solid compound **BODIPY 1** (1.4 g, 36%). <sup>1</sup>H NMR (400 MHz, CDCl<sub>3</sub>) δ: 6.04 (s, 2H), 2.92 (t, J = 7.79 Hz, 2H), 2.51 (s, 6H), 2.41 (s, 6H), 1.67–1.55 (m, 2H), 1.53–1.43 (p, J = 6.4 Hz, 2H), 1.27 (m, 10H), 0.89 (t, J = 6.82 Hz, 3H); <sup>13</sup>C NMR (100 MHz, CDCl<sub>3</sub>) δ: 153.66, 146.72, 140.28, 131.42, 121.52, 31.88, 31.83, 30.39, 29.50, 29.39, 29.22, 28.48, 22.62, 16.33, 14.41, 14.07.

**BODIPY 2:** Following the procedure for compound **BODIPY 1**, using 2, 4-dimethylpyrrole (1.92 g, 20.2 mmol) and 2-(2-(2-methoxyethoxy)ethoxy)acetyl chloride (1.98 g, 10.1 mmol), Compound **BODIPY 2** (1.2 g, 32%) was synthesized. <sup>1</sup>H NMR (500 MHz, CDCl<sub>3</sub>) δ: 6.04 (s, 2H), 4.63 (s, 2H), 3.73 (t, 2H), 3.66 (t, 2H), 3.60 (t, 2H), 3.50 (t, 2H), 3.35 (s, 3 H), 2.50 (s, 6H), 2.41 (s, 6H); <sup>13</sup>C NMR (125 MHz, CDCl<sub>3</sub>) δ: 155.76, 141.84, 136.01, 132.96, 121.82, 71.91, 70.70, 70.50, 63.90, 59.04, 15.37, 14.61.

**BODIPY 3:** Following the procedure for compound **BODIPY 1**, using 2-methylpyrrole (1.7 g, 21 mmol), compound **BODIPY 3** (1.1 g, 30%) was synthesized. <sup>1</sup>H NMR (400 MHz, CDCl<sub>3</sub>) δ: 7.07 (d, J = 4.12 Hz, 2H), 6.25 (d, J = 4.12 Hz, 2H), 2.79 (t, J = 8 Hz, 2H), 2.60 (s, 6 H), 1.76–1.68 (m, 2H), 1.40 (p, J = 7.33 Hz, 2H), 1.26 (m, 10H), 0.88 (t, J = 7 Hz, 3H); <sup>13</sup>C NMR (100 MHz, CDCl<sub>3</sub>) δ: 156.49, 145.63, 134.62, 126.66, 118.64, 33.79, 31.81, 30.36, 29.99, 29.39, 29.23, 22.61, 14.74, 14.06.

**BODIPY 4:** Following the procedure for compound BODIPY 1, using 2-methylpyrrole (1.46 g, 18 mmol) and 2-(2-(2-methoxyethoxy)ethoxy)acetyl chloride (1.76 g, 9.0 mmol), **BODIPY 4** (950 mg, 30%) was synthesized.  $^1\text{H}$  NMR (200 MHz,  $\text{CDCl}_3$ )  $\delta$ : 7.29 (d, 2H), 6.26 (d, 2H), 4.73 (s, 2 H), 3.68 – 3.52 (m, 8H), 3.38 (s, 3H), 2.61 (s, 6H);  $^{13}\text{C}$  NMR (50 MHz,  $\text{CDCl}_3$ ):  $\delta$  158.03, 137.79, 134.46, 128.21, 119.36, 71.90, 70.71, 70.57, 69.86, 67.11, 59.06, 14.93.

**2,6-diiodo-BODIPY 1a:** To the solution of BODIPY dye **1** (1.1 g, 2.94 mmol) in  $\text{CH}_2\text{Cl}_2$  (21 mL), a solution of N-iodosuccinimide (1.98 g, 8.82 mmol) in anhydrous and degassed DMF (7 mL) was added drop wise and the reaction mixture was stirred vigorously for 24 h at room temperature. After completion, the reaction mixture was repeatedly washed with water and once with brine. The organic layer was then dried over anhydrous  $\text{Na}_2\text{SO}_4$  and solvent was removed under reduced pressure. The crude product was purified by silica gel column chromatography (eluent: EtOAc/pet.ether) to furnish **1a** (1.0 g, 54%).  $^1\text{H}$  NMR (400 MHz,  $\text{CDCl}_3$ )  $\delta$ : 3.00 (t,  $J = 8.8$  Hz, 2H), 2.61 (s, 6H), 2.48 (s, 6H), 1.61(m, 2H), 1.50 (p,  $J = 7.3$  Hz, 2H), 1.27 (m, 10H), 0.89 (t,  $J = 6.85$  Hz, 3H);  $^{13}\text{C}$  NMR (100 MHz,  $\text{CDCl}_3$ )  $\delta$ : 155.14, 146.40, 142.20, 131.34, 86.35, 31.80, 31.66, 30.29, 29.47, 29.37, 29.30, 29.22, 22.63, 18.93, 16.09, 14.09.

**2,6-diiodo-BODIPY 2a:** Following the procedure for the compound **1a**, using BODIPY **2** (200 mg, 0.53 mmol) and N-iodosuccinimide (283 mg, 1.26 mmol), compound **2a** (260 mg, 78%) was synthesized.  $^1\text{H}$  NMR (500 MHz,  $\text{CDCl}_3$ )  $\delta$ : 4.66 (s, 2H), 3.75 (t, 2H), 3.68 (t, 2H), 3.61 (t, 2H), 3.52 (t, 2H), 3.38 (s, 3H), 2.60 (s, 6H), 2.47 (s, 6H);  $^{13}\text{C}$  NMR (125 MHz,  $\text{CDCl}_3$ ): 157.15, 143.88, 135.30, 132.94, 86.57, 71.93, 70.77, 70.74, 70.49, 59.11, 29.70, 17.75, 16.22.

**2,6-diiodo-BODIPY 3a:** Following the procedure for the compound **1a**, using BODIPY **3** (1.0 g, 2.90 mmol) and N-iodosuccinimide (1.95 g, 8.6 mmol), compound **3a** (960 mg, 55%) was synthesized.  $^1\text{H}$  NMR (400 MHz,  $\text{CDCl}_3$ )  $\delta$ : 7.29 (s, 2H), 2.71 (t,  $J = 8.07$  Hz, 2H), 2.61 (s, 6H), 1.69 (p,  $J = 7.58$  Hz, 2H), 1.39 (p,  $J = 7.56$  Hz, 2H), 1.27 (m, 10H), 0.89 (t,  $J = 7.02$  Hz, 3H);  $^{13}\text{C}$  NMR (100 MHz,  $\text{CDCl}_3$ )  $\delta$ : 157.74, 144.67, 135.27, 133.34, 33.79, 31.80, 30.51, 30.03, 29.38, 29.25, 29.23, 22.63, 15.34, 14.09.

**2,6-diiodo-BODIPY 4a:** Following the procedure for the compound 1a, using BODIPY 4 (160 mg, 0.45 mmol) and N-iodosuccinimide (247 mg, 1.1 mmol), compound **4a** (85 mg, 31%) was synthesized. (Caution: compound 4b was purified by quick column chromatography)  $^1\text{H}$  NMR (400 MHz,  $\text{CDCl}_3$ )  $\delta$ : 7.53 (s, 2H), 4.68 (s, 2H), 3.70 – 3.63 (m, 6 H), 3.60 – 3.57 (m 2 H), 3.41 (s, 3H), 2.62 (s, 6H).

### CSMs (1-4)

**Compound 1: 1a** (100 mg, 0.16 mmol), 4-(diphenylamino)phenylboronic acid (109 mg, 0.38 mmol),  $\text{Pd}(\text{dppf})\text{Cl}_2$  (6 mg) and  $\text{Na}_2\text{CO}_3$  (168 mg, 1.6 mmol) were taken in a schlenk tube. The tube was evacuated and back-filled with argon three times, after which a degassed solvent mixture of toluene (15 mL), ethanol (6 mL) and water (7.5 mL) was transferred to the schlenk tube through a septum and the reaction was carried out at 85 °C for 6 h under argon atmosphere. After completion of the reaction, the solvent was removed under reduced pressure and then the residue was dissolved in ethyl acetate and washed with water. The organic layer was passed through a short pad of celite and dried over anhydrous  $\text{Na}_2\text{SO}_4$ . The filtrate was concentrated under reduced pressure and the crude product was purified by column chromatography (eluent: EtOAc/pet.ether) to furnish **1** (104 mg, 75%) as a red solid.  $^1\text{H}$  NMR (500 MHz,  $\text{CDCl}_3$ )  $\delta$ : 7.33 – 7.29 (m ,8H), 7.19 – 7.06 (m 20 H), 3.11 (t, 2H), 2.55 (s, 6H), 2.41 (s, 6H), 1.73 (m, 2 H), 1.53 (m, 2H), 1.44 – 1.29 (m ,10H), 0.90 (t, 3H);  $^{13}\text{C}$  NMR (125 MHz,  $\text{CDCl}_3$ ): 152.62, 147.68, 146.78, 146.69, 136.30, 133.45, 131.45, 131.18, 129.33, 127.59, 124.56, 123.12, 123.03, 31.99, 31.84, 30.44, 29.57, 29.48, 29.28, 28.80, 22.67, 14.58, 14.13, 13.42. MALDI-TOF/TOF:  $\text{M}^+$  ( $\text{C}_{58}\text{H}_{59}\text{BF}_2\text{N}_4$ ) calcd  $m/z$  = 860.4801, found  $m/z$  = 860.3278.

**Compound 2:** Following the procedure for the compound 1, using BODIPY **2a** (100 mg, 0.16 mmol) and 4-(diphenylamino)phenylboronic acid (109 mg, 0.38 mmol), dark red solid compound **2** (100 mg, 72%) was synthesized.  $^1\text{H}$  NMR (500 MHz,  $\text{CDCl}_3$ )  $\delta$ : 7.33 – 7.29 (m 8H), 7.19 – 7.06 (m 20H), 4.83 (s, 2H), 3.81 (t, 2H), 3.73 (t, 2H), 3.65 (t, 2H), 3.54 (t, 2H), 3.37 (s, 3H), 2.56 (s, 6H), 2.45 (s, 6H);  $^{13}\text{C}$  NMR (125 MHz,  $\text{CDCl}_3$ ): 154.72, 147.59, 146.80, 137.38, 135.51, 133.75, 133.10, 130.99, 129.28, 127.16, 124.55, 123.03, 122.97, 71.88, 70.67, 70.52, 70.49, 64.40, 59.01, 13.63, 13.43. MALDI-TOF/TOF:  $\text{M}^+$  ( $\text{C}_{55}\text{H}_{53}\text{BF}_2\text{N}_4\text{O}_3$ ) calcd  $m/z$  = 866.4179, found  $m/z$  = 866.2792.

**Compound 3:** Following the procedure for the compound 1, using BODIPY **3a** (100 mg, 0.17 mmol) and 4-(diphenylamino)phenylboronic acid (109 mg, 0.38 mmol), blue coloured compound **3** (100 mg, 71%) was synthesized.  $^1\text{H}$  NMR (400 MHz,  $\text{CDCl}_3$ )  $\delta$ : 7.29 – 7.26 (m, 12H), 7.15 – 7.02 (m, 18 H), 2.84 (t, 2H), 2.72 (s, 6H), 1.77 (m, 2H), 1.43 (m, 2H), 1.36 – 1.20 (m, 10H), 0.86 (t, 3H);  $^{13}\text{C}$  NMR (100 MHz,  $\text{CDCl}_3$ ): 154.18, 147.58, 146.88, 144.41, 133.68, 132.91, 129.29, 128.82, 128.21, 124.46, 123.71, 123.49, 123.01, 33.77, 33.19, 31.82, 30.51, 30.13, 29.69, 29.44, 29.35, 29.27, 26.72, 22.63, 14.08, 13.92. MALDI-TOF/TOF:  $\text{M}^+$  ( $\text{C}_{56}\text{H}_{55}\text{BF}_2\text{N}_4$ ) calcd  $m/z$  = 832.4488, found  $m/z$  = 832.3201.

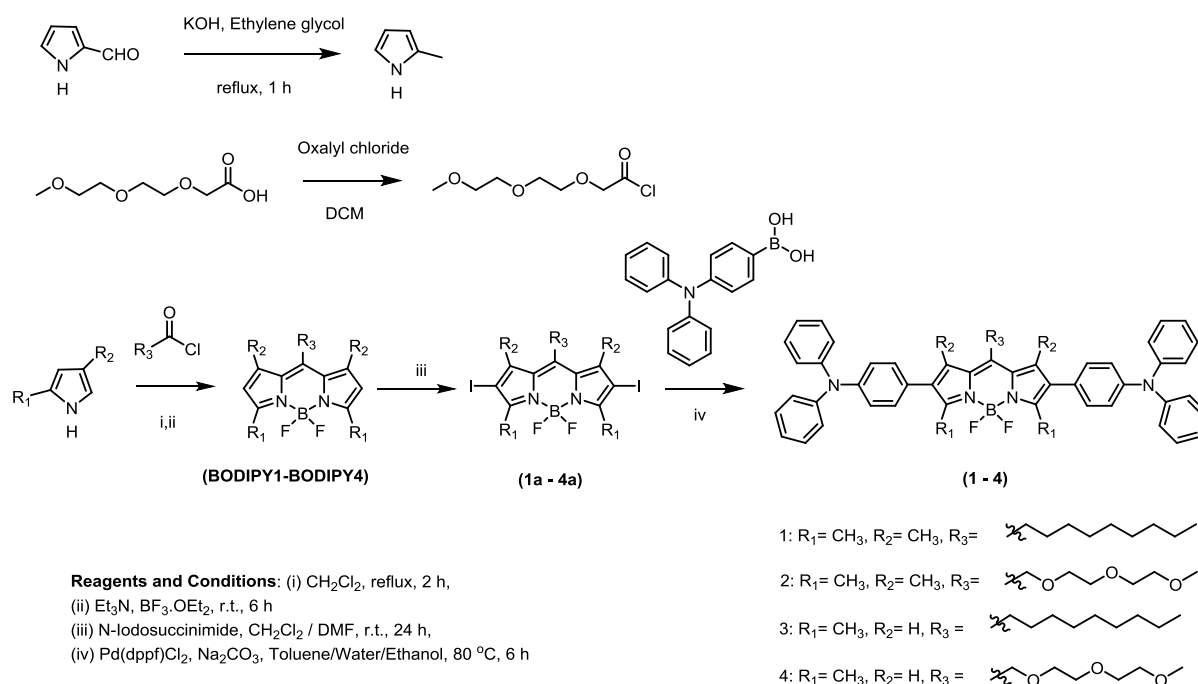
**Compound 4:** Following the procedure for the compound 1, using BODIPY **4a** (85 mg, 0.14 mmol) and 4-(diphenylamino)phenylboronic acid (97 mg, 0.33 mmol), blue coloured compound **4** (30 mg, 33%) was synthesized.  $^1\text{H}$  NMR (400 MHz,  $\text{CDCl}_3$ )  $\delta$ : 7.30 – 7.26 (m, 14H), 7.15 – 7.02 (m, 16H), 4.78 (s, 2H), 3.71 (t, 2H), 3.67 (t, 2H), 3.61 (t, 2H), 3.50 (t, 2H), 3.31 (s, 3H), 2.73 (s, 6H);  $^{13}\text{C}$  NMR (100 MHz,  $\text{CDCl}_3$ ): 155.85, 147.59, 147.02, 136.51, 133.58, 129.33, 128.85, 127.96, 124.54, 123.44, 123.09, 71.85, 70.72, 70.57, 69.94, 67.20, 58.99, 14.11. MALDI-TOF/TOF:  $\text{M}^+$  ( $\text{C}_{53}\text{H}_{49}\text{BF}_2\text{N}_4\text{O}_3$ ) calcd  $m/z$  = 838.3866, found  $m/z$  = 838.2918.

### 3.3 Results and Discussion

#### 3.3.1 Synthesis and Thermal Characterization

Tetramethyl and dimethyl BODIPY cores were synthesized from 2, 4-dimethylpyrrole and 2-methylpyrrole respectively as starting materials. Synthesis of BODIPY dyes (1 - 4) involves acid-catalyzed condensation of pyrroles with corresponding acid chlorides that produces unstable dipyrromethene hydrochloride salt intermediates. Further complexation reaction with boron trifluoride etherate ( $\text{BF}_3\cdot\text{OEt}_2$ ) in the presence of a base yields BODIPY dyes (about 30 – 35% yield).<sup>25</sup> Iodination of the BODIPY core at the 2- and 6-position using N-iodosuccinimide resulted in 2,6-diiodo-BODIPY (1a – 4a). Target molecules (1 – 4) were synthesized using  $\text{Pd}(\text{dppf})\text{Cl}_2$  as a catalyst and  $\text{Na}_2\text{CO}_3$  as a base in the Suzuki coupling reaction under an inert atmosphere (33 – 75% yield) (Scheme 3.1).<sup>26</sup>

These molecules were characterized by  $^1\text{H}$ ,  $^{13}\text{C}$  NMR spectroscopy, and MALDI-TOF analysis (Appendix II).



### Scheme 3.1 Synthetic route to CSMs (1 – 4).

The thermal characteristics of the CSMs were studied by thermogravimetric analysis (TGA) and differential scanning calorimetry (DSC). These CSMs **1**, **2**, **3**, and **4** are thermally stable up to 352 °C, 279 °C, 321 °C, and 248 °C respectively with 5% weight loss and hence can be thermally annealed during device fabrication without degradation (Figure 3.2). The DSC data were obtained from the second heating and cooling cycles (Figure 3.3). For **1** and **3** only melting transitions ( $T_m$ ) was observed at 238 °C and 189 °C respectively. **2** and **4** show  $T_m$  at 192 °C and 215 °C in the first heating and  $T_g$  at 88 °C and 70 °C in the second heating cycle respectively.

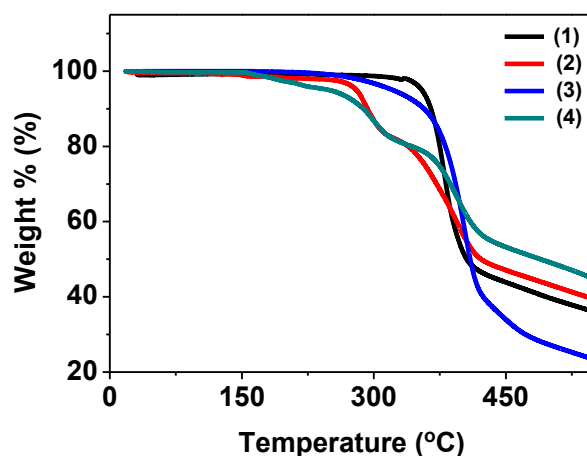
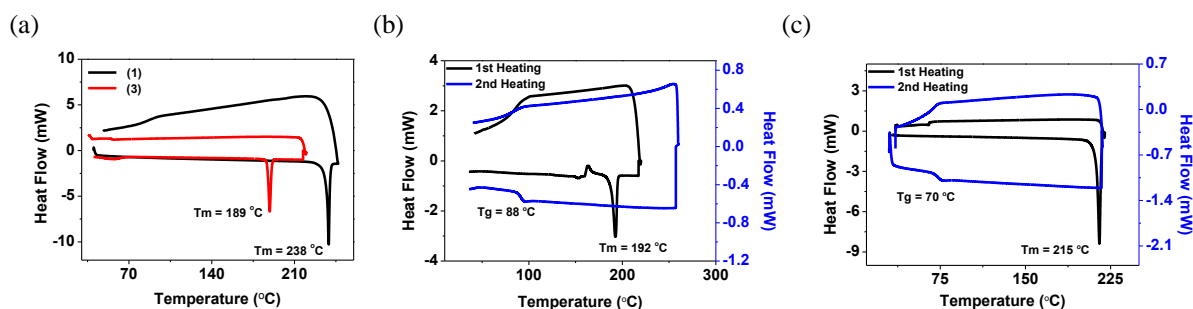


Figure 3.2 TGA curves of CSMs (1 – 4).



**Figure 3.3** DSC plots for **1** and **3** (a), **2** (b), and **4** (c).

### 3.3.2 Molecular Geometry and Electronic Structure Calculations from DFT

Theoretical calculations using density functional theory (DFT) with B3LYP functional and 6-31G\*\* basis set were carried out to calculate frontier orbital energy levels and distribution of wave function in the monomers and the target CSMs. Frontier molecular orbital (FMO)

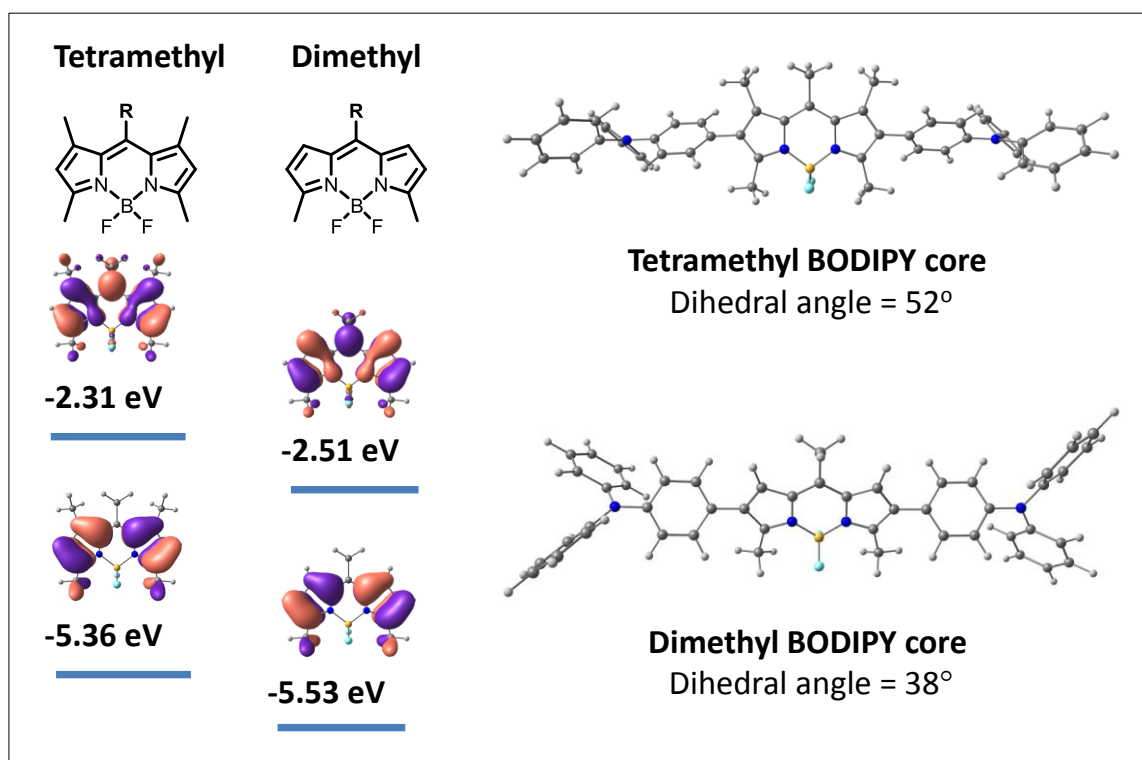


**Figure 3.4** Surface plots and electronic structure of tetramethyl and dimethyl BODIPY core and molecular geometry of CSMs.

energy levels for all BODIPY dyes and CSMs (**1** – **4**) are given in table 3.1. Triphenylamine is an electron rich moiety and LUMO and HOMO energy levels are -0.32 eV and -4.96 eV respectively. For BODIPY moiety, frontier orbital energy levels have gone deeper from tetramethyl to dimethyl BODIPY core while energy bandgap remains the same (Figure 3.4). It shows that removal of methyl groups stabilizes both LUMO and HOMO equally and

hence, energy bandgap did not alter. Side chains at meso are varied from alkyl (nonyl) to OEG (triethylene glycol). In triethylene glycol substituted **BODIPY 2** and **4**, LUMO energy levels are lowered down by 0.19 eV and 0.09 eV from their alkyl chain counterparts **BODIPY 1** and **3**. Though, only minor lowering of 0.04 eV and 0.02 eV is calculated for HOMO energy levels upon triethylene glycol substitution. It is evident from the fact that the electronic density at meso is higher in the LUMO than in the HOMO, and hence, triethylene glycol substitution has affected LUMO energy levels more than HOMO energy levels in both tetramethyl and dimethyl BODIPY cores. This lowering of LUMO for **BODIPY 2** and **BODIPY 4** than alkyl chain analogs should be ascribed to the presence of the -OCH<sub>2</sub> group which reduces the inductive donor character of the substituent.<sup>23</sup>

**Table 3.1** Frontier molecular orbital (FMO) energy levels for BODIPY dyes and CSMs (**1** – **4**) from DFT.

Molecules	BODIPY <b>1</b>	BODIPY <b>2</b>	BODIPY <b>3</b>	BODIPY <b>4</b>	<b>1</b>	<b>2</b>	<b>3</b>	<b>4</b>
LUMO (eV)	-2.29	-2.48	-2.48	-2.57	-2.29	-2.47	-2.49	-2.58
HOMO (eV)	-5.33	-5.37	-5.50	-5.52	-4.89	-4.89	-4.83	-4.83
E <sub>g</sub> (eV) <sup>DFT</sup>	3.04	2.89	3.02	2.95	2.60	2.43	2.34	2.26

The twist in the conjugated backbone reduced from dihedral angle 52° to 38° after removal of methyl groups from 1 and 7 positions (Figure 3.4). As these molecules are designed following donor acceptor strategy and in principle, the HOMO and LUMO energy levels of target molecules depend on the relative placement of the HOMO and LUMO energy levels of the donor and acceptor monomers respectively. Here, contribution to the HOMO comes from the triphenylamine and to LUMO comes from the BODIPY monomers. Molecule **4** has deepest LUMO energy level and lowest energy bandgap among the CSMs (**1** – **4**). The HOMO and LUMO surface plots for CSMs (**1** – **4**) are shown in Figure 3.5. The surface plots indicate that the HOMO wave function is distributed over the entire conjugated backbone. The LUMO wave function, on the other hand, is localized on the BODIPY core. These calculations predict that these CSMs could be possible hole transporting materials.



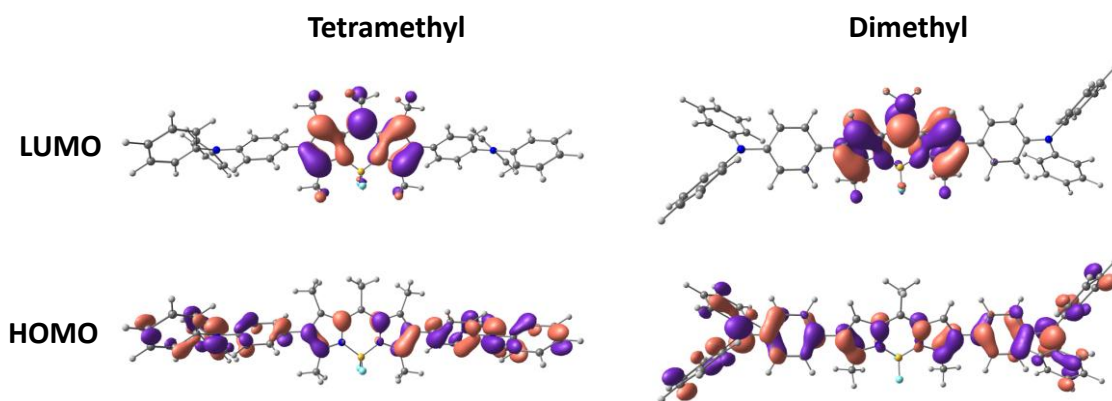


**Figure 3.5** HOMO and LUMO surface plots of CSMs containing tetramethyl (left) and dimethyl (right) BODIPY core.

### 3.3.3 Optical and Electrochemical Properties

The UV-vis absorption spectra of the CSMs were recorded in chloroform as solvent and as thin films (Figure 3.6). The absorption spectra exhibit two clear peaks, a high energy peak for triphenylamine and a low energy peak for BODIPY moiety. The absorption maxima of **1**, **2**, **3**, and **4** in chloroform solutions at room temperature are 538, 564, 586, 606 nm respectively (Figure 3.6a). Absorption maxima for dimethyl BODIPY core are red shifted in comparison

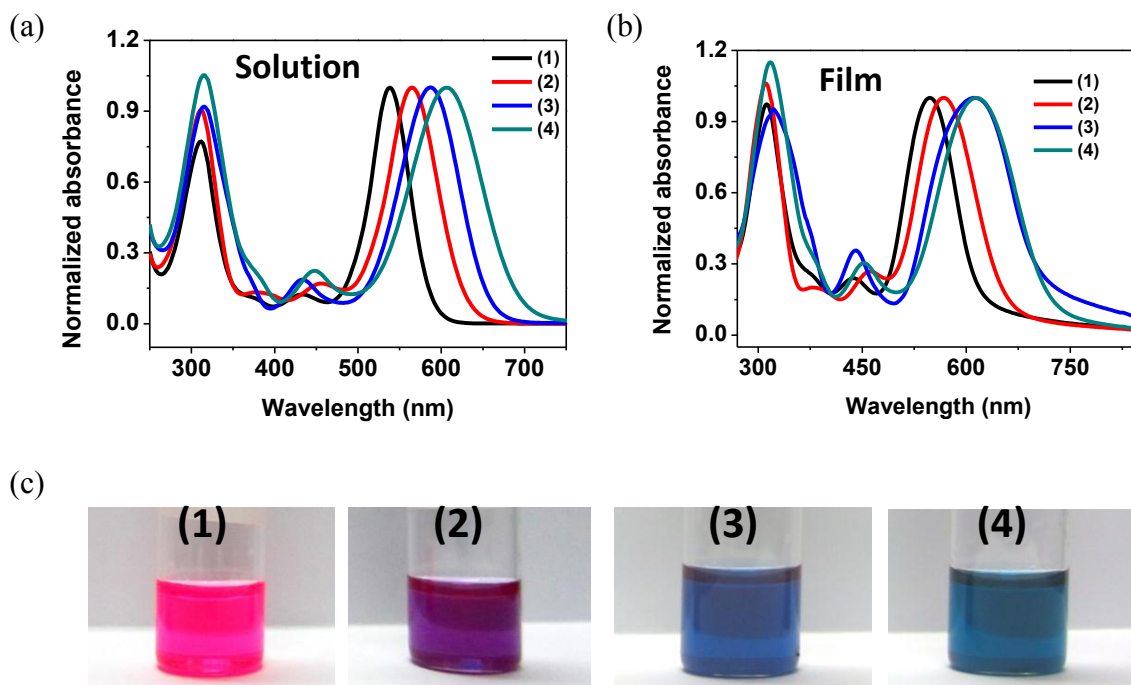


**Figure 3.6** UV-vis absorption spectra of CSMs (**1** – **4**) in dilute chloroform solution (a), as thin-film on quartz substrates (b), and (c) colour of chloroform solution of **1** to **4**, from pink to blue.

to that of tetramethyl core and the shift is 48 nm with nonyl side chain and 42 nm with triethylene glycol side chain. In the case of CSMs with tetramethyl BODIPY core, the absorption spectra of triethylene glycol containing **2** shows a 26 nm red shift to that of **1** with nonyl side chain. Similar absorption pattern was observed for CSMs with dimethyl BODIPY core, that is the absorption of **4** is 20 nm red shifted relative to that of **3** (Table 3.2). Thin film absorption spectra of CSMs **1**, **2**, **3**, **4** are broader and 10, 4, 24, 8 nm red shifted compared to the solution-state spectra, presumably due to planarization of the conjugated backbone (Figure 3.6b). Energy bandgap calculated from low energy absorption edges for **1**, **2**, **3**, and **4** are 1.97, 1.87, 1.72, and 1.69 respectively. Colour of chloroform solution of these molecules also changes from **1** to **4** (Figure 3.6c). Molecule **4** with dimethyl BODIPY core and triethylene glycol side chain has lowest bandgap among CSMs, and that is in agreement with the results from the DFT calculations.

Cyclic voltammetry of CSMs (**1** – **4**) were recorded using CSMs coated Pt wire as working electrode, Ag/Ag<sup>+</sup> as a reference electrode and Pt foil as the counter electrode. The CVs were recorded by sweeping the working electrode potential in the anodic and cathodic segments in 0.1 M tetrabutylammonium hexafluorophosphate in dry acetonitrile (Figure 3.7). Redox processes in both anodic and cathodic sweeps are quasi reversible as the  $\Delta E_p$  was found to be higher than 59 mV. The orbital energy levels with respect to vacuum level were determined by calibrating the oxidation and reduction onsets of CSMs using ferrocene as an internal standard.<sup>27</sup> The orbital energy level values and calculated energy bandgaps are provided in Table 3.2.

**Table 3.2** Optical and electrochemical data for **1** – **4**.

CSM	$\lambda_{\max}^{\text{sol}}$ (nm)	$\lambda_{\max}^{\text{Film}}$ (nm)	$\lambda_{\text{onset}}$ (nm)	$E_g^{\text{Optical}}$ (eV)	$E_{\text{ox, onset/}}$ HOMO(eV)	$E_{\text{red, onset}}$ /LUMO(eV)	$E_g^{\text{elect}}$ (eV)
<b>1</b>	538	548	627	1.97	0.39/-5.13	-1.17/-3.57	1.56
<b>2</b>	564	568	662	1.87	0.35/-5.09	-1.15/ -3.59	1.50
<b>3</b>	586	610	718	1.72	0.40/-5.14	-1.10/ -3.64	1.50
<b>4</b>	606	614	730	1.69	0.37/-5.11	-1.10/-3.64	1.47

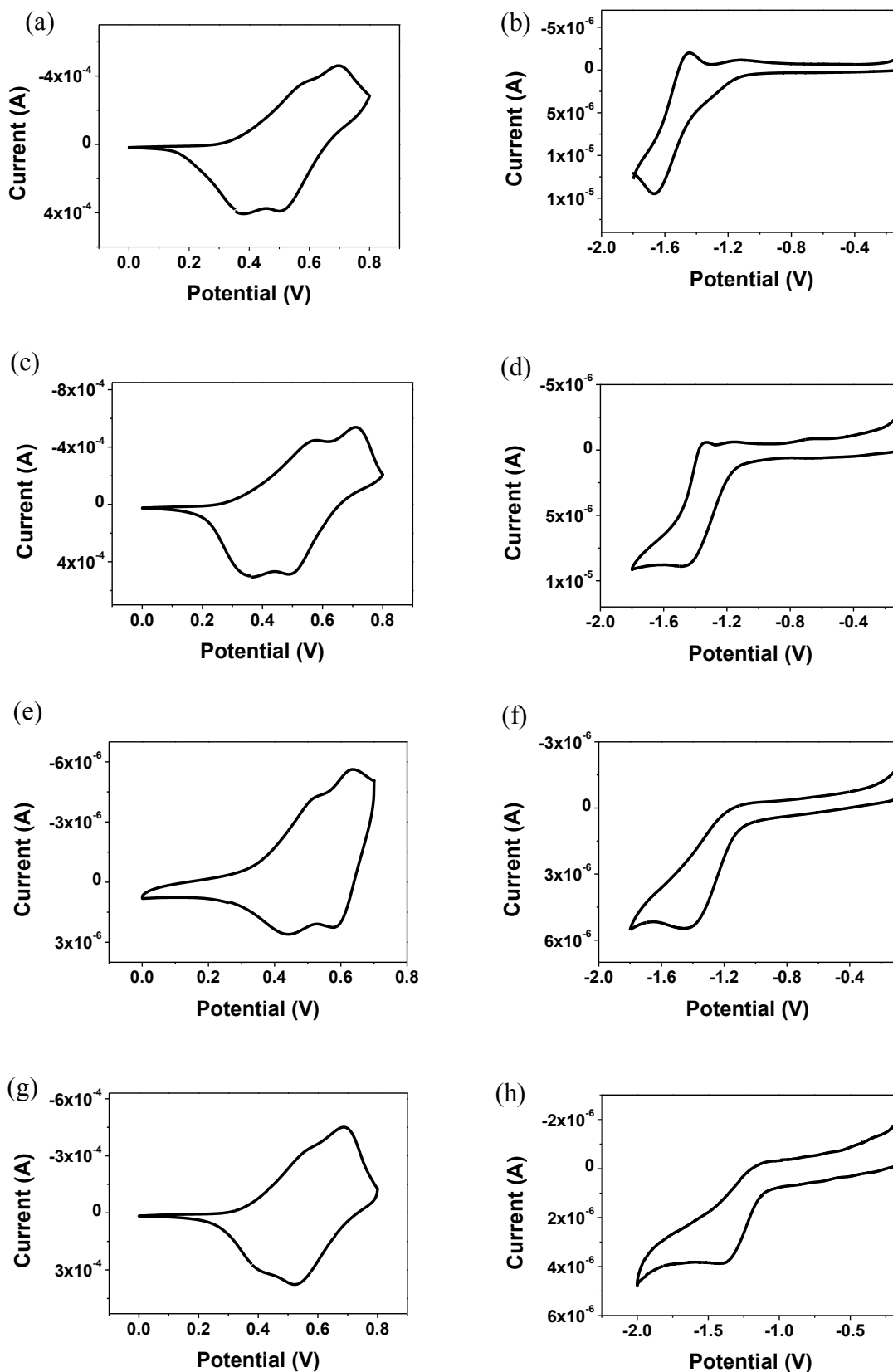


**Figure 3.7** Cyclic voltammograms of molecule **1**: (a) oxidation scan, (b) reduction scan, **2**: (c) oxidation scan, (d) reduction scan, **3**: (e) oxidation scan, (f) reduction scan, **4**: (g) oxidation scan, (h) reduction scan.

### 3.3.4 Crystallinity and Thin Film Morphology

Crystals grown from CSMs (**1** – **4**) were not large enough to be mounted on the single crystal XRD instrument. Hence, to understand solid state packing, thin film XRD of CSMs was recorded (Figure 3.8a). Film XRD pattern of **1** and **2** with tetramethyl core didn't show any peak indicating phase transition while preparing films. Sharp peaks for **3** and **4** were observed at a  $2\theta$  of 19.90 and 19.93 which corresponds to a  $d$  spacing of 4.46 and 4.45 Å, respectively. The interplanar spacing for **3** and **4** are very close which indicates that variation in nature of side chain from hydrophobic to hydrophilic did not impact solid state packing much. And this observation can be attributed to the presence of propeller shaped triphenylamine which limits the close packing after a certain extent. A similar pattern was observed in the film absorption spectra for **3** and **4**. The absorption spectrum for **4**, recorded in chloroform solution, is 20 nm red shifted relative to that of **3** whereas thin film absorption spectra show only 4 nm red shift.

Hydrophilic SiO<sub>2</sub> surface and hexamethyldisilazane (HMDS) treated hydrophobic SiO<sub>2</sub> surface were used for this study. These substrates were used for morphological studies because same substrates were used for the fabrication of Field Effect Transistors (FETs). CSMs (**1** – **4**) were spin coated from chloroform solution on both types of substrates (Figure

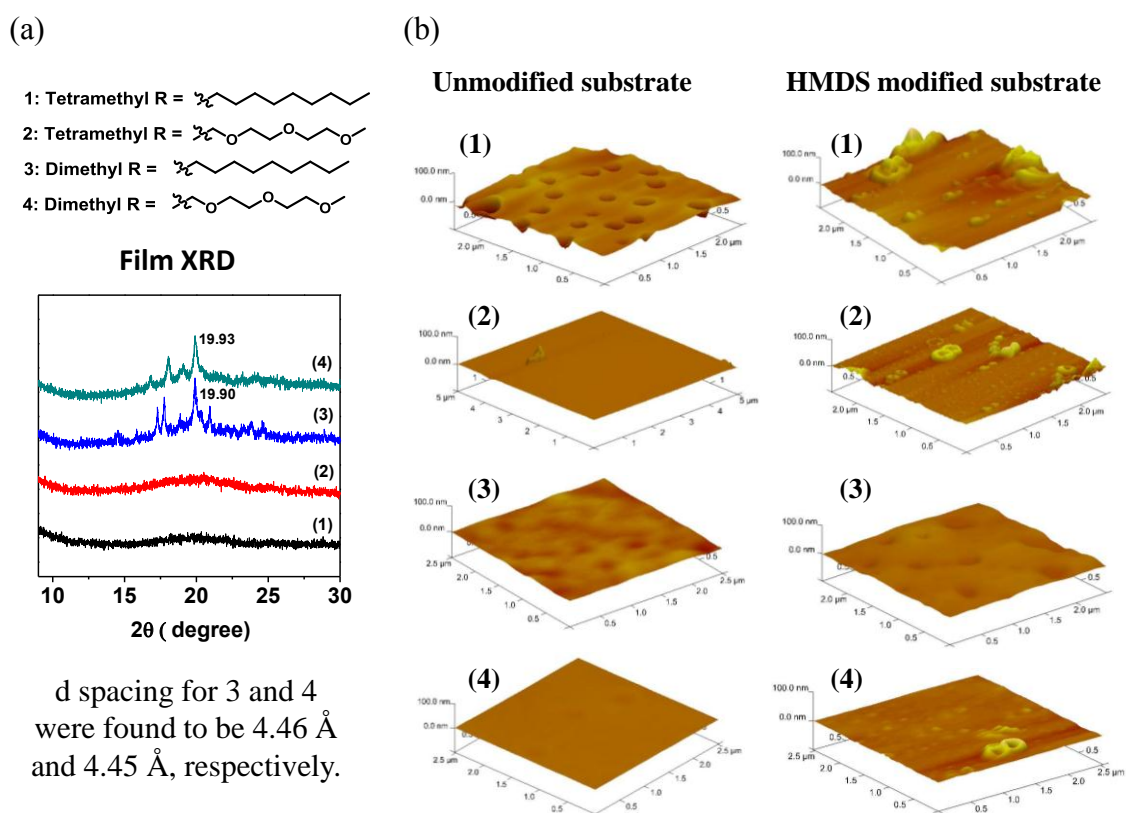


**Figure 2.3** (a) Powder XRD pattern of **1**– **4** and AFM images of thin films of **1**–**4** on unmodified and on HMDS modified SiO<sub>2</sub> substrate (b).

3.8b). For **1**, the film spin coated on unmodified silica substrate showed rough surface morphology with a large number of pinholes. The film of **1** coated on HMDS modified surface exhibited absence of pinholes due to better interaction with hydrophobic than the hydrophilic surface, but the film remains rough. For **3**, the films spin coated on both modified and unmodified SiO<sub>2</sub> have troughs and crests indicating a rough surface though the quality of the film has improved on HMDS modified surface. For **2** and **4** on unmodified silica substrates, the films were uniform, indicating the formation of a very smooth film. Contrary to this, thin film morphology of **2** and **4** spin coated on HMDS modified surface was rough, which is apparently caused by the incompatibility between hydrophilic triethylene glycol substituted **2** and **4** and hydrophobic HMDS modified substrate.<sup>1</sup>

### 3.3.5 Characterization of Field-Effect Transistor Devices

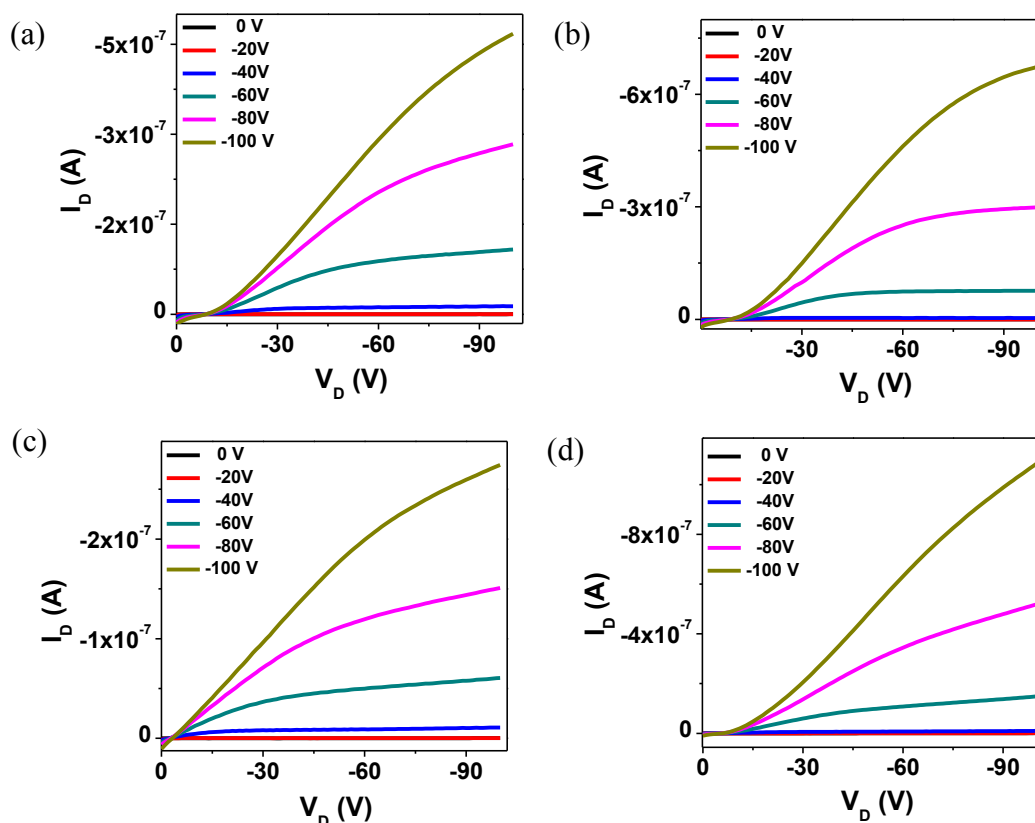


**Figure 3.9** Output characteristic curves of **1**(a), **2** (b), **3** (c), and **4** (d) on unmodified FET

Field effect transistors were fabricated using SiO<sub>2</sub> as a gate dielectric, heavily n doped Si as a gate electrode and gold as source and drain electrodes. The prefabricated substrate has a bottom gate, bottom contact configuration. Two types of devices were fabricated (i) without

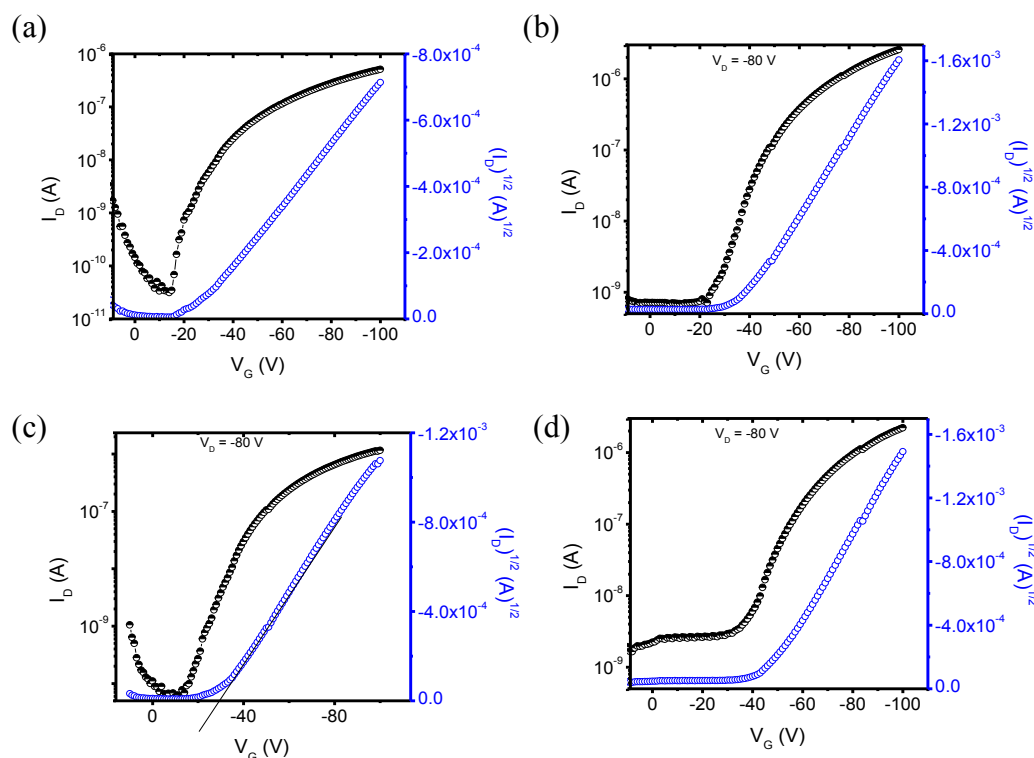


**Figure 3.10** Transfer characteristic curves of **1**(a), **2** (b), **3** (c), and **4**(d) on unmodified FET substrate.

silane (HMDS) modification which is hydrophilic in nature and (ii) with silane modification which is hydrophobic in nature. Conventionally, enhancement in charge carrier mobility has been attributed to the better interaction of organic molecules and silane modified hydrophobic surface.<sup>1</sup> In our studies, The CSMs were spin coated on top of the substrates from chloroform solutions. Output characteristic curves were recorded while sweeping the drain voltage ( $V_D$ ) between 0 and -100V while applying a constant gate voltage ( $V_G$ ). The output characteristic curves of CSMs (**1** – **4**) on unmodified FET substrates are given in figure 3.9. The output characteristic curves showed standard linear and saturation regimes with a gate modulation as a function of applied gate voltage ( $V_G$ ). The linear regime for CSMs (**1** – **4**) didn't start at 0V, which is likely due to contact resistance (Figure 3.9). Device data are given in table 3.3. The hole carrier mobility ( $\mu$ ) calculated for **1** and **3** for unmodified devices was found to be  $1.4 \times 10^{-5}$  and  $1.26 \times 10^{-5}$   $\text{cm}^2/\text{Vs}$  respectively. Devices fabricated on silane modified surface show a slight increase in mobility. Molecules **2** and **4** with triethylene glycol side chains exhibit higher hole mobility than their alkyl chain counterparts on unmodified devices. But for devices fabricated on silane modified surface, hole mobilities decrease by one order. And that is because of incompatibility of the hydrophobic gate dielectric surface with the hydrophilic **2** and **4**. Device characteristics for HMDS modified substrates are given in Appendix II.

**Table 3.3:** OFET device metrics of CSMs 1 – 4.

CSMs	$\mu^a$ (cm <sup>2</sup> /Vs) ( $\mu^{\text{max}}$ )	$V_T^a$ (V)	$I_{\text{on/off}}^a$	$\mu^b$ (cm <sup>2</sup> /Vs) ( $\mu^{\text{max}}$ )	$V_T^b$ (V)	$I_{\text{on/off}}^b$
<b>1</b>	$9.39 \times 10^{-6}$ ( $1.40 \times 10^{-5}$ )	-15	$6.88 \times 10^3$	$1.25 \times 10^{-5}$ ( $1.90 \times 10^{-5}$ )	-45	$3.68 \times 10^3$
<b>2</b>	$1.02 \times 10^{-5}$ ( $1.47 \times 10^{-5}$ )	-36	$4.64 \times 10^5$	$1.58 \times 10^{-6}$ ( $2.11 \times 10^{-6}$ )	-52	$1.22 \times 10^4$
<b>3</b>	$8.96 \times 10^{-6}$ ( $1.26 \times 10^{-5}$ )	-25	$1.07 \times 10^3$	$1.36 \times 10^{-5}$ ( $4.22 \times 10^{-5}$ )	-35	$1.68 \times 10^2$
<b>4</b>	$1.19 \times 10^{-5}$ ( $1.47 \times 10^{-5}$ )	-32	$5.91 \times 10^3$	$3.18 \times 10^{-6}$ ( $4.91 \times 10^{-6}$ )	-30	$1.59 \times 10^3$

(a – Unmodified SiO<sub>2</sub> substrate, b – HMDS modified SiO<sub>2</sub> substrates,  $\mu^{\text{max}}$  = maximum mobility)

### 3.4 Summary

In summary, a systematic study was carried to understand the impact of nature of side chain on both electronic and physical properties of conjugated small molecules. Four different BODIPY dyes with two types of structural variations were used for this work (i) methyl groups removal from 1 and 7 positions of BODIPY core and (ii) Side chain variation from the hydrophobic alkyl (nonyl) chain to hydrophilic OEG (triethylene glycol) chain. First, DFT calculations were performed to understand the impact of these variations on the electronic structure of BODIPY dyes and target molecules. Methyl group removal resulted in deep lying LUMO and HOMO energy levels for dimethyl BODIPY core, and also, a decrease in dihedral angle of 14° in the target molecules. Side chain variation also affected electronic nature of target molecules. The presence of -OCH<sub>2</sub> group in the triethylene glycol side chain caused a reduction in inductive donor character of the substituent at meso position and that led to stabilization of LUMO energy level in respective molecules. Absorption spectra of triethylene glycol containing molecules are red shifted in comparison to the alkyl chain analogs. CSMs substituted with triethylene glycol show higher hole mobility on unmodified FET substrates than alkyl chain substituted CSMs. After silane modification, hole carrier mobilities improve slightly for alkyl chain substituted CSMs but decrease by one order for triethylene glycol substituted CSMs.

### 3.5 References

- 1) Singh, S.; Venugopalan, V.; Krishnamoorthy, K. *Phys. Chem. Chem. Phys.* **2014**, *16*, 13376.
- 2) Piliago, C.; Holcombe, T. W.; Douglas, J. D.; Woo, C. H.; Beaujuge, P. M.; Fréchet, J. M. J. *J. Am. Chem. Soc.* **2010**, *132*, 7595.
- 3) Zoombelt, A. P.; Leenen, M. A. M.; Fonrodona, M.; Nicolas, Y.; Wienk, M. M.; Janssen, R. A. J. *Polymer* **2009**, *50*, 4564.
- 4) Lei, T.; Dou, J.-H.; Pei, J. *Adv. Mater.* **2012**, *24*, 6457.
- 5) Meager, I.; Ashraf, R. S.; Mollinger, S.; Schroeder, B. C.; Bronstein, H.; Beatrup, D.; Vezie, M. S.; Kirchartz, T.; Salleo, A.; Nelson, J.; McCulloch, I. *J. Am. Chem. Soc.* **2013**, *135*, 11537.
- 6) Zhang, F.; Hu, Y.; Schuettfort, T.; Di, C.-a.; Gao, X.; McNeill, C. R.; Thomsen, L.; Mannsfeld, S. C. B.; Yuan, W.; Siringhaus, H.; Zhu, D. *J. Am. Chem. Soc.* **2013**, *135*, 2338.
- 7) Mei, J.; Graham, K. R.; Stalder, R.; Reynolds, J. R. *Org. Lett.* **2010**, *12*, 660.
- 8) Wang, E.; Ma, Z.; Zhang, Z.; Vandewal, K.; Henriksson, P.; Inganäs, O.; Zhang, F.; Andersson, M. R. *J. Am. Chem. Soc.* **2011**, *133*, 14244.
- 9) Loudet, A.; Burgess, K. *Chem. Rev.* **2007**, *107*, 4891.
- 10) Ulrich, G.; Ziessel, R.; Harriman, A. *Angew. Chem., Int. Ed.* **2008**, *47*, 1184.
- 11) Boens, N.; Leen, V.; Dehaen, W. *Chem. Soc. Rev.* **2012**, *41*, 1130.
- 12) Rousseau, T.; Cravino, A.; Bura, T.; Ulrich, G.; Ziessel, R.; Roncali, J. *Chem. Commun.* **2009**, 1673.
- 13) Rousseau, T.; Cravino, A.; Ripaud, E.; Leriche, P.; Rihn, S.; De Nicola, A.; Ziessel, R.; Roncali, J. *Chem. Commun.* **2010**, *46*, 5082.
- 14) Kim, B.; Ma, B.; Donuru, V. R.; Liu, H.; Fréchet, J. M. J. *Chem. Commun.* **2010**, *46*, 4148.
- 15) Lin, H.-Y.; Huang, W.-C.; Chen, Y.-C.; Chou, H.-H.; Hsu, C.-Y.; Lin, J. T.; Lin, H.-W. *Chem. Commun.* **2012**, *48*, 8913.
- 16) Shrestha, M.; Si, L. P.; Chang, C.-W.; He, H. S.; Sykes, A.; Lin, C.-Y.; Diao, E. W.-G. *J. Phys. Chem. C* **2012**, *116*, 10451.
- 17) Cortizo-Lacalle, D.; Howells, C. T.; Gambino, S.; Vilela, F.; Vobecka, Z.; Findlay, N. J.; Inigo, A. R.; Thomson, S. A. J.; Skabara, P. J.; Samuel, I. D. W. *J. Mater. Chem.* **2012**, *22*, 14119.



- 18) López Arbeloa, F.; Bañuelos, J.; Martínez, V.; Arbeloa, T.; López Arbeloa, I. *Int. Rev. Phys. Chem.* **2005**, *24*, 339.
- 19) Lu, H.; Mack, J.; Yang, Y.; Shen, Z. *Chem. Soc. Rev.* **2014**, *43*, 4778.
- 20) Gómez-Durán, C. F. A.; García-Moreno, I.; Costela, A.; Martín, V.; Sastre, R.; Bañuelos, J.; López Arbeloa, F.; López Arbeloa, I.; Peña-Cabrera, E. *Chem. Commun.* **2010**, *46* (28), 5103.
- 21) Nepomnyashchii, A. B.; Bröring, M.; Ahrens, J.; Krüger, R.; Bard, A. J. *J. Phys. Chem. C* **2010**, *114*, 14453.
- 22) Dhokale, B.; Jadhav, T.; Mobin, S. M.; Misra, R. *J. Org. Chem.* **2015**, *80*, 8018.
- 23) Bañuelos, J.; Arroyo-Córdoba, I. J.; Valois-Escamilla, I.; Alvarez-Hernández, A.; Peña-Cabrera, E.; Hu, R.; Zhong Tang, B.; Esnal, I.; Martínez, V.; López Arbeloa, I. *RSC Adv.* **2011**, *1*, 677.
- 24) Usta, H.; Yilmaz, M. D.; Avestro, A.-J.; Boudinet, D.; Denti, M.; Zhao, W.; Stoddart, J. F.; Facchetti, A. *Adv. Mater.* **2013**, *25*, 4327.
- 25) Popere, B. C.; Della Pelle, A. M.; Thayumanavan, S. *Macromolecules* **2011**, *44*, 4767.
- 26) Zhu, S.; Dorh, N.; Zhang, J.; Vegesna, G.; Li, H.; Luo, F. -T.; Tiwari, A.; Liu, H. *J. Mater. Chem.*, **2012**, *22*, 2781.
- 27) Popere, B. C.; Della Pelle, A. M.; Poe, A.; Balaji, G.; Thayumanavan, S. *Chem. Sci.*, **2012**, *3*, 3093.

## Chapter 4

# BODIPY in Conjugation with Diketopyrrolopyrrole (DPP) Core for Solution-Processable Small Molecule Organic Field Effect Transistors

## 4.1 Introduction

Small molecule semiconductors are easy to synthesize and can be solution-processed into field effect transistor (FET) devices just like polymers. There is no issue of polydispersity like polymeric materials, hence, they maintain batch to batch consistency.<sup>1-3</sup> The performance of devices based on small molecules depends on many factors such as the electronic structure of conjugated system, side chains, and solid state packing.<sup>4,5</sup> Earlier, small conjugated molecules were mainly acenes, fused heteroacene, and oligothiophene derivatives, and they were mostly fabricated via thermal evaporation methods.<sup>6-9</sup> To make solution processable, high performing molecules, over past few years, organic dyes such as diketopyrrolopyrrole (DPP),<sup>10-13</sup> isoindigo,<sup>14-16</sup> rylene imides,<sup>17,18</sup> squaraines,<sup>19</sup> merocyanines,<sup>20</sup> and BODIPY<sup>21-26</sup> are being extensively explored. These  $\pi$  conjugated dyes demonstrate excellent thermal and (photo-)chemical stability, and are accessible by straightforward synthetic protocols.<sup>27</sup> BODIPY is comparatively less explored, and moderate performer for OFET applications amongst these dyes.

In previous works, CSMs containing central BODIPY and terminal triphenylamine moieties were synthesized and Impact of side chains variation on physical and electronic properties was studied. BODIPY dye has a rigid structure and it facilitates  $\pi$  -  $\pi$  stacking in the solid state,<sup>22</sup> but in both studies, we had modest hole mobilities in the range of  $10^{-5}$ . One possible reason could be the limited intermolecular connectivity due to BODIPY being in the middle and terminal propeller shaped triphenylamine. In the present work, we have hypothesized that the CSMs with terminal  $\pi$ -stacking BODIPY moiety would show enhanced interconnectivity (Figure 4.1), leading to improvement in charge transport.<sup>28</sup> In the case of conventional BODIPY dyes, introduction of bulky substitution is one of the methods to achieve solid state fluorescence.<sup>29,30</sup> But, bulky substituents suppress the  $\pi$  stacking, resulting in poor interconnectivity. In our approach, terminal moieties are selected with

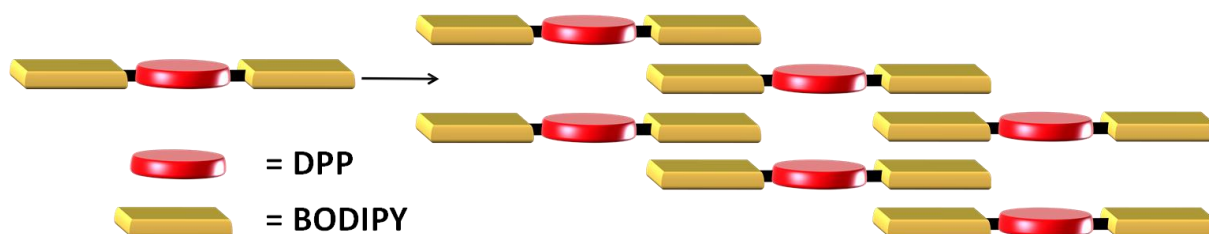


**Figure 4.1** CSMs with DPP and terminal  $\pi$ -stacking BODIPY moiety to enhance interconnectivity.

varying degree of planarity. Substituents on BODIPY core affecting  $\pi - \pi$  stacking and causing twisting in the conjugated backbone are systematically removed. In this way we have three types of BODIPY cores, BODIPY **1** with methyl groups at 1, 3, 5, 7- positions and phenyl ring at meso position, BODIPY **2** with the same tetramethyl core with phenyl ring at meso is replaced by a methyl group and BODIPY **3** with methyl groups at 3, 7, and meso positions (Chart 4.1).

Our previous study shows that removal of two methyl groups results in a reduction in dihedral angle as well modulation of frontier molecular orbital (FMO) energy levels. BODIPY **3** with 3, 7 dimethyl groups has low lying LUMO and HOMO energy levels than BODIPY **2**. Replacement of phenyl ring with methyl ring did not alter FMO energy levels much from BODIPY **1** to BODIPY **2**. To achieve long range interconnectivity in the small molecules we connected terminal BODIPYs with another planar dye DPP. Unlike BODIPY,

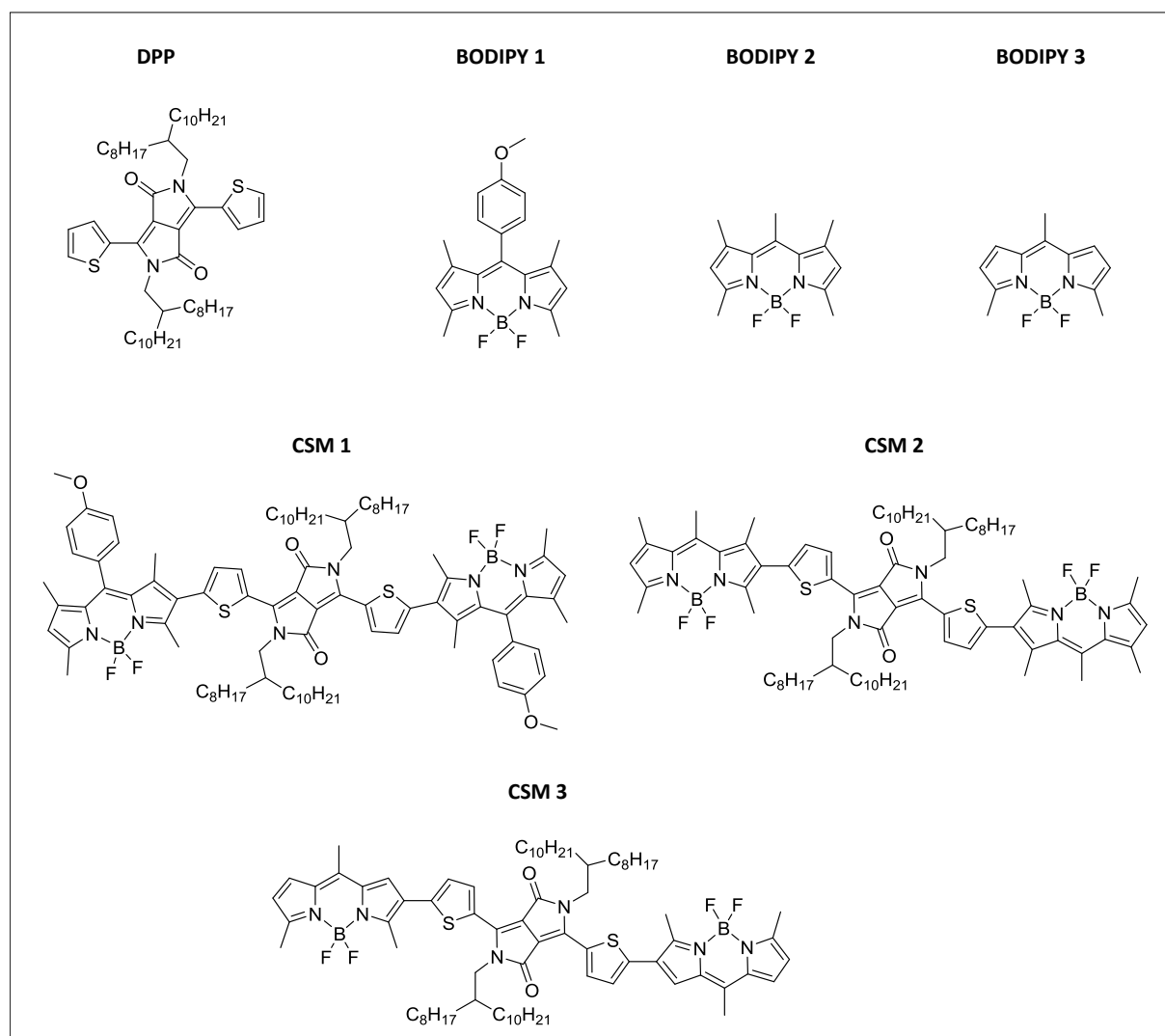


**Chart 4.1** Chemical structures of DPP and BODIPY monomers, and CSMs (**1 – 3**).

a significant number of reports of DPP based systems, small molecules, and polymers for OFET applications are available. They exhibit promising optical and charge transport properties,<sup>10-13,31</sup> and their solution-processability and solid-state molecular ordering can be controlled by varying N-alkylation.<sup>32</sup> DPP core is electron deficient and in most of the research work, it is incorporated in an alternative manner with an electron rich unit to yield low band gap materials. Small molecules and polymers incorporating DPP demonstrate p-type, n-type, and ambipolar charge transport with high mobility values.<sup>33-37</sup> Thus, the approach, connecting pi-stacking BODIPY as terminal moiety with DPP core that can improve charge transport of BODIPY containing systems, would help in material design for OFETs. CSMs (**1** – **3**) contain DPP substituted with 2-octyldodecyl side chain and BODIPY **1**, BODIPY **2**, and BODIPY **3** are synthesized and field effect transistors (FET) have been fabricated using these CSMs and charge transport properties are studied.

## 4.2. Experimental Section

### 4.2.1 Materials

2,4-dimethylpyrrole, pyrrole-2-carboxaldehyde, Acetyl chloride, DDQ, boron trifluoride diethyl etherate, N-iodosuccinimide, 2-thiophenecarbonitrile, diethyl succinate, 2-octyl-1-dodecanol, 2-isopropoxy-4,4,5,5-tetramethyl-1,3,2-dioxaborolane, n-butyllithium, diisopropylamine, anhydrous N,N-dimethylformamide, and 1,4-dioxane were obtained from commercial sources and used directly as received. Tetrahydrofuran (THF) was passed through alumina and distilled over Na/benzophenone before use. Dry DCM and dry acetone were obtained from stirring and distillation over CaH<sub>2</sub> and K<sub>2</sub>CO<sub>3</sub> respectively. Synthesis of DPP dye was carried out by following procedure reported previously.<sup>38</sup>

### 4.2.2 Instrumentation Details

Cyclic voltammetry (CVs) experiments were performed on BioLogic Science Instruments. CSMs coated Pt wire was used as a working electrode, Ag/Ag<sup>+</sup> as a reference electrode and Pt foil as the counter electrode. CVs were recorded under inert condition in 0.1 M solution of tetrabutylammonium hexafluorophosphate in dry acetonitrile at a scan rate of 100 mV/s. E<sup>ox</sup> and E<sup>red</sup> are determined from the onset potential of oxidation and reduction waves. HOMO and LUMO energy levels were calculated following the equation  $E^{\text{HOMO}} = -(E^{\text{ox}} + 4.8) \text{ eV}$

and  $E^{\text{LUMO}} = -(E^{\text{Red}} - 4.8) \text{ eV}$ , and calibrated with respect to the internal standard  $\text{Fc}/\text{Fc}^+$  couple.<sup>39</sup>

### 4.2.3 Device Fabrication (OFET)

Bottom-gate bottom-contact field-effect transistors substrates were purchased from Fraunhofer IPMS (interdigitated S/D electrodes, with channel lengths (L) 2.5, 5, 10 and 20  $\mu\text{m}$  and channel width (W) of 10  $\mu\text{m}$ ). Cleaning of FET substrates were done with acetone followed by isopropanol, and dried by heat gun. The device fabrication and measurements were done inside argon filled glove box. Modification of  $\text{SiO}_2$  surface was done using a chloroform solution of OTS (octyltrichlorosilane). Thin films were prepared by spin-coating (concentration  $\cong 10 \text{ mg/mL}$  in chloroform, 1500 rpm for 60 seconds). OFET measurements were performed on Agilent 4156C semiconductor probe analyser and semi probe station. Charge carrier mobilities were calculated using the standard saturation regime quadratic model equation  $\mu = I_{DS}/(V_{GS}-V_{th})^2 \times 2L/WC_{OX}$ .

### 4.2.4 Synthetic Procedures and Characterization Data

#### Monomers synthesis:

**BODIPY 1:** To a solution of 4-methoxybenzaldehyde (1.36 g, 10 mmol) in anhydrous dichloromethane (800 mL), 2,4-dimethylpyrrole (1.90 g, 20 mmol) was added drop wise and the reaction mixture was purged with argon for 5 minutes. 0.2 mL of TFA was added to the solution and the reaction mixture was stirred overnight at room temperature under an argon atmosphere. The reaction mixture was then washed with 2N NaOH solution and then with water. The organic layer was dried over anhydrous  $\text{Na}_2\text{SO}_4$  and solvent was evaporated under reduced pressure. The residue was then dissolved in toluene (35 mL) and a solution of DDQ (2.5 g, 11 mmol) in toluene (15 mL) was added slowly to it, under argon atmosphere. After 5 minutes of stirring, triethylamine (8 mL) and borontrifluoride etherate (7 mL) were added and the reaction mixture was stirred at room temperature for 1.5 h. The reaction mixture was then diluted with diethylether and was repeatedly washed with water. The organic layer was dried over anhydrous  $\text{Na}_2\text{SO}_4$  and was evaporated under reduced pressure. The crude product was purified by column chromatography (eluent: EtOAc/pet.ether) to furnish **BODIPY 1** (800 mg, 23%) as a bright orange solid with a metallic luster.  $^1\text{H NMR}$  (200 MHz,  $\text{CDCl}_3$ )  $\delta$ : 7.21 (d,  $J = 8.72$ , 2 H), 7.04 (d,  $J = 8.72$ , 2 H), 5.98 (s, 2 H), 3.88 (s, 3 H), 2.56 (s, 6 H), 1.44 (s, 6

H);  $^{13}\text{C}$  NMR (50 MHz,  $\text{CDCl}_3$ )  $\delta$ : 160.12, 155.25, 143.20, 141.87, 131.86, 129.20, 127.02, 121.12, 114.54, 55.33, 14.59.

**BODIPY 2:** To a solution of 2,4-methylpyrrole (2.5 mL, 2.28 g, 24 mmol) in DCM (60 mL), acetyl chloride (0.8 mL, 12 mmol) was added slowly and the reaction mixture was refluxed for 2 h. Triethylamine (12 mL) was added, followed by an addition of  $\text{BF}_3 \cdot \text{Et}_2\text{O}$  (12 mL) and stirring was continued for 2 h at rt. The reaction mixture was quenched with 10% aq HCl and extracted with EtOAc. The organic extracts were washed with water, dried over anhydrous  $\text{Na}_2\text{SO}_4$  and was evaporated under reduced pressure. The crude product was purified by column chromatography (eluent: EtOAc/pet.ether) to furnish **BODIPY 2** (1.23 g, 39%) as a red solid.  $^1\text{H}$  NMR (400 MHz,  $\text{CDCl}_3$ )  $\delta$ : 6.05 (s, 2H), 2.57 (s, 3H), 2.51 (s, 6H), 2.41 (s, 6H);  $^{13}\text{C}$  NMR (100 MHz,  $\text{CDCl}_3$ )  $\delta$ : 153.56, 141.40, 140.98, 132.03, 121.21, 29.69, 17.29, 16.34, 14.40.

**BODIPY 3:** Following the procedure for the compound BODIPY 2, using 2-methylpyrrole (1.95 g, 24 mmol), compound **BODIPY 3** (1.12 g, 40%) was synthesized.  $^1\text{H}$  NMR (400 MHz,  $\text{CDCl}_3$ )  $\delta$ : 7.09 (d, 2H), 6.26 (d, 2H), 2.60 (s, 6H), 2.46 (s, 3H);  $^{13}\text{C}$  NMR (100 MHz,  $\text{CDCl}_3$ )  $\delta$ : 156.62, 140.17, 134.99, 126.93, 118.72, 15.21, 14.75.

**Monoiodo-BODIPY 1a:** To the solution of BODIPY 1 (177 mg, 0.5 mmol) in  $\text{CH}_2\text{Cl}_2$  (10 mL), a solution of N-iodosuccinimide (123 mg, 0.55 mmol) in anhydrous and degassed DMF (3 mL) was added drop wise and the reaction mixture was stirred vigorously for 12 h at room temperature. After completion, the reaction mixture was repeatedly washed with water and once with brine. The organic layer was then dried over anhydrous  $\text{Na}_2\text{SO}_4$  and solvent was removed under reduced pressure. The crude product was purified by silica gel column chromatography (eluent: EtOAc/pet.ether) to furnish **1a** (150 mg, 63%).  $^1\text{H}$  NMR (400 MHz,  $\text{CDCl}_3$ ): 7.14 (d, 2H), 7.01 (d, 2H), 3.88 (s, 3H), 2.63 (s, 3H), 2.56 (s, 3H), 1.43 (s, 6H);  $^{13}\text{C}$  NMR (100 MHz,  $\text{CDCl}_3$ )  $\delta$ : 160.31, 157.58, 154.31, 145.19, 143.23, 141.65, 132.26, 131.34, 129.12, 126.80, 122.17, 114.68, 84.15, 55.33, 16.80, 15.75, 14.78.

**Monoiodo-BODIPY 2a:** Following the procedure for the compound 1a, using BODIPY 2 (136 mg, 0.52 mmol), compound **2a** (130 mg, 65%) was synthesized.  $^1\text{H}$  NMR (400 MHz,  $\text{CDCl}_3$ )  $\delta$ : 6.12 (s, 1H), 2.60 (d, 6H), 2.53 (s, 3H), 2.46 (s, 3H), 2.43 (s, 3H);  $^{13}\text{C}$  NMR (100

MHz, CDCl<sub>3</sub>)  $\delta$ : 155.95, 152.69, 143.13, 141.29, 140.82, 132.54, 131.66, 122.40, 84.29, 19.41, 17.58, 17.05, 16.13, 15.80, 14.61.

**Monoiodo-BODIPY 3a:** Following the procedure for the compound 1a, using BODIPY 3 (117 mg, 0.50 mmol), compound **3a** (110 mg, 61%) was synthesized. <sup>1</sup>H NMR (400 MHz, CDCl<sub>3</sub>)  $\delta$ : 7.23 (s, 1H), 7.17 (d, 1H), 6.32 (d, 1H), 2.59 (d, 6H), 2.46 (s, 3H); <sup>13</sup>C NMR (100 MHz, CDCl<sub>3</sub>)  $\delta$ : 159.21, 155.37, 139.58, 135.39, 135.28, 131.87, 128.71, 126.92, 120.20, 75.10, 15.28, 15.08, 14.97.

**2,5-bis(2-octyldodecyl)-3,6-di(thiophen-2-yl)-2,5-dihydropyrrolo[3,4-c]pyrrole-1,4-dione**

**D1:** To a solution of DPP (6.0 g, 20 mmol) and anhydrous potassium carbonate (38 g, 240 mmol) in 120 mL of N,N-dimethylformamide, 1-Iodo-2-octyldodecane (21.0 g, 52 mmol) was injected by syringe under argon protection. The reaction mixture was stirred for 20 h at 110 °C, cooled to room temperature, and then poured into water. Organic phase was extracted with CH<sub>2</sub>Cl<sub>2</sub>, washed with brine and dried over anhydrous Na<sub>2</sub>SO<sub>4</sub>. After removal of solvent under reduced pressure, the crude product was purified by silica gel column chromatography (eluent: EtOAc/pet.ether) to furnish red solid compound **D1** (8.5 g, 49%). <sup>1</sup>H NMR (400 MHz, CDCl<sub>3</sub>)  $\delta$ : 8.87 (d, 2H), 7.61 (d, 2H), 7.25 (d, 2H), 4.00 (d, 4H), 1.90 (m, 2H), 1.25 (m, 64H), 0.87 (m, 12H); <sup>13</sup>C NMR (100 MHz, CDCl<sub>3</sub>)  $\delta$ : 161.82, 140.49, 135.29, 130.52, 129.92, 128.46, 108.00, 46.29, 37.81, 31.99, 31.96, 31.25, 30.09, 29.71, 29.63, 29.57, 29.43, 26.27, 22.77, 22.75, 14.19.

**2,5-bis(2-octyldodecyl)-3,6-bis(5-(4,4,5,5-tetramethyl-1,3,2-dioxaborolan-2-yl)thiophen-**

**2-yl)-2,5-dihydropyrrolo[3,4-c]pyrrole-1,4-dione D2:** LDA solution was prepared by adding n-Butyllithium in n-hexane (1.52 mL, 3.8 mmol) slowly at 0 °C to diisopropylamine (0.67 mL, 4.8 mmol) in 20 mL of dry THF under argon atmosphere. This freshly prepared LDA solution was added within 15 min to the THF (10 mL) solution of D1 (1.38 g, 1.6 mmol) and 2-isopropoxy-4,4,5,5-tetramethyl-1,3,2-dioxaborolane (1.31 mL, 6.4 mmol) at -25 °C. After 2 h of stirring at 0 °C, the reaction was quenched with 10 mL of 1 M HCl solution. Organic layer was extracted with chloroform and concentrated under reduced pressure. The residue was dissolved in dichloromethane, and the solution was poured into 400 mL of cold acetone under vigorous stirring. Product was filtered off and washed with cold acetone to afford **D2** (920 mg, 52%) as a pink solid. <sup>1</sup>H NMR (400 MHz, CDCl<sub>3</sub>)  $\delta$ : 8.90 (d, 2H), 7.70



(d, 2H), 4.04 (d, 4H), 1.88 (m, 2H), 1.36 (s, 24H), 1.32 – 1.20 (m, 64H), 0.85 (m, 12H);  $^{13}\text{C}$  NMR (100 MHz,  $\text{CDCl}_3$ )  $\delta$ : 161.75, 140.51, 137.67, 136.18, 135.66, 108.72, 84.59, 46.24, 37.77, 31.93, 31.89, 30.03, 29.65, 29.61, 29.54, 29.37, 29.30, 26.32, 24.78, 22.70, 22.68, 14.15.

### CSMs (1 – 3)

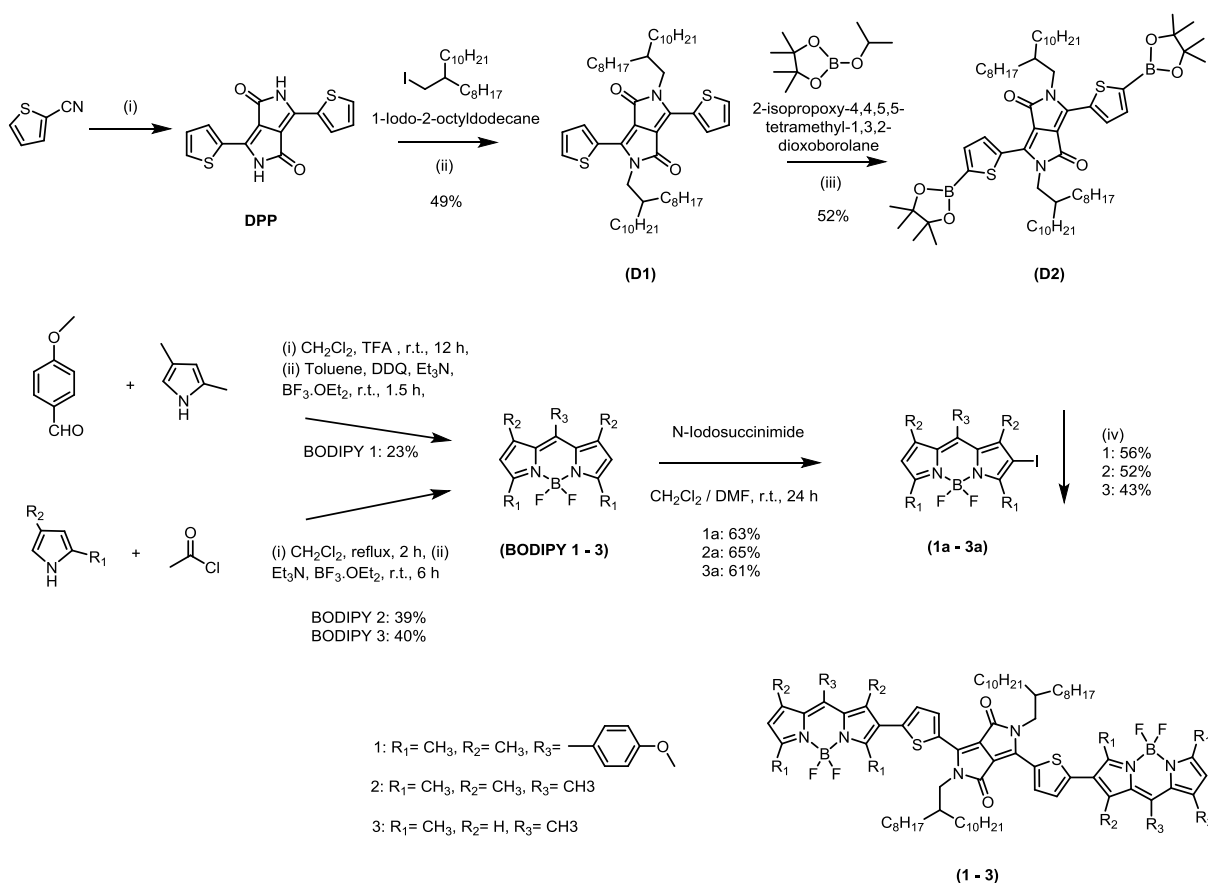
**Compound 1:** DPP monomer D2 (70 mg, 0.063 mmol), 1a (72 mg, 0.15 mmol),  $\text{Pd}(\text{dppf})\text{Cl}_2$  (5 mg) and  $\text{Na}_2\text{CO}_3$  (66 mg, 0.63 mmol) were taken in a schlenk tube. The tube was evacuated and back-filled with argon three times. Degassed solvent mixture of toluene (13 mL), ethanol (5 mL) and water (7 mL) was transferred to the schlenk tube through a septum and the reaction was carried out at 85 °C for 6 h under argon atmosphere. After completion of the reaction, solvent was removed under reduced pressure and then the residue was dissolved in ethyl acetate and washed with water. Organic layer was passed through a short pad of celite and dried over anhydrous  $\text{Na}_2\text{SO}_4$ . The filtrate was concentrated under reduced pressure and the crude product was purified by column chromatography (eluent: DCM/pet.ether) to furnish **1** (55 mg, 56%) as a dark blue solid.  $^1\text{H}$  NMR (400 MHz,  $\text{CDCl}_3$ )  $\delta$ : 8.96 (d, 2H), 7.19 (d, 2H), 7.02 (d, 2H), 7.00 (d, 2H), 6.06 (s, 2H), 3.99 (d, 4H), 3.88 (s, 6H), 2.65 (s, 6H), 2.59 (s, 6H), 1.94 (m, 2H), 1.49 (s, 6H), 1.47 (s, 6H), 1.19 (m, 64H), 0.85 (m, 12H);  $^{13}\text{C}$  NMR (100 MHz,  $\text{CDCl}_3$ )  $\delta$ : 161.71, 160.33, 157.88, 152.67, 145.00, 142.48, 141.01, 139.89, 139.21, 135.94, 132.96, 131.08, 129.74, 129.15, 128.85, 126.77, 124.17, 122.31, 114.72, 107.81, 55.32, 46.36, 37.98, 31.90, 31.83, 31.12, 30.02, 29.60, 29.54, 29.46, 29.35, 29.27, 26.21, 22.64, 14.83, 14.10, 13.48, 13.07. MALDI-TOF/TOF:  $\text{M}^+$  ( $\text{C}_{94}\text{H}_{126}\text{B}_2\text{F}_4\text{N}_6\text{O}_4\text{S}_2$ ) calcd  $m/z = 1564.9404$ , found  $m/z = 1564.8358$ .

**Compound 2:** Following the procedure for the compound 1, using DPP monomer D2 (100 mg, 0.089 mmol), 2a (89 mg, 0.23 mmol),  $\text{Pd}(\text{dppf})\text{Cl}_2$  (6 mg) and  $\text{Na}_2\text{CO}_3$  (93 mg, 0.89 mmol), compound **2** (64 mg, 52%) was synthesized.  $^1\text{H}$  NMR (400 MHz,  $\text{CDCl}_3$ )  $\delta$ : 9.03 (d, 2H), 7.06 (d, 2H), 6.14 (s, 2H), 4.03 (d, 4h), 2.66 (s, 6H), 2.60 (s, 6H), 2.56 (s, 6H), 2.45 (d, 12H), 1.98 (m, 2h), 1.21 (m, 64H), 0.85 (m, 12H);  $^{13}\text{C}$  NMR (100 MHz,  $\text{CDCl}_3$ )  $\delta$ : 161.69, 156.19, 151.04, 142.88, 142.09, 141.01, 139.90, 137.04, 136.05, 133.23, 131.59, 130.02, 129.24, 123.96, 122.49, 107.84, 46.44, 38.05, 31.91, 31.87, 31.18, 30.10, 29.66, 29.63, 29.59, 29.35, 29.31, 26.27, 22.67, 17.59, 16.94, 15.43, 14.63, 14.10, 13.34. MALDI-TOF/TOF:  $\text{M}^+$  ( $\text{C}_{82}\text{H}_{118}\text{B}_2\text{F}_4\text{N}_6\text{O}_2\text{S}_2$ ) calcd  $m/z = 1380.8880$ , found  $m/z = 1381.0433$ .

**Compound 3:** Following the procedure for the compound 1, using DPP monomer D2 (100 mg, 0.089 mmol), 3a (83 mg, 0.23 mmol), Pd(dppf)Cl<sub>2</sub> (6 mg) and Na<sub>2</sub>CO<sub>3</sub> (93 mg, 0.89 mmol), compound **3** (50 mg, 43%) was synthesized. <sup>1</sup>H NMR (500 MHz, CDCl<sub>3</sub>) δ: 8.95 (d, 2H), 7.27 (s, 2h), 7.23 (s, 2H), 7.20 (d, 2H), 6.35 (d, 2H), 4.05 (d, 4H), 2.82 (s, 6H), 2.65 (s, 6H), 2.54 (s, 6H), 1.98 (m, 2H), 1.21 (m, 64H), 0.84 (m, 12H); <sup>13</sup>C NMR (100 MHz, CDCl<sub>3</sub>) δ: 161.59, 159.59, 152.13, 142.33, 140.16, 139.38, 136.36, 135.93, 133.57, 128.39, 128.05, 125.04, 124.23, 122.28, 120.33, 107.95, 46.31, 38.06, 31.91, 31.87, 31.29, 30.13, 29.69, 29.64, 29.57, 29.37, 29.33, 26.37, 22.66, 15.43, 15.01, 14.43, 14.10. MALDI-TOF/TOF: M<sup>+</sup> (C<sub>78</sub>H<sub>110</sub>B<sub>2</sub>F<sub>4</sub>N<sub>6</sub>O<sub>2</sub>S<sub>2</sub>) calcd m/z = 1324.8254, found m/z = 1324.6819.

## 4.3 Results and Discussion

### 4.3.1 Synthesis and Thermal Characterization



**Reagents and Conditions:** (i) Diethylsuccinate, t-BuOK, t-amyl alcohol, 120 °C, (ii) K<sub>2</sub>CO<sub>3</sub>, DMF, 100 °C, 24 h, (iii) THF, LDA, -25°C- rt, 1h, (iv) Pd(dppf)Cl<sub>2</sub>, Na<sub>2</sub>CO<sub>3</sub>, Toluene/Water/Ethanol, 85 °C, 6 h

### Scheme 4.1 Synthetic routes to DPP and BODIPY monomers, and CSMs (1 – 3).

The synthetic routes for DPP and BODIPY monomers and CSMs (**1** – **3**) are illustrated in Scheme 4.1. BODIPY **1** was synthesized following the procedure given in chapter 1. BODIPY **2** and **3** were synthesized by acid-catalyzed condensation of 2,4-dimethylpyrrole and 2-methylpyrrole respectively with the acetyl chloride that produces unstable dipyrromethene hydrochloride salt intermediates. Further complexation reaction with boron trifluoride etherate ( $\text{BF}_3 \cdot \text{OEt}_2$ ) in the presence of a base yields BODIPY dyes (40% yield). N-iodosuccinimide was used to synthesize monoiodo BODIPY (**1a** – **3a**) in about 60 – 64% yield. DPP dye was synthesized in high yield (about 70%) according to the reported procedure.<sup>40</sup> This insoluble DPP dye was then subjected to N-alkylation with two solubilizing 2-octyldodecyl side chains and afforded the compound D1 in 50% yield. Diborylated DPP monomer was obtained in 51% yield by treating a reaction mixture of D1 and 2-isopropoxy-4,4,5,5-tetramethyl-1,3,2-dioxaborolane with freshly prepared LDA solution.<sup>38</sup> CSMs (**1** – **3**) were synthesized by Suzuki coupling between diborylated DPP monomer and monoiodo BODIPY monomers in about 42 – 56% yield.<sup>41</sup>

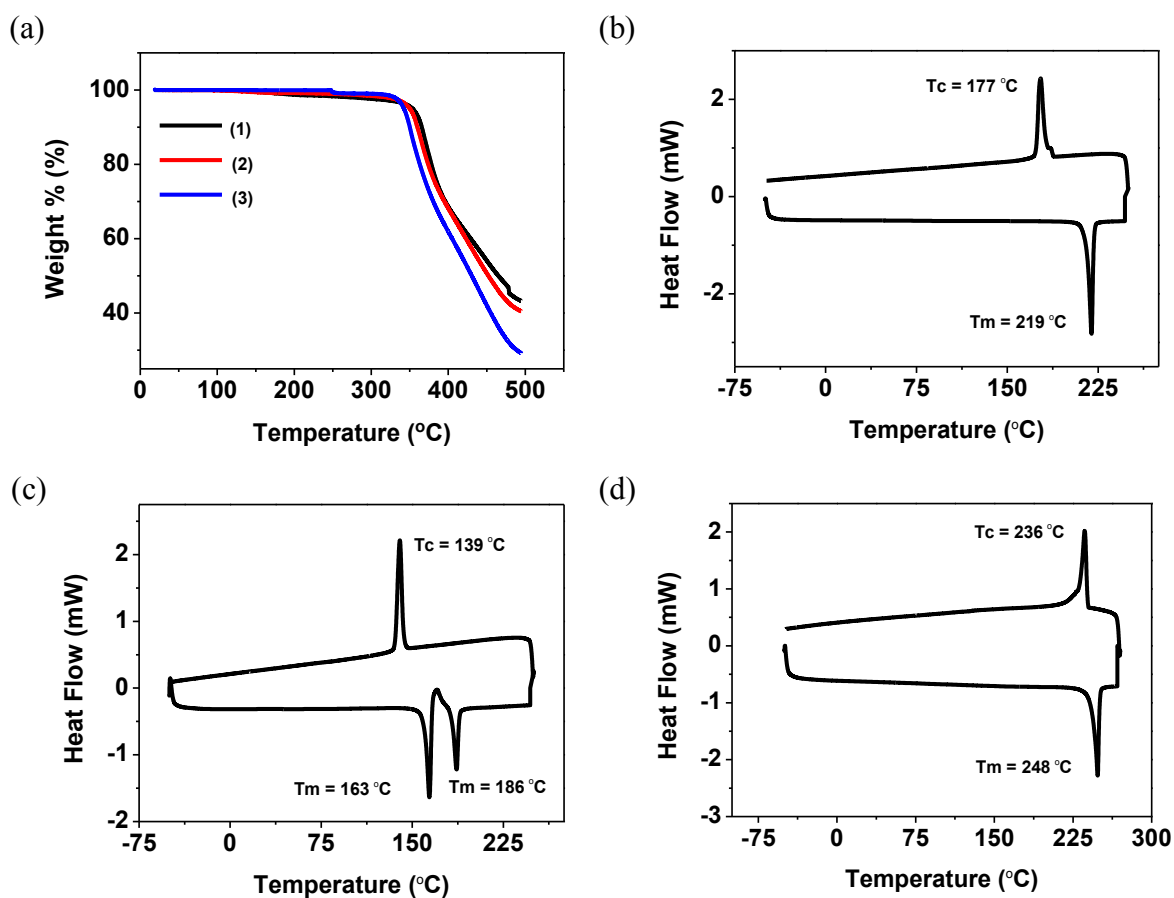


**Figure 4.2** (a) TGA curves for CSMs (**1** – **3**), and DSC plots for **1** (b), **2** (c), and **3** (d).

Synthesized monomers and small molecules were characterized by  $^1\text{H}$ ,  $^{13}\text{C}$  NMR spectroscopy, and MALDI-TOF analysis (Appendix IV).

The thermal characteristics of the CSMs were studied by thermogravimetric analysis (TGA) and differential scanning calorimetry (DSC). These CSMs **1**, **2**, and **3** are thermally stable upto 354 °C, 350 °C, and 342 °C respectively with 5% weight loss, and hence can be thermally annealed during device fabrication without degradation (Figure 4.2a). The DSC data were obtained from the second heating and cooling cycles (Figure 4.2b - d). For **1** and **3**, melting transitions ( $T_m$ ) were observed at 218 °C and 248 °C, and crystallization transitions ( $T_c$ ) at 177 °C and 238 °C respectively. Molecule **2** shows two melting transitions at 163 °C, 186 °C and one  $T_c$  at 139 °C. Since it shows two melting transitions we studied its crystallization behavior using polarizing light microscopy. We allowed it to melt with 5 °C heating rate till 200 °C and then hold at isotherm for 2 min and then cooled at the rate of 5 °C. On cooling, it forms spherulitic crystalline texture (Figure 4.3).

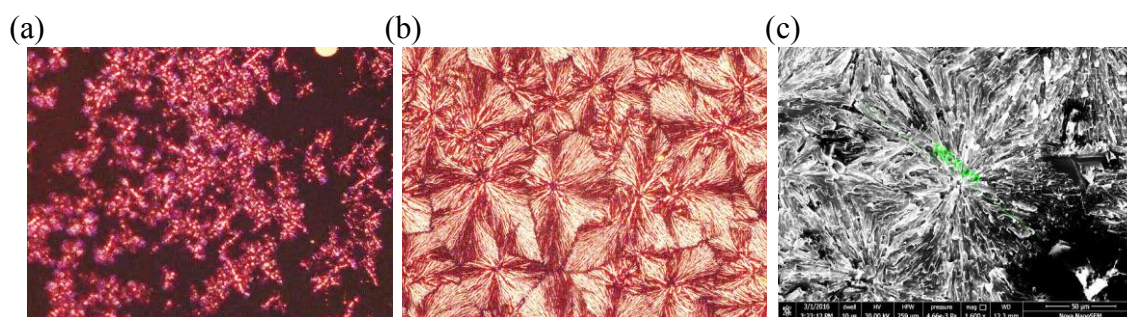


**Figure 4.3** Polarized light microscopy image of molten film of **2** while cooling (a) starting of crystallization (5 X), (b) crystalline film in 20X, (c) SEM image of crystalline film.

### 4.3.2 Molecular Geometry and Electronic Structure Calculations from DFT

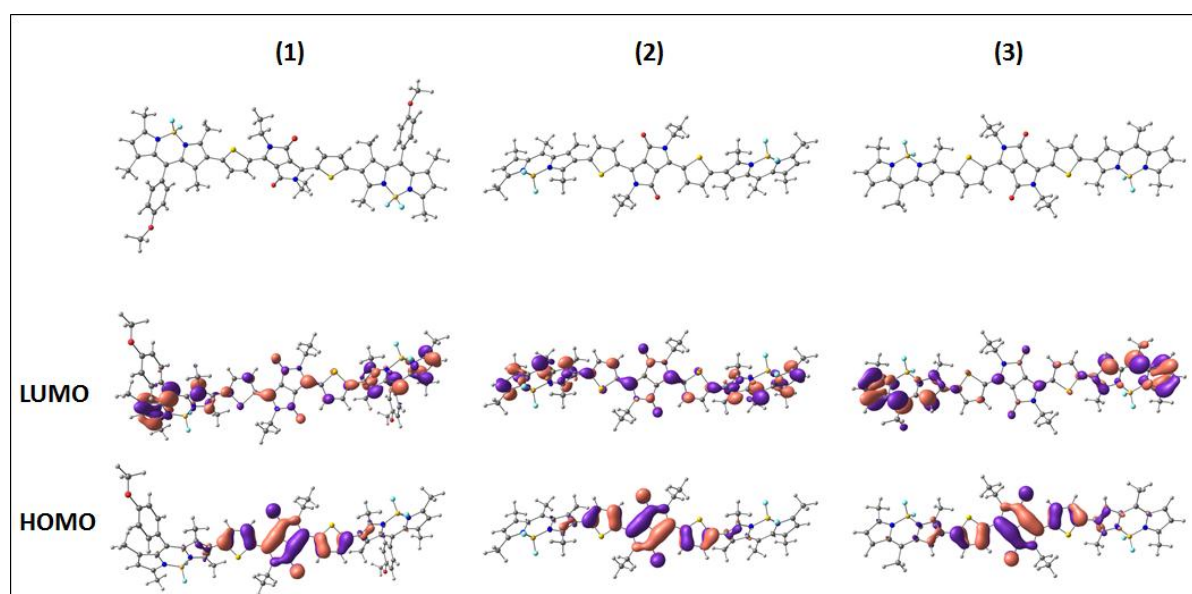
Density functional theory (DFT) analysis was carried out to investigate the optimal geometric structure and the electronic properties of CSMs (**1** – **3**). DFT calculations were done at B3LYP/6-31G \*\* level using Gaussian 09 on model compounds representing the DPP, BODIPY monomers, and CSMs (**1** – **3**).<sup>42,43</sup> The theoretical HOMO and LUMO levels are given in table 4.1, and compared with the experimental data. The HOMO/LUMO levels for DPP monomer, are -4.95/-2.50 eV, and for BODIPY (**1** – **3**) are -5.28/-2.28 eV, -5.36/-2.31 eV, and -5.53/-2.51 eV. From BODIPY **1** to **2**, replacement of phenyl ring with alkyl group affected energy levels to some extent, while removal of two methyl groups from BODIPY **2** at 1,7 positions resulted in deeper HOMO/LUMO for BODIPY **3**. These BODIPY monomers

exhibit strong molecular dipoles, oriented toward the 4,4'-fluorine substituents, and the values are 5.42 D, 4.14 D, and 3.36 D for BODIPY **1**, **2**, and **3** respectively.

**Table 4.1** Frontier molecular orbital (FMO) energy levels for monomers and CSMs from DFT.

Molecules	DPP	BODIPY <b>1</b>	BODIPY <b>2</b>	BODIPY <b>3</b>	<b>1</b>	<b>2</b>	<b>3</b>
LUMO (eV)	-2.50	-2.28	-2.31	-2.51	-2.60	-2.65	-2.84
HOMO (eV)	-4.95	-5.28	-5.36	-5.53	-4.65	-4.74	-4.68
$E_g^{DFT}$ (eV)	2.45	3.00	3.05	3.02	2.05	2.09	1.84

Since substituent groups and orbital energy levels are different for BODIPY (**1** – **3**), corresponding CSMs (**1** - **3**) exhibit variation in orbital energy levels and degree of planarity in the conjugated backbones. The geometrically optimized structures of model compounds are given in figure 4.4. The inter-ring torsion angles are  $\approx 42^\circ$ ,  $\approx 46^\circ$ , and  $\approx 25^\circ$  for **1**, **2**, and **3** respectively. With the lowest inter-ring torsion angle, **3**, containing dimethyl BODIPY core has the most coplanar conjugated backbone compared to other two molecules. In each of the model compounds, both LUMO and HOMO wave functions are delocalized along the backbone, and this is a characteristic feature of ambipolar molecules reported in the



**Figure 4.4** Molecular geometry and HOMO, LUMO surface plots of CSMs (**1** – **3**).

literature.<sup>44-47</sup> The theoretical HOMO/LUMO energies are -4.65/-2.60 eV for **1**, -4.74/-2.65 eV for **2**, and -4.68/-2.84 eV for **3**. The energy band gaps are 2.05, 2.09, and 1.84 eV for **1**, **2**, and **3** respectively. Furthermore, amongst the CSMs (**1** – **3**), **3** has the most planar conjugated backbone and the lowest energy band gap, which are important factors for efficient inter and intramolecular charge transport.

### 4.3.3 Optical and Electrochemical Properties

The UV-vis absorption spectra of the CSMs were recorded in chloroform as solvent and as thin films (Figure 4.5). The absorption spectra of CSMs exhibit two distinct absorption bands, a higher energy band below 450 nm that could result from  $\pi$ - $\pi^*$  transitions whereas the lower-energy (450–750 nm) bands due to intramolecular charge transfer (ICT). The absorption maxima of **1**, **2**, and **3** in chloroform solutions at room temperature are 596, 591, and 647 nm respectively (Figure 4.5a). The absorption maximum of CSM **2** is 5 nm blue shifted than that of **1** while **3** shows a considerable (51 nm) red shift relative to that of **1**.

Thin film absorption spectra of CSMs **1**, **2**, and **3** are broader and 66, 81, and 85 nm red shifted compared to the solution-state spectra, presumably due to planarization of the conjugated backbone (Figure 4.5b). On thermal annealing of thin films of CSMs, a bathochromic shift in absorption spectra was observed for **1** and **2** but remain nearly unchanged for **3**. This could be due to the lack of further planarization of the conjugated

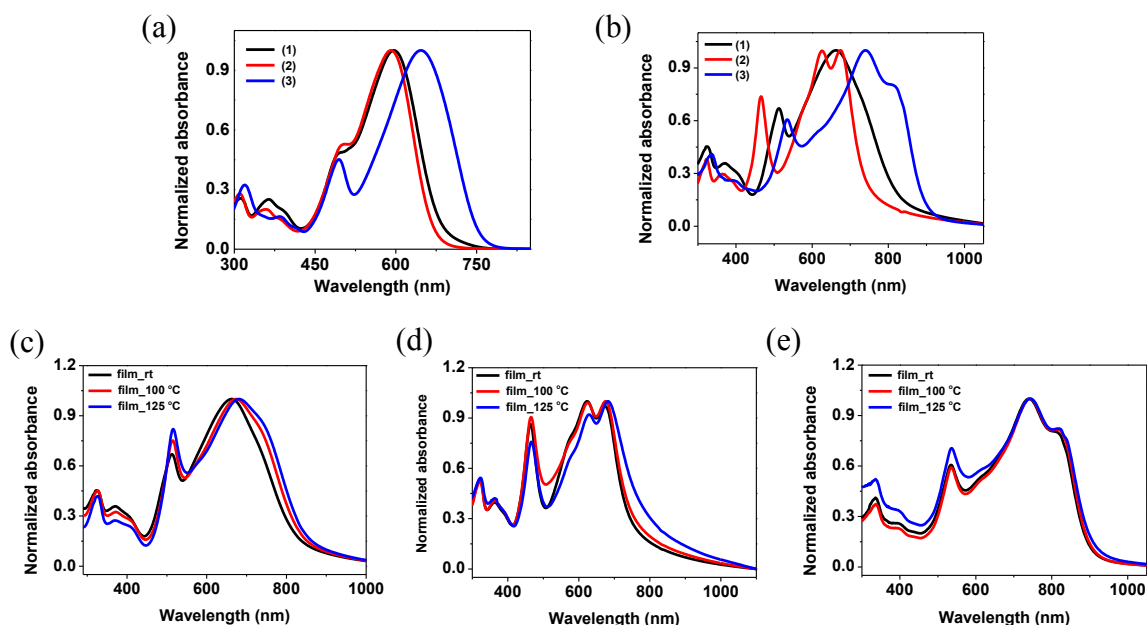


**Figure 4.5** UV-vis absorption spectra of CSMs (**1** – **3**) in dilute chloroform solution (a), as thin-film on quartz substrates (b), and of thermally annealed film (c) of **1**, (d) of **2**, and (e) of **3**.

backbone of **3**. Energy band gaps calculated from low energy absorption edges for **1**, **2**, and **3** are 1.46, 1.61, 1.36 eV respectively. Molecule **3** containing dimethyl BODIPY core has the lowest band gap among the CSMs (**1** – **3**). These observations (Table 4.2) are consistent with the computationally optimized geometries and estimated frontier molecular orbital energy levels.

**Table 4.2** Optical and electrochemical data for **1–3**.

Molecules	$\lambda_{\max}^{\text{sol}}$ (nm)	$\lambda_{\max}^{\text{Film}}$ (nm)	$\lambda_{\text{onset}}$ (nm)	$E_g^{\text{Optical}}$ (eV)	$E_{\text{ox, onset}}$ / HOMO(eV)	$E_{\text{red, onset}}$ /LUMO(eV)	$E_g^{\text{elect}}$ (eV)
<b>1</b>	596	662	850	1.46	0.39/-5.10	-1.40/-3.31	1.79
<b>2</b>	591	672	770	1.61	0.48/-5.19	-1.22/-3.49	1.70
<b>3</b>	647	732	910	1.36	0.36/-5.07	-1.14/-3.57	1.50

Cyclic voltammetry of CSMs (**1** – **3**) were recorded using CSMs coated Pt wire as working electrode, Ag/Ag<sup>+</sup> as a reference electrode and Pt foil as the counter electrode. The CVs were recorded by sweeping the working electrode potential in the anodic and cathodic segments in 0.1 M solution of tetrabutylammonium hexafluorophosphate in dry acetonitrile (Figure 4.6). The orbital energy levels with respect to vacuum level were determined by calibrating the oxidation and reduction onsets of CSMs using ferrocene as an internal standard.<sup>39</sup> The orbital energy level values and calculated energy band gaps are provided in

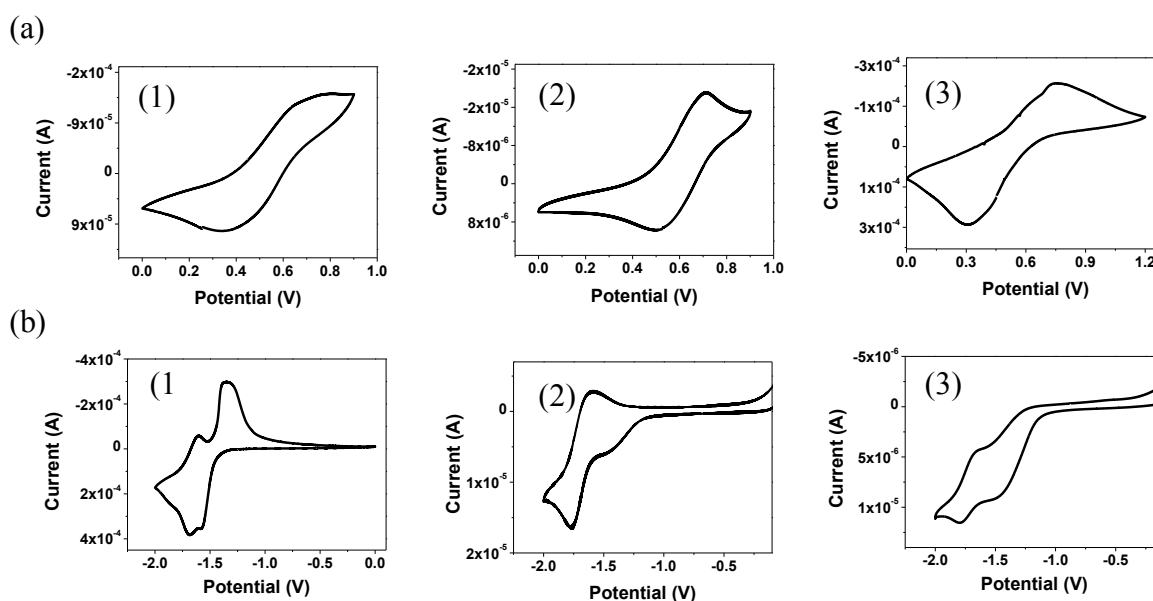


**Figure 4.6** Cyclic voltammograms of molecules **1** – **3**: (a) oxidation scan, (b) reduction scan.

Table 4.2. Similar to results obtained from computational and optical studies, energy level calculated from cyclic voltammetry show that among the CSMs (**1** – **3**), **3** has the lowest band gap. This could be attributed to deeper LUMO and HOMO energy levels of BODIPY **3** and lowest inter-ring torsion angles of CSM **3** compared to other two molecules.

#### 4.3.4 Thin Film Morphology

OTS (octyltrichlorosilane) modified SiO<sub>2</sub> surface was used to study the morphology of thin films as the same substrates were used for the fabrication of field effect transistors (FETs). CSMs (**1** – **3**) were spin coated on the substrate from chloroform solution (Figure 4.7a). Molecule **1** forms a continuous film with few pinholes. The film of **2** shows small domains throughout and discontinuity in the film. In comparison to CSM **1** and **2**, **3** forms smoother and continuous film without any pinholes. As these molecules have twisted conjugated backbone and long branched alkyl side chains, thermal annealing of thin films was done for planarization of the conjugated backbone and for better solid state

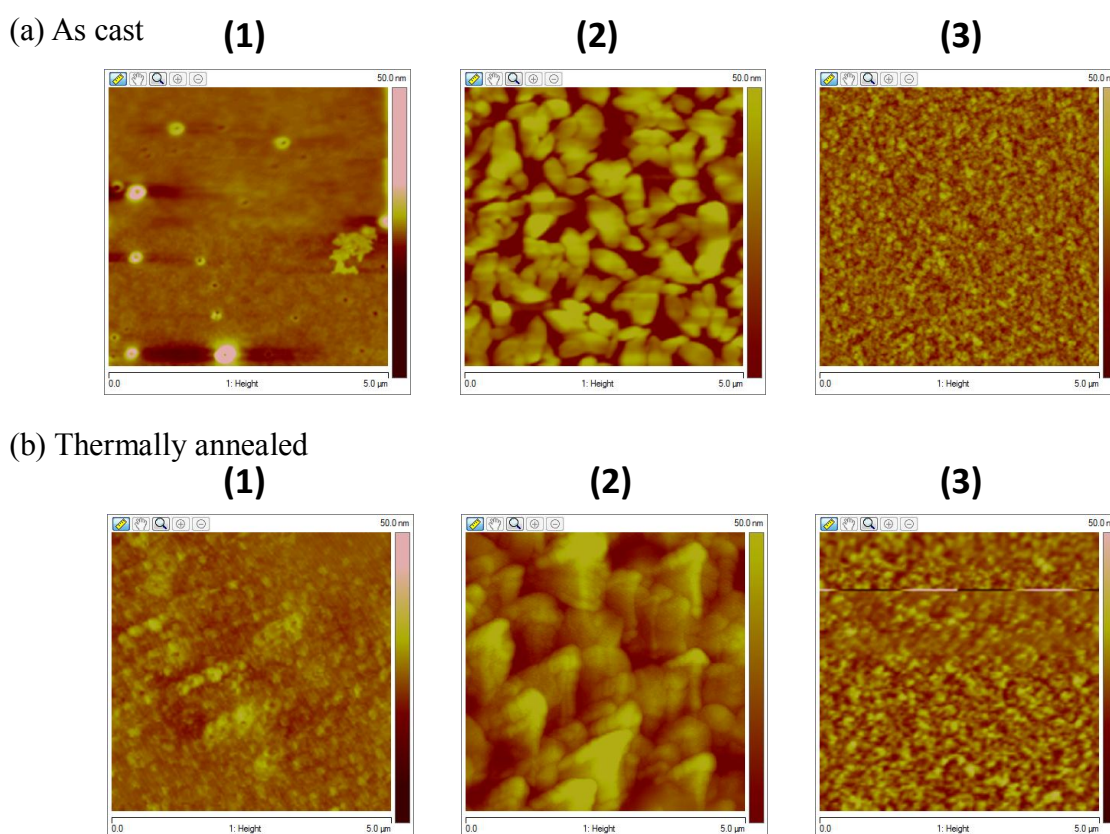


**Figure 4.7** AFM images of thin films of **1** – **3**: (a) As cast film, (b) Thermally annealed film.

packing. These films were thermally annealed at 125 °C and further morphological changes were studied (Figure 4.7b). The thin film of **1** develops small ring like structure throughout



and the possible reason can be due to the evaporation of trapped solvent on heating. Random lumps in thin film of **2** arrayed in triangular shapes upon thermal annealing and film becomes continuous, unlike pristine film. There was no significant effect of annealing for the film of **3**.

### 4.3.5 Characterization of Field-Effect Transistor Devices

Field effect transistors were fabricated using SiO<sub>2</sub> as a gate dielectric, heavily n doped Si as a gate electrode and gold as source and drain electrodes. The prefabricated substrate has a bottom gate, bottom contact configuration. These CSMs contains long branched alkyl chains, hence hydrophilic SiO<sub>2</sub> surface was modified using OTS (octyltrichlorosilane) for favourable contact between molecules and channels. In our studies, The CSMs were spin coated on top of the substrates from chloroform solutions. Output and transfer characteristic curves for device fabricated with as cast film of CSMs (**1** – **3**) are given in figure 4.8. Output characteristic curves were recorded by sweeping the drain voltage (V<sub>D</sub>) between 0 and –100V while keeping the gate voltage (V<sub>G</sub>) constant. The output characteristic curves showed standard linear and saturation regimes with a good gate modulation as a function of applied gate voltage (V<sub>G</sub>) (Figure 4.8a). Hole carrier mobilities are calculated using the standard saturation regime quadratic model equation  $\mu = I_{DS}/(V_{GS}-V_{th})^2 \times 2L/WC_{OX}$ . From the transfer characteristic curves, the threshold voltages for CSMs (**1** – **3**) are calculated (Figure 4.8b). Device data are given in table 4.3.

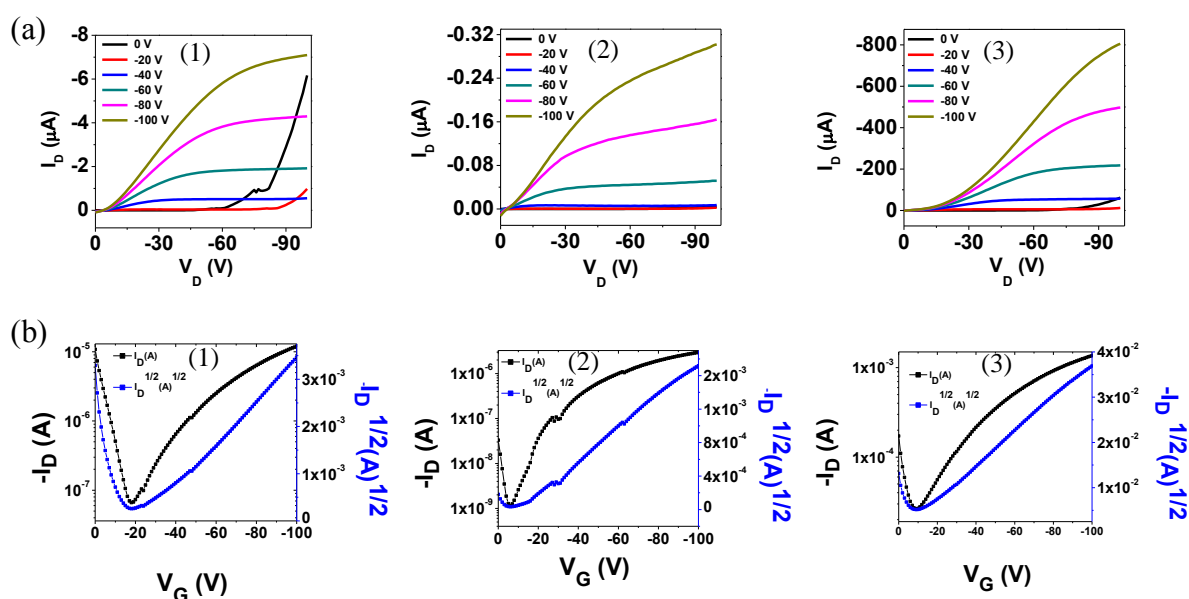


**Figure 4.8** (a) Output characteristic curves and (b) transfer characteristic curves of OFET devices of CSMs (**1** – **3**) for as cast film while measuring hole transport.

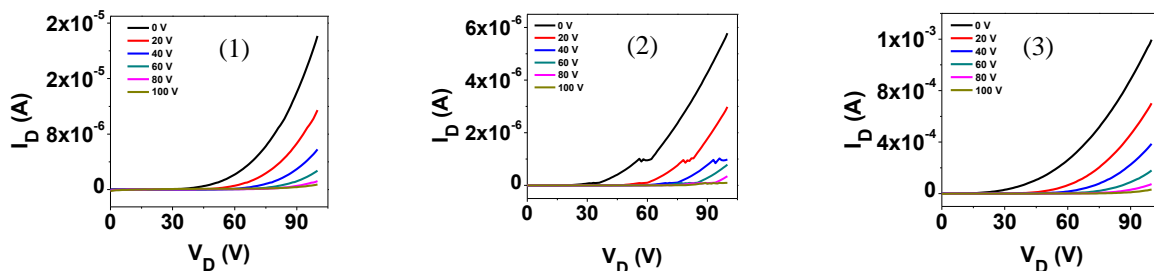


**Figure 4.9** Output characteristic curves for OFET devices of CSMs (1 – 3) while measuring electron transport.

Electron transport properties of these molecules were also studied as DFT calculations suggest that these molecules could be ambipolar in nature. Also, Output and transfer characteristic curves for negative sweep show a typical ambipolar nature. Output characteristic curves for CSMs (1 – 3), recorded while sweeping the drain voltage ( $V_D$ ) between 0 and 100V while applying a constant gate voltage ( $V_G$ ), did not show standard linear and saturation regimes (Figure 4.9). One possible reason could be the improper contact between the channel and the material coated. As the high work function gold source and drain electrodes are not very suitable for electron injection and  $\text{SiO}_2$  gate dielectric acts as an electron trap, it could be another possible reason for such behavior. Hole mobilities  $\mu_h$  for CSMs (1 – 3) are  $1.9 \times 10^{-4} \text{ cm}^2/\text{Vs}$ ,  $3.5 \times 10^{-5} \text{ cm}^2/\text{Vs}$ , and  $1.1 \times 10^{-2} \text{ cm}^2/\text{Vs}$ . Molecule 3, which has lowest energy band gap and lowest inter-ring torsion angle, calculated from theoretical and experimental studies, shows the highest hole mobility values amongst CSMs (1 – 3). OFET devices were thermally annealed at  $125^\circ \text{C}$  hoping that annealing would help

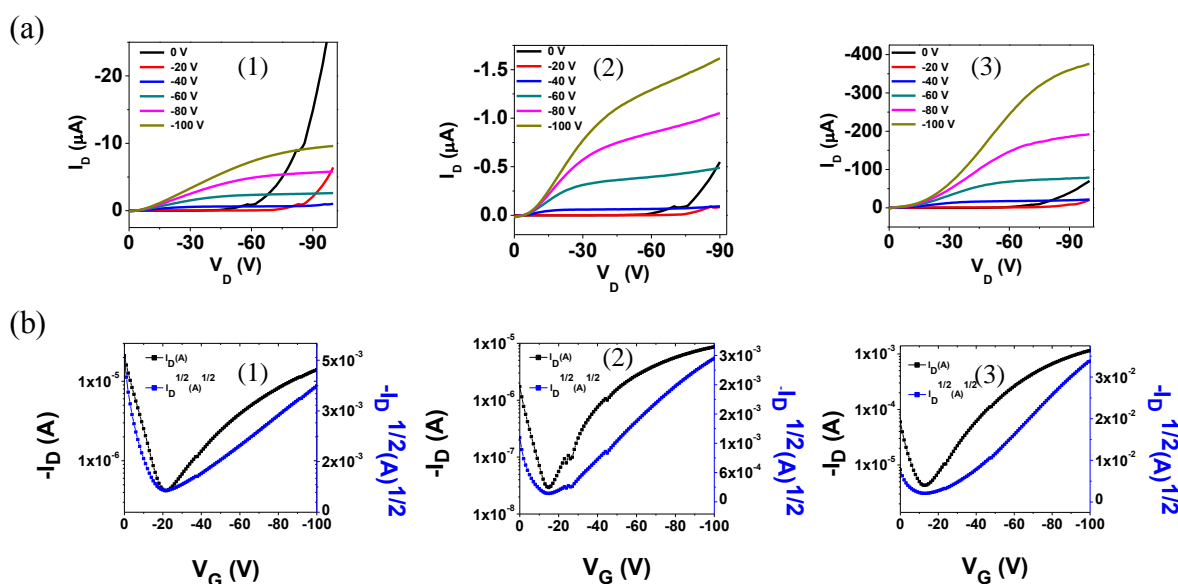


**Figure 4.10** (a) Output characteristic curves and (b) transfer characteristic curves of CSMs (1 – 3) for thermally annealed OFET devices while measuring hole transport.

further planarization of the twisted conjugated backbone, and better intermolecular connectivity and that in turn would improve charge carrier mobility values. For **1**, on thermal annealing, hole mobility remain nearly same and no standard output characteristics curves were observed for electron transport. Hole mobility of **2** improves by one order after annealing. Owing to the relatively planar backbone of **3**, thermal annealing did not impact hole transport much.

**Table 4.3** OFET device metrics of CSMs **1-3**.

Molecules	As cast film			After annealing at 125 °C		
	$\mu_h$ ( $\text{cm}^2\text{V}^{-1}\text{s}^{-1}$ ) ( $\mu_{\text{max}}$ )	$V_T$ (V)	$I_{\text{on/off}}$	$\mu_h$ ( $\text{cm}^2\text{V}^{-1}\text{s}^{-1}$ ) ( $\mu_{\text{max}}$ )	$V_T$ (V)	$I_{\text{on/off}}$
<b>1</b>	$1.7 \times 10^{-4}$ ( $1.9 \times 10^{-4}$ )	-21	$2 \times 10^2$	$1.6 \times 10^{-4}$ ( $2.0 \times 10^{-4}$ )	-15	40
<b>2</b>	$2.5 \times 10^{-5}$ ( $3.5 \times 10^{-5}$ )	-5.6	$3 \times 10^3$	$9.3 \times 10^{-5}$ ( $1.2 \times 10^{-4}$ )	-12	$3 \times 10^2$
<b>3</b>	$8.4 \times 10^{-3}$ ( $1.1 \times 10^{-2}$ )	-8	$10^2$	$1.0 \times 10^{-2}$ ( $1.3 \times 10^{-2}$ )	-15	$3 \times 10^2$

Since molten film of **2** forms crystalline structure on cooling, we thought of studying its OFET properties. **2** in powder form was allowed to melt on the FET channels and then slowly cooled down to the room temperature. Charge transport properties were calculated from output and transport characteristic curve (Figure 4.11). The output characteristic curves are linear, and obtained values, hole mobility ( $\mu_h = 4.2 \times 10^{-6} \text{ cm}^2/\text{Vs}$ ), threshold voltage ( $V_T$

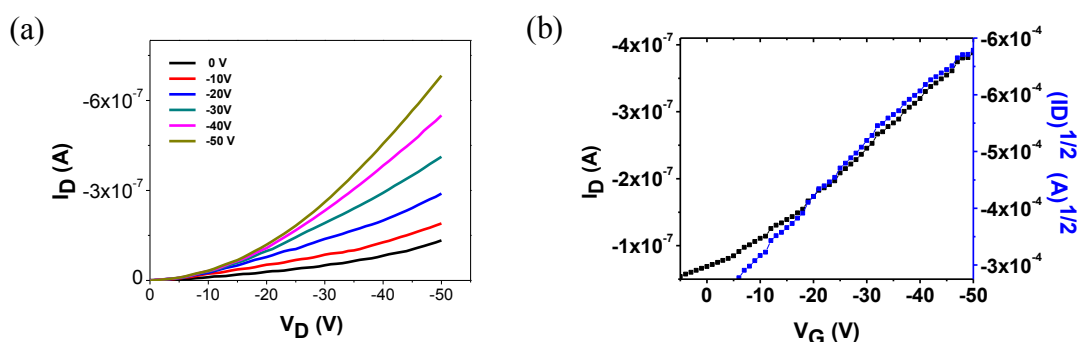


**Figure 4.11** Output characteristic curves and (a) transfer characteristic curves (b) of OFET device fabricated from molten film of **2**.

= -10 V), and  $I^{\text{on/off}}$  (11.3), are also lower than that of solution processed OFET. This observation shows that the OFET fabricated for **2** by solution processing method is better than that by solution free method.

#### 4.4 Summary

In summary, solution processable conjugated small molecules containing central planar DPP moiety and terminal BODIPY dyes were synthesized and characterized. Three types of BODIPY dyes (**1** – **3**) were selected with varying substitution on the core in order to improve solid state packing. Replacing phenyl ring with a methyl group at meso from BODIPY **1** to **2** resulted in slightly higher energy band gap in the corresponding CSM **2** as observed from DFT, optical and electrochemical studies. Furthermore, it degrades film quality as evident from the thin film morphology studies using AFM. Smoother and continuous film for **1** and small domain like structures in the thin film for **2**, demonstrates that phenyl ring helps in intermolecular interactions. CSM **3** with dimethyl BODIPY core and methyl group at meso position has deeper HOMO/LUMO energy levels, lowest band gap and most planar conjugated backbone amongst three. The absorption spectrum is broad and spans most of the visible spectrum (300 – 900 nm). OFET devices fabricated using these molecules exhibit hole transport. **3** shows highest mobility with a hole mobility of  $1.3 \times 10^{-2} \text{ cm}^2/\text{Vs}$ . This study demonstrates that careful combination of DPP and BODIPY subunits results in high performing molecules.

#### 4.5 References

- 1) Roncali, J. *Acc. Chem. Res.* **2009**, *42*, 1719.
- 2) Walker, B.; Kim, C.; Nguyen, T.-Q. *Chem. Mater.* **2011**, *23*, 470.
- 3) Sun, Y.; Welch, G. C.; Leong, W. L.; Takacs, C. J.; Bazan, G. C.; Heeger, A. J. *Nat. Mater.* **2012**, *11*, 44.
- 4) Hsu, W. P.; Levon, K.; Ho, K. S.; Myerson, A. S.; Kwei, T. K. *Macromolecules* **1993**, *26*, 1318.
- 5) Keg, P.; Lohani, A.; Fichou, D.; Lam, Y. M.; Wu, Y.; Ong, B. S.; Mhaisalkar, S. G. *Macromol. Rapid Commun.* **2008**, *29*, 1197.
- 6) Dodabalapur, A.; Torsi, L.; Katz, H. E. *Science* **1995**, 268.
- 7) Zeis, R.; Besnard, C.; Siegrist, T.; Schlockermann, C.; Chi, X.; Kloc, C. *Chem. Mater.* **2006**, *18*, 244.
- 8) Katz, H. E.; Torsi, L.; Dodabalapur, A. *Chem. Mater.* **1995**, *7*, 2235.

- 9) Lin, Y. Y.; Gundlach, D. J.; Nelson, S. F.; Jackson, T. N. *IEEE Electron Device Letters*. **1997**, 606.
- 10) Chen, H.; Guo, Y.; Yu, G.; Zhao, Y.; Zhang, J.; Gao, D.; Liu, H.; Liu, Y. *Adv. Mater.* **2012**, 24, 4618.
- 11) Nielsen, C. B.; Turbiez, M.; McCulloch, I. *Adv. Mater.* **2013**, 25, 1859.
- 12) Kim, H. G.; Kang, B.; Ko, H.; Lee, J.; Shin, J.; Cho, K. *Chem. Mater.* **2015**, 27, 829.
- 13) Park, J.-M.; Park, S. K.; Yoon, W. S.; Kim, J. H.; Kim, D. W.; Choi, T.-L.; Park, S. Y. *Macromolecules* **2016**, 49, 2985.
- 14) Zhang, G.; Fu, Y.; Xie, Z.; Zhang, Q. *Macromolecules* **2011**, 44, 1414.
- 15) Mei, J.; Graham, K. R.; Stalder, R.; Reynolds, J. R. *Org. Lett.* **2010**, 12, 660.
- 16) Mei, J.; Graham, K. R.; Stalder, R.; Reynolds, J. R. **2010**, 12, 660.
- 17) Zhan, X.; Facchetti, A.; Barlow, S.; Marks, T. J.; Ratner, M. A.; Wasielewski, M. R.; Marder, S. R. *Adv. Mater.* **2011**, 23, 268.
- 18) Forrest, S. R. *Chem. Rev.* **1997**, 97, 1793.
- 19) Zhang, C.; Zhang, X.; Zhang, X.; Ou, X.; Zhang, W.; Jie, J.; Chang, J. C.; Lee, C.-S.; Lee, S.-T. *Adv. Mater.* **2009**, 21, 4172–4175.
- 20) Kudo, K.; Yamashina, M.; Moriizumi, T. *Jpn. J. Appl. Phys.* **1984**, 23, 130.
- 21) Popere, B. C.; Della Pelle, A. M.; Thayumanavan, S. *Macromolecules* **2011**, 44, 4767.
- 22) Usta, H.; Yilmaz, M. D.; Avestro, A.-J.; Boudinet, D.; Denti, M.; Zhao, W.; Stoddart, J. F.; Facchetti, A. *Adv. Mater.* **2013**, 25, 4327.
- 23) Yoshii, R.; Yamane, H.; Nagai, A.; Tanaka, K.; Taka, H.; Kita, H.; Chujo, Y. *Macromolecules* **2014**, 47, 2316.
- 24) Debnath, S.; Singh, S.; Bedi, A.; Krishnamoorthy, K.; Zade, S. S. *J. Polym. Sci. A: Polym. Chem.* **2016**, 54, 1978.
- 25) Debnath, S.; Singh, S.; Bedi, A.; Krishnamoorthy, K.; Zade, S. S. *J. Phys. Chem. C* **2015**, 119, 15859.
- 26) Singh, S.; Venugopalan, V.; Krishnamoorthy, K. *Phys. Chem. Chem. Phys.* **2014**, 16, 13376.
- 27) Gsänger, M.; Bialas, D.; Huang, L.; Stolte, M.; Würthner, F. *Adv. Mater* **2016**, 28, 3615.
- 28) Lee, O. P.; Yiu, A. T.; Beaujuge, P. M.; Woo, C. H.; Holcombe, T. W.; Millstone, J. E.; Douglas, J. D.; Chen, M. S.; Fréchet, J. M. J. *Adv. Mater.* **2011**, 23, 5359.
- 29) Loudet, A.; Burgess, K. *Chem. Rev.* **2007**, 107, 4891.
- 30) Ulrich, G.; Ziessel, R.; Harriman, A. *Angew. Chem., Int. Ed.* **2008**, 47, 1184.

- 31) Kaur, M.; Choi, D. H. *Chem. Soc. Rev.* **2015**, *44*, 58.
- 32) Tamayo, A. B.; Tantiwiwat, M.; Walker, B.; Nguyen, T.-Q. *J. Phys. Chem. C* **2008**, *112*, 15543.
- 33) Bürgi, L.; Turbiez, M.; Pfeiffer, R.; Bienewald, F.; Kirner, H.-J.; Winnewisser, C. *Adv. Mater.* **2008**, *20*, 2217.
- 34) Bijleveld, J. C.; Zoombelt, A. P.; Mathijssen, S. G. J.; Wienk, M. M.; Turbiez, M.; de Leeuw, D. M.; Janssen, R. A. J. *J. Am. Chem. Soc.* **2009**, *131*, 16616.
- 35) Li, Y.; Sonar, P.; Singh, S. P.; Soh, M. S.; van Meurs, M.; Tan, J. *J. Am. Chem. Soc.* **2011**, *133*, 2198.
- 36) Lee, J.; Han, A.-R.; Yu, H.; Shin, T. J.; Yang, C.; Oh, J. H. *J. Am. Chem. Soc.* **2013**, *135*, 9540.
- 37) Kang, I.; Yun, H.-J.; Chung, D. S.; Kwon, S.-K.; Kim, Y.-H. *J. Am. Chem. Soc.* **2013**, *135*, 14896.
- 38) Burckstummer, H.; Weissenstein, A.; Bialas, D.; Wurthner, F. *J. Org. Chem.* **2011**, *76*, 2426.
- 39) Popere, B. C.; Pelle, A. M. D.; Poe, A.; Balaji, G.; Thayumanavan, S. *Chem. Sci.* **2012**, *3*, 3093.
- 40) Huo, L.; Hou, J.; Chen, H. Y.; Zhang, S.; Jiang, Y.; Chen, T. L.; Yang, Y. *Macromolecules* **2009**, *42*, 6564.
- 41) Zhu, S.; Dorh, N.; Zhang, J.; Vegesna, G.; Li, H.; Luo, F.-T.; Tiwari, A.; Liu, H. *J. Mater. Chem.* **2012**, *22*, 2781.
- 42) Sonar, P.; Ng, G.-M.; Lin, T. T.; Dodabalapur, A.; Chen, Z.-K. *J. Mater. Chem.* **2010**, *20*, 3626.
- 43) Tamayo, A. B.; Tantiwiwat, M.; Walker, B.; Nguyen, T.-Q. *J. Phys. Chem. C* **2008**, *112*, 15543.
- 44) Lei, T.; Dou, J.-H.; Ma, Z.-J.; Liu, C.-J.; Wang, J.-Y.; Pei, J. *Chem. Sci.* **2013**, *4*, 2447.
- 45) Gao, Y.; Zhang, X.; Tian, H.; Zhang, J.; Yan, D.; Geng, Y.; Wang, F. *Adv. Mater.* **2015**, *27*, 6753.
- 46) Hwang, H.; Khim, D.; Yun, J.-M.; Jung, E.; Jang, S.-Y.; Jang, Y. H.; Noh, Y.-Y.; Kim, D.-Y. *Adv. Funct. Mater.* **2015**, *25*, 1146.
- 47) Lin, G.; Qin, Y.; Zhang, J.; Guan, Y.-S.; Xu, H.; Xu, W.; Zhu, D. *J. Mater. Chem. C* **2016**, *4*, 4470.

## Chapter 5

# BODIPY based Copolymers as p- Channel and Ambipolar Semiconductors for Organic Field Effect Transistors

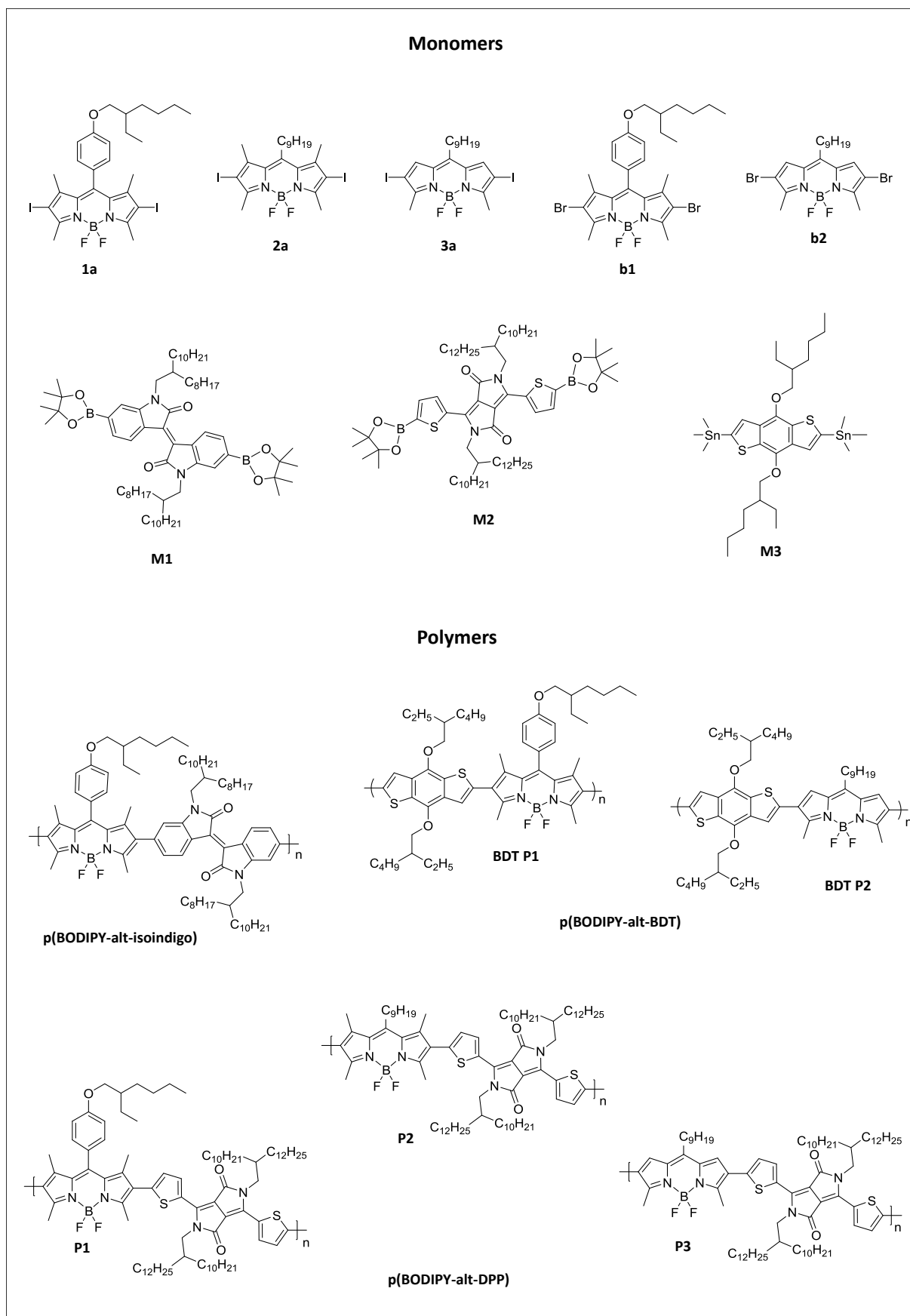
## 5.1 Introduction

Small molecule semiconductors are easy to purify, maintain batch to batch consistency and field effect transistors devices fabricated using them exhibit high charge carrier mobility values.<sup>1-3</sup> Such devices are generally fabricated by thermal evaporation techniques which is expensive and not suitable for making large area devices.<sup>4</sup> For making cost effective and large area devices, solution processing methods are preferred as flexible devices can be fabricated by roll to roll printing methods using organic solutions.<sup>5-7</sup> Linear and branched side chains are substituted on conjugated small molecules to enhance solubility in common organic solvents.<sup>8-12</sup> But, small molecule FET devices fabricated using solution processing methods often lag behind FETs based on polymeric materials. Polymers generally demonstrate better wettability on FET substrate and form uniform and smooth thin films and hence show better contact between channel and material. Though their molecular weight and polydispersity index (PDI) varies batch to batch, it affects device performance to some extent but not drastically.<sup>13-15</sup> Therefore, conjugated polymers have always been attractive option for development of organic electronics.

BODIPY based polymers are reported for different applications such as sensing, solar cells, biological labeling etc.<sup>16-21</sup> They are rarely attempted for OFET applications and charge transport properties have been moderate. BODIPY core can be conjugated either at  $\alpha$  or at  $\beta$  positions and substitutions on the core can also be varied. As unsubstituted BODIPY is unstable, substituents groups are chosen selectively.<sup>22-23</sup> First report of conjugated polymer containing this dye for OFET came in by Popere et al. where BODIPY was in the conjugation with other electron deficient moieties and obtained hole and electron mobility were in the range of  $10^{-5}$ .<sup>24</sup> Other p and n type polymers reported by different groups show mobility in the range of  $10^{-2}$  to  $10^{-8}$ .<sup>25-28</sup> Highest hole mobility so far is 0.17 reported by Usta et al.<sup>29</sup>

Previous chapters were focused on improvement of charge transport properties of BODIPY based small molecules. Side chains were varied and structural modulations were done on BODIPY core towards this endeavor. This work explores BODIPY based conjugated polymers for FET applications. BODIPY is connected with isoindigo, Diketopyrrolopyrrole (DPP), Benzodithiophenedione (BDT) monomers. These monomers are selected due to the difference in their electron affinity nature. Isoindigo<sup>30-32</sup> and DPP<sup>33-35</sup> dyes are electron deficient while BDT<sup>36-38</sup> is electron rich in nature. Three different types of conjugated polymers are designed and synthesized and their physical, thermal and electronic properties are studied. Chemical structure of BODIPY monomers and polymers are given in chart 5.1.





## 5.2. Experimental Section

### 5.2.1 Materials

2,4-dimethylpyrrole, 4-hydroxybenzaldehyde, 2-ethylhexyl bromide, pyrrole-2-carboxaldehyde, DDQ, boron trifluoride diethyletherate, N-iodosuccinimide, 6-bromooxindole, 6-bromoisatin, 2-octyl-1-dodecanol, Bis(pinacolato)diboron, 2-thiophenecarbonitrile, diethyl succinate, 2-decyl-1-tetradecanol, 2-isopropoxy-4,4,5,5-tetramethyl-1,3,2-dioxaborolane, n-butyllithium, diisopropylamine, thiophene-3-carboxylic acid, anhydrous N,N-dimethylformamide, and 1,4-dioxane were obtained from commercial sources and used directly as received. Tetrahydrofuran (THF) was passed through alumina and distilled over Na/benzophenone before use. Dry DCM and dry acetone were obtained from stirring and distillation over CaH<sub>2</sub> and K<sub>2</sub>CO<sub>3</sub> respectively.

### 5.2.2 Instrumentation Details

Cyclic voltammetry (CVs) experiments were performed on BioLogic Science Instruments. Polymers coated Pt wire was used as a working electrode, Ag/Ag<sup>+</sup> as a reference electrode and Pt foil as the counter electrode. CVs were recorded under inert condition in 0.1 M solution of tetrabutylammonium hexafluorophosphate in dry acetonitrile at a scan rate of 100 mV/s. E<sup>ox</sup> and E<sup>red</sup> are determined from the onset potential of oxidation and reduction waves. HOMO and LUMO energy levels were calculated following the equation  $E^{\text{HOMO}} = -(E^{\text{ox}} + 4.8)$  eV and  $E^{\text{LUMO}} = -(E^{\text{red}} - 4.8)$  eV, and calibrated with respect to the internal standard Fc/Fc<sup>+</sup> couple.

### 5.2.3 Device Fabrication (OFET)

Bottom-gate bottom-contact field-effect transistors substrates were purchased from Fraunhofer IPMS (interdigitated S/D electrodes), with channel lengths (L) 2.5, 5, 10 and 20 μm and channel width (W) of 10 mm. Cleaning of prefabricated FET substrates were done with acetone followed by isopropanol, and dried by heat gun. The device fabrication and measurements were done inside argon filled glove box. Modification of SiO<sub>2</sub> surface was done using a chloroform solution of OTS (octadecyltrichlorosilane). Thin films were prepared by spin-coating (concentration  $\cong$  10 mg/mL in chloroform, 1500 rpm for 60 seconds). OFET measurements were performed on Agilent 4156C semiconductor probe

analyzer and semi probe station. Charge carrier mobilities were calculated using the standard saturation regime quadratic model equation  $\mu = I_{DS}/(V_{GS}-V_{th})^2 \times 2L/WC_{OX}$ .

#### 5.2.4 Synthetic Procedures and Characterization Data

- Synthesis route of 2,6-diiodoBODIPY, 1a is described earlier in the chapter 2, and that of 2a and 3a are given in the chapter 3.
- Synthesis of DPP was carried out by following procedure reported previously.<sup>39</sup>

##### i) BODIPY Monomer synthesis:

**2,6-diiodo-BODIPY 1a:** <sup>1</sup>H NMR (400 MHz, CDCl<sub>3</sub>) δ: 7.11 (d, *J* = 8.60 Hz, 2 H), 7.02 (d, *J* = 8.60 Hz, 2 H), 3.91 (d, *J* = 5.87, 2 H), 2.64 (s, 6 H), 1.78 (m, 1 H), 1.45 (s, 6 H), 1.35 (m, 8 H), 0.94 (m, 6 H); <sup>13</sup>C NMR (100 MHz, CDCl<sub>3</sub>) δ: 160.36, 156.46, 145.38, 141.78, 131.73, 128.97, 126.34, 115.44, 85.49, 70.90, 39.35, 30.50, 29.11, 23.84, 23.02, 17.18, 15.98, 14.09, 11.14. MALDI-TOF/TOF: M<sup>+</sup> (C<sub>27</sub>H<sub>33</sub>BF<sub>2</sub>I<sub>2</sub>N<sub>2</sub>O) calcd m/z = 704.0743, found m/z = 704.1264. Yield 80%.

**2,6-diiodo-BODIPY 2a:** <sup>1</sup>H NMR (400 MHz, CDCl<sub>3</sub>) δ: 3.00 (t, *J* = 8.8 Hz, 2H), 2.61 (s, 6H), 2.48 (s, 6H), 1.61(m, 2H), 1.50 (p, *J* = 7.3 Hz, 2H), 1.27 (m, 10H), 0.89 (t, *J* = 6.85 Hz, 3H); <sup>13</sup>C NMR (100 MHz, CDCl<sub>3</sub>) δ: 155.14, 146.40, 142.20, 131.34, 86.35, 31.80, 31.66, 30.29, 29.47, 29.37, 29.30, 29.22, 22.63, 18.93, 16.09, 14.09. MALDI-TOF/TOF: M<sup>+</sup> (C<sub>22</sub>H<sub>31</sub>BF<sub>2</sub>I<sub>2</sub>N<sub>2</sub>) calcd m/z = 626.0638, found m/z = 626.1882. Yield 54%.

##### **2,6-diiodo-BODIPY 3a:**

<sup>1</sup>H NMR (400 MHz, CDCl<sub>3</sub>) δ: 7.29 (s, 2H), 2.71 (t, *J* = 8.07 Hz, 2H), 2.61 (s, 6H), 1.69 (p, *J* = 7.58 Hz, 2H), 1.39 (p, *J* = 7.56 Hz, 2H), 1.27 (m, 10H), 0.89 (t, *J* = 7.02 Hz, 3H); <sup>13</sup>C NMR (100 MHz, CDCl<sub>3</sub>) δ: 157.74, 144.67, 135.27, 133.34, 33.79, 31.80, 30.51, 30.03, 29.38, 29.25, 29.23, 22.63, 15.34, 14.09. MALDI-TOF/TOF: M<sup>+</sup> (C<sub>20</sub>H<sub>27</sub>BF<sub>2</sub>I<sub>2</sub>N<sub>2</sub>) calcd m/z = 598.0325, found m/z = 598.1432. Yield 56%.

**2,6-dibromo-BODIPY b1:** A solution of N-bromosuccinimide (396 mg, 2.23 mmol) in dichloromethane (10 mL) was added dropwise to a solution of BODIPY 1 (420 mg, 0.93 mmol) in DMF/ DCM (20 mL/ 20 mL) under an inert atmosphere. The reaction mixture was

stirred at room temperature for 1 h, washed with water and extracted with dichloromethane. The organic phase was dried over  $\text{Na}_2\text{SO}_4$ . After removal of solvent under reduced pressure, the crude product was purified by silica gel column chromatography (eluent: DCM/pet. ether) to furnish shiny red solid compound **b1** (400 mg, 71%).  $^1\text{H}$  NMR ( $\text{CDCl}_3$ )  $\delta$ : 7.12 (d,  $J = 8.4$  Hz, 2H), 7.03 (d,  $J = 8.4$  Hz, 2H), 3.91 (d,  $J = 5.36$  Hz, 2H), 2.59 (s, 6H), 1.81-1.73 (m, 1H), 1.54-1.44 (m, 4H), 1.43 (s, 6H), 1.37-1.31 (m, 4H), 0.98-0.86 (m, 6H).  $^{13}\text{C}$  NMR (100 MHz,  $\text{CDCl}_3$ ):  $\delta$  160.3, 153.6, 142.5, 140.6, 130.8, 128.9, 125.9, 115.4, 111.5, 70.8, 39.3, 30.5, 29.6, 29.1, 23.8, 23.0, 13.9, 13.6, 11.1.

**2,6-dibromo-BODIPY b2:** Following the procedure for compound **b1**, using BODIPY 3 (200 mg, 0.58 mmol), Compound **b2** (220 mg, 75%) was synthesized.  $^1\text{H}$  NMR (400 MHz,  $\text{CDCl}_3$ )  $\delta$ : 7.15 (s, 2H), 2.72 (t,  $J=7.80$  Hz, 2H), 2.58 (s, 6H), 1.70 (m, 2H), 1.40 (m, 2H), 1.27 (m, 10H), 0.88 (t,  $J=7.75$  Hz, 3H).

## ii) Isoindigo monomer synthesis:

**6,6'-dibromoisindigo a:** To a suspension of 6-bromooxindole (500 mg, 2.36 mmol) and 6-bromoisatin (533 mg, 2.36 mmol) in AcOH (15 mL), conc. HCl solution (0.1 ml) was added and reaction mixture was refluxed for 24 h. The reaction mixture was allowed to cool to room temperature and filtered. The solid material was washed with water, EtOH and AcOEt. After drying under vacuum, it yielded brown 6,6-dibromoisindigo (810 mg, 80%). Obtained product was used as such for next step without further purification.

**6,6'-(N,N'-2-octyldodecyl)-dibromoisindigo b:** To a suspension of 6,6'-dibromoisindigo (700 mg, 1.67 mmol) and potassium carbonate (1.4 g, 10 mmol) in DMF (30 mL), 2-octyl-iodododecane (2.0 g, 5 mmol) was injected through a septum under argon. The reaction mixture was stirred for 15 h at 100 °C and then poured into water (200 mL). The organic phase was extracted by  $\text{CH}_2\text{Cl}_2$ , washed with brine and dried over  $\text{Na}_2\text{SO}_4$ . After removal of the solvent under reduced pressure, the crude product was purified by silica gel column chromatography (eluent: EtOAc/pet.ether) to furnish **b** (1.10 g, 70 %) as dark red solids.  $^1\text{H}$  NMR ( $\text{CDCl}_3$ )  $\delta$ : 9.04 (d,  $J = 9$  Hz, 2H), 7.14 (dd,  $J = 9$  Hz,  $J_2 = 1.8$  Hz, 2H), 6.83 (d,  $J = 1.8$  Hz, 2H), 3.56 (d,  $J = 7.5$  Hz, 4H), 1.83 (m, 2H), 1.40-1.24 (m, 64H), 0.88-0.84 (m, 12H).

**6,6'-(N,N'-2-octyldodecyl)-pinacoldiboronisoindigo M1:** 6,6'-(N,N'-2-octyldodecyl)-dibromoisoindigo (980 mg, 1.0 mmol), pinacol ester of diboron (760 mg, 3 mmol), [Pd(dppf)Cl<sub>2</sub>] (55 mg), and potassium acetate (590 mg, 6 mmol) were taken under an argon atmosphere. Anhydrous 1,4-dioxane (10 mL) was injected to the reaction mixture via a syringe through a septum. The solution was heated at 80 °C for 30 h and then cooled to room temperature. The reaction mixture was passed through a short pad of silica gel and washed by a mixture of CH<sub>2</sub>Cl<sub>2</sub> and hexane (1:1). The collected organic part was concentrated and precipitated into cold methanol. The product was filtered and dried to furnish a dark red shiny powder **M1** (750 mg, 70%). <sup>1</sup>H NMR (CDCl<sub>3</sub>) δ: 9.15 (d, J = 7.2 Hz, 2H), 7.48 (d, J<sub>1</sub> = 8.1 Hz, J<sub>2</sub> = 0.6 Hz, 2H), 7.15 (d, J = 0.6 Hz, 2H), 3.70 (d, J = 7.5 Hz, 2H), 1.95 (m, 2H), 1.59-1.19 (m, 86H), 0.85 (t, J = 6.6 Hz, 6H).

### iii) DPP monomer synthesis:

**2,5-bis(2-decyltetradecyl)-3,6-di(thiophen-2-yl)-2,5-dihydropyrrolo[3,4-c]pyrrole-1,4-dione D1:** To a solution of DPP (1.2 g, 4 mmol) and anhydrous potassium carbonate (5.52 g, 40 mmol) in 50 mL of N,N-dimethylformamide, 1-Iodo-2-decyltetradecane (6.96 g, 15 mmol) was injected by syringe under argon protection. The reaction mixture was stirred for 20 h at 110 °C, cooled to room temperature, and then poured into water. Organic phase was extracted with CH<sub>2</sub>Cl<sub>2</sub>, washed with brine and dried over anhydrous Na<sub>2</sub>SO<sub>4</sub>. After removal of solvent under reduced pressure, the crude product was purified by silica gel column chromatography (eluent: EtOAc/pet.ether) to furnish red solid compound **D1** (1.95 g, 50%). <sup>1</sup>H NMR (200 MHz, CDCl<sub>3</sub>) δ: 8.87 (dd, J=1.0 Hz, 3.9 Hz, 2H), 7.62 (dd, J=1.1 Hz, 5.1 Hz, 2H), 7.26 (dd, J=3.9 Hz, 5.0 Hz, 2H), 4.01 (d, J=7.6 Hz, 4H), 1.90 (m, 2H), 1.22 (m, 80 H), 0.87 (m, 12 H). <sup>13</sup>C NMR (100 MHz, CDCl<sub>3</sub>) δ: 161.72, 140.40, 135.20, 130.42, 129.83, 128.36, 107.92, 46.20, 37.73, 31.92, 31.18, 30.00, 29.69, 29.64, 29.55, 29.36, 26.20, 22.68, 14.11.

**2,5-bis(2-decyltetradecyl)-3,6-bis(5-(4,4,5,5-tetramethyl-1,3,2-dioxaborolan-2-yl)thiophen-2-yl)-2,5-dihydropyrrolo[3,4-c]pyrrole-1,4-dione M2:** LDA solution was prepared by adding n-butyllithium in n-hexane (1.52 mL, 3.8 mmol) slowly at 0 °C to diisopropylamine (0.67 mL, 4.8 mmol) in 20 mL of dry THF under argon atmosphere. This freshly prepared LDA solution was added within 15 min to the THF (10 mL) solution of D1

(1.56 g, 1.6 mmol) and 2-isopropoxy-4,4,5,5-tetramethyl-1,3,2-dioxaborolane (1.31 mL, 6.4 mmol) at -25 °C. After 2 h of stirring at 0 °C, the reaction was quenched with 10 mL of 1 M HCl solution. Organic layer was extracted with chloroform and concentrated under reduced pressure. The residue was dissolved in dichloromethane, and the solution was poured into 400 mL of cold acetone under vigorous stirring. Product was filtered off and washed with cold acetone to afford **M2** (1.10 g, 56%) as a pink solid. <sup>1</sup>H NMR (400 MHz, CDCl<sub>3</sub>) δ: 8.90 (d, *J* = 3.9 Hz, 2H), 7.70 (d, *J* = 3.9 Hz, 2H), 4.04 (d, *J* = 7.6 Hz, 4H), 1.89 (m, 2H), 1.36 (s, 24H), 1.25 (m, 80H), 0.87 (m, 12H), <sup>13</sup>C NMR (100 MHz, CDCl<sub>3</sub>) δ: 161.75, 140.52, 137.66, 136.15, 135.66, 108.72, 84.58, 46.26, 37.78, 31.93, 31.28, 30.03, 29.64, 29.60, 29.37, 26.34, 24.77, 22.70, 14.13. MALDI-TOF/TOF: M<sup>+</sup> (C<sub>74</sub>H<sub>126</sub>B<sub>2</sub>N<sub>2</sub>O<sub>6</sub>S<sub>2</sub>) calcd m/z = 1224.9243, found m/z = 1224.1948.

#### iv) BDT monomer synthesis:

##### Thiophene-3-carbonyl chloride 1:

To a solution of thiophene-3-carboxylic acid (10 g, 78.03 mmol) in dichloromethane, oxalyl chloride (20.1 g, 13.7 mL, and 158.66 mmol) was added dropwise at 0 °C under an inert atmosphere. Reaction mixture was stirred at 0 °C for 30 min and then warm to room temperature and further stirred overnight. Unreacted oxalyl chloride and solvent was removed under high vacuum. Thiophene-3-carbonyl chloride was obtained as a colourless solid and was used in the next reaction without further purification.

**N,N-diethylthiophene-3-carboxamide 2:** A solution of thiophene-3-carbonyl chloride (11.1 g, 75.71 mmol) in dichloromethane was kept at 0 °C for 15 min. To this, diethylamine (12.5 g, 17.0 mL 171.20 mmol) in dichloromethane (30 mL) was added over a period of 15 min. Then the reaction mixture was brought to room temperature and further stirred for 30 min. It was then diluted with dichloromethane and washed with water. Organic phase was dried over anhydrous Na<sub>2</sub>SO<sub>4</sub> and concentrated under reduced pressure to afford the required product as a pale yellow oil (11.8 g, 85%). <sup>1</sup>H NMR (CDCl<sub>3</sub>, 200 MHz): δ, 7.47 (dd, 1H), 7.32 (dd, 1H), 7.18 (dd, 1H), 3.43 (q, 4H), 1.19 (t, 6H); <sup>13</sup>C NMR (CDCl<sub>3</sub>, 50 MHz) δ: 166.2, 137.0, 126.4, 125.4, 124.7, 42.8, 39.3, 14.1, 12.6.

**Benzo[1,2-b:4,5-b']dithiophene-4,8-dione 3:** N,N-diethylthiophene-3-carboxamide (8.7 g, 47.52 mmol) was dissolved in anhydrous THF (50 mL) under an inert atmosphere and the reaction mixture was cooled down to 0 °C. *n*-butyl lithium (19.0 mL, 47.52 mmol, 2.5 M in hexane) was added drop wise to the solution via syringe. Then, the reaction was stirred at ambient temperature for 1 h. After that, the reaction mixture was poured into ice water (60 mL) and stirred for several hours. The yellow-green precipitate was filtered, washed with water (100 mL), methanol (50 mL), and hexane (50 mL) and dried under high vacuum to afford the yellow-green solid **3** (4.0 g, 77 %), <sup>1</sup>H NMR (CDCl<sub>3</sub>, 200 MHz) δ: 7.68 (d, 2H), 7.64 (d, 2H).

**4,8-bis((2-ethylhexyl)oxy)benzo[1,2-b:4,5-b']dithiophene 4:**

Compound **3** (1.0 g, 4.54 mmol), zinc dust (0.653 g, 10.0 mmol), NaOH (2.72 g, 68.1 mmol) and 20 mL of water were taken in a two neck round bottom flask and refluxed for 2 h. During the reflux, the colour of the reaction mixture changed from yellow to orange. The reaction mixture was cooled to room temperature and to it, tetrabutylammonium bromide (0.150 g, 0.465 mmol) and 2-ethylhexyl bromide (3.23 mL, 3.51 g, 18.2 mmol) were added and mixture was then further refluxed overnight. The reaction mixture was poured into ice water and extracted with CH<sub>2</sub>Cl<sub>2</sub>. The combined organic layers were dried with anhydrous Na<sub>2</sub>SO<sub>4</sub>, concentrated under reduced pressure and purified by column chromatography using pet ether as the eluent to afford the required compound as pale yellow liquid (1.74 g, 86%) <sup>1</sup>H NMR (CDCl<sub>3</sub>, 200 MHz) δ: 7.46 (d, 2H), 7.35 (d, 2H) 4.18 (d, 4H) 1.62-1.50 (m, 2H), 1.38-1.10 (m, 16H), 0.90-0.72 (m, 12H).

**4,8-bis((2-ethylhexyl)oxy)benzo[1,2-b:4,5-b']dithiophene-2,6-diylbis(trimethylstannane)**

**M3:** compound **4** (1.0 g, 2.24 mmol) was dissolved in 25 mL of anhydrous THF under an inert atmosphere. Reaction mixture was cooled down to -78 °C and to it, *n*-butyl lithium (2.33 mL, 5.82 mmol, 2.5 M solution in hexane,) was added dropwise and then reaction was stirred for 1 h. while maintaining the temperature at -78 °C, Trimethyltinchloride (1.79 g, 8.96 mmol) solution in 25 mL anhydrous THF was added slowly to the reaction mixture. After that, the mixture was stirred overnight at room temperature. The reaction mixture was poured into ice-cold water and extracted with diethyl ether dried over anhydrous Na<sub>2</sub>SO<sub>4</sub> and evaporated to dryness in vacuum. Recrystallization of the crude product from ethanol afforded the compound **M3** as colourless needles (1.2 g, 70%). <sup>1</sup>H NMR (CDCl<sub>3</sub>, 200 MHz)

$\delta$ : 7.52 (s, 2H), 4.19 (d, 4H), 1.82 (m, 2H), 1.74-1.25 (m, 18H), 1.10-0.90 (m, 12H),  $\delta$  0.45 (s, 18H).

#### v) Polymer synthesis

**Synthesis of Polymer p(BODIPY-*alt*-isoindigo):** 2,6-DiiodoBODIPY 1a (70 mg, 0.1 mmol), 6,6'-(N,N'-2-octyldodecyl)-pinacoldiboron-isoindigo M1 (107 mg, 0.1 mmol), Pd(dppf)Cl<sub>2</sub> (3.0 mg) and Na<sub>2</sub>CO<sub>3</sub> (105 mg, 1 mmol) were taken in a schlenk tube, and was evacuated and back-filled with argon three times. A degassed solvent mixture of toluene (12 mL), ethanol (4 mL) and water (6 mL) was transferred to the schlenk tube through a septum, and the reaction mixture was purged with argon for 15 min. The mixture was stirred at 85 °C under a nitrogen atmosphere for 12 h. After removal of the solvent, the residue was dissolved in ethyl acetate and washed with water twice. The organic layer was collected, dried over anhydrous Na<sub>2</sub>SO<sub>4</sub>, and filtered. The filtrate was concentrated under reduced pressure and precipitated into cold methanol. Crude polymer was subjected to soxhlet extraction with methanol to remove catalyst, acetone to remove monomers and oligomers from polymer and finally with chloroform to collect polymer in pure form (90 mg, 70%). <sup>1</sup>H NMR (200 MHz, CDCl<sub>3</sub>)  $\delta$ : 9.14 (d, 2H), 7.16 (d, 2H), 7.01 (d, 2H), 6.83 (d, 2H), 6.58 (d, 2H), 3.88 (d, 2H), 3.64 (br, 4H), 1.88-1.76 (br, 3 H), 1.22 (br), 0.85 (br), GPC (RT in THF): M<sub>n</sub> = 16509 g·mol<sup>-1</sup>, M<sub>w</sub> = 37547 g·mol<sup>-1</sup>, and PDI = 2.27 (against PS standard).

**Synthesis of Polymer p(BODIPY-*alt*-DPP) P1:** 1a (115 mg, 0.16 mmol), M2 (200 mg, 0.16 mmol), Pd(dppf)Cl<sub>2</sub> (13 mg) and Na<sub>2</sub>CO<sub>3</sub> (171.2 mg, 1.63 mmol) were taken in a schlenk tube, and was evacuated and back-filled with argon three times. A degassed solvent mixture of toluene (26 mL), ethanol (10 mL) and water (14 mL) was transferred to the schlenk tube through a septum, and the reaction mixture was purged with argon for 15 min. The reaction was carried out at 85 °C for 12 h under argon atmosphere, and then end capping was done by adding monoiodobodipy, stirred for 30 min, followed by addition of 2-thienylboronic acid, and the reaction was continued for another 1 h. After completion, the reaction mixture was washed once with water, dried over anhydrous Na<sub>2</sub>SO<sub>4</sub>, and then the organic layer was passed through celite to remove metal catalyst. After removal of solvent under reduced pressure, the residue was dissolved in 20 mL of chloroform, and the solution was poured slowly into 250 mL of cold methanol under vigorous stirring. After 15 min of stirring, the polymer was



collected by vacuum filtration. The crude polymer was purified by sequential soxhlet extraction with methanol, acetone, to remove catalyst residue and low molecular weight species, acetone/ chloroform mixture to remove oligomers and lower molecular weight polymers, and finally with chloroform. The volume of chloroform fraction was reduced and was poured slowly into cold methanol to precipitate final 130 mg (57%) of dark blue solid polymer **P1**.  $^1\text{H NMR}$  (400 MHz,  $\text{CDCl}_3$ )  $\delta$ : 8.97 (s, 2H), 7.21 (br, 2H), 7.04 (br, 4H), 4.01 (br, 4H), 3.91 (br, 2 H), 2.69 (s, 6H), 1.95 (br, 2 H), 1.77 (m, 1 H), 1.54 (s, 6H), 1.40- 1.20 (br), 1.00-0.85(br), GPC (RT in  $\text{CHCl}_3$ ):  $M_n = 11700 \text{ g}\cdot\text{mol}^{-1}$ ,  $M_w = 32400 \text{ g}\cdot\text{mol}^{-1}$ , and PDI = 2.77 (against PS standard).

**Synthesis of Polymer p(BODIPY-*alt*-DPP) P2:** Following the procedure for polymer P1, using 2a (102 mg, 0.16 mmol), M2 (200 mg, 0.16 mmol), Pd(dppf) $\text{Cl}_2$  (13 mg) and  $\text{Na}_2\text{CO}_3$  (171.2 mg, 1.63 mmol), polymer **P2** (150 mg, 69%) was synthesized.  $^1\text{H NMR}$  (400 MHz,  $\text{CDCl}_3$ )  $\delta$ : : 9.02 (s, 2H), 7.12 (s, 2H), 4.06 (br, 4H), 3.12 (br, 2 H), 2.64 (s, 6H), 2.52 (s, 6 H), 2.00 (br, 2 H), 1.72 (m, 2 H), 1.23 (br), 0.87(br), GPC (RT in  $\text{CHCl}_3$ ):  $M_n = 19700 \text{ g}\cdot\text{mol}^{-1}$ ,  $M_w = 48600 \text{ g}\cdot\text{mol}^{-1}$ , and PDI = 2.46 (against PS standard).

**Synthesis of Polymer p(BODIPY-*alt*-DPP) P3:** Following the procedure for polymer P1, using 3a (100 mg, 0.17 mmol), M2 (204 mg, 0.17 mmol), Pd(dppf) $\text{Cl}_2$  (14 mg) and  $\text{Na}_2\text{CO}_3$  (178.5 mg, 1.7 mmol), polymer **P3** (110 mg, 49%) was synthesized.  $^1\text{H NMR}$  (400 MHz,  $\text{CDCl}_3$ )  $\delta$ : 9.16 (br), 7.00(br), 4.07 (br), 2.88(br), 1.97 (br), 1.22 (m), 0.87 (br), GPC (RT in  $\text{CHCl}_3$ ):  $M_n = 18800 \text{ g}\cdot\text{mol}^{-1}$ ,  $M_w = 80500 \text{ g}\cdot\text{mol}^{-1}$ , and PDI = 4.27 (against PS standard).

**Synthesis of Polymer p(BODIPY-*alt*-BDT) BDT P1:** b1 (122 mg, 0.2 mmol), bistannyl-functionalized BDT monomer M3 (154 mg, 0.2 mmol) and Pd( $\text{PPh}_3$ ) $_4$  (23 mg, 10 mol %) were taken in a schlenk tube, and the tube was evacuated and back-filled with argon three times. 10 mL of the degassed toluene was added to the reaction mixture through a septum, and the reaction was carried out at 90 °C for 16 h. After completion, reaction mixture was poured into cold MeOH. After stirring for 1 h, crude polymer was collected by vacuum filtration and it was subjected to soxhlet extraction with methanol to remove catalyst, acetone to remove monomers and oligomers from polymer and finally with chloroform. Chloroform solution was precipitated into cold MeOH with vigorous stirring. The extraction and precipitation procedure was repeated once. The final pure polymer was collected by vacuum

filtration and dried under reduced pressure (55 mg, 30%).  $^1\text{H}$  NMR (400 MHz,  $\text{CDCl}_3$ )  $\delta$ : 7.66 (br), 7.23 (br), 7.21 (br), 7.07 (br), 4.19 (br), 3.92 (br), 2.73 (m), 2.66 (br), 1.80 (m), 1.49 – 1.28 (m), 1.12 – 0.79 (m), GPC (RT in THF):  $M_n = 6680 \text{ g}\cdot\text{mol}^{-1}$ ,  $M_w = 8890 \text{ g}\cdot\text{mol}^{-1}$ , and PDI = 1.33 (against PS standard).

**Synthesis of Polymer p(BODIPY-*alt*-BDT) BDT P2:** Following the procedure for polymer BDT P1, using b2 (100 mg, 0.2 mmol), M3 (154 mg, 0.2 mmol), and  $\text{Pd}(\text{PPh}_3)_4$  (23 mg, 10 mol %) polymer **BDT P2** (40 mg, 25%) was synthesized.  $^1\text{H}$  NMR (400 MHz,  $\text{CDCl}_3$ )  $\delta$ : 7.74 (br), 7.47 (br), 4.24 (br), 2.95 (br), 2.04 – 0.63 (br), GPC (RT in  $\text{CHCl}_3$ ):  $M_n = 5000 \text{ g}\cdot\text{mol}^{-1}$ ,  $M_w = 23000 \text{ g}\cdot\text{mol}^{-1}$ , and PDI = 4.61 (against PS standard).

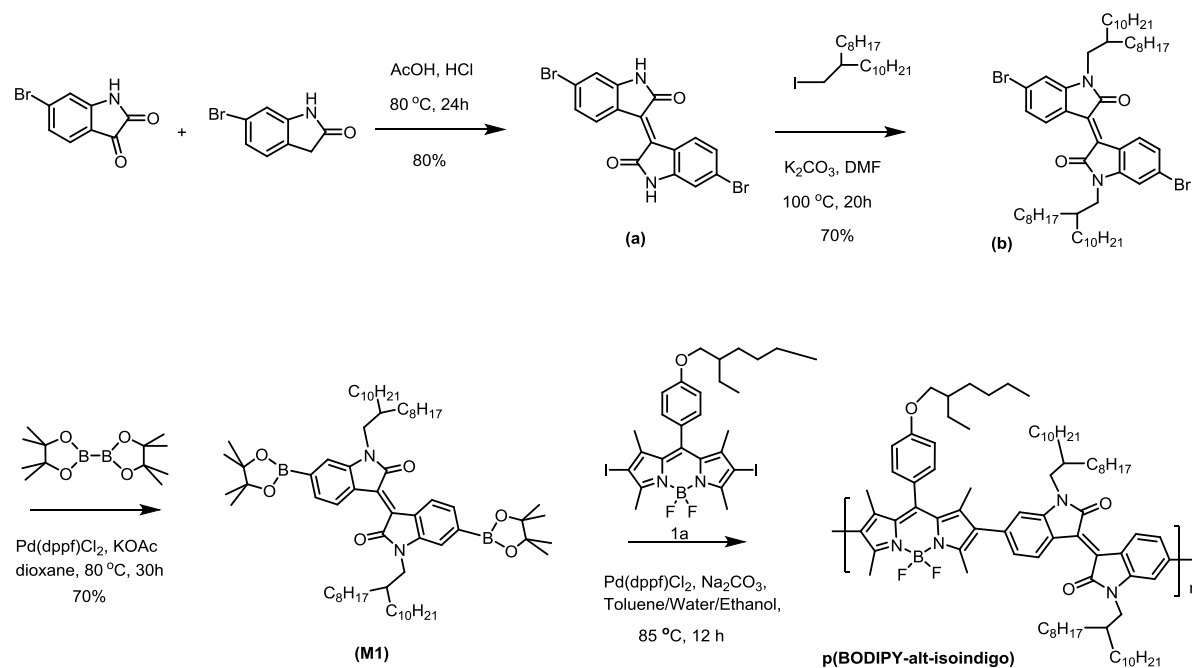
### 5.3 Results and Discussion: p(BODIPY-*alt*-isoindigo)

BODIPY is connected in alternate manner at  $\beta$  position with isoindigo to synthesize conjugated polymer. Isoindigo, a symmetrical molecule consisting of two lactam rings, is an electron-deficient dye.<sup>40-43</sup> The low-lying frontier orbital energy levels, planar  $\pi$ -conjugated structure, and ease of N-alkylation make it an ideal monomer for low band gap conjugated polymer.<sup>44,45</sup> It can be synthesized in large scale with easy synthetic methods. In this work, 2-octyldecyl side chain is substituted on isoindigo while 2-ethylhexyl side chain is substituted on BODIPY to ensure good solubility of the polymer.

#### 5.3.1 Synthesis and Thermal Characterization

Synthesis of 2,6-diiodoBODIPY monomer **1a** is discussed in chapter 1. Isoindigo monomer was synthesized following the scheme 5.1. 6,6'-Dibromoisindigo (**a**) was synthesized in high yield (about 80%) by refluxing the commercially available 6-bromoisatin and 6-bromooxindole in a mixture of acetic acid and hydrochloric acid.<sup>46</sup> This insoluble product was N-alkylated with 2-octyldecyl side chain at both lactam nitrogen atoms in 70% yield. Diborylated isoindigo monomer was synthesized from N-alkylated isoindigo (**b**) under Miyaura borylation conditions and purified by successive dissolution and reprecipitation in methanol (70% yields). Polymer p(BODIPY-*alt*-isoindigo) was synthesized under Suzuki polycondensation conditions using  $\text{Pd}(\text{dppf})\text{Cl}_2$  as a catalyst, and  $\text{Na}_2\text{CO}_3$  as a base.<sup>47</sup> The crude polymer was purified by soxhlet extraction using methanol and acetone to remove residual catalyst, monomers, and oligomers. A final chloroform fraction was collected and

precipitated into methanol to obtain pure polymer in overall 70 % yield.  $M_n = 16509 \text{ g}\cdot\text{mol}^{-1}$ ,  $M_w = 37547 \text{ g}\cdot\text{mol}^{-1}$ , and PDI = 2.27 (against PS standard).



**Scheme 5.1** Synthetic routes to isoindigo monomer and polymer.

Synthesized monomers and polymer were characterized by <sup>1</sup>H and <sup>13</sup>C NMR spectroscopy, MALDI-TOF analysis, and GPC analysis (Appendix IV).

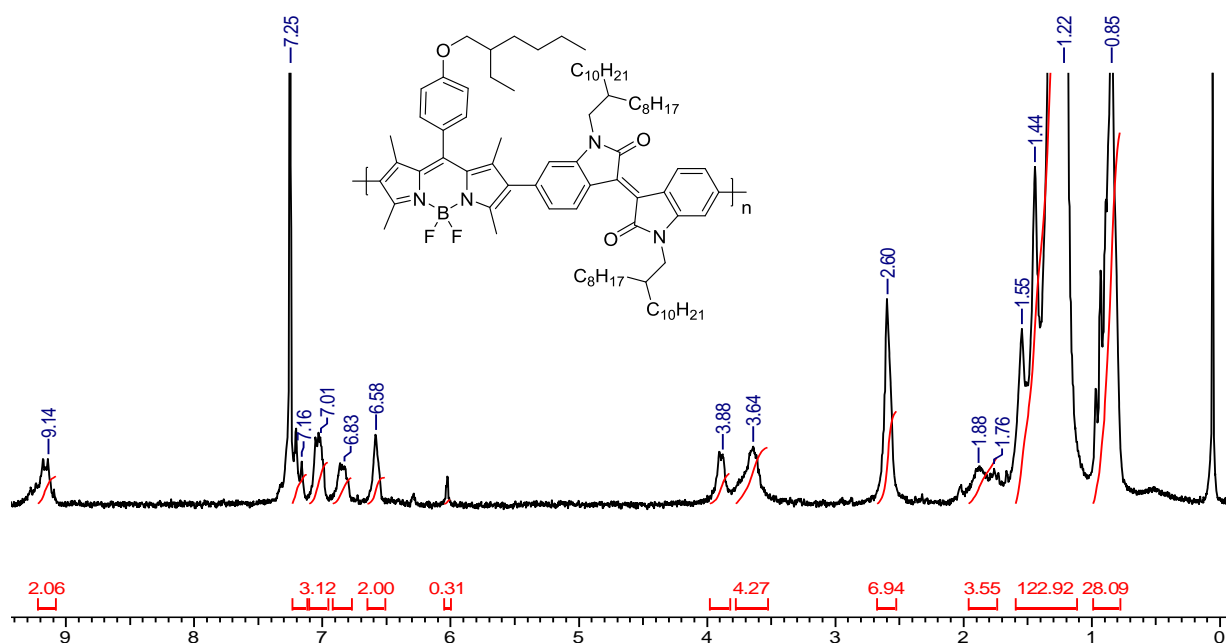


**Figure 5.1** 200 MHz <sup>1</sup>H NMR spectrum of Polymer p(BODIPY-*alt*-isoindigo) in CDCl<sub>3</sub>.

The thermal stability of the polymer was studied by thermogravimetric analysis (TGA) and it was found that the polymer is thermally stable upto 225 °C with 5% weight loss, and hence can be thermally annealed during device fabrication without degradation (Figure 5.2b).

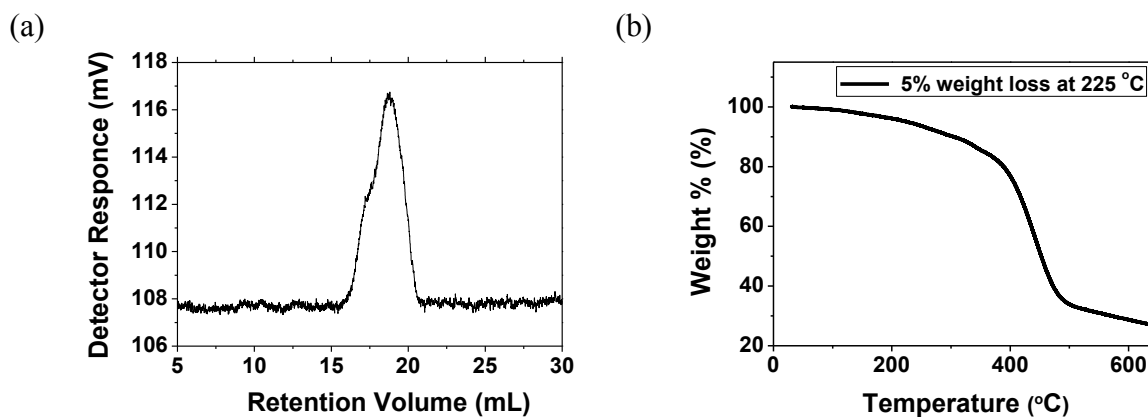


**Figure 5.2** (a) GPC chromatogram and (b) TGA curve of Polymer p(BODIPY-*alt*-isoindigo).

### 5.3.2 Molecular Geometry and Electronic Structure Calculations from DFT

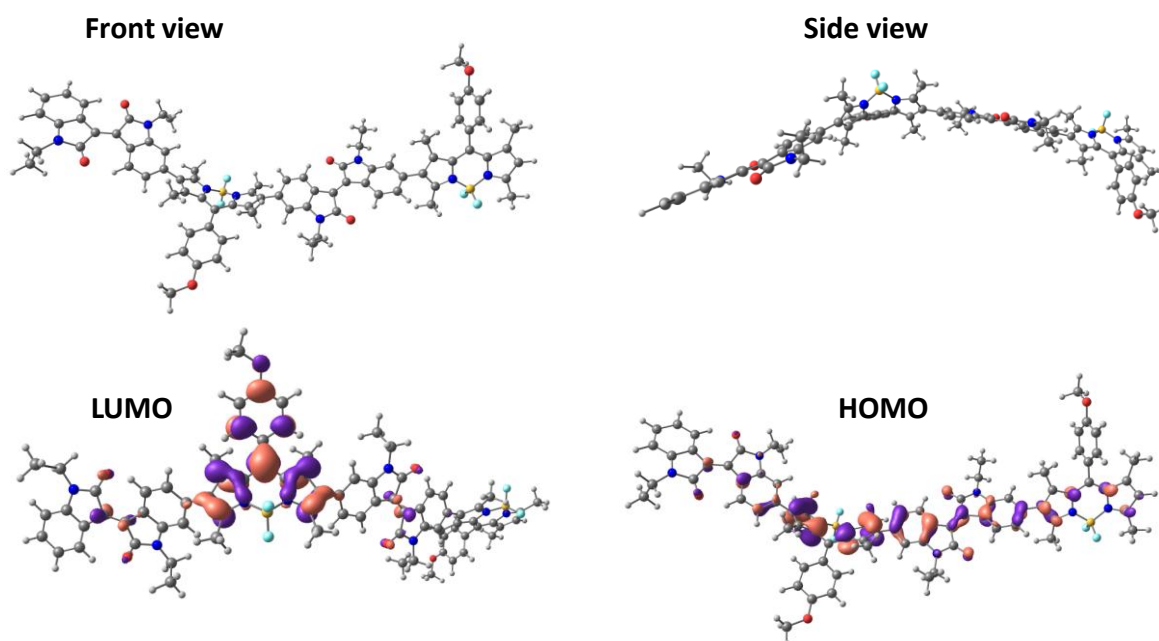


**Figure 5.3** Molecular geometry and HOMO, LUMO surface plots of p(BODIPY-*alt*-isoindigo).

Density functional theory (DFT) analysis was carried out to investigate the optimal geometric structure and the electronic properties of polymer p(BODIPY-*alt*-isoindigo). DFT calculations were done at B3LYP/6-31G \*\* level using Gaussian 09 on model compounds representing the isoindigo and BODIPY monomers, and the repeat units in the polymer.<sup>48</sup>

The theoretical HOMO and LUMO energy levels are calculated theoretically and compared with the experimental data. The theoretical HOMO/LUMO levels for isoindigo monomer, are -5.55/-2.65 eV, and for BODIPY are -5.28/-2.28 eV. The geometrically optimized structure of two repeating units representing the polymer is given in figure 5.3 and the inter-ring torsion angle is  $\sim 46^\circ$ . Side view of the conjugated backbone of model compound demonstrates that the polymer has a twisted structure. HOMO wave function is delocalized along the backbone but LUMO is primarily located on BODIPY core. The theoretical HOMO/LUMO energies are -5.11/-2.95 eV and the energy band gap is 2.16 eV.

### 5.3.3 Optical and Electrochemical Properties

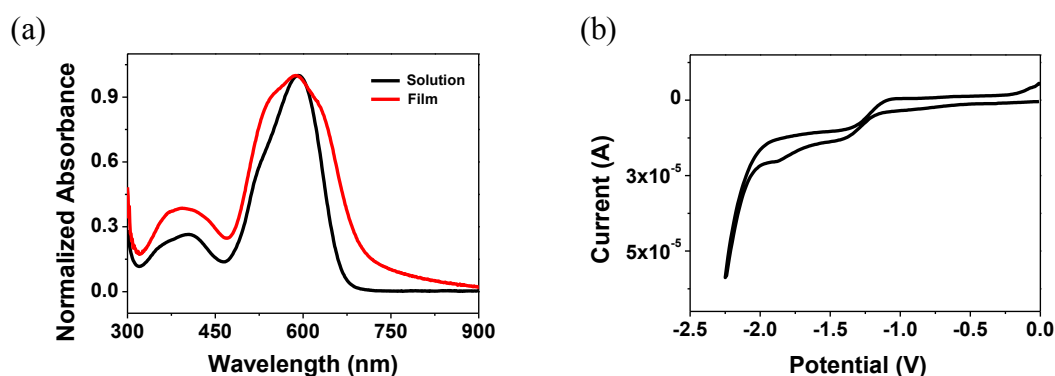


**Figure 5.4** (a) UV-vis absorption spectra, (b) reduction scan cyclic voltammogram of p(BODIPY-*alt*-isoindigo).

The UV-vis absorption spectrum of the polymer was recorded in dilute chloroform solution and as thin film. The absorption spectra of the polymer in solution exhibits two distinct absorption bands, a higher energy band below 450 nm that could result from  $\pi$ - $\pi^*$  transitions whereas the lower-energy (450–750 nm) band due to intramolecular charge transfer (ICT). The absorption maximum is 595 nm and onset is 672 nm. Thin film absorption spectrum of the polymer is broader than that of the solution, presumably due to planarization of the conjugated backbone (Figure 5.4a). p(BODIPY-*alt*-isoindigo) is a medium band gap polymer as energy band gap is 1.74 eV, calculated from the low energy absorption edge.

Orbital energy levels were experimentally calculated from cyclic voltammetry experiment coupled with optical studies. The polymer was coated on Pt wire as working electrode, Ag/Ag<sup>+</sup> as a reference electrode and Pt foil as the counter electrode. The cyclic voltammogram was recorded by sweeping the working electrode potential in the cathodic segments in 0.1 M tetrabutylammonium hexafluorophosphate in dry acetonitrile (Figure 5.4b).

Calculated LUMO energy level was -3.62 eV. HOMO energy level was calculated by subtraction of the optical band gap from the LUMO value and was found to be -5.36 eV.

**Table 5.1** Optical and electrochemical data for (BODIPY-*alt*-isoindigo).

Polymer	Solution		Film		$E_g^{\text{opt}}$ (eV)	$E^{\text{red}}$ (V)	LUMO (eV)	HOMO (eV)
	$\lambda_{\text{max}}$ (nm)	$\lambda_{\text{onset}}$ (nm)	As cast $\lambda_{\text{max}}$ (nm)	Annealed $\lambda_{\text{onset}}$ (nm)				
p(BODIPY -alt- isoindigo)	595	672	591	713	1.74	-1.18	- 3.62	-5.36

$$\text{LUMO} = - (E^{\text{red, onset}} + 4.8) \text{ eV}$$

$$\text{HOMO} = \text{LUMO} - E_g^{\text{opt}}$$

### 5.3.4 Characterization of Field-Effect Transistor Devices

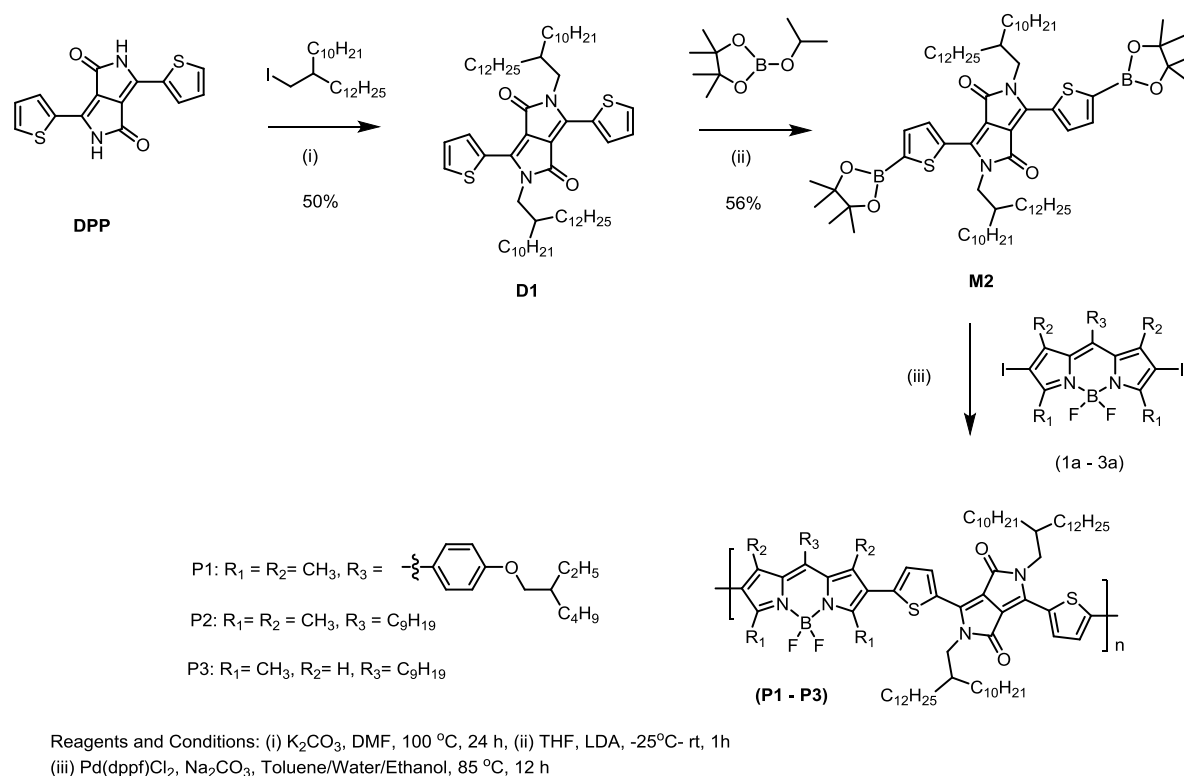
Field effect transistors were fabricated using SiO<sub>2</sub> as a gate dielectric, heavily n doped Si as a gate electrode and gold as source and drain electrodes. The prefabricated substrate has a bottom gate, bottom contact configuration. The polymer contains long branched alkyl chains hence hydrophilic SiO<sub>2</sub> surface was modified using OTS (octadecyltrichlorosilane) for favourable contact between molecules and channels. In our studies, polymer was spin coated on top of the substrates from chloroform solution. The device fabrication and measurements were carried out inside an argon filled glove box. Output characteristic curves were recorded while sweeping the drain voltage ( $V_D$ ) between 0 and -100V while applying a constant gate voltage ( $V_G$ ). Surprisingly, OFET device did not show any charge transport property. n-type measurements were also performed while sweeping the drain voltage ( $V_D$ ) between 0 and 100V while applying a constant gate voltage ( $V_G$ ). This experiment also did not show any semiconducting property of the material. The possible reason could be the twisted backbone of the polymer and an ineffective orbital mixing in the polymer.

### 5.4 Results and Discussion: p(BODIPY-*alt*-DPP)

Previously designed polymer p(BODIPY-*alt*-isoindigo), containing BODIPY and electron deficient isoindigo dye, did not show any charge transport property. The possible reason could be the twisted backbone and ineffective orbital mixing of BODIPY and isoindigo energy levels in the polymer. In this work we have selected DPP as comonomer which is also electron deficient, planar and has two lactam ring.<sup>49-52</sup> Here, BODIPY unit has three variants

similar to chapter 4, the only difference is presence of long alkyl chains to ensure good solubility while synthesizing polymers. BODIPY **1** has methyl groups at 1,3,5,7 positions and 2-ethylhexyl substituted phenyl ring at meso position, BODIPY **2** has the same tetramethyl core with phenyl ring at meso is replaced by alkyl (nonyl) chain, and BODIPY **3** has 3,7 dimethyl core with nonyl chain at the meso position (Chart 5.1).

### 5.4.1 Synthesis and Thermal Characterization



**Scheme 5.2** Synthetic routes to DPP monomers, and polymers p(BODIPY-*alt*-DPP) (P1 – P3).

BODIPY **1** was synthesized following the procedure given in the chapter 2. Synthetic procedure of BODIPY **2** and **3** are discussed in detail in chapter 3. N-iodosuccinimide was used to synthesize diiodo BODIPY (**1a – 3a**). DPP dye was synthesized in high yield (about 80%) according to the reported procedure.<sup>39</sup> This insoluble DPP dye was then subjected to N-alkylation with two solubilizing 2-decyltetradecyl side chains and afforded the compound D1 in 50% yield (Scheme 5.2). Diborylated DPP monomer was obtained in 56% yield by treating a reaction mixture of D1 and 2-isopropoxy-4,4,5,5-tetramethyl-1,3,2-dioxaborolane with freshly prepared LDA solution.<sup>53</sup> polymers (**P1 – P3**) were synthesized by Suzuki coupling between diborylated DPP monomer and diiodo BODIPY monomers in about 50 – 70% yield.<sup>54</sup>

These monomers and polymer were characterized by  $^1\text{H}$  and  $^{13}\text{C}$  NMR spectroscopy, MALDI-TOF analysis, and GPC analysis (Appendix IV).

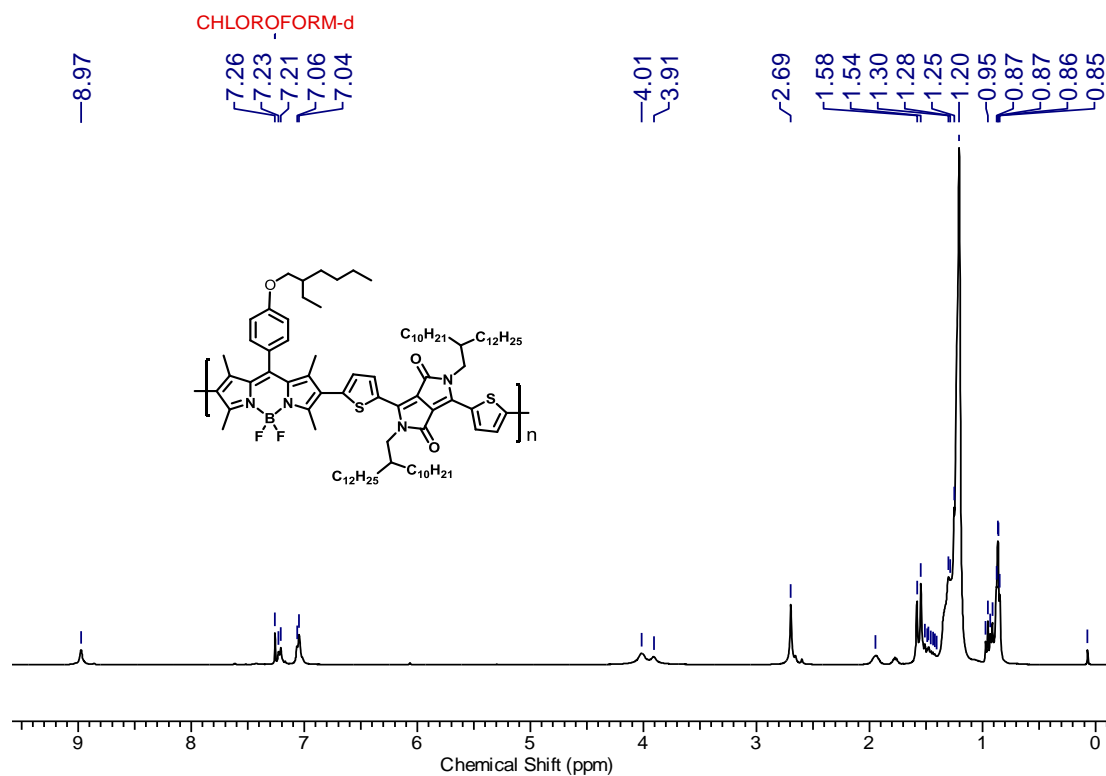


**Figure 5.5**  $^1\text{H}$  NMR (400 MHz,  $\text{CDCl}_3$ ) spectrum of polymer **P1**

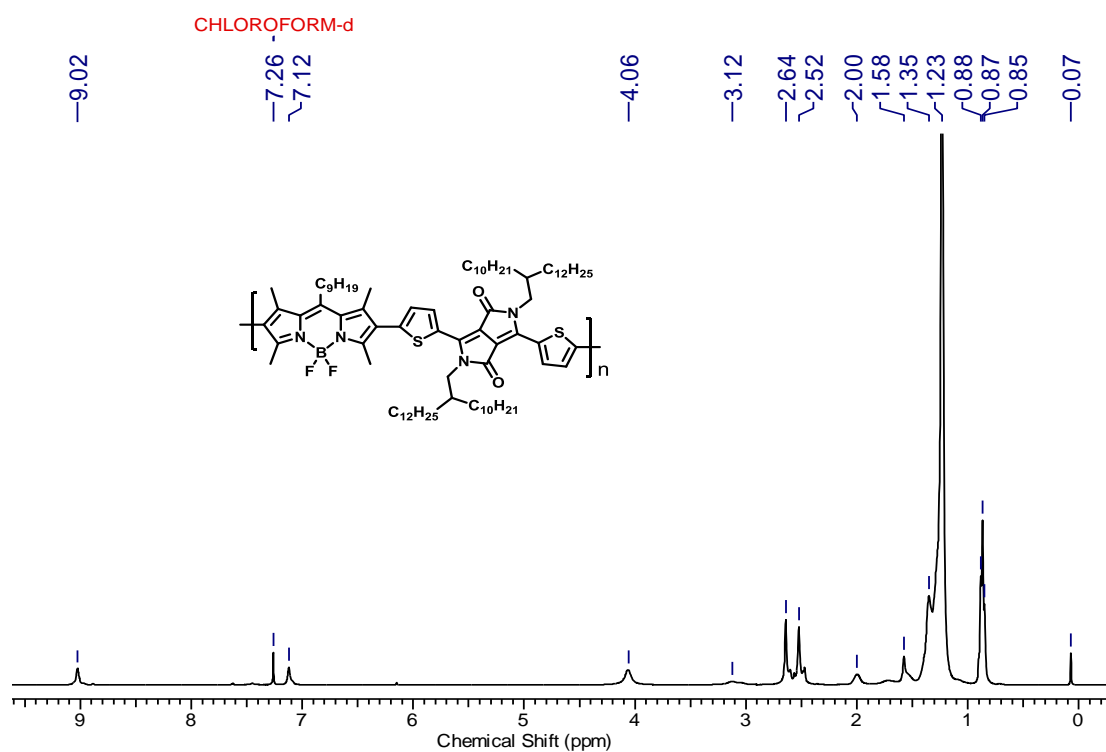


**Figure 5.6**  $^1\text{H}$  NMR (400 MHz,  $\text{CDCl}_3$ ) spectrum of polymer **P2**



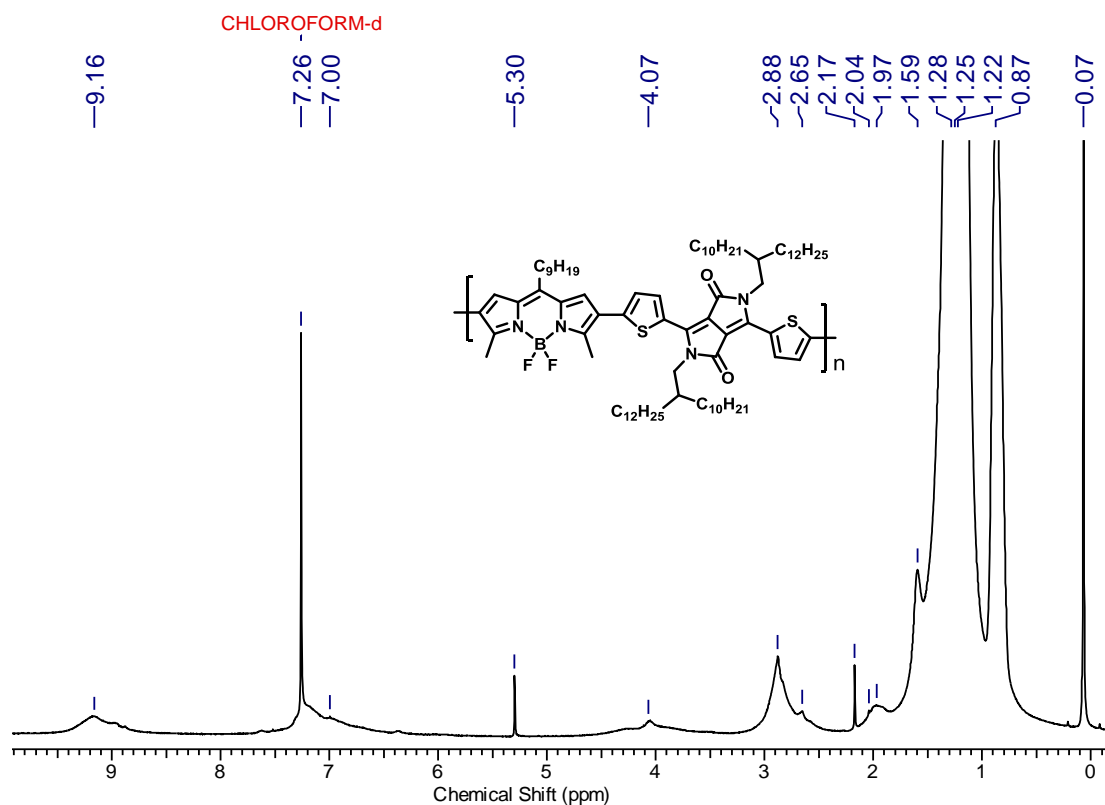


**Figure 5.7**  $^1\text{H}$  NMR (400 MHz,  $\text{CDCl}_3$ ) spectrum of polymer **P3**

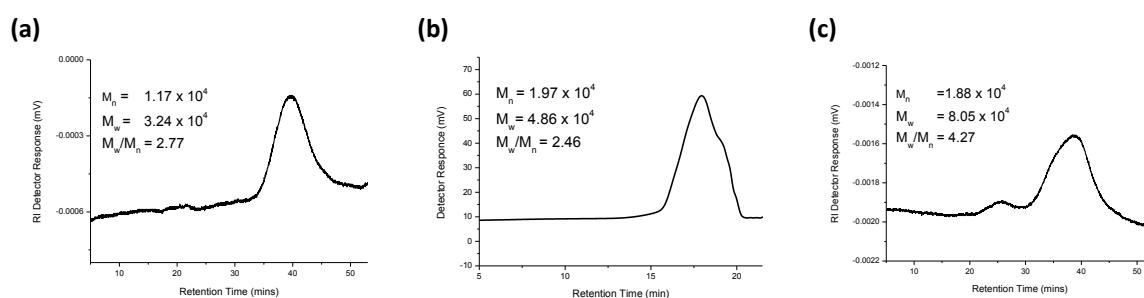


**Figure 5.8** GPC chromatograms of polymer **P1** (a), **P2** (b), and **P3** (c).

The thermal characteristics of three polymers (**P1–P3**) were studied by thermogravimetric analysis (TGA) and differential scanning calorimetry (DSC). These polymers are thermally stable upto 362 °C, 331 °C, and 355 °C respectively with 5% weight loss which is suitable for thermal annealing during device fabrication without degradation (Figure 5.9a). Differential scanning calorimetry (DSC) results of the polymers were obtained from the second heating and cooling cycles (Figure 5.9b). DSC of **P2** and **P3** did not show any clear phase transition when heated till 280 °C, indicating the amorphous nature of the polymers. Though, **P1** shows melting (276 °C) and crystallization transition (226 °C) in heating and cooling cycles.

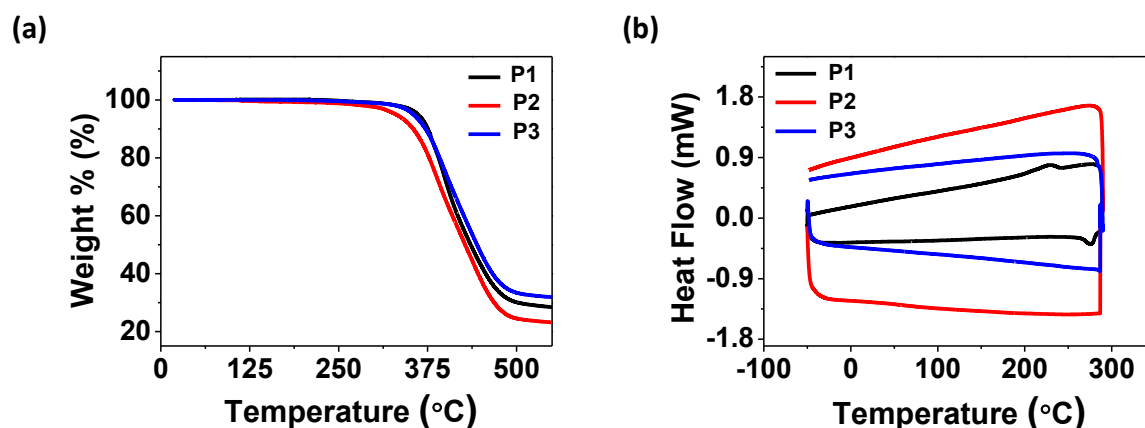


**Figure 5.9** (a) TGA curves (a) and DSC plots (b) of polymers P1, P2 and P3.

#### 5.4.2 Molecular Geometry and Electronic Structure Calculations from DFT

Density functional theory (DFT) analysis was carried out to investigate the optimal geometric structure and the electronic properties of polymers (**P1** – **P3**). DFT calculations were done at B3LYP/6-31G \*\* level using Gaussian 09 on model compounds representing the DPP, BODIPY monomers, and the repeat units in the corresponding polymers. The theoretical HOMO and LUMO levels are given in table 5.2 and compared with the experimental data. The HOMO/LUMO levels for DPP monomer, are -4.95/-2.50 eV, and for BODIPY (**1** – **3**) are -5.28/-2.28 eV, -5.36/-2.31 eV, and -5.53/-2.51 eV. From BODIPY **1** to **2**, replacement of phenyl ring with alkyl group affected energy levels to some extent, while removal of two methyl groups from BODIPY **2** at 1,7 positions resulted in deeper HOMO/LUMO for BODIPY **3**. These BODIPY monomers exhibit strong molecular dipoles, oriented toward the 4,4'-fluorine substituents, and the values are 5.42 D, 4.14 D, and 3.36 D for BODIPY **1**, **2**, and **3** respectively.

**Table 5.2:** FMO energy levels from DFT calculations for model compounds

Molecules	DPP	BODIPY 1	BODIPY 2	BODIPY 3	P1	P2	P3
LUMO (eV)	-2.50	-2.28	-2.31	-2.51	-2.77	-2.78	-3.03
HOMO (eV)	-4.95	-5.28	-5.36	-5.53	-4.74	-4.82	-4.74
$E_g^{\text{DFT}}$ (eV)	2.45	3.00	3.05	3.02	1.97	2.04	1.71

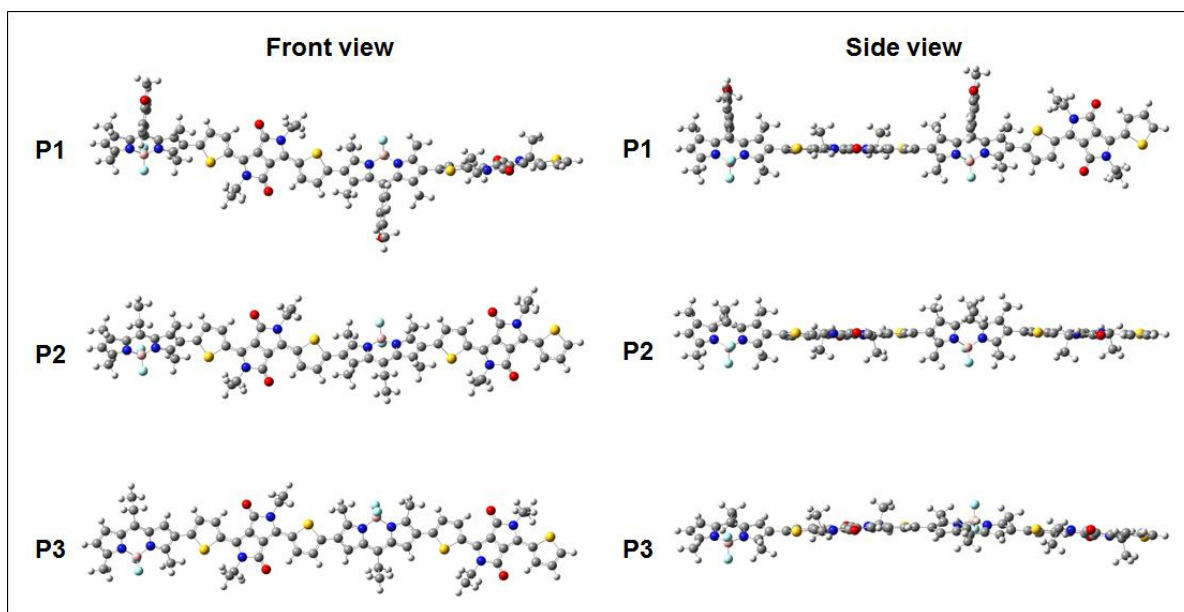


**Figure 5.10** Front and side view of model compounds representing polymers (**P1 – P3**) obtained from DFT calculations.

In polymers (**P1 – P3**), DPP and BODIPY (**1 – 3**) monomers are connected in an alternate fashion. Since substituent groups and orbital energy levels are different for BODIPY (**1 – 3**), corresponding polymers (**P1 - P3**) will exhibit variation in orbital energy levels and degree of planarity in the conjugated backbones. The geometrically optimized structures of two repeating units representing polymers are given in figure 5.10. The inter-ring torsion angles are  $\sim 47^\circ$ ,  $\sim 51^\circ$ , and  $\sim 27^\circ$  for **P1**, **P2**, and **P3** respectively. Side views of conjugated backbones of model compounds demonstrate that **P1** has a twisted coiled structure while **P2** and **P3** have an alternate twist in the backbone. With the lowest inter-ring torsion angle, **P3** containing dimethyl BODIPY core has the most coplanar conjugated backbone compared to the other two polymers. In each of the model compounds, both LUMO and HOMO wave functions are delocalized along the backbone, and this is a characteristic feature of ambipolar molecules reported in the literature.<sup>55-58</sup> LUMO and HOMO electron densities for **P1** to **P3** change with the inter-ring torsional angles (Figure 5.11).

HOMO is primarily located on the DPP moiety and the LUMO is on the BODIPY moiety which reflects that DPP is the donor and BODIPY is the acceptor in our polymeric systems. The theoretical HOMO/LUMO energies are -4.74/-2.77 eV for **P1**, -4.82/-2.78 eV for **P2**, and -4.74/-3.03 eV for **P3**. The energy band gap are 1.97, 2.04, and 1.71 eV for **P1**, **P2**, and **P3** respectively, where **P3** has the lowest band gap. Furthermore, amongst the polymers (**P1 – P3**), **P3** has the most coplanar conjugated backbone, well delocalized LUMO

and HOMO, and the lowest energy band gap, which are the important factors for efficient inter and intramolecular charge transport.

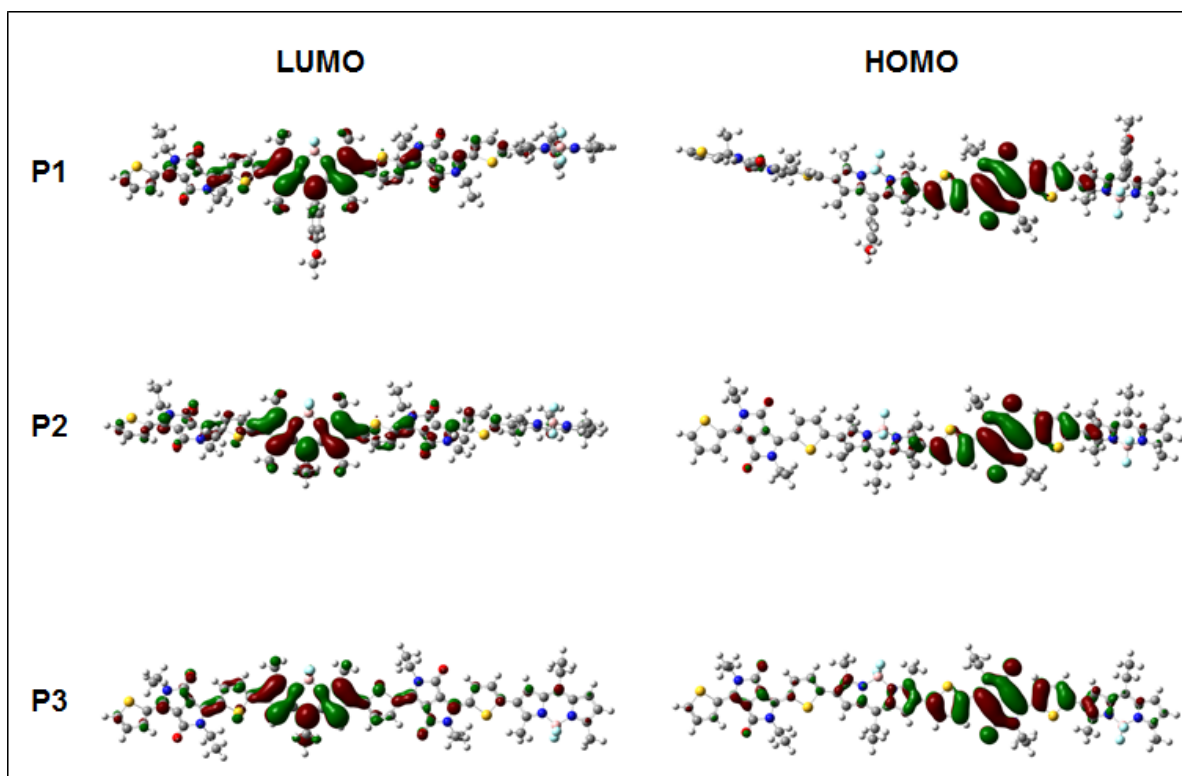


**Figure 5.11** HOMO and LUMO surface plots from DFT calculations for model compounds for polymers (P1 – P3).

### 5.4.3 Optical and Electrochemical Properties

The UV-vis absorption spectra of polymers were recorded in dilute chloroform solution and as thin films. The absorption maxima of **P1**, **P2**, and **P3** in chloroform solutions at room temperature are 647, 630, and 878 nm respectively (Figure 5.12a). The absorption maximum of **P2** is 17 nm blue shifted than that of **P1** and the reason could be the slightly higher energy band gap for **P2** than **P1** as obtained from DFT calculations. **P3** has a significant 230 nm red shift in the absorption maximum than **P1** and that may be attributed to the lower band gap and highly coplanar backbone (from DFT studies) than other two polymers. Charge transfer band of **P3** shows vibronic splitting with 0 – 0 vibrational (880 nm) and 0 – 1 vibrational peaks (797 nm), a characteristic of highly ordered structures.<sup>59-61</sup>

Thin film absorption spectra of polymers (**P1** – **P3**) are broader and red shifted (Table 5.3) compared to their solution-state spectra, presumably due to planarization of the conjugated backbone (Figure 5.12b). These films were then thermally annealed and that resulted in further broadening and red shift in the absorption spectra (Figure 5.12c). On

thermal annealing above 100 °C, polymers **P1** and **P2** displays emergence of low energy shoulder peaks, indicating interchain  $\pi$ - $\pi$  stacking interactions.<sup>62-64</sup> The impact of thermal annealing on the absorption spectra of the **P3** was not very pronounced, only a slight red shift was observed. This implies that **P3** with planar backbone forms an ordered structure even in the pristine film form. Energy band gap calculated from low energy absorption edges for **P1**, **P2** and **P3** are 1.37, 1.43, 1.17 eV respectively. Polymer **P3** containing dimethyl BODIPY core has the lowest band gap among the polymers (**P1** – **P3**). These observations are in agreement with the computationally optimized geometries and estimated frontier molecular orbital energy levels.

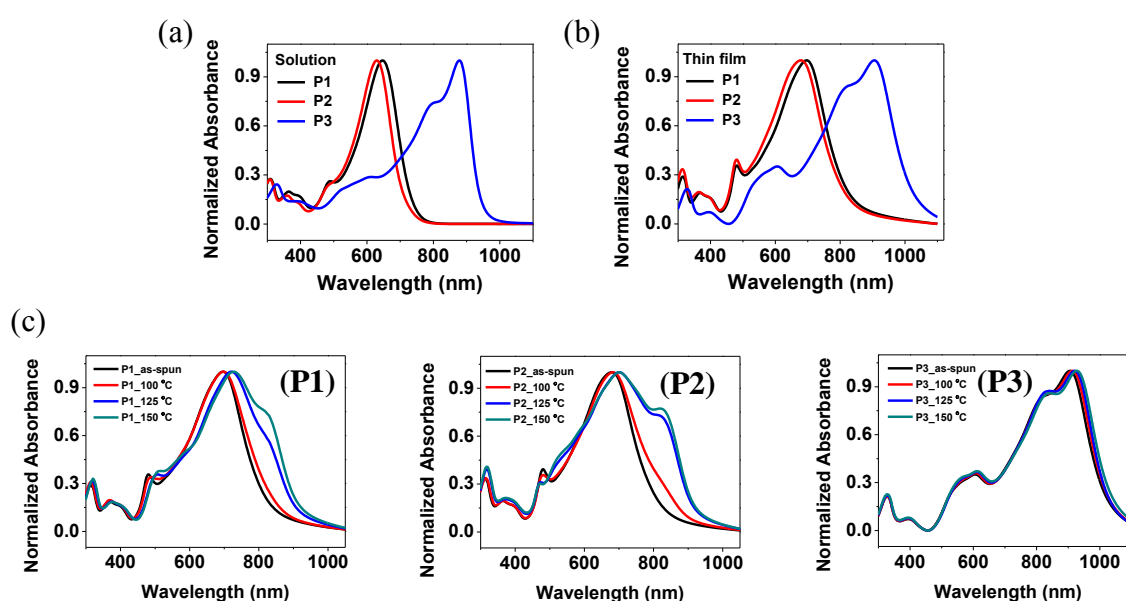


**Figure 5.12** UV-vis absorption spectra of polymers in dilute chloroform solution (a), as thin-film on quartz substrates (b), and of thermally annealed film (c).

**Table 5.3:** Thermal, optical, and electrochemical properties of polymers (**P1** – **P3**)

Polymer	$T_d$ (°C)	$\lambda_{\max}^{\text{sol}}$ (nm)	$\lambda_{\max}^{\text{Film}}$ (nm)	$\lambda_{\text{onset}}$ (nm)	$E_g^{\text{Optical}}$ (eV)	$E^{\text{ox}}/\text{HOMO}$ (eV)	$E^{\text{red}}/\text{LUMO}$ (eV)	$E_g^{\text{elect}}$ (eV)
<b>P1</b>	362	647	696	890	1.39	0.65/-5.36	-1.25/-3.46	1.90
<b>P2</b>	331	630	678	863	1.43	0.68/-5.39	-1.25/-3.46	1.93
<b>P3</b>	355	878	905	1052	1.17	0.57/-5.28	-1.12/-3.59	1.69

Energy levels were experimentally calculated from cyclic voltammetry experiments using polymer coated Pt wire as working electrode,  $\text{Ag}/\text{Ag}^+$  as a reference electrode and Pt

foil as the counter electrode. Working electrode potential was swept in the anodic and cathodic segments in 0.1 M tetrabutylammonium hexafluorophosphate in dry acetonitrile (Figure 5.13). HOMO and LUMO energy levels with respect to vacuum level were determined by calibrating the oxidation and reduction of polymers using ferrocene as an internal standard.<sup>65</sup> The orbital energy level values and calculated energy band gap are provided in table 5.3. Energy band gap for **P1**, **P2**, and **P3** are 1.90, 1.93, and 1.69 eV respectively. Results obtained from electrochemical studies are consistent with the optical and computational studies. Polymer **P3** has the lowest band gap amongst three and this could be attributed to the deeper LUMO and HOMO energy levels of BODIPY **3** and lowest inter-ring torsion angles in **P3** compared to **P1** and **P2**.

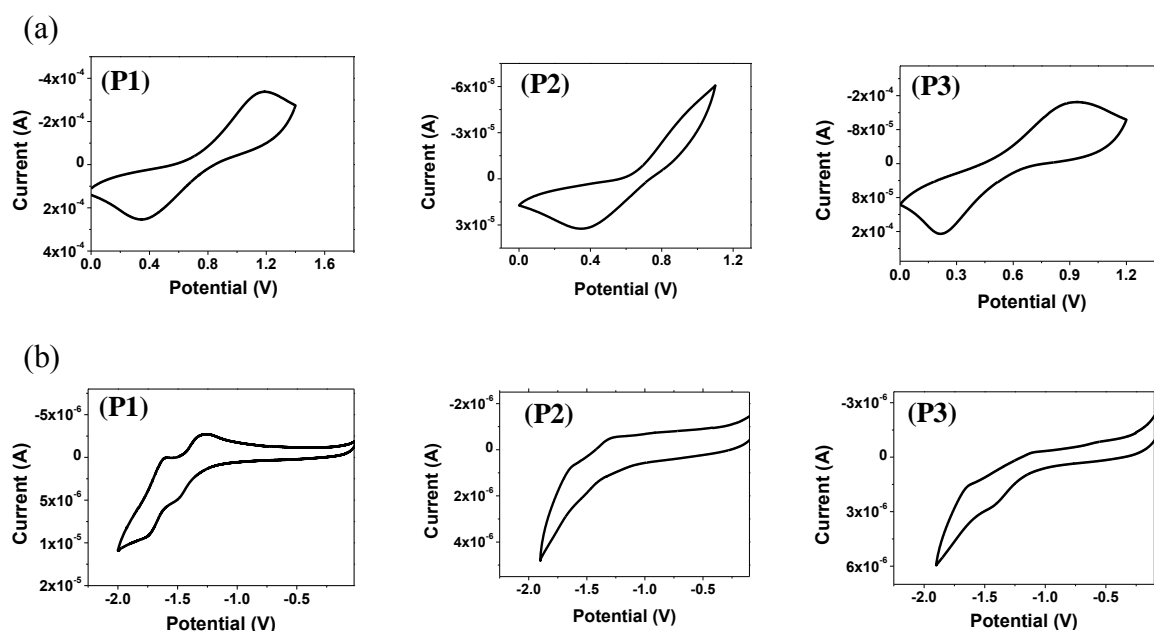


**Figure 5.13** Cyclic voltammograms of polymers (**P1 – P3**): (a) oxidation scan, (b) reduction scan.

#### 5.4.4 Thin Film Morphology

OTS (octadecyltrichlorosilane) modified SiO<sub>2</sub> surface was used to study the morphology of thin films as same substrates were used for the fabrication of Field Effect Transistors (FETs) (Figure 5.14). Polymers (**P1 – P3**) were spin coated on top of the substrate from chloroform solution. **P1** forms lumpy domains throughout in the film. **P2** film shows rough, fibrous structure. In comparison to **P1** and **P2**, **P3** film is continuous and evenly distributed. As these molecules have twisted conjugated backbone and long branched alkyl side chains, thermal annealing was done for planarization of the conjugated backbone and better solid state packing. These films were thermally annealed and further morphological changes were

studied. Unevenness in the film was reduced in annealed films of **P1** and **P2**, though, it was not very pronounced for **P3** as film morphology remains nearly same.

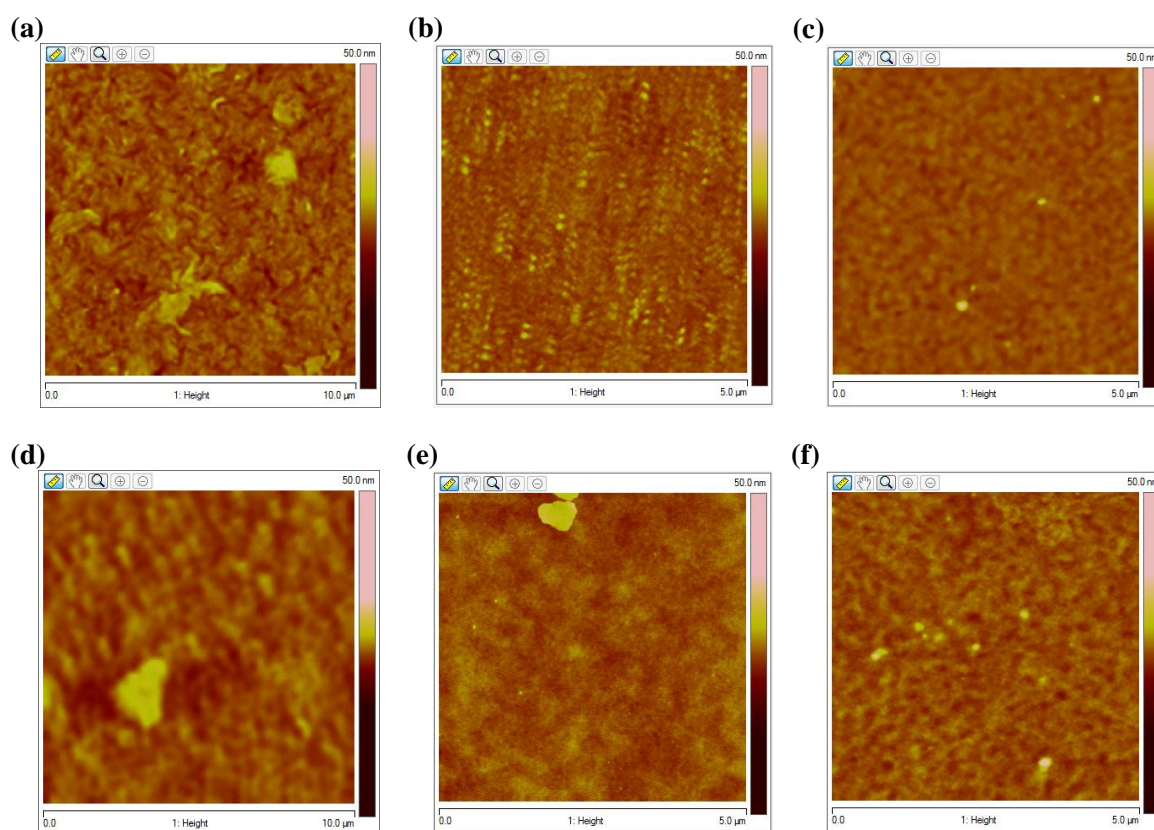


**Figure 5.14** AFM height images of spin coated films: as-spun film of **P1** (a), **P2** (b), **P3** (c) and thermally annealed film of **P1** (d), **P2** (e), and **P3** (f).

### 5.4.5 Characterization of Field-Effect Transistor Devices

Charge transport properties, both p-type and n-type of these polymers were investigated by fabricating OFET devices. The prefabricated FET substrate, with bottom gate, bottom contact configuration, consists of  $\text{SiO}_2$  as a gate dielectric, heavily n doped Si as a gate electrode and gold as source and drain electrodes. FET substrates were modified by forming single assembled monolayer of OTS (octadecyltrichlorosilane) on hydrophilic  $\text{SiO}_2$  surface to achieve favourable contact between the channel and long branched alkyl chains containing polymers. In our studies, polymers were spin coated on top of the substrates from chloroform solutions. The device fabrication and measurements were carried out inside an argon filled glove box. Output characteristic curves were recorded by sweeping the drain voltage ( $V_D$ ) between 0 and -100V while applying a constant gate voltage ( $V_G$ ). The output characteristic curves for **P1**, **P2**, and **P3** showed standard linear and saturation regimes with a good gate modulation as a function of applied gate voltage ( $V_G$ ) though curves were somewhat noisy

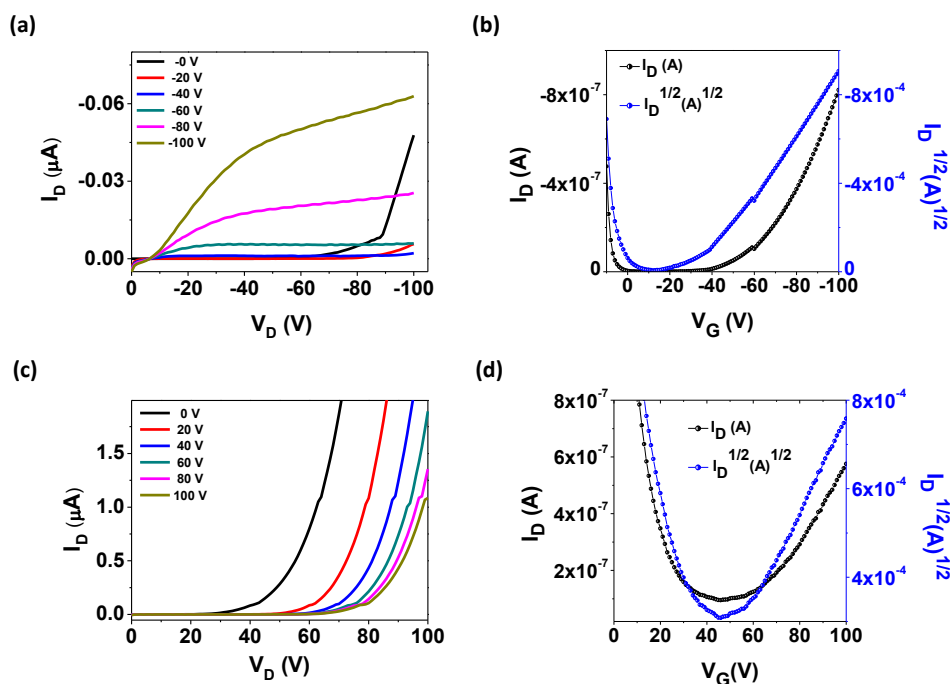


**Figure 5.15** Output (a) and transfer (b) for hole transport, and output (c) and transfer (d) characteristics curves for electron transport of as-spun film of **P1** ( $W = 10 \text{ nm}$ ,  $L = 5 \text{ }\mu\text{m}$ ).

for **P2** (Figure 5.16a). The threshold voltages were calculated from the transfer characteristic curves. Device data are given in table 5.4.

**Table 5.4** Summary of OFET properties of polymers **P1**, **P2** and **P3**.

Polymer	$T^a$ ( $^{\circ}\text{C}$ )	Hole			Electron		
		$\mu_h$ ( $\text{cm}^2\text{V}^{-1}\text{s}^{-1}$ ) ( $\mu_{\text{max}}$ ) <sup>b</sup>	$V_T$ (V)	$I_{\text{on}}/I_{\text{off}}$	$\mu_e$ ( $\text{cm}^2\text{V}^{-1}\text{s}^{-1}$ ) ( $\mu_{\text{max}}$ ) <sup>b</sup>	$V_T$ (V)	$I_{\text{on}}/I_{\text{off}}$
<b>P1</b>	as-spun	$2.53 \times 10^{-5}$	-30	$6.5 \times 10^3$	-	-	-
	100	$8.44 \times 10^{-4}$	-37	$3.6 \times 10^3$	$5.43 \times 10^{-4}$	52	$3.2 \times 10^3$
	150	$5.25 \times 10^{-3}$ ( $6.08 \times 10^{-3}$ )	-17	$3.1 \times 10^5$	$1.05 \times 10^{-3}$ ( $3.37 \times 10^{-3}$ )	58	$7.5 \times 10^4$
<b>P2</b>	as-spun	$6.0 \times 10^{-5}$	-32	$1.11 \times 10^3$	-	-	-
	100	$1.62 \times 10^{-4}$ ( $3.1 \times 10^{-4}$ )	-25	$6.91 \times 10^3$	-	-	-
	150	$7.4 \times 10^{-5}$	-28	$8.08 \times 10^3$	-	-	-
<b>P3</b>	as-spun	$6.74 \times 10^{-3}$	-24	$10^2$	$5.24 \times 10^{-3}$	40	$0.2 \times 10^2$
	150	$2.44 \times 10^{-2}$ ( $3.08 \times 10^{-2}$ )	-30	$1.3 \times 10^2$	$4.80 \times 10^{-3}$	50	$0.3 \times 10^2$
	175	$1.76 \times 10^{-2}$	-33	$8.08 \times 10^3$	$1.12 \times 10^{-2}$ ( $1.53 \times 10^{-2}$ )	40	$0.3 \times 10^2$



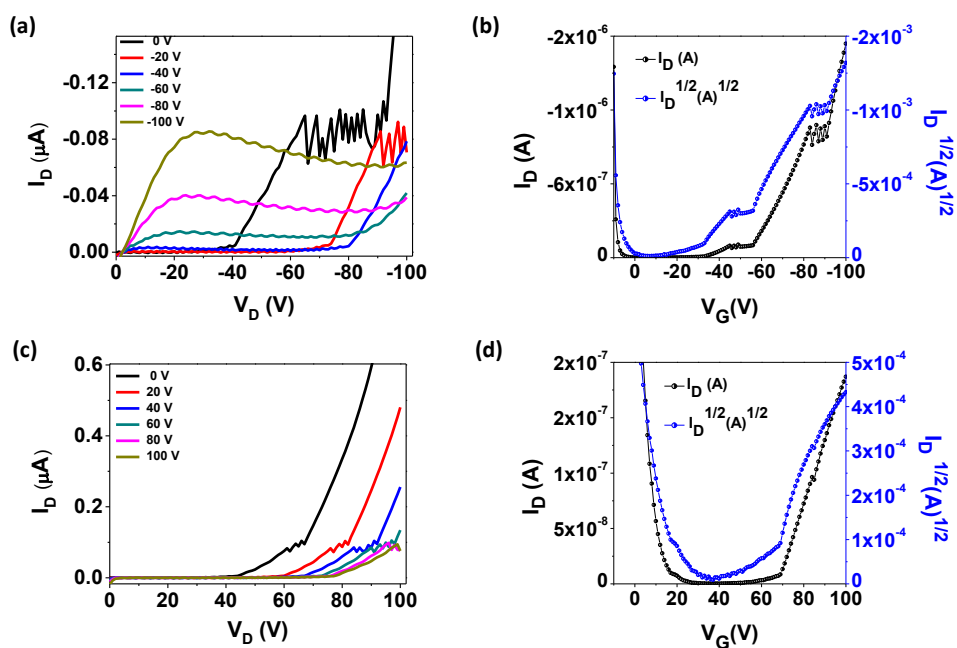


**Figure 5.16** Output (a) and transfer (b) for hole transport, and output (c) and transfer (d) characteristics curves for electron transport of as-spun film of **P2** (W = 10 mm, L = 5 μm).

Electron transport properties of these polymers were also studied. Output characteristic curves were recorded by sweeping the drain voltage ( $V_D$ ) between 0 and 100V while applying a constant gate voltage ( $V_G$ ). **P1** (Figure 5.15c) and **P2** (Figure 5.16c) did not show standard linear and saturation regimes in their output characteristics curves, but **P3** (Figure 5.17c) displayed standard curves. Hole mobility  $\mu_h$  for polymers **P1** and **P2** are

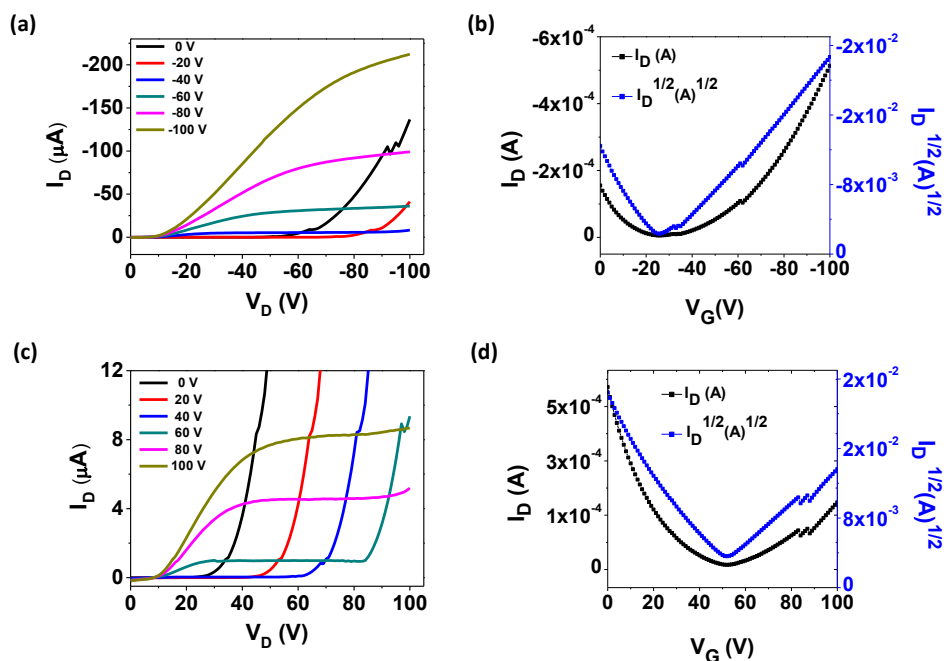


**Figure 5.17** Output (a) and transfer (b) for hole transport and output (c) and transfer (d) characteristics curves for electron transport of as-spun film of **P3** (W = 10 mm, L = 5 μm).

$2.53 \times 10^{-5}$  and  $6.0 \times 10^{-5} \text{ cm}^2/\text{Vs}$ .  $\mu_h/\mu_e$  for **P3** are  $6.74 \times 10^{-3}/ 5.24 \times 10^{-3} \text{ cm}^2/\text{Vs}$ . **P3** exhibits highest hole and electron mobility for devices fabricated at room temperature. These observations could be attributed to the fact that **P3** is the lowest band gap material and has the most coplanar backbone among three polymers, and hence higher chances of intra and intermolecular charge transport.

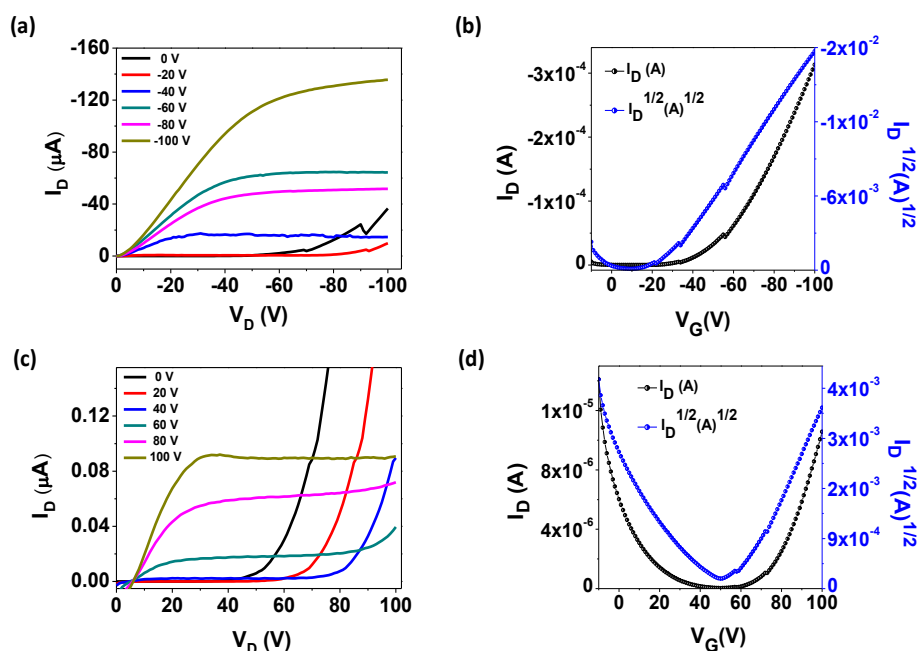


**Figure 5.18** Output (a), transfer (b) for hole transport and output (c) and transfer (d) characteristic curves for electron transport of thermally annealed film of **P1** ( $W = 10 \text{ mm}$ ,  $L = 5 \text{ }\mu\text{m}$ ).

OFET devices were then thermally annealed at different temperatures and device characteristics were recorded. Hole and electron mobilities for **P1** was improved after annealing at  $100 \text{ }^\circ\text{C}$ . improvement in mobility values was observed till  $150 \text{ }^\circ\text{C}$  annealing ( $\mu_h/\mu_e = 6.08 \times 10^{-3}/ 3.37 \times 10^{-3} \text{ cm}^2/\text{Vs}$ ) but a slight decrease was noticed for temperature higher than  $150 \text{ }^\circ\text{C}$  (Table 5.4). Also, **P1** displayed standard curves n type output characteristic curves after annealing (Figure 5.18c). On thermal annealing, hole mobility improved by one order for **P2** ( $\mu_h = 3.1 \times 10^{-4} \text{ cm}^2/\text{Vs}$ ) but it did not help n type charge transport (Figure 5.19c). For **P3**, after thermal annealing at  $150 \text{ }^\circ\text{C}$ , hole mobility improves to  $3.08 \times 10^{-2} \text{ cm}^2/\text{Vs}$  but electron mobility nearly remains same. Further annealing at  $175 \text{ }^\circ\text{C}$ , led to improvement in electron transport by one order ( $\mu_e = 1.50 \times 10^{-2} \text{ cm}^2/\text{Vs}$ ), though no further improvement in hole mobility was observed (Figure 5.20c). Overall, **P3** shows

highest hole and electron mobility values which is one order higher than that of **P1** and two to four order higher than that of **P2**.

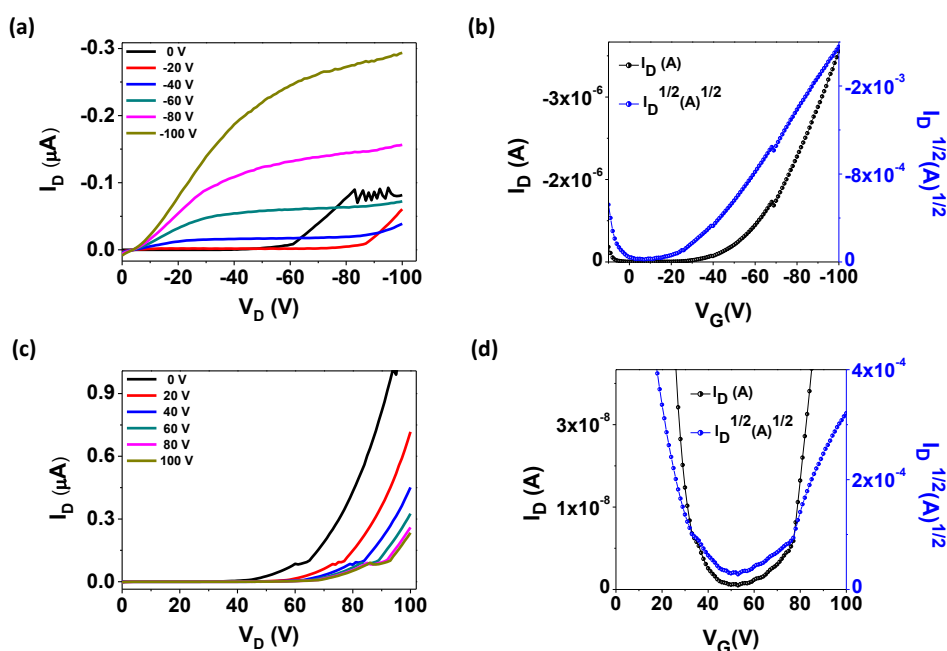


**Figure 5.19** Output (a), transfer (b) for hole transport and output (c), transfer (d) characteristic curves for electron transport of thermally annealed film of **P2** (W = 10 mm, L = 5 μm).

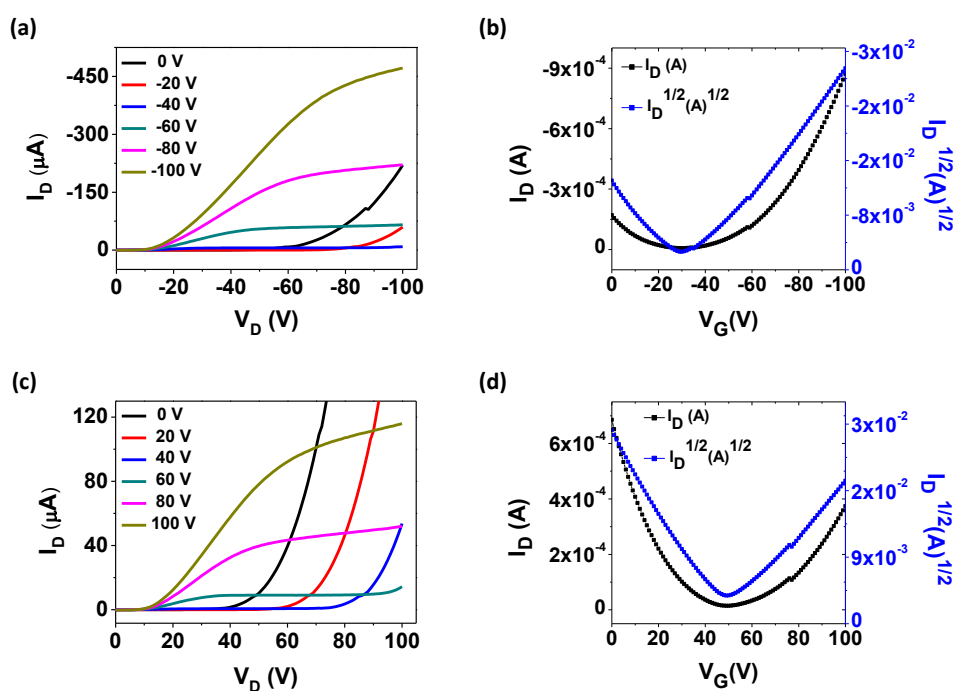
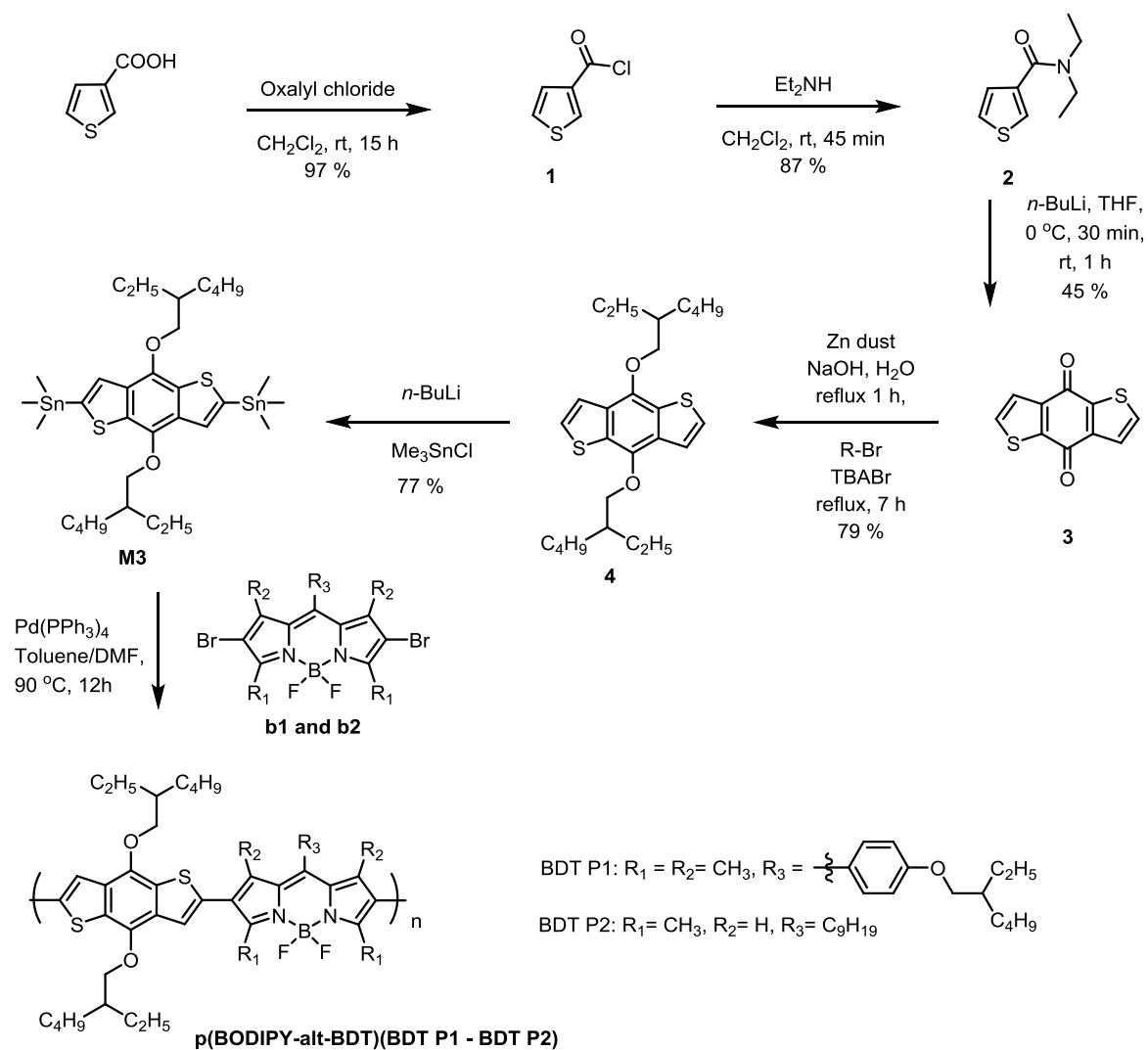


**Figure 5.20** Output (a), transfer (b) for hole transport and output (c), transfer (d) characteristics curves for electron transport of thermally annealed film of **P3** (W = 10 mm, L = 5 μm).

## 5.5 Results and Discussion: p(BODIPY-*alt*-BDT)

In the previous polymers, BODIPY was connected with a planar, lactam rings connecting isoindigo dye and DPP. Isoindigo and DPP are electron deficient in nature and have low lying LUMO and HOMO energy levels. Here, conjugated polymers p(BODIPY-*alt*-BDT), containing BODIPY and benzo[1,2-*b*:4,5-*b'*]dithiophene (BDT) are synthesized. BDT has planar conjugated core and is electron rich in nature.<sup>36-38,66-69</sup> 2-ethylhexyl side chains are connected on BDT monomer to ensure good solubility of the polymer. There are two types of BODIPY moieties used in this work, BODIPY **1**, consisting of methyl groups at 1,3,5,7 positions and 2-ethylhexyl substituted phenyl ring at meso position and BODIPY **3**, consisting of 3,7 dimethyl core with nonyl chain at meso. Two methyl groups are removed to reduce twist in the backbone and to achieve better solid state packing in the polymer film.

### 5.5.1 Synthesis and Thermal Characterization



**Scheme 5.3** Synthetic routes to BDT monomer and p(BODIPY-*alt*-BDT) polymers.

Synthetic routes to BDT monomers and p(BODIPY-*alt*-BDT) polymers are illustrated in scheme 5.3. BDT monomer **M3** was synthesized in 77% yield from thiophene-3-carboxylic acid as starting material following the reported procedure.<sup>70</sup> Synthetic procedures for BODIPY dyes have been discussed in previous chapters. Dibromination of the BODIPY 1 and 3 at the 2- and 6-position using N-bromosuccinimide resulted in 2,6-dibromo BODIPY (70 - 75% yield). Polymers were synthesized by the Stille coupling reaction using Pd(PPh<sub>3</sub>) as a catalyst. Crude polymers were purified by soxhlet extraction using methanol and acetone to remove residual catalyst, monomers, and oligomers. A final chloroform fraction was collected and precipitated into methanol to obtain pure polymers. For **BDT P1**:  $M_n = 6680 \text{ g}\cdot\text{mol}^{-1}$ ,  $M_w = 8890 \text{ g}\cdot\text{mol}^{-1}$ , and PDI = 1.33 (against PS standard), for **BDT P2**:  $M_n = 5000 \text{ g}\cdot\text{mol}^{-1}$ ,  $M_w = 23000 \text{ g}\cdot\text{mol}^{-1}$ , and PDI = 4.61 (against PS standard).

Chemical structures of all synthesized monomers and polymers are given in the Chart 5.1. These monomers and polymer were characterized by <sup>1</sup>H and <sup>13</sup>C NMR spectroscopy, MALDI-TOF analysis, and GPC analysis (Appendix IV).

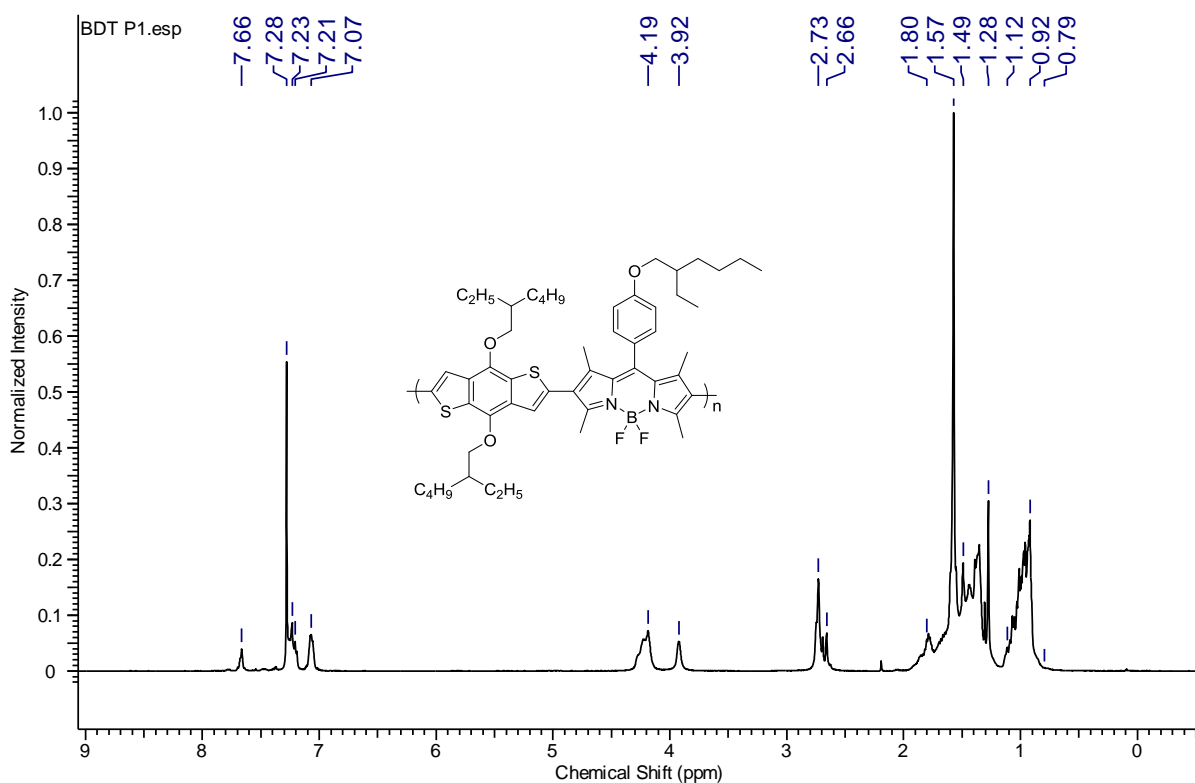


**Figure 5.21** <sup>1</sup>H NMR (400 MHz, CDCl<sub>3</sub>) spectrum of polymer BDT P1

Thermal stability of the polymers was studied by thermogravimetric analysis (TGA). **BDT P1** and **BDT P2** are thermally stable upto 300 °C with 5% weight loss, and hence can be thermally annealed during device fabrication without degradation (Figure 5.24).

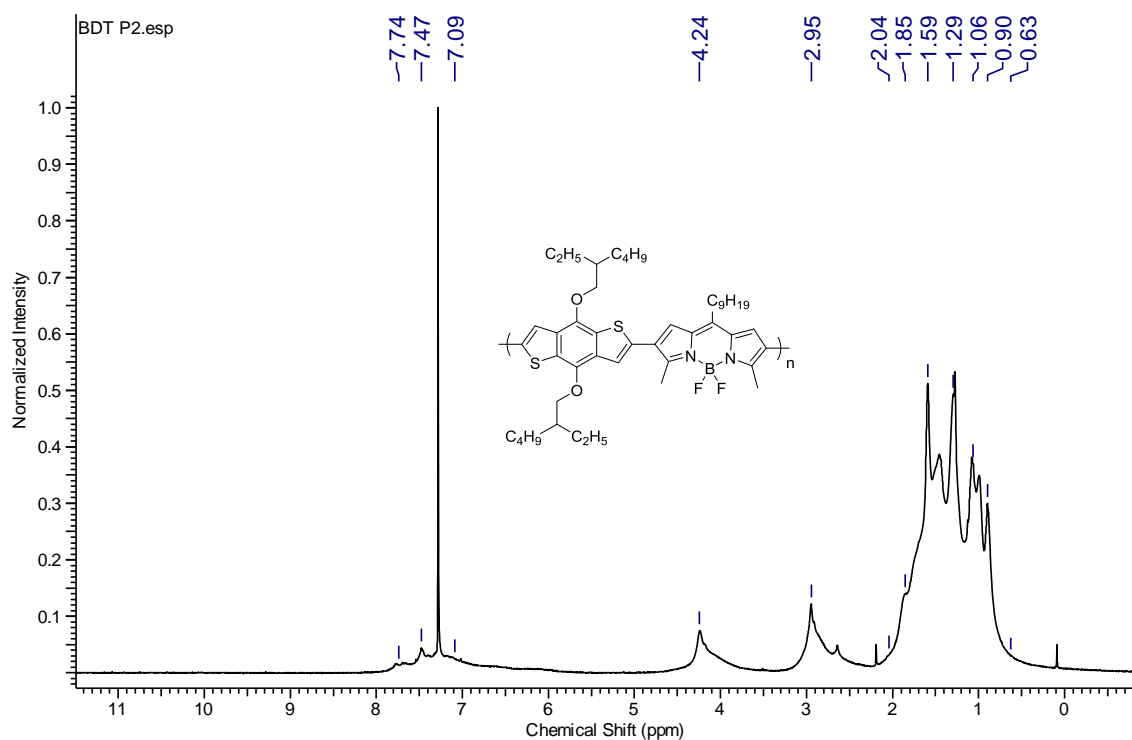


Figure 5.22 <sup>1</sup>H NMR (400 MHz, CDCl<sub>3</sub>) spectrum of polymer **BDT P2**

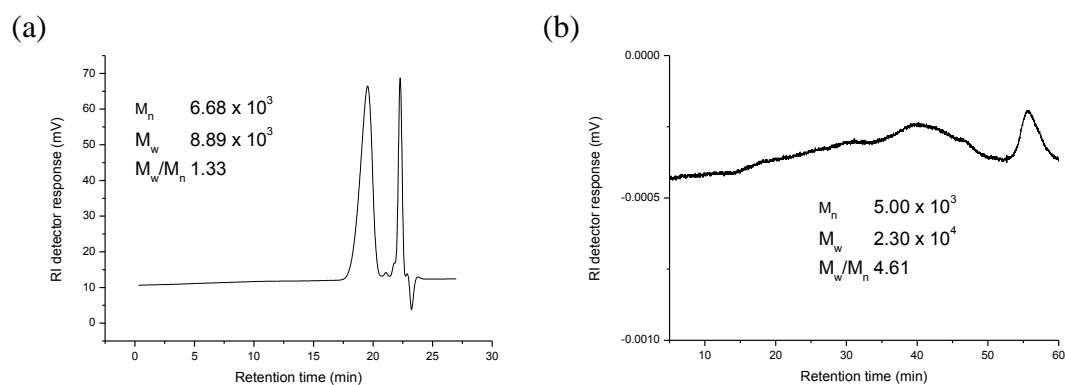


Figure 5.23 GPC chromatograms of polymers (a) **BDT P1** (b) **BDT P2**.

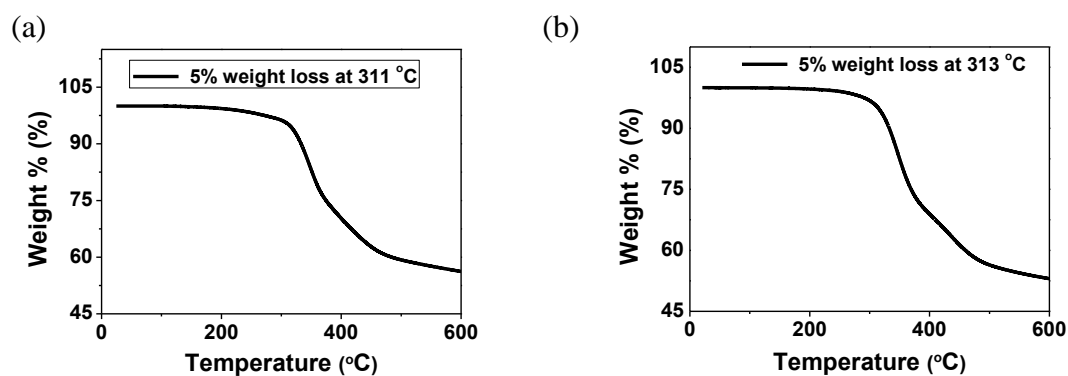
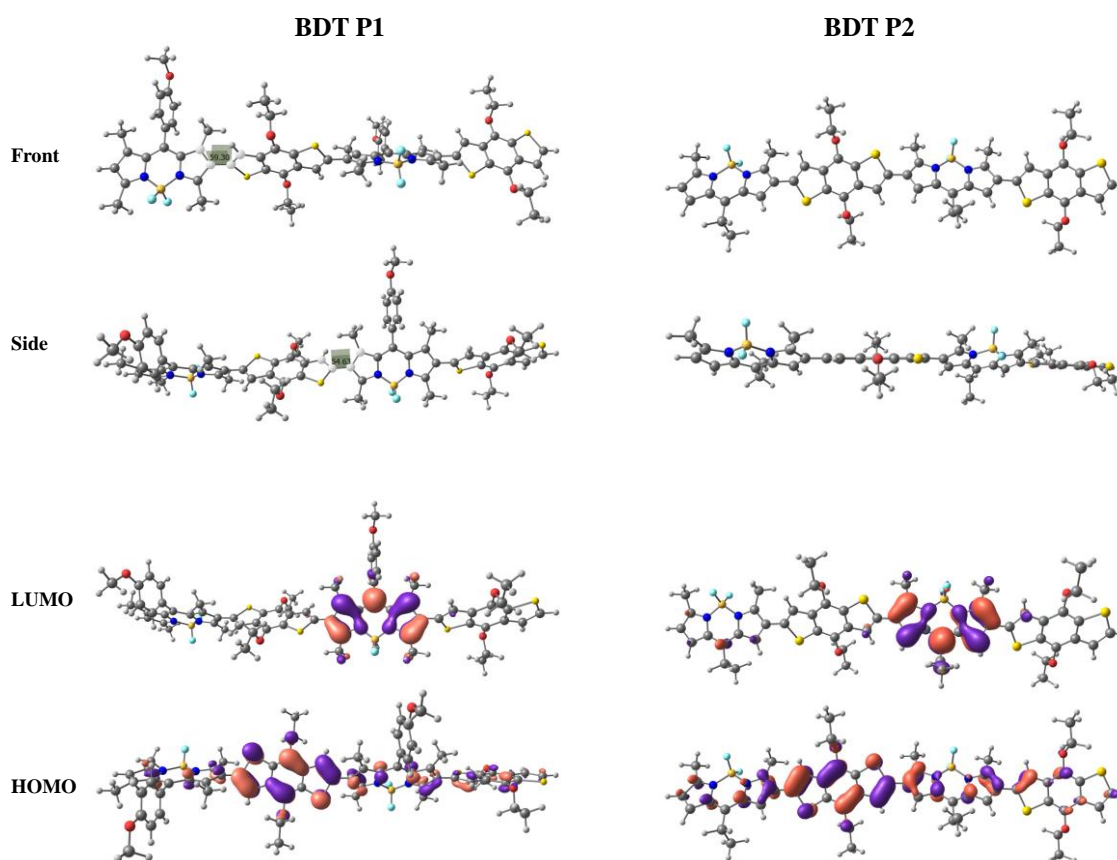


Figure 5.24 TGA curves for (a) **BDT P1** (b) **BDT P2**.

### 5.5.2 Molecular Geometry and Electronic Structure Calculations from DFT

Density functional theory (DFT) analysis was carried out to investigate the optimal geometric structure and the electronic properties of the polymers. DFT calculations were done at B3LYP/6-31G \*\* level using Gaussian 09 on model compounds representing the BDT and BODIPY monomers, and the repeat units in the polymers. The theoretical HOMO/LUMO levels for BDT monomer, are -4.65/-0.77 eV, and for BODIPY **1** and **2** are -5.28/-2.28 eV and -5.53/-2.51 eV. Geometrically optimized structures of two repeating units representing polymers are given in figure 5.25 and the inter-ring torsion angles are  $\sim 54^\circ$  and  $\sim 32^\circ$  for **BDT P1** and **BDT P2** respectively. Side views of conjugated backbones demonstrate that polymer BDT P1 has a very twisted structure. **BDT P2** is relatively planar. HOMO wave function is delocalized along the backbone but LUMO is primarily located on the electron deficient BODIPY moiety. This type of delocalization behaviour is characteristic of a hole transporting material. The theoretical HOMO/LUMO energy levels for **BDT P1** and **BDT P2** are -5.06/-2.50 eV and -5.02/-2.77 eV and the energy band gap are 2.56 eV and 2.25 eV respectively.



**Figure 5.25** Front and side view and HOMO, LUMO surface plots of model compounds for polymers **BDT P1** and **BDT P2** obtained from DFT calculations.

### 5.5.3 Optical and Electrochemical Properties

The UV-vis absorption spectra of the polymers were recorded in dilute chloroform solutions and as thin films. Similar to other BODIPY based small molecules and polymers, these polymers also exhibit two distinct absorption bands, a higher energy band below 450 nm and a lower-energy (450–800 nm) band. The absorption maxima of **BDT P1** and **BDT P2** in chloroform solutions at room temperature are 552 and 720 nm respectively (Figure 5.26). This 168 nm red shift in the absorption spectrum of **BDT P2** indicates better coplanarity and conjugation in the polymer backbone after removal of two methyl groups. Thin film absorption spectra are broader and red shifted compared to the solution-state spectra, presumably due to planarization of the conjugated backbone. Energy band gap calculated from low energy absorption edges for **BDT P1** and **BDT P2** are 1.78 and 1.48 eV respectively. These observations (Table 5.5) are consistent with the computationally calculated frontier molecular orbital energy levels.

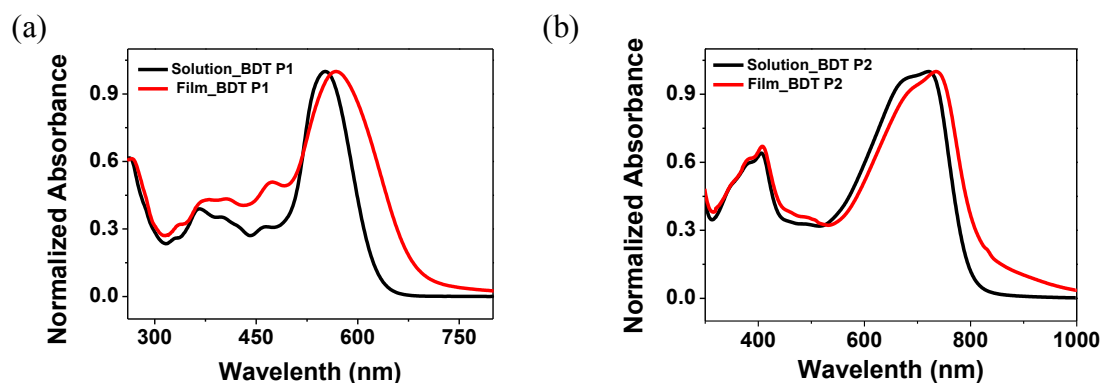


**Figure 5.26** UV-vis absorption spectra of Polymers in dilute chloroform solution and as thin-film on quartz substrates (a) **BDT P1** (b) **BDT P2**.

Cyclic voltammograms of polymers were recorded using polymer coated Pt wire as working electrode, Ag/Ag<sup>+</sup> as a reference electrode and Pt foil as the counter electrode. Working electrode potential was swept in the anodic and cathodic segments in 0.1 M tetrabutylammonium hexafluorophosphate in dry acetonitrile (Figure 5.27). HOMO and LUMO energy levels with respect to vacuum level were determined by calibrating the oxidation and reduction of polymers using ferrocene as an internal standard.<sup>65</sup> The orbital energy level values and calculated energy band gap are provided in Table 5.5 Energy band gap for **BDT P1** and **BDT P2** were found to be 1.61 and 1.46 eV respectively. Results obtained from electrochemical studies are consistent with the optical and computational



studies that **BDT P2**, with planar conjugated backbone, has a lower band gap than the **BDT P1**.

**Table 5.5** Optical and electrochemical properties of polymers **BDT P1** and **BDT P2**.

Polymer	$\lambda_{\max}^{\text{solution}}$ (nm)	$\lambda_{\max}^{\text{film}}$ (nm)	$\lambda_{\text{onset}}$ (nm)	$E_g^{\text{Optical}}$ (eV)	$E^{\text{ox}}$ (V)	$E^{\text{red}}$ (V)	HOMO (eV)	LUMO (eV)	$E_g^{\text{Elect}}$ (eV)
<b>BDT P1</b>	552	568	695	1.78	0.68	0.93	-5.41	-3.80	1.61
<b>BDT P2</b>	720	735	838	1.48	0.52	0.94	-5.25	-3.79	1.46

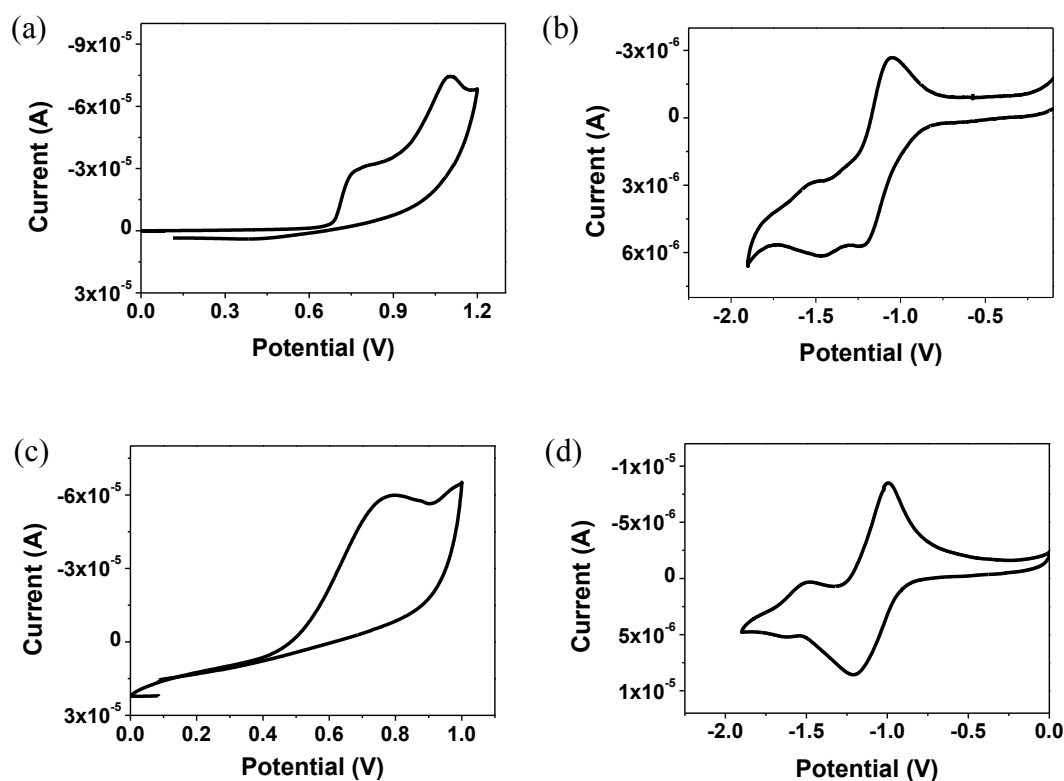


**Figure 5.27** Cyclic voltammograms of **BDT P1**: (a) oxidation scan, (b) reduction scan and **BDT P2**: (c) oxidation scan, (d) reduction scan.

#### 5.5.4 Characterization of Field-Effect Transistor Devices

Field effect transistors were fabricated using  $\text{SiO}_2$  as a gate dielectric, heavily n doped Si as a gate electrode and gold as source and drain electrodes. Hydrophilic  $\text{SiO}_2$  surface was modified using OTS (octyltrichlorosilane) solution. In our studies, polymers were spin coated

on top of the FET substrates from chloroform solution and thermally annealed at 100 °C. Output characteristic curves were recorded while sweeping the drain voltage ( $V_D$ ) between 0 and -100V while applying a constant gate voltage ( $V_G$ ). The output and transfer characteristic curves are given in figure 5.28. Device data are given in table 5.6. Hole mobility ( $\mu_h$ ) for **BDT P1** is  $3.37 \times 10^{-6}$  and for **BDT P2** is  $1.35 \times 10^{-5} \text{ cm}^2/\text{Vs}$ . Removal of two methyl group led to planarity in the conjugated backbone of polymer **BDT P2** but could improve mobility value by one order only. Electron transport measurements were also performed but these polymers did show electron transport.

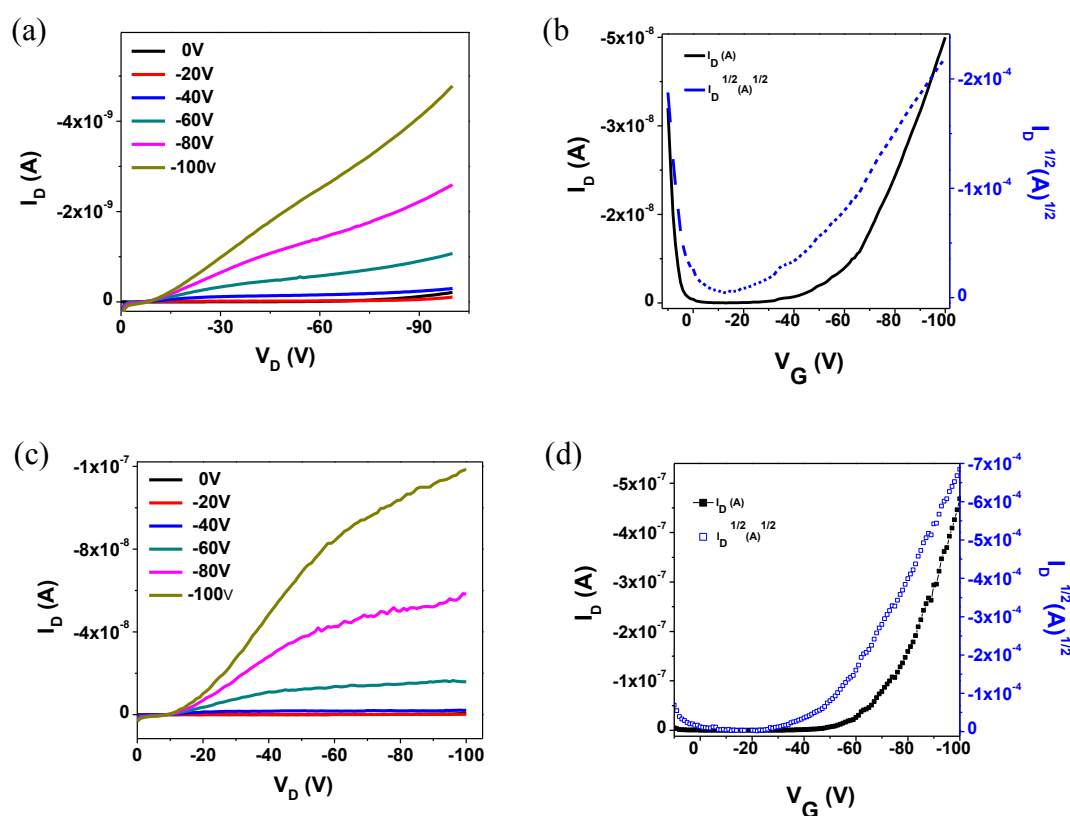


**Figure 5.28** Output (a), transfer (b) for **BDT P1** and output (c), transfer (d) characteristic curves for **BDT P2** ( $W = 10 \text{ nm}$ ,  $L = 2.5 \text{ }\mu\text{m}$ ).

**Table 5.6** Summary of OFET properties of polymers P1, P2 and P3.

Polymer	Mobility	$V_T$ (V)	$I_{\text{on/off}}$
<b>BDT P1</b>	$3.37 \times 10^{-6}$ ( $1.32 \times 10^{-6}$ )	-22	$6.90 \times 10^1$
<b>BDT P2</b>	$1.35 \times 10^{-5}$ ( $9.60 \times 10^{-6}$ )	-42	$7.80 \times 10^3$

## 5.6 Summary

In summary, solution processable conjugated copolymers containing BODIPY are synthesized and their charge transport properties were measured. Comonomers were varied from electron deficient isoindigo and DPP to electron rich BDT. They have high to low torsional angles and variation in the orbital energy levels.

p(BODIPY-alt-isoindigo) has low lying HOMO/LUMO energy levels, medium energy band gap, and is thermally stable upto 225 °C with 5% weight loss. DFT calculations show that it has highly twisted backbone. OFET devices were fabricated using this polymer and both p and n-type of measurements were performed but they did not show any charge transport property. Three p(BODIPY-alt-DPP) polymers (**P1** – **P3**) were synthesized with a variation on the BODIPY core, and their physical, thermal, and electronic properties are studied. HOMO and LUMO orbital energy levels were determined theoretically from DFT and experimentally from optical and electrochemical studies. Replacing 2-ethylhexyl side chain phenyl ring with a nonyl side chain at meso from **P1** to **P2** resulted in slightly higher energy band gap as observed from DFT, optical and electrochemical studies. Inter torsion angle calculated from DFT studies was also found to be higher for **P2** than that of **P1**. **P3** containing dimethyl core exhibits most coplanar and has the lowest band gap among three polymers. These polymers are thermally well stable up to 300 °C without significant weight loss, hence suitable for higher temperature device fabrication. Field effect transistors devices fabricated from these polymers show ambipolar charge transport. **P3** exhibits highest mobility values with a hole mobility of  $3.1 \times 10^{-2} \text{ cm}^2/\text{Vs}$  and electron mobility of  $1.5 \times 10^{-2} \text{ cm}^2/\text{Vs}$ . p(BODIPY-alt-BDT) polymers have medium to low energy band gap and they are thermally stable upto 300 °C with 5% weight loss. DFT calculations show that **BDT P1** has a highly twisted backbone while **BDT P2** has a comparatively less twisted backbone. OFET devices fabricated from **BDT P2** exhibit hole mobility of  $1.35 \times 10^{-5} \text{ cm}^2/\text{Vs}$  which is one order higher than that obtained for **BDT P1**.

## 5.7 References

- 1) Roncali, J. *Acc. Chem. Res.* **2009**, *42*, 1719.
- 2) Walker, B.; Kim, C.; Nguyen, T.-Q. *Chem. Mater.* **2011**, *23*, 470.
- 3) Sun, Y.; Welch, G. C.; Leong, W. L.; Takacs, C. J.; Bazan, G. C.; Heeger, A. J. *Nat. Mater.* **2012**, *11*, 44.

- 4) Zeis, R.; Besnard, C.; Siegrist, T.; Schlockermann, C.; Chi, X.; Kloc, C. *Chem. Mater.* **2006**, *18*, 244.
- 5) Afzali, A.; Dimitrakopoulos, C. D.; Breen, T. L. *J. Am. Chem. Soc.* **2002**, *124*, 8812.
- 6) Afzali, A.; Kagan, C. R.; Traub, G. P. *Synth. Met.* **2005**, *155*, 490.
- 7) Anthony, J. E.; Brooks, J. S.; Eaton, D. L.; Parkin, S. R. *J. Am. Chem. Soc.* **2001**, *123*, 9482.
- 8) Cheng, Y.-J.; Yang, S.-H.; Hsu, C.-S. *Chem. Rev.* **2009**, *109*, 5868.
- 9) Lei, T.; Wang, J.-Y.; Pei, J. *Chem. Mater.* **2013**, DOI: 10.1021/cm4018776.
- 10) Mei, J.; Bao, Z. *Chem. Mater.* **2013**, DOI: 10.1021/cm4020805.
- 11) Facchetti, A. *Chem. Mater.* **2011**, *23*, 733.
- 12) Cabanetos, C.; El Labban, A.; Bartelt, J. A.; Douglas, J. D.; Mateker, W. R.; Fréchet, J. M. J.; McGehee, M. D.; Beaujuge, P. M. *J. Am. Chem. Soc.* **2013**, *135*, 4656.
- 13) Kline, R.J.; McGehee, M.D.; Kadnikova, E.N.; Liu, J.; Fréchet, J.M.J.; Toney, M.F. *Macromolecules*, **2005**, *38*, 3312.
- 14) Chang, J.-F.; Sub, B.; Breiby, D.W.; Nielsen, M.M.; Spelling, T.I.; Giles, M.; McCulloch, I.; Sirringhaus, H. *Chem. Mater.* **2004** *16*, 4772.
- 15) Majewski, L.A.; Kingsley, J.W.; Balocco, C.; Song, A.M. *Appl. Phys. Lett.* **2008**, *88*, 222108.
- 16) Karolin, J.; Johansson, L. B.-A.; Strandberg, L.; Ny, T. *J. Am. Chem. Soc.* **1994**, *116*, 7801.
- 17) Tan, K.; Jaquinod, L.; Paolesse, R.; Nardis, S.; Di Natale, C.; Di Carlo, A.; Prodi, L.; Montalti, M.; Zaccheroni, N.; Smith, K. M. *Tetrahedron* **2004**, *60*, 1099.
- 18) Yee, M.-c.; Fas, S. C.; Stohlmeyer, M. M.; Wandless, T. J.; Cimprich, K. A. *J. Biol. Chem.* **2005**, *280*, 29053.
- 19) Turfan, B.; Akkaya, E. U. *Org. Lett.* **2002**, *4*, 2857.
- 20) Arbeloa, T. L.; Arbeloa, F. L.; Arbeloa, I. L.; Garcia-Moreno, I.; Costela, A.; Sastre, R.; Amat-Guerri, F. *Chem. Phys. Lett.* **1999**, *299*, 315.
- 21) Kim, B.; Ma, B.; Donuru, V. R.; Liu, H.; Fréchet, J. M. J. *Chem. Commun.* **2010**, *46*, 4148.
- 22) Loudet, A.; Burgess, K. *Chem. Rev.* **2007**, *107*, 4891.
- 23) Ulrich, G.; Ziessel, R.; Harriman, A. *Angew. Chem., Int. Ed.* **2008**, *47*, 1184.
- 24) Popere, B. C.; Della Pelle, A. M.; Thayumanavan, S. *Macromolecules* **2011**, *44*, 4767.

- 25) Yoshii, R.; Yamane, H.; Nagai, A.; Tanaka, K.; Taka, H.; Kita, H.; Chujo, Y. *Macromolecules* **2014**, *47*, 2316.
- 26) Debnath, S.; Singh, S.; Bedi, A.; Krishnamoorthy, K.; Zade, S. S. *J. Phys. Chem. C* **2015**, *119*, 15859.
- 27) Debnath, S.; Singh, S.; Bedi, A.; Krishnamoorthy, K.; Zade, S. S. *J. Polym. Sci. A: Polym. Chem.* **2016**, *54*, 1978.
- 28) Cortizo-Lacalle, D.; Howells, C. T.; Gambino, S.; Vilela, F.; Vobecka, Z.; Findlay, N. J.; Inigo, A. R.; Thomson, S. A. J.; Skabara, P. J.; Samuel, I. D. W. *J. Mater. Chem.* **2012**, *22*, 14119.
- 29) Usta, H.; Yilmaz, M. D.; Avestro, A.-J.; Boudinet, D.; Denti, M.; Zhao, W.; Stoddart, J. F.; Facchetti, A. *Adv. Mater.* **2013**, *25*, 4327.
- 30) Zhang, G.; Fu, Y.; Xie, Z.; Zhang, Q. *Macromolecules* **2011**, *44*, 1414.
- 31) Mei, J.; Graham, K. R.; Stalder, R.; Reynolds, J. R. *Org. Lett.* **2010**, *12*, 660.
- 32) Wang, E.; Ma, Z.; Zhang, Z.; Henriksson, P.; Inganäs, O.; Zhang, F.; Andersson, M. R. *Chem. Commun.* **2011**, *47*, 4908.
- 33) Nielsen, C. B.; Turbiez, M.; McCulloch, I. *Adv. Mater.* **2013**, *25*, 1859.
- 34) Kaur, M.; Choi, D. H. *Chem. Soc. Rev.* **2015**, *44*, 58.
- 35) Chen, H.; Guo, Y.; Yu, G.; Zhao, Y.; Zhang, J.; Gao, D.; Liu, H.; Liu, Y. *Adv. Mater.* **2012**, *24*, 4618.
- 36) Liang, Y.; Feng, D.; Wu, Y.; Tsai, S. T.; Li, G.; Ray, C.; Yu, L. *J. Am. Chem. Soc.* **2009**, *131*, 7792.
- 37) Hou, J.; Park, M.-H.; Zhang, S.; Yao, Y.; Chen, L.-M.; Li, J.-H.; Yang, Y. *Macromolecules* **2008**, *41*, 6012.
- 38) Qu, B.; Tian, D.; Cong, Z.; Wang, W.; An, Z.; Gao, C.; Gao, Z.; Yang, H.; Zhang, L.; Xiao, L.; et al. *J. Phys. Chem. C* **2013**, *117*, 3272.
- 39) Huo, L.; Hou, J.; Chen, H. Y.; Zhang, S.; Jiang, Y.; Chen, T. L.; Yang, Y. *Macromolecules* **2009**, *42*, 6564.
- 40) Lei, T.; Wang, J. Y.; Pei, J. *Acc. Chem. Res.* **2014**, *47*, 1117.
- 41) Huang, J.; Mao, Z.; Chen, Z.; Gao, D.; Wei, C.; Zhang, W.; Yu, G. *Chem. Mater.* **2016**, *28*, 2209.
- 42) Shin, J.; Um, H. A.; Lee, D. H.; Lee, T. W.; Cho, M. J.; Choi, D. H. *Polym. Chem.* **2013**, *4*, 5688.

- 43) Stalder, R.; Mei, J.; Graham, K. R.; Estrada, L. a; Reynolds, J. R. *Chem. Mater.* **2014**, *26*, 664.
- 44) Zhao, N.; Ai, N.; Cai, M.; Wang, X.; Pei, J.; Wan, X. *Polym. Chem.* **2016**, *7*, 235.
- 45) Estrada, L. A.; Stalder, R.; Abboud, K. A.; Risko, C.; Bre, J.; Reynolds, J. R. *Macromolecules* **2013**, *46*, 8832.
- 46) Stalder, R.; Mei, J.; Subbiah, J.; Grand, C.; Estrada, L. A.; So, F.; Reynolds, J. R. *Macromolecules* **2011**, *44*, 6303.
- 47) Zhu, S.; Dorh, N.; Zhang, J.; Vegesna, G.; Li, H.; Luo, F.-T.; Tiwari, A.; Liu, H. *J. Mater. Chem.* **2012**, *22*, 2781.
- 48) Tamayo, A. B.; Tantiwivat, M.; Walker, B.; Nguyen, T-Q. *J. Phys. Chem. C* **2008**, *112*, 15543.
- 49) Huo, L.; Hou, J.; Chen, H.-Y.; Zhang, S.; Jiang, Y.; Chen, T. L.; Yang, Y. *Macromolecules* **2009**, *42*, 6564.
- 50) Park, J.-M.; Park, S. K.; Yoon, W. S.; Kim, J. H.; Kim, D. W.; Choi, T.-L.; Park, S. Y. *Macromolecules* **2016**, *49*, 2985.
- 51) Khim, D.; Cheon, Y. R.; Xu, Y.; Park, W.-T.; Kwon, S.-K.; Noh, Y.-Y.; Kim, Y.-H. *Chem. Mater.* **2016**, *28*, 2287.
- 52) Kim, H. G.; Kang, B.; Ko, H.; Lee, J.; Shin, J.; Cho, K. *Chem. Mater.* **2015**, *27*, 829–838.
- 53) Burckstummer, H.; Weissenstein, A.; Bialas, D.; Wurthner, F. *J. Org. Chem.* **2011**, *76*, 2426.
- 54) Zhu, S.; Dorh, N.; Zhang, J.; Vegesna, G.; Li, H.; Luo, F.-T.; Tiwari, A.; Liu, H. *J. Mater. Chem.* **2012**, *22*, 2781.
- 55) Lei, T.; Dou, J.-H.; Ma, Z.-J.; Liu, C.-J.; Wang, J.-Y.; Pei, J. *Chem. Sci.* **2013**, *4*, 2447.
- 56) Gao, Y.; Zhang, X.; Tian, H.; Zhang, J.; Yan, D.; Geng, Y.; Wang, F. *Adv. Mater.* **2015**, *27*, 6753.
- 57) Hwang, H.; Khim, D.; Yun, J.-M.; Jung, E.; Jang, S.-Y.; Jang, Y. H.; Noh, Y.-Y.; Kim, D.-Y. *Adv. Funct. Mater.* **2015**, *25*, 1146.
- 58) Lin, G.; Qin, Y.; Zhang, J.; Guan, Y.-S.; Xu, H.; Xu, W.; Zhu, D. *J. Mater. Chem. C* **2016**, *4*, 4470.
- 59) Lei, T.; Dou, J. H.; Pei, J. *Adv. Mater.* **2012**, *24*, 6457.
- 60) Kang, I.; Yun, H. J.; Chung, D. S.; Kwon, S. K.; Kim, Y. H. *J. Am. Chem. Soc.* **2013**, *135*, 14896.
- 61) Lei, T.; Dou, J. H.; Cao, X. Y.; Wang, J. Y.; Pei, J. *Adv. Mater.* **2013**, *25*, 6589.

- 62) Na, J. Y.; Kang, B.; Sin, D. H.; Cho, K.; Park, Y. D. *Sci. Rep.* **2015**, *5*, 13288.
- 63) Hu, Z.; Willard, A. P.; Ono, R. J.; Bielawski, C. W.; Rossky, P. J.; Vanden Bout, D. A. *Nat. Commun.* **2015**, *6*, 8246.
- 64) Li, G.; Shrotriya, V.; Huang, J.; Yao, Y.; Moriarty, T.; Emery, K.; Yang, Y. *Nature Mater.* **2005**, *4*, 864.
- 65) Popere, B. C.; Pelle, A. M. D.; Poe, A.; Balaji, G.; Thayumanavan, S. *Chem. Sci.* **2012**, *3*, 3093.
- 66) Cabanetos, C.; El Labban, A.; Bartelt, J. A.; Douglas, J. D.; Mateker, W. R.; Fréchet, J. M. J.; McGehee, M. D.; Beaujuge, P. M. *J. Am. Chem. Soc.* **2013**, *135*, 4656.
- 67) Huang, Y.; Wu, F.; Zhang, M.; Mei, S.; Shen, P.; Tan, S. *Dye. Pigment.* **2015**, *115*, 58.
- 68) Kastinen, T.; Niskanen, M.; Risko, C.; Cramariuc, O.; Hukka, T. I. *J. Phys. Chem. A* **2016**, *120*, 1051.
- 69) Yao, H.; Ye, L.; Zhang, H.; Li, S.; Zhang, S.; Hou, J. *Chem. Rev.* **2016**, *116*, 7397.
- 70) Kang, T. E.; Cho, H. H.; Cho, C. H.; Kim, K. H.; Kang, H.; Lee, M.; Lee, S.; Kim, B.; Im, C.; Kim, B. J. *ACS Appl. Mater. Interfaces* **2013**, *5*, 861.

## **Chapter 6**

# Summary and Future Directions



## 6.1 Summary

BODIPY dyes are now being explored in the area of organic electronics particularly for organic field effect transistors (OFET). Polymers and small molecules comprising BODIPY were used as donor in organic solar cells, but it's in 2011 when Popere et al developed BODIPY based polymers for OFET for the first time.<sup>1</sup> Mobility values were low but the findings were exciting as these dyes were not considered suitable for electronic applications before. Since then many reports of BODIPY based small molecules and polymers have come.<sup>2-4</sup> Most of them are unipolar charge transport materials and mobility values have been modest so far. Perhaps the reason is that knowledge of structure-property relationship is limited and this fluorophore is not being utilized to its full potential. Towards this objective, the thesis entitled "BODIPY based small molecules and polymers for organic field effect transistors" was focused on the development of BODIPY based organic semiconductor materials and study of their charge transport behaviour. The main goal was to understand the impact of substituents on the core on charge transport properties. As BODIPY dyes are conventionally used as small dyes for fluorescence labelling, sensors, etc., bulky groups are introduced into the core to increase fluorescence quantum yields. A variety of such dyes are reported by different groups. But, introducing such cores in conjugated systems leads to a twist in the backbone and poor solid state packing. Closer solid state packing is one essential criterion for faster charge transport. Another important criterion is a selection of suitable long alkyl side chains for solubility purposes. They are not only helpful in bringing solubility but also impact solid state packing.

In first two working chapters, a series of small conjugated molecules (CSMs) were synthesized with varying side chains and their charge transport properties were measured. First, side chain was varied from linear and branched alkyl chain to the OEG side chain and impact on physical properties were studied. Side chains were substituted on CSMs containing triphenylamine as donor and BODIPY as acceptor. CSM with OEG side chain was found to be soluble in common organic solvents and forms smooth films while processed from organic solvents.<sup>4</sup> It facilitates better intermolecular contact and shows superior device efficiencies than its alkyl chain counterparts. Next, a systematic study was carried to understand the impact of nature of side chain on both electronic and physical properties of BODIPY based conjugated small molecules. BODIPY core was varied by methyl groups removal from 1 and 7 positions and side chains were varied from the hydrophobic alkyl (nonyl) chain to hydrophilic OEG (triethylene glycol) chain. These side chains have different electronic and

physical properties. Methyl group removal resulted in deep lying LUMO and HOMO energy levels for dimethyl BODIPY core and also a decrease in dihedral angle in the target molecules was observed. Absorption spectra of triethylene glycol containing molecules are red shifted in comparison to the alkyl chain analogs. In this way, by varying side chain substitution on meso position FMO orbital levels were finely tuned. OFET devices fabricated from these molecules show better performance for triethylene glycol containing CSMs on unmodified FET substrates than alkyl chain substituted ones. After silane modification, hole carrier mobilities improve slightly for alkyl chain substituted CSMs but decrease by one order for triethylene glycol substituted ones.

In another design, BODIPY was selected as terminal moiety to explore the potential of the rigid core in solid state stacking and hence better interconnectivity in the film form. Three types of BODIPY dyes (**1** – **3**) were selected with varying substitution on the core in order to improve solid state packing. Planar DPP moiety was selected as a central unit. Electronic behaviour of these molecules was studied theoretically and experimentally. It was found that CSM **3** with dimethyl BODIPY core and methyl group at meso position has deeper HOMO/LUMO energy levels, lowest band gap and most planar conjugated backbone amongst three. OFET devices fabricated using these molecules exhibit hole transport. **3** shows highest mobility values with a hole mobility of  $1.3 \times 10^{-2} \text{ cm}^2/\text{Vs}$ . Here, a judicious combination of DPP and BODIPY subunits resulted in high performing solution processable small molecules for OFETs.

In addition to small molecules, BODIPY based copolymers were also synthesized and studied. Comonomers were varied from electron deficient isoindigo and DPP to electron rich BDT moieties. All of these polymers were well soluble in common organic solvents. Though p(BODIPY-alt-isoindigo) is a thermally stable medium energy band gap material, it does not transport charges while used in OFET device configuration. Three p(BODIPY-alt-DPP) polymers (**P1** – **P3**) were synthesized with a variation on the BODIPY core. These polymers are thermally well stable, low band gap materials. One of the polymers, **P3**, with dimethyl BODIPY core exhibits highest mobility values with a hole mobility of  $3.1 \times 10^{-2} \text{ cm}^2/\text{Vs}$  and electron mobility of  $1.5 \times 10^{-2} \text{ cm}^2/\text{Vs}$ . this is the highest value reported so far for a BODIPY containing material for ambipolar charge transport. Two copolymers containing BDT and BODIPY were synthesized. They are medium to low energy band gap materials and are hole transporter. OFET devices fabricated from **BDT P2** exhibit hole mobility of  $1.35 \times 10^{-5} \text{ cm}^2/\text{Vs}$  which is one order higher than that obtained for **BDT P1**. To summarise, conjugated

materials containing BODIPY were developed and studied for OFET applications. A p(BODIPY-alt-DPP), **P3** was synthesized and an ambipolar charge transport with hole and electron mobilities in the range of  $0.01 \text{ cm}^2/\text{Vs}$  was found which is highest so far for a BODIPY based ambipolar semiconductor polymer.

## 6.2 Future Directions

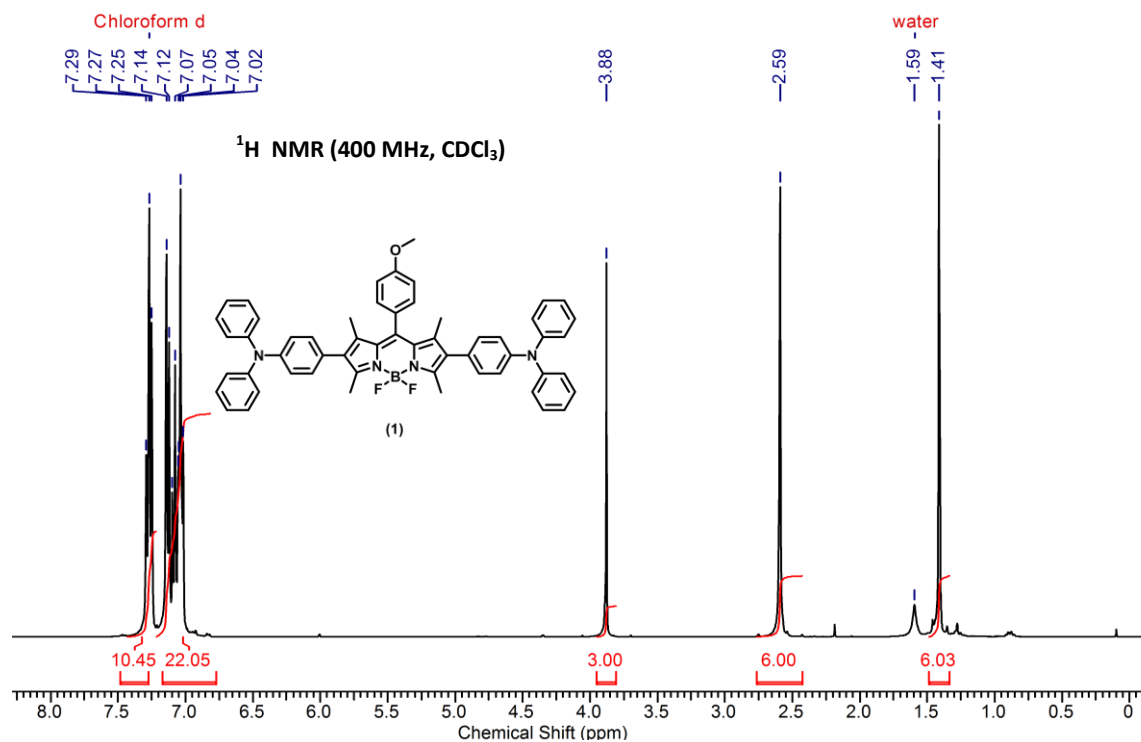
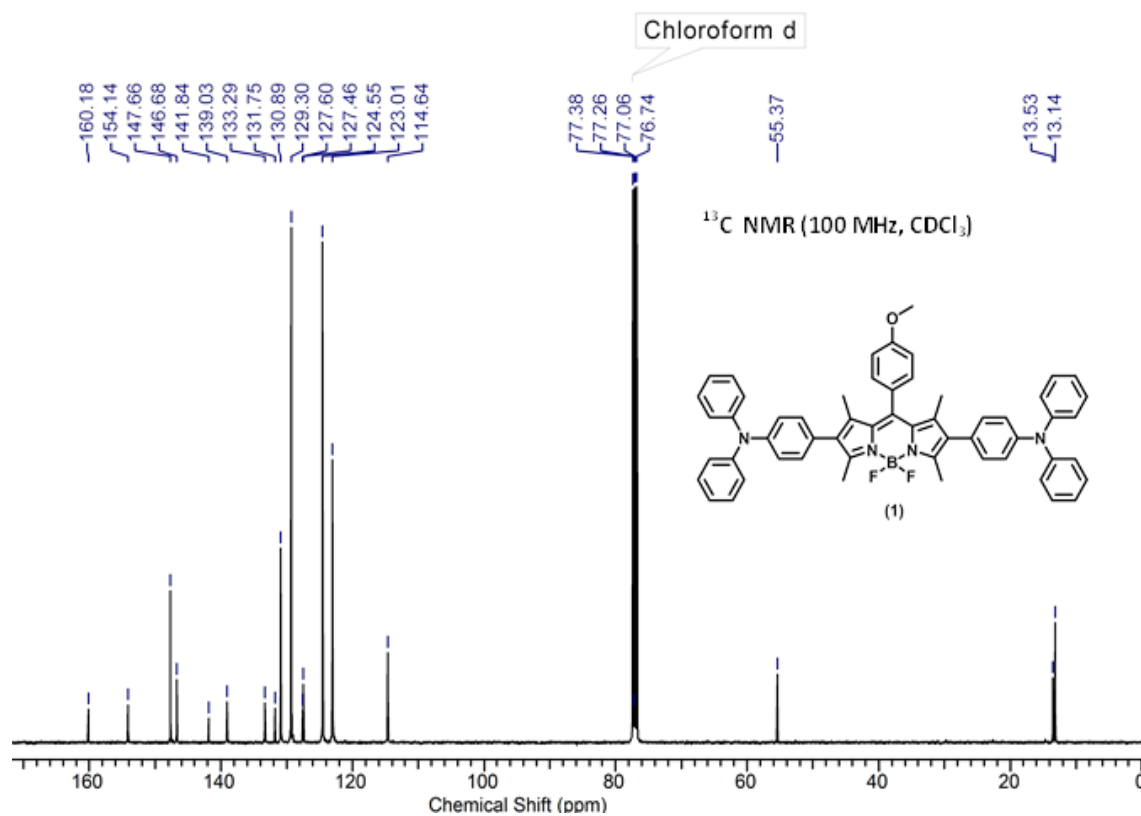
Based on the findings in this work, a number of BODIPY derivatives can be designed and synthesized. As BODIPY core is robust and synthetic protocols are straight forward, substituent groups can be varied as per requirements. We found that OEG side chain helps in ordered solid state packing. Though in our work we used triphenylamine as a terminal moiety that limits close packing after a certain distance, planar terminal moieties can be used for long range and closer solid state packing. By placing side chains directly on meso position, FMO energy levels can be finely tuned. This property can be used for materials with varying band gaps and degree of self-assembly in the solid state. BODIPY was used as a terminal group in conjugation with DPP and the small molecule was found to have mobility in the range of  $0.01 \text{ cm}^2/\text{Vs}$  which is a considerable number for a small molecule by solution processing method. BODIPY can be conjugated with other planar moieties for developing low band gap materials. Also, copolymers of BODIPY dyes in conjugation with other planar monomers with suitable orbital mixing can be developed as high performing p-channel, n-channel, and ambipolar semiconductors.

## 6.3 References

- 1) Popere, B. C.; Della Pelle, A. M.; Thayumanavan, S. *Macromolecules* **2011**, *44*, 4767.
- 2) Debnath, S.; Singh, S.; Bedi, A.; Krishnamoorthy, K.; Zade, S. S. *J. Phys. Chem. C* **2015**, *119*, 15859.
- 3) Debnath, S.; Singh, S.; Bedi, A.; Krishnamoorthy, K.; Zade, S. S. *J. Polym. Sci. A: Polym. Chem.* **2016**, *54*, 1978.
- 4) Singh, S.; Venugopalan, V.; Krishnamoorthy, K. *Phys. Chem. Chem. Phys.* **2014**, *16*, 13376.

## Appendix I

## I.1 NMR and MALDI-TOF spectra for Chapter 2

**Figure I.1:** 400 MHz  $^1\text{H}$  NMR spectrum of compound (1) in  $\text{CDCl}_3$ .**Figure I.2** 400 MHz  $^{13}\text{C}$  NMR spectrum of compound (1) in  $\text{CDCl}_3$ .

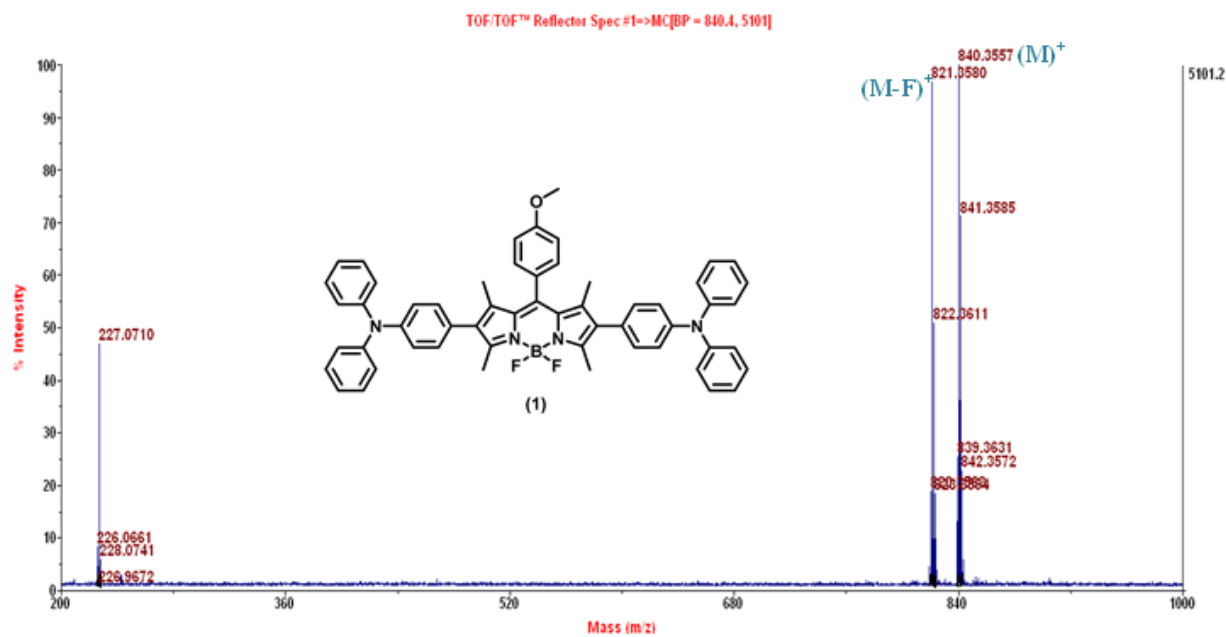


Figure I.3 Mass spectrum of compound (1)

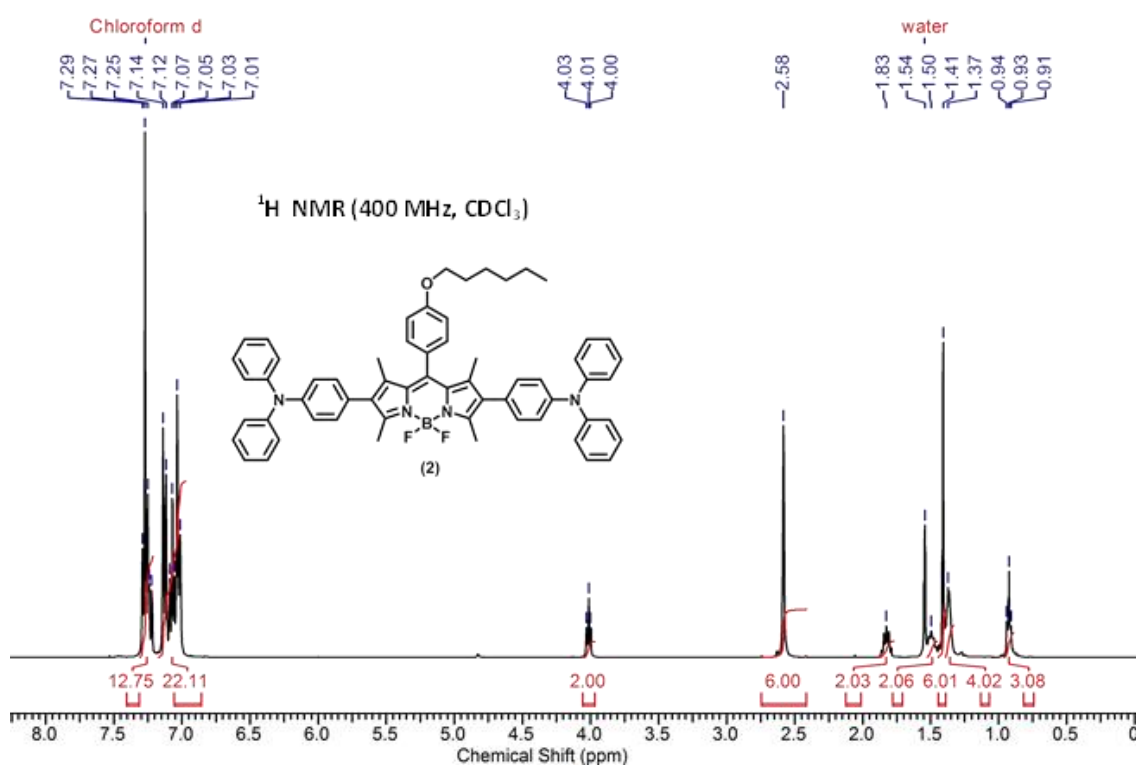
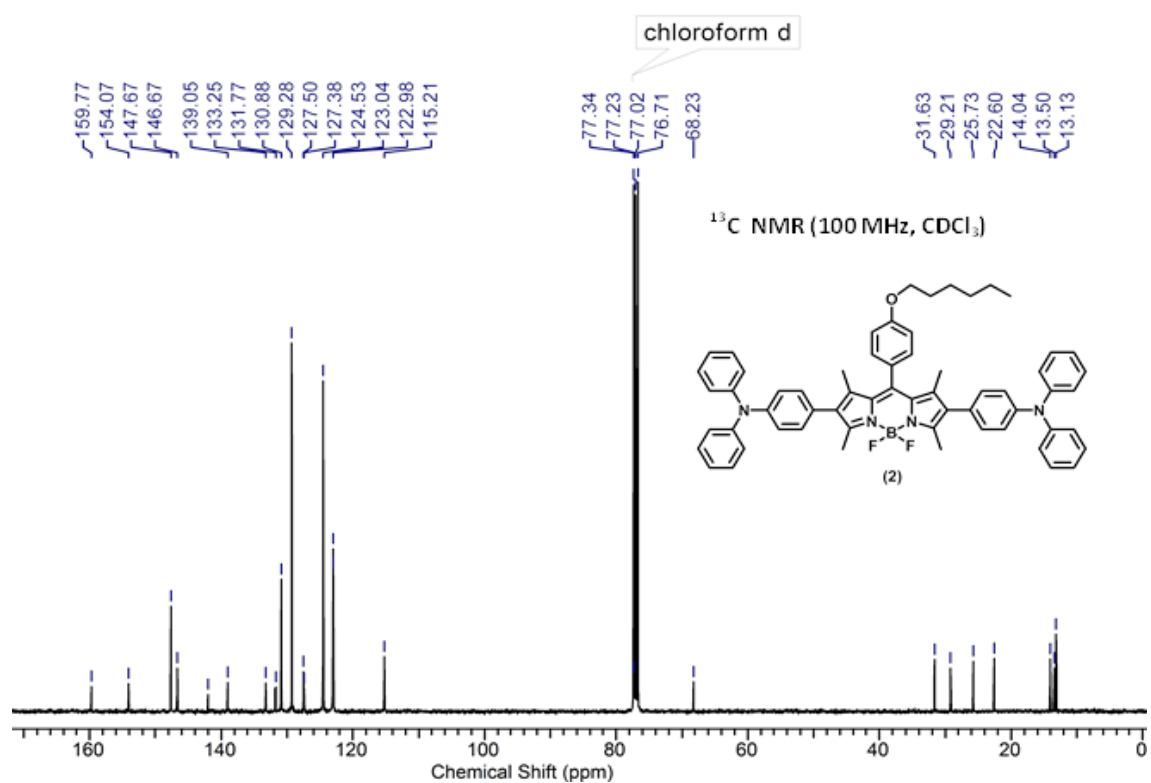
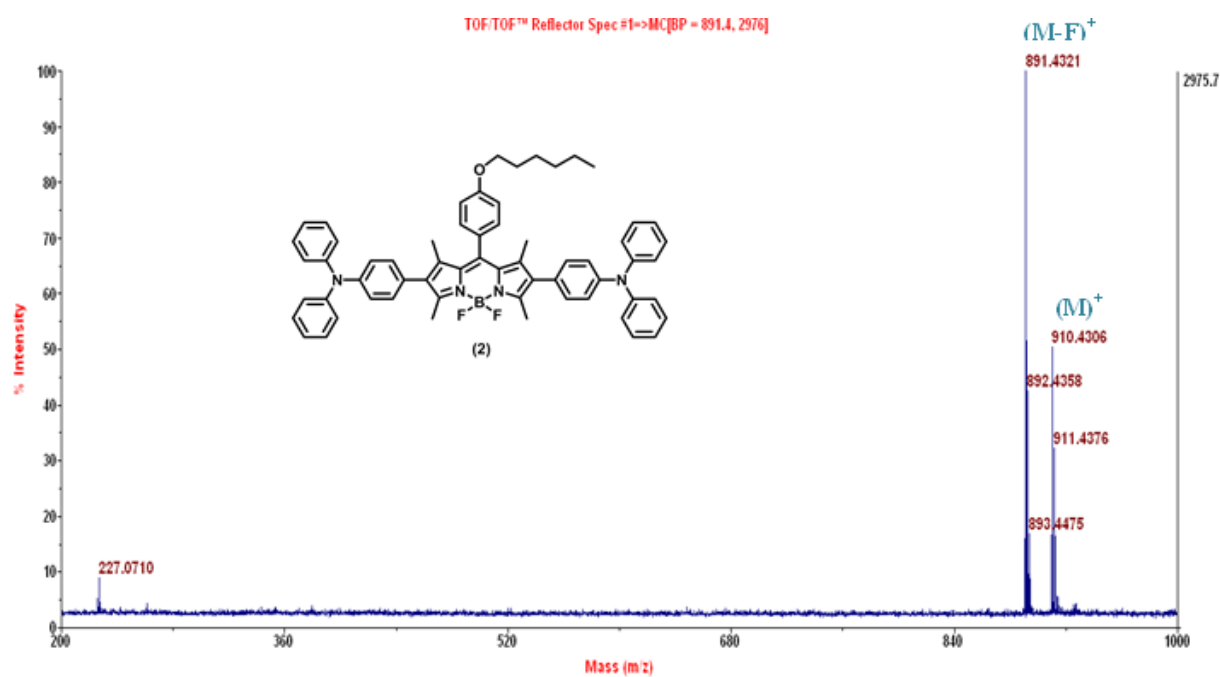


Figure I.4 400 MHz <sup>1</sup>H NMR spectrum of compound (2) in CDCl<sub>3</sub>.



**Figure I.5** 400 MHz <sup>13</sup>C NMR spectrum of compound (2) in CDCl<sub>3</sub>.



**Figure I.6** Mass spectrum of compound (2)

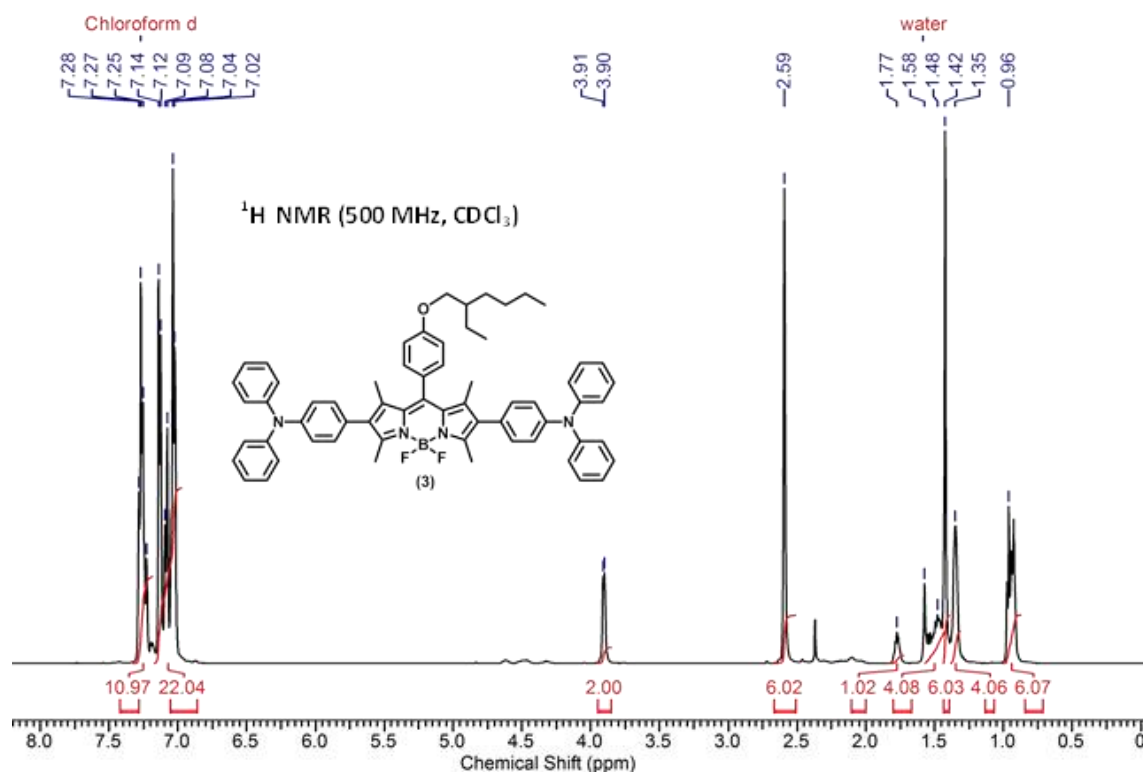


**Figure I.7** 400 MHz <sup>1</sup>H NMR spectrum of compound (3) in CDCl<sub>3</sub>.

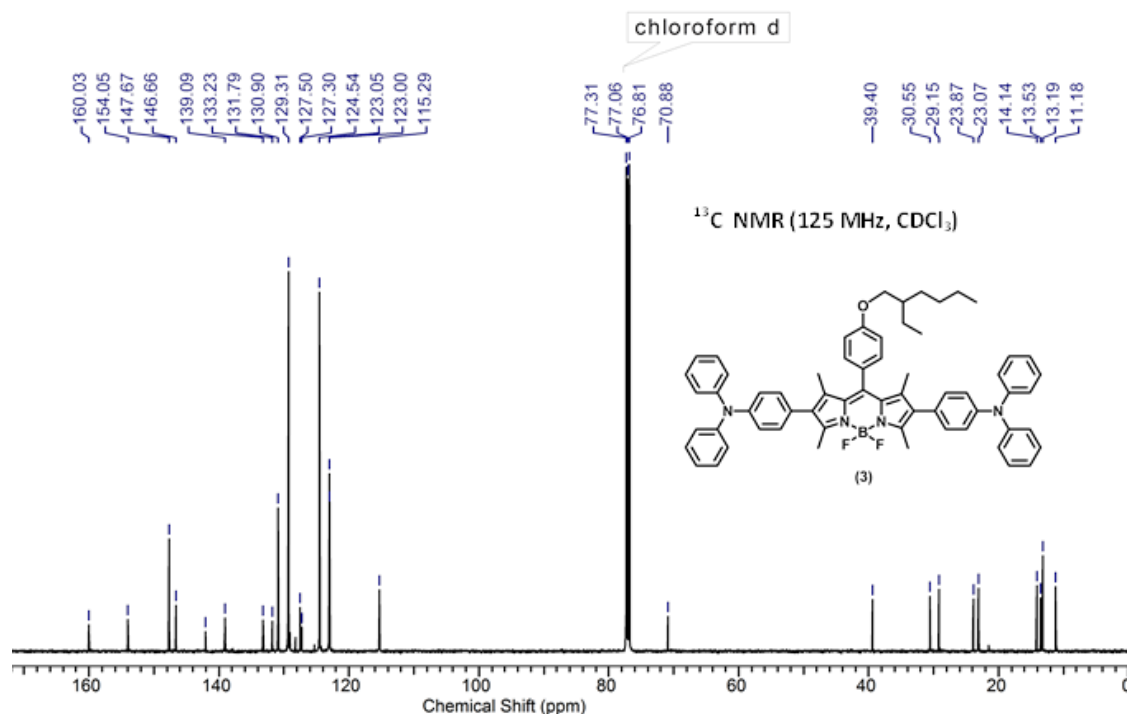


**Figure I.8** 400 MHz <sup>13</sup>C NMR spectrum of compound (2) in CDCl<sub>3</sub>.

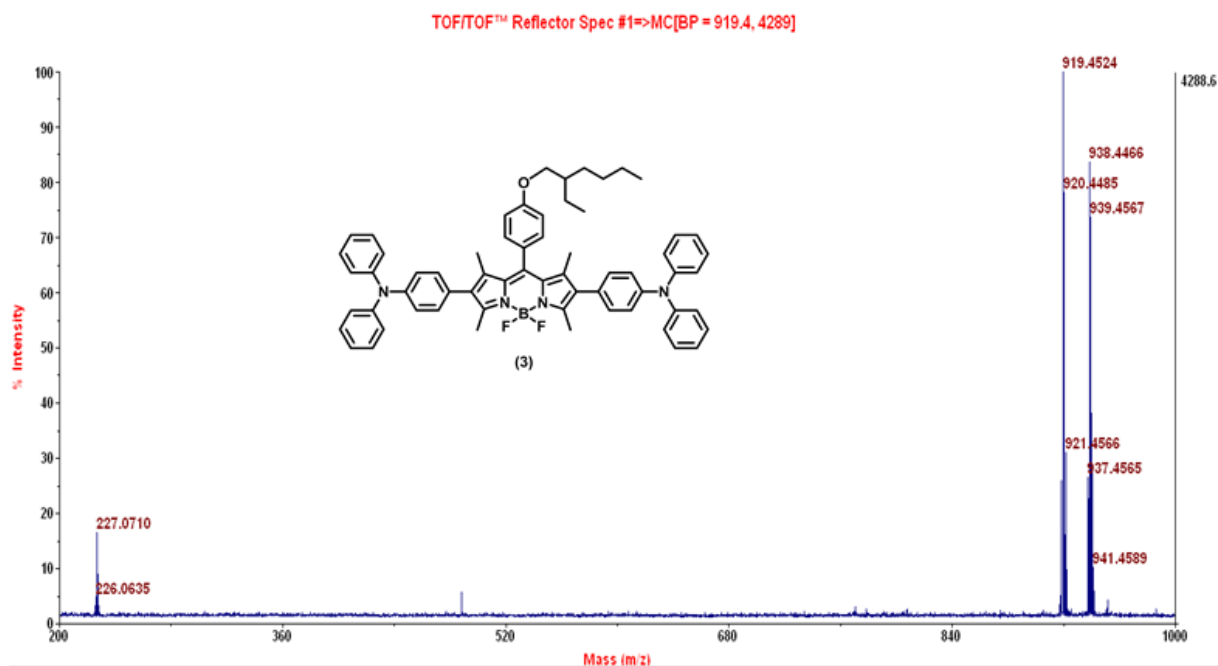


Figure I.9 Mass spectrum of compound (3)

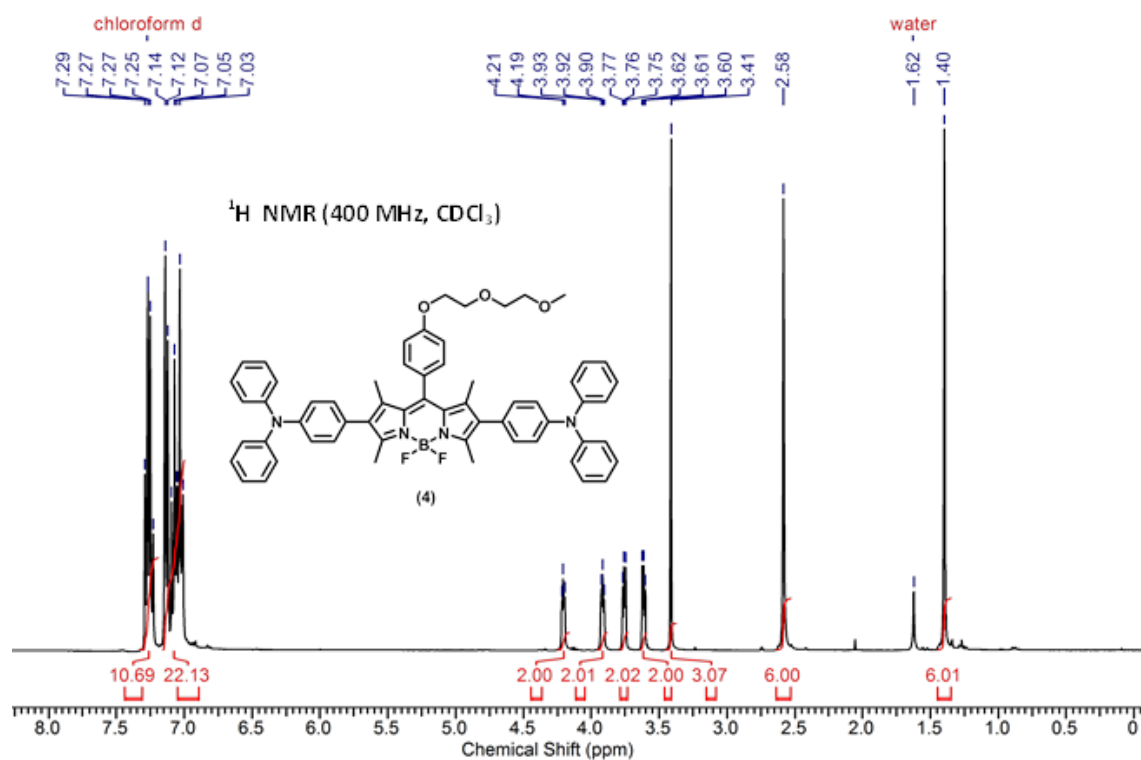


Figure I.10 400 MHz <sup>1</sup>H NMR spectrum of compound (4) in CDCl<sub>3</sub>.



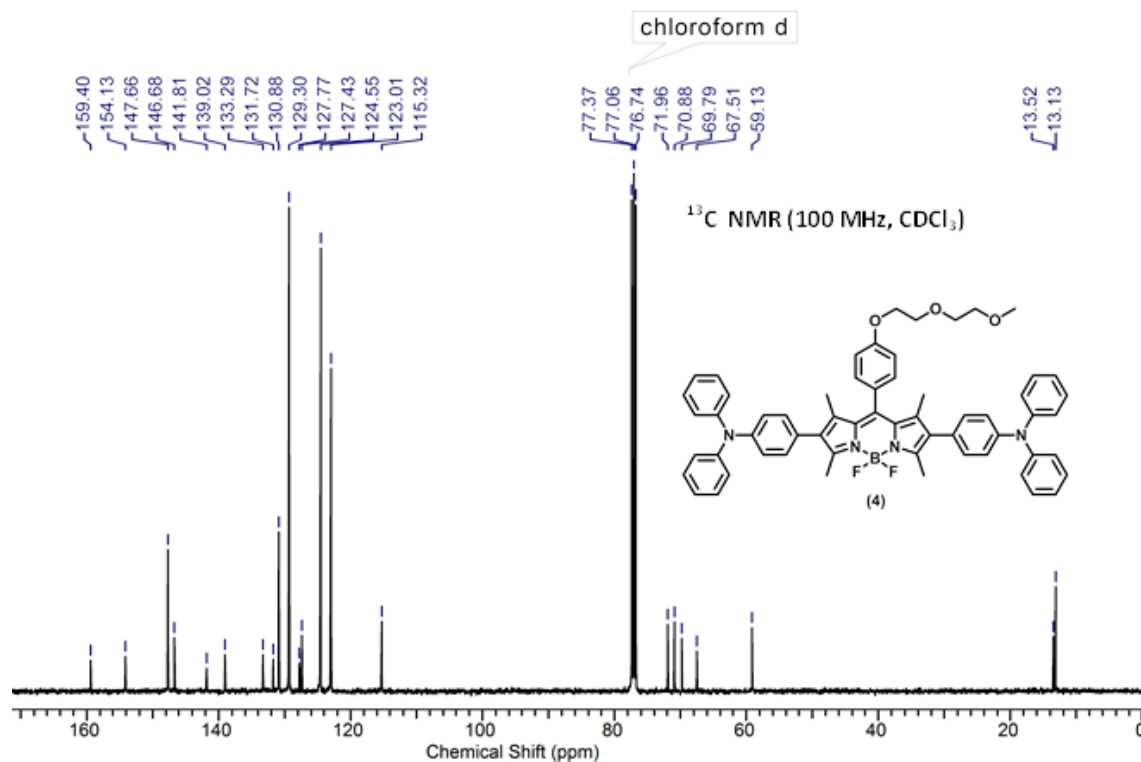


Figure I.11 400 MHz <sup>13</sup>C NMR spectrum of compound (4) in CDCl<sub>3</sub>.

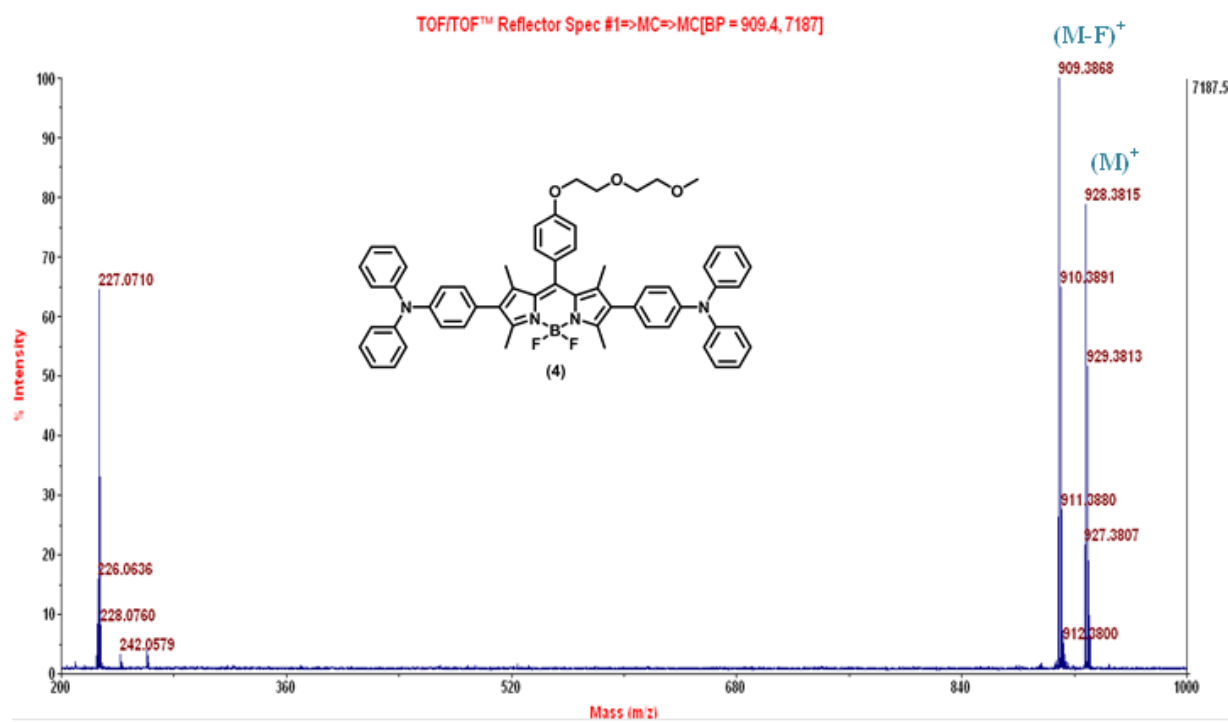
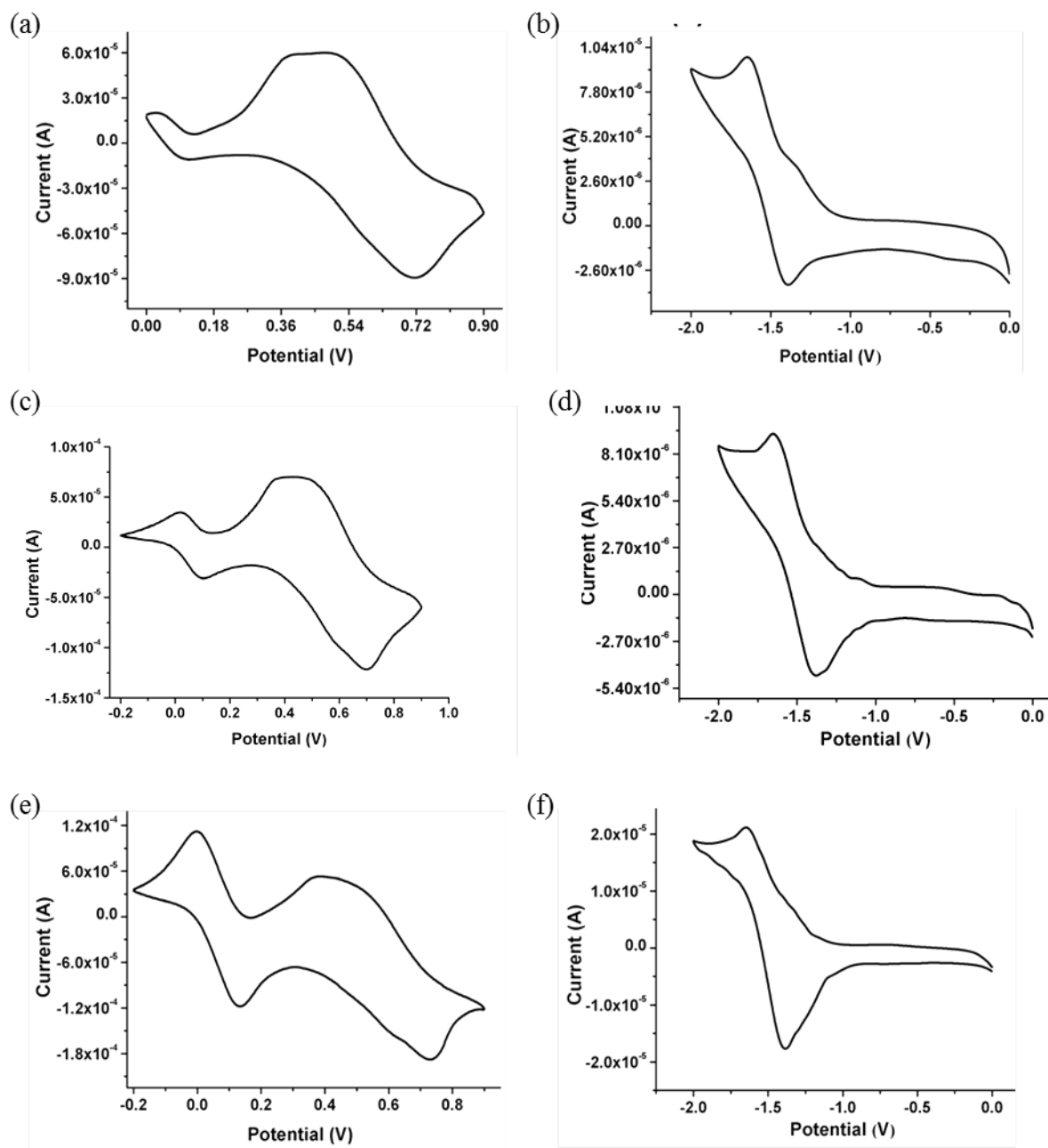


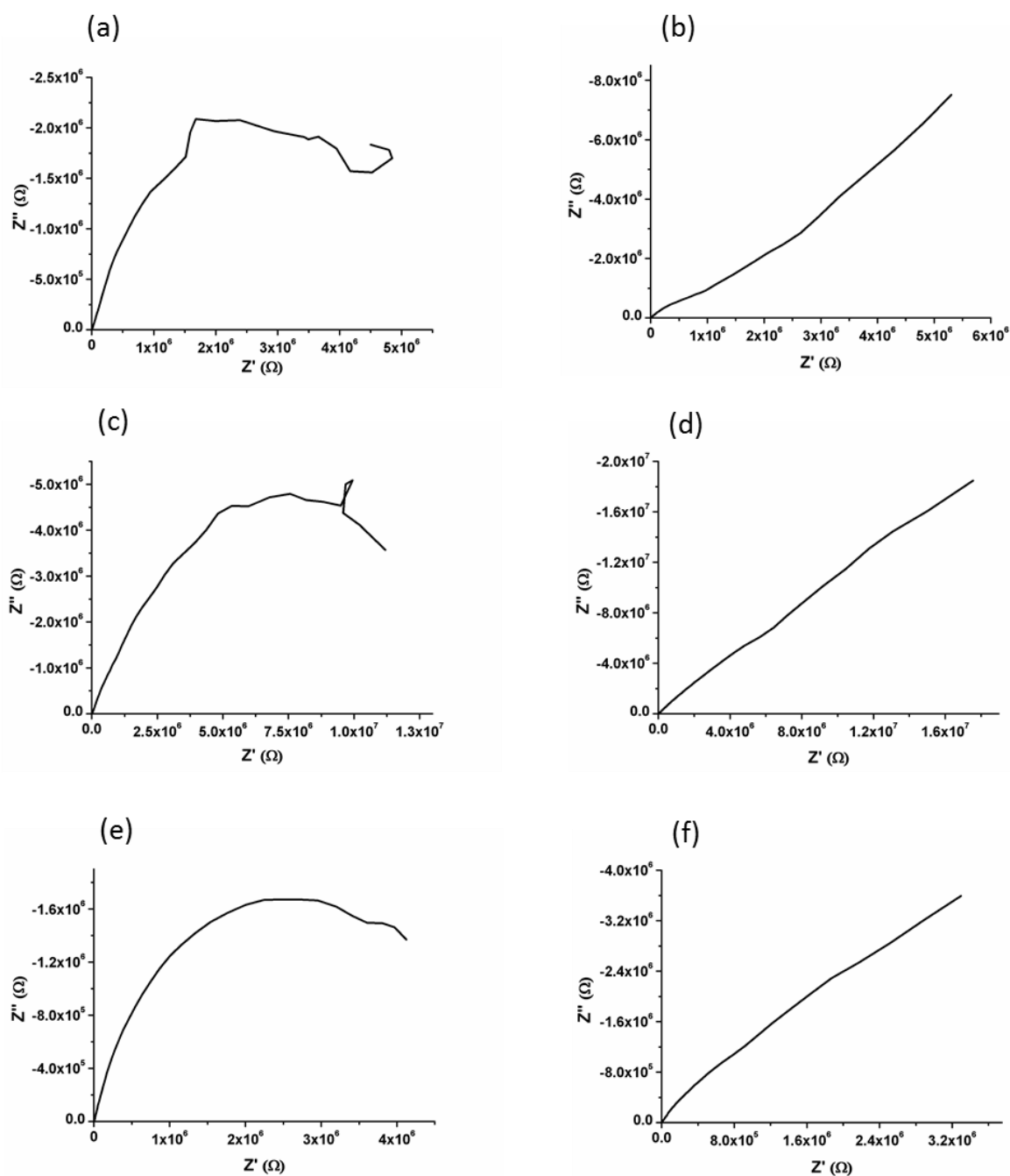
Figure I.12 Mass spectrum of compound (4)

## I.2 Electrochemical Properties: Cyclic voltammetry

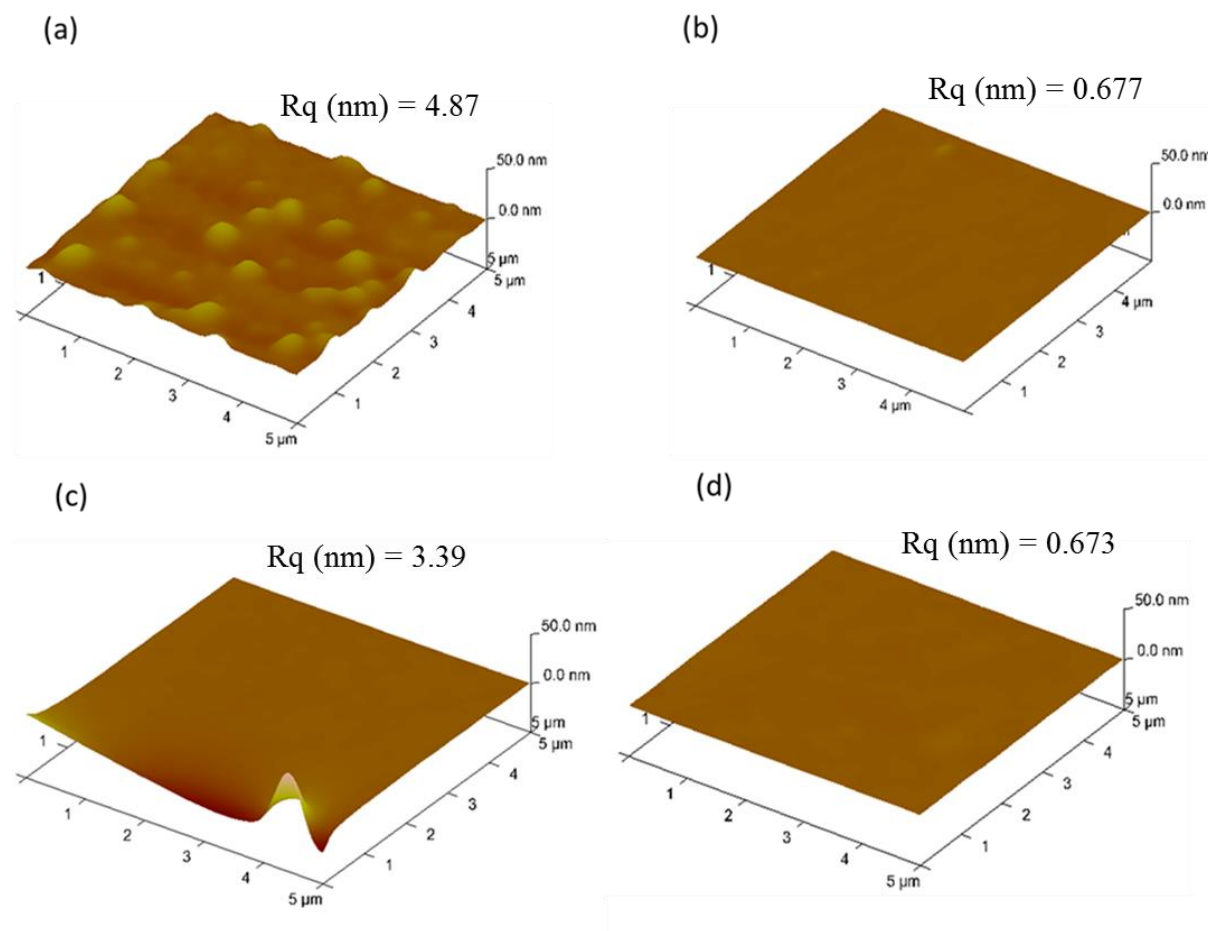


**Figure I.13** Cyclic voltammograms of molecules **2**, **3** and **4**: (a) oxidation scan of **2**, (b) reduction scan of **2**, (c) oxidation scan of **3**, (d) reduction scan of **3**, (e) oxidation scan of **4**, (f) reduction scan of **4**.

## I.3 Electrochemical Properties: Impedance



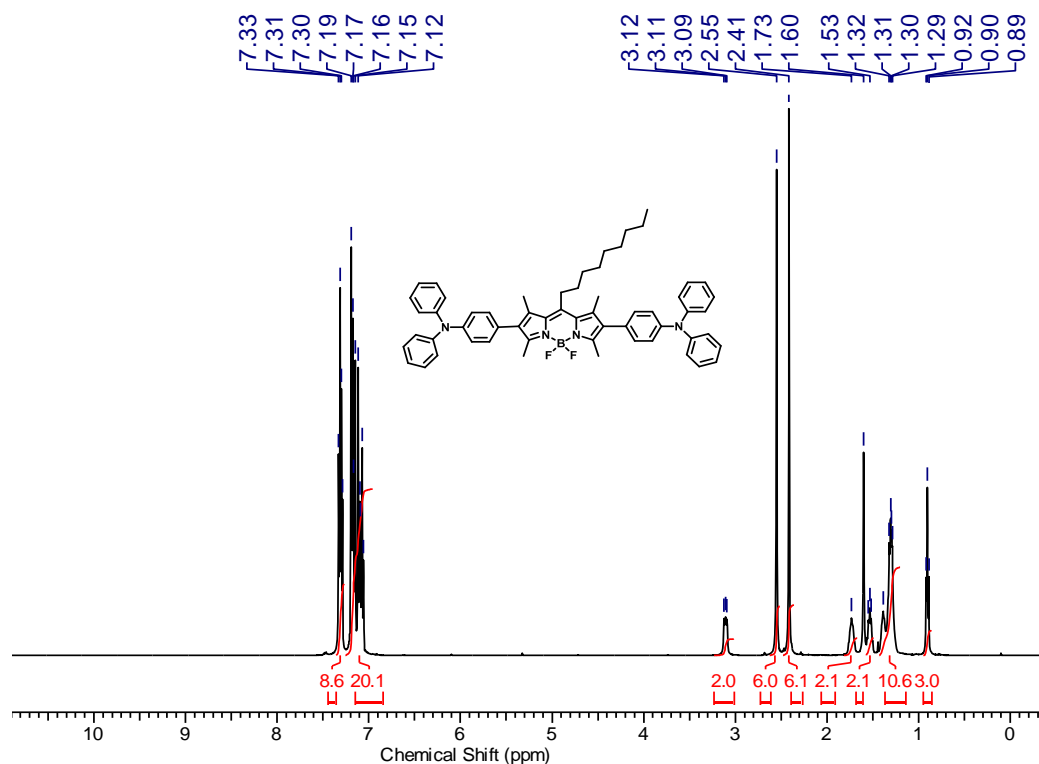
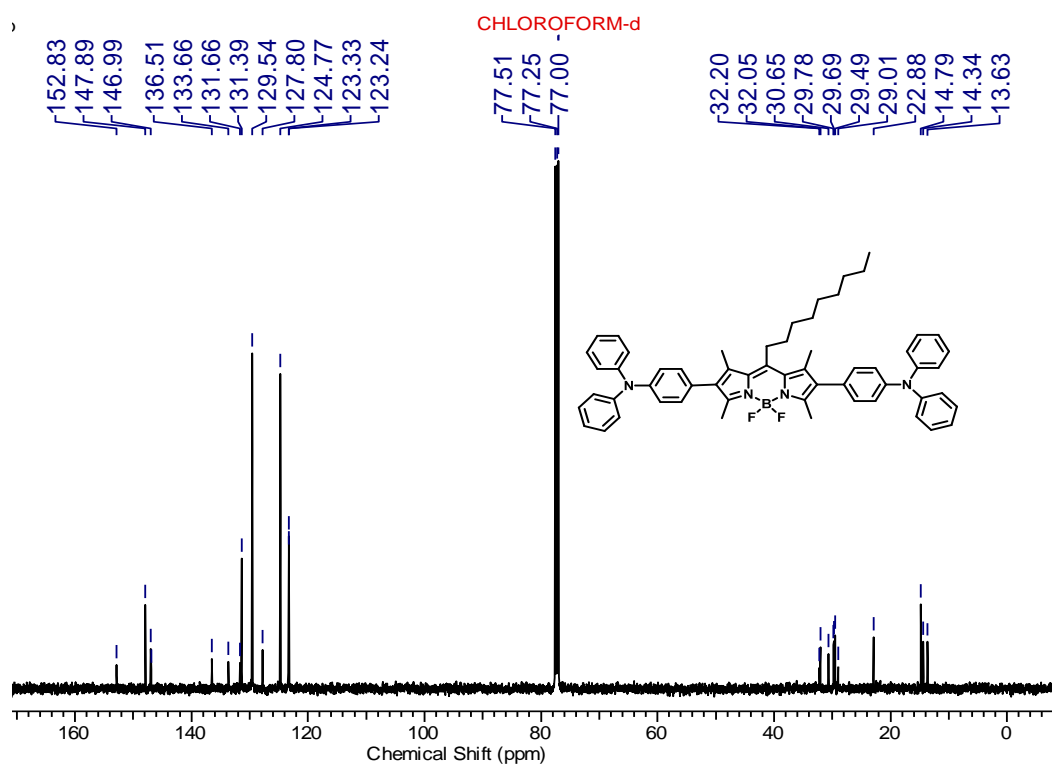
**Figure I.14** Nyquist plots for molecules **1**, **2** and **3**: (a) Nyquist plot at 0 V for **1**, (b) Nyquist plot at 0.6 V for **1**, (c) Nyquist plot at 0 V for **2**, (d) Nyquist plot at 0.6 V for **2**, (e) Nyquist plot at 0 V for **3** and (f) Nyquist plot at 0.6 V for **3**.

**I.4 Thin film morphology studies: AFM images**

**Figure I.15** AFM height images and root mean square roughness ( $R_q$ ) of thin films of **1** (a) and **3** (b) on modified  $\text{SiO}_2$ , **2** (c) on unmodified  $\text{SiO}_2$  and **2** (d) on HMDS modified  $\text{SiO}_2$  substrate.

## Appendix II

## II.1 NMR and MALDI-TOF spectra for Chapter 3

Figure II.1 400 MHz  $^1\text{H}$  NMR spectrum of compound (1) in  $\text{CDCl}_3$ .Figure II.2 400 MHz  $^{13}\text{C}$  NMR spectrum of compound (1) in  $\text{CDCl}_3$ .

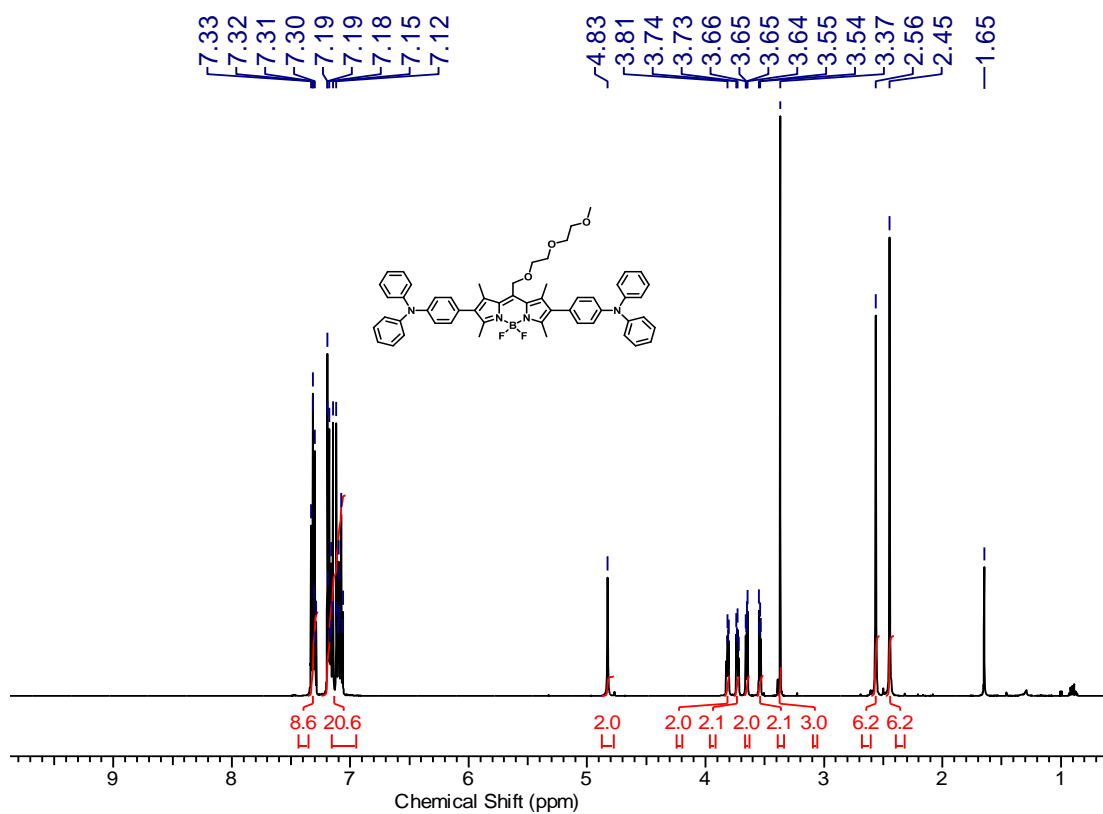


**Figure II.3** 400 MHz <sup>1</sup>H NMR spectrum of compound (2) in CDCl<sub>3</sub>.

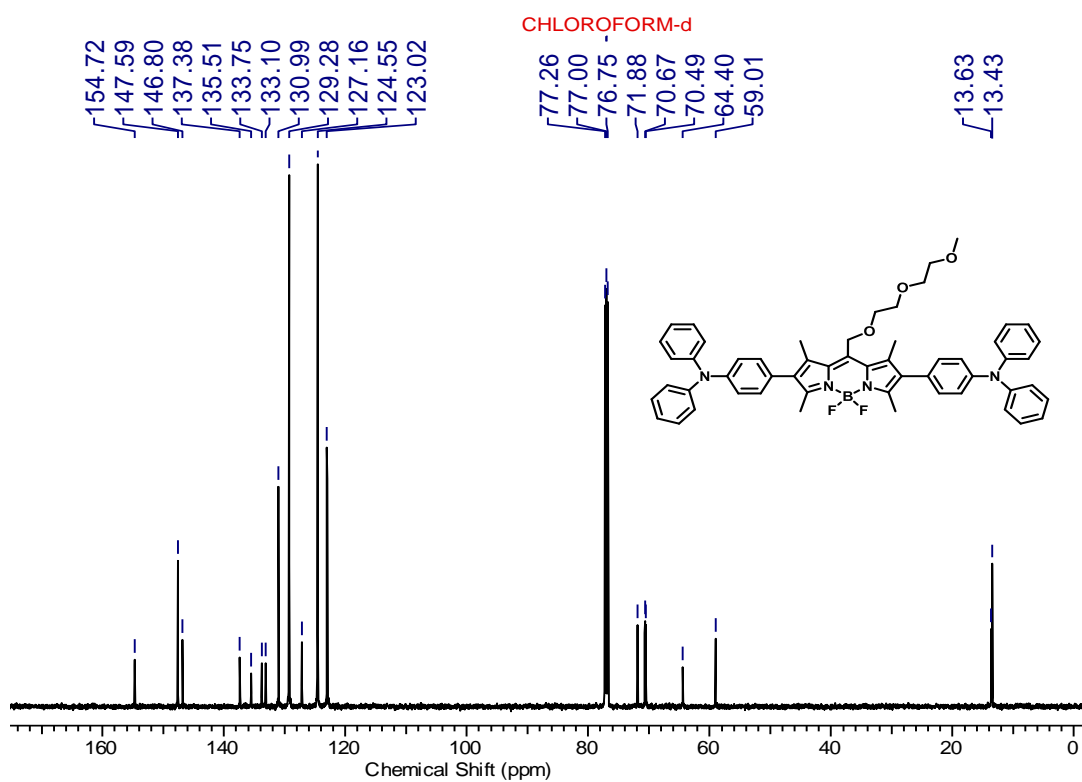


**Figure II.4** 400 MHz <sup>13</sup>C NMR spectrum of compound (2) in CDCl<sub>3</sub>.

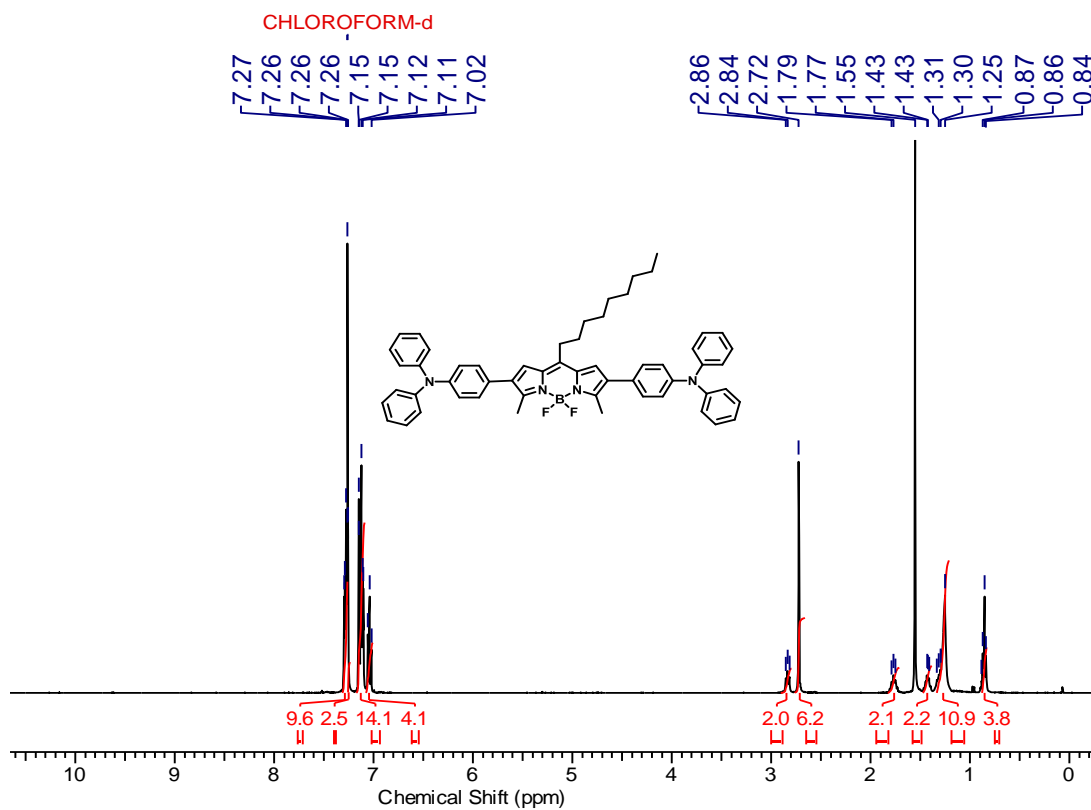


**Figure II.5** 400 MHz  $^1\text{H}$  NMR spectrum of compound (3) in  $\text{CDCl}_3$ .

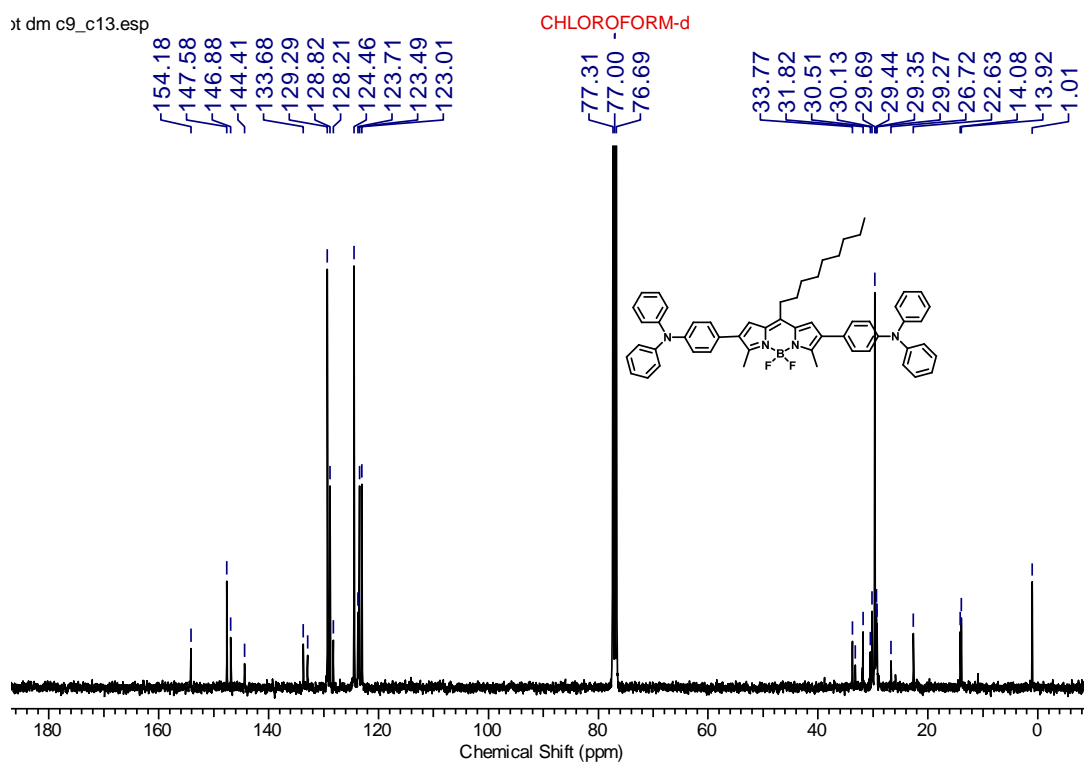


**Figure II.6** 400 MHz  $^{13}\text{C}$  NMR spectrum of compound (3) in  $\text{CDCl}_3$ .

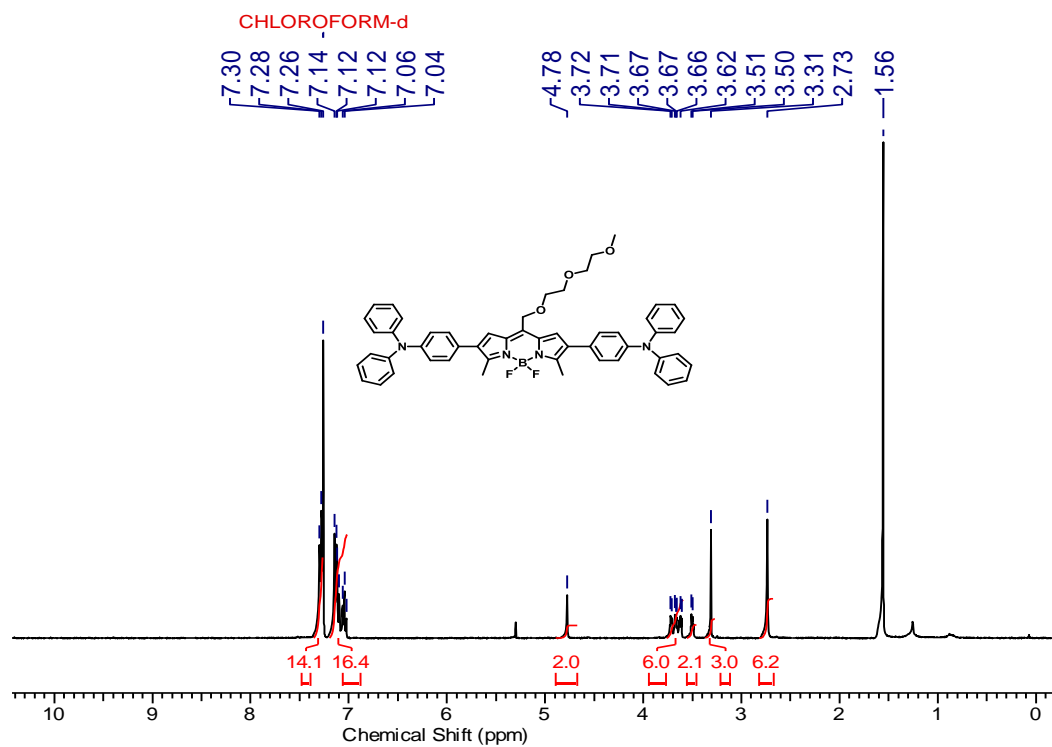


**Figure II.7** 400 MHz  $^1\text{H}$  NMR spectrum of compound (4) in  $\text{CDCl}_3$ .

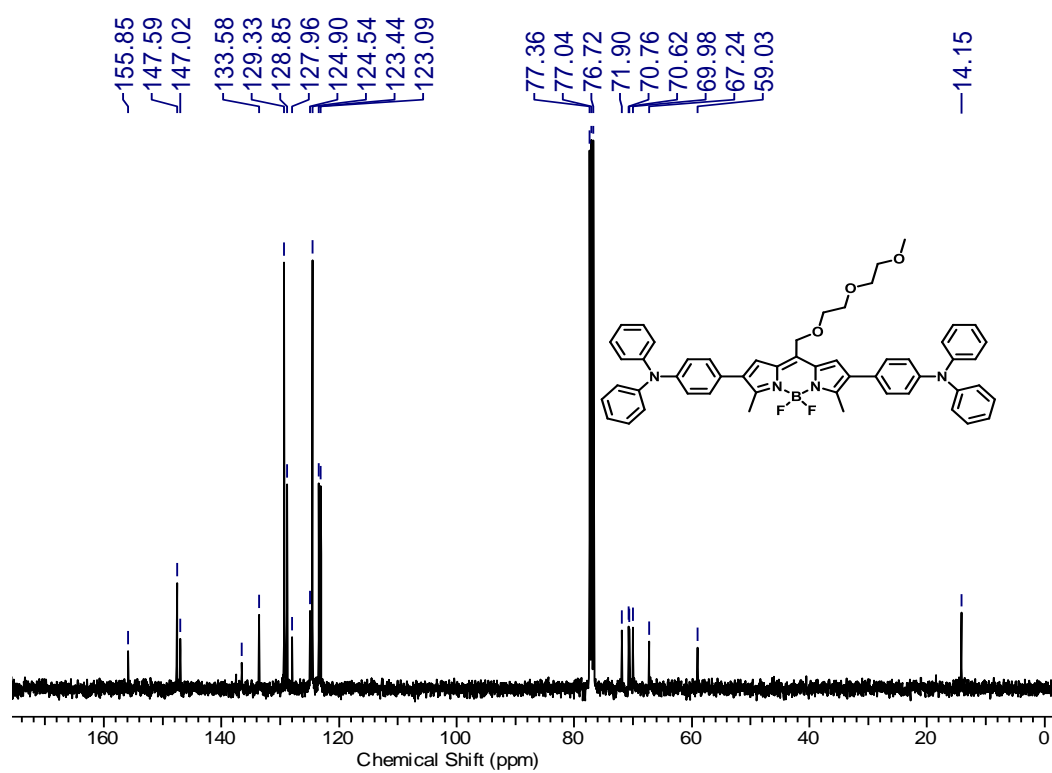


**Figure II.8** 400 MHz  $^{13}\text{C}$  NMR spectrum of compound (4) in  $\text{CDCl}_3$ .



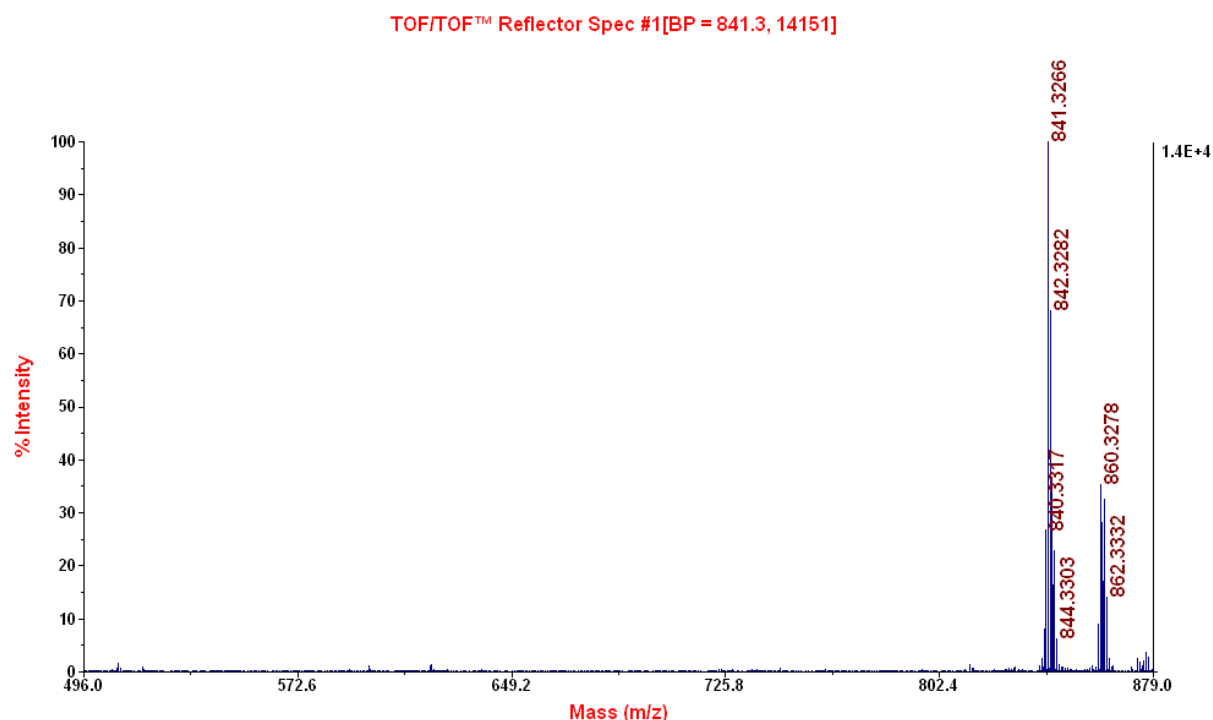


Figure II.9 Mass spectrum of compound (1).

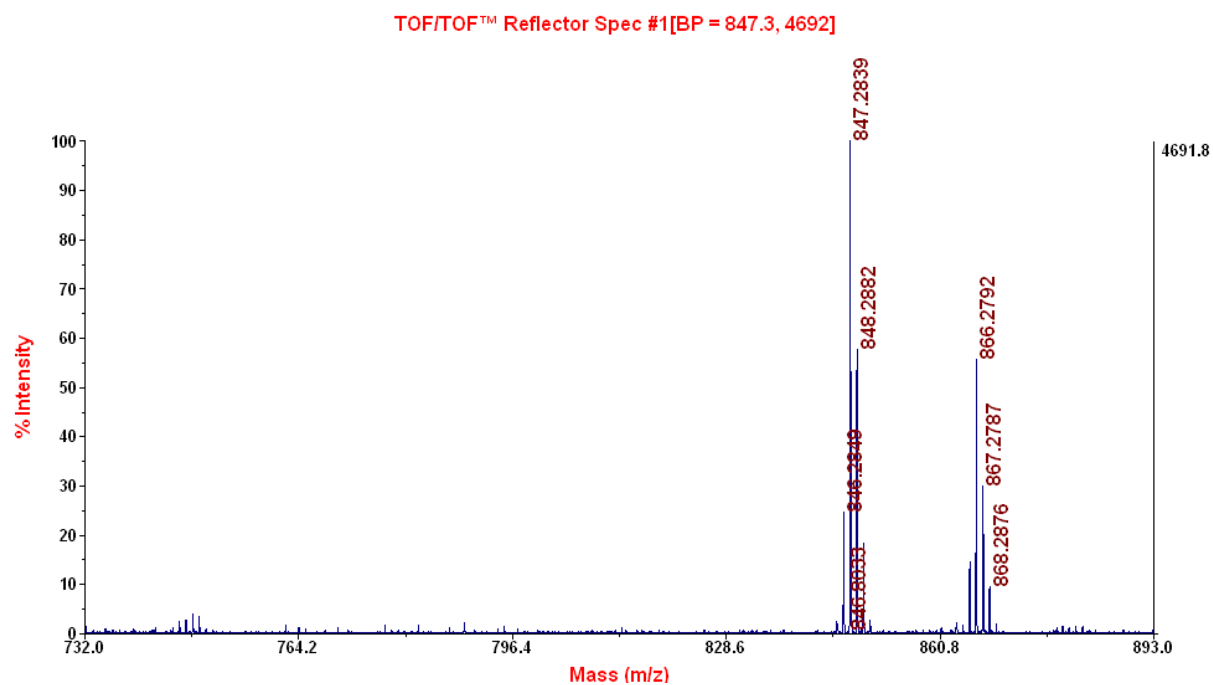


Figure II.10 Mass spectrum of compound (2).

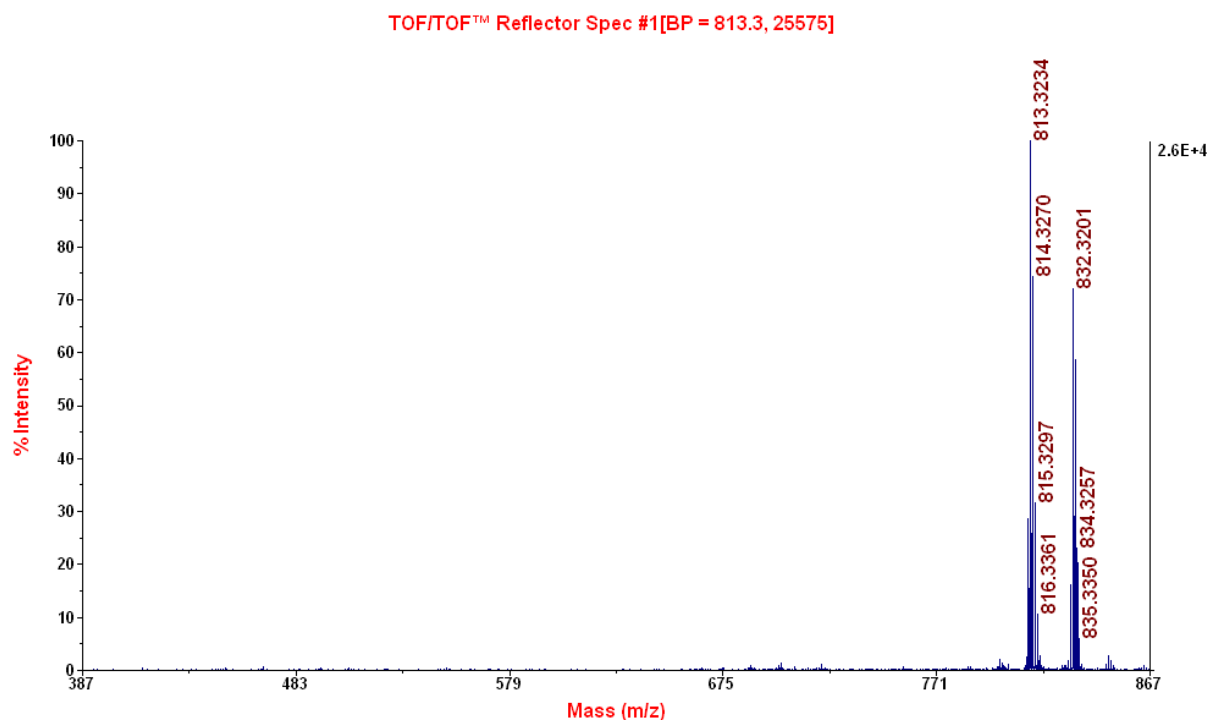


Figure II.11 Mass spectrum of compound (3).

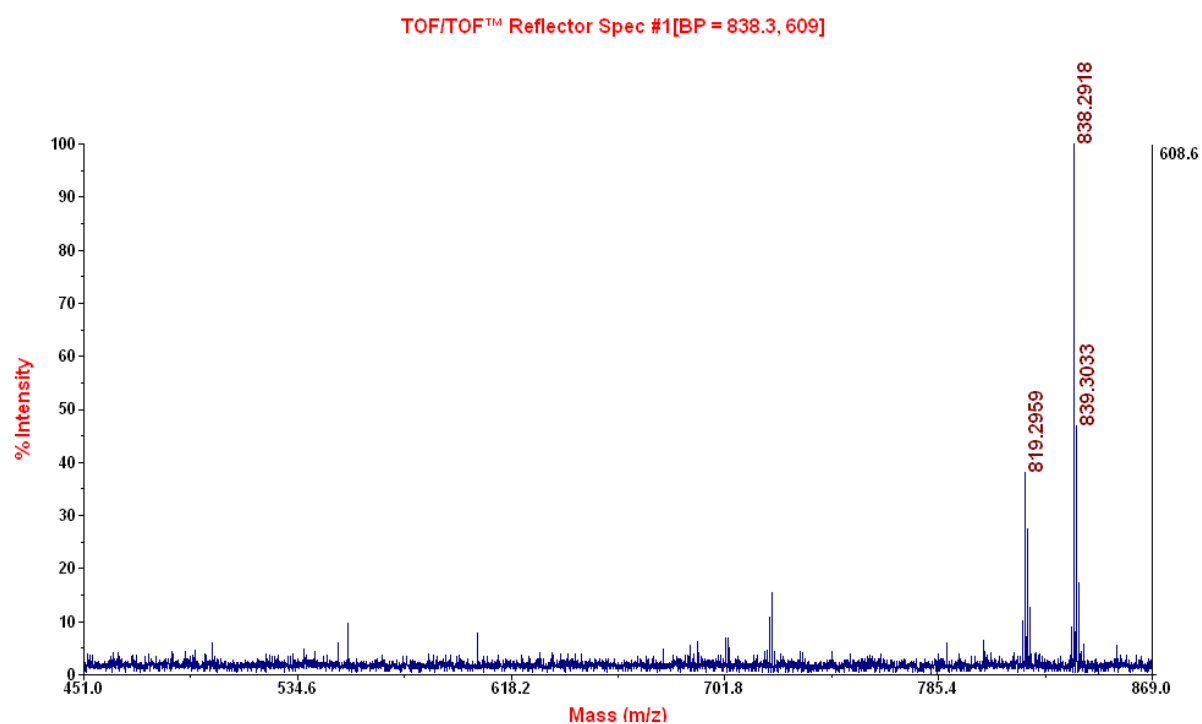
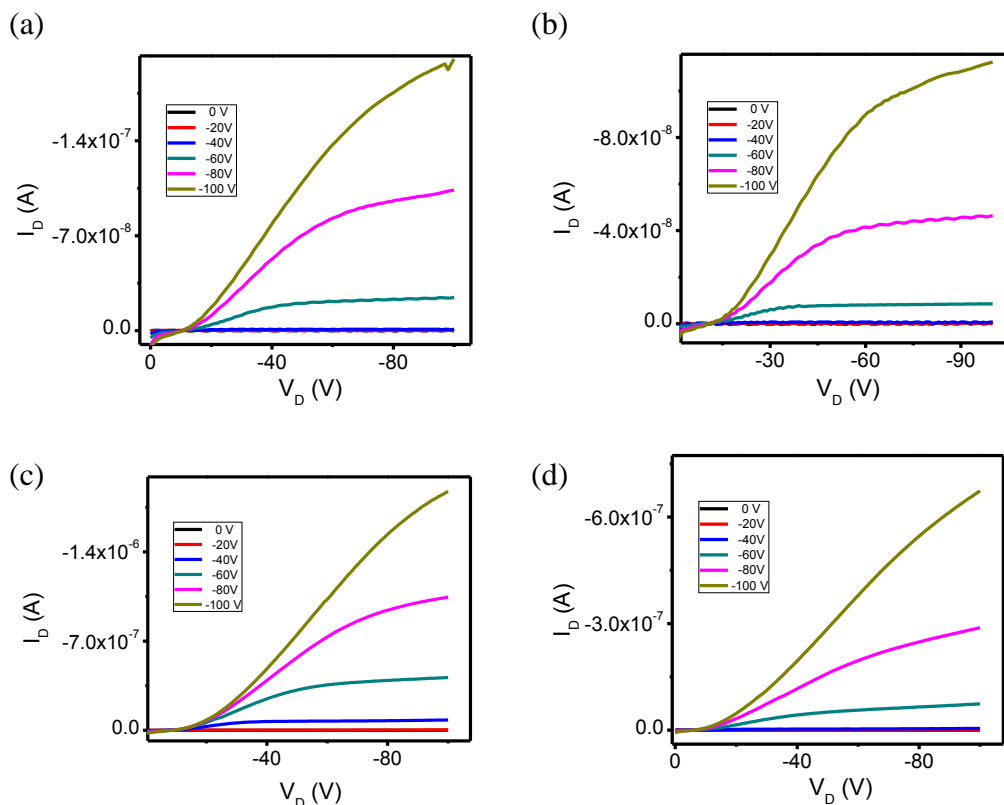
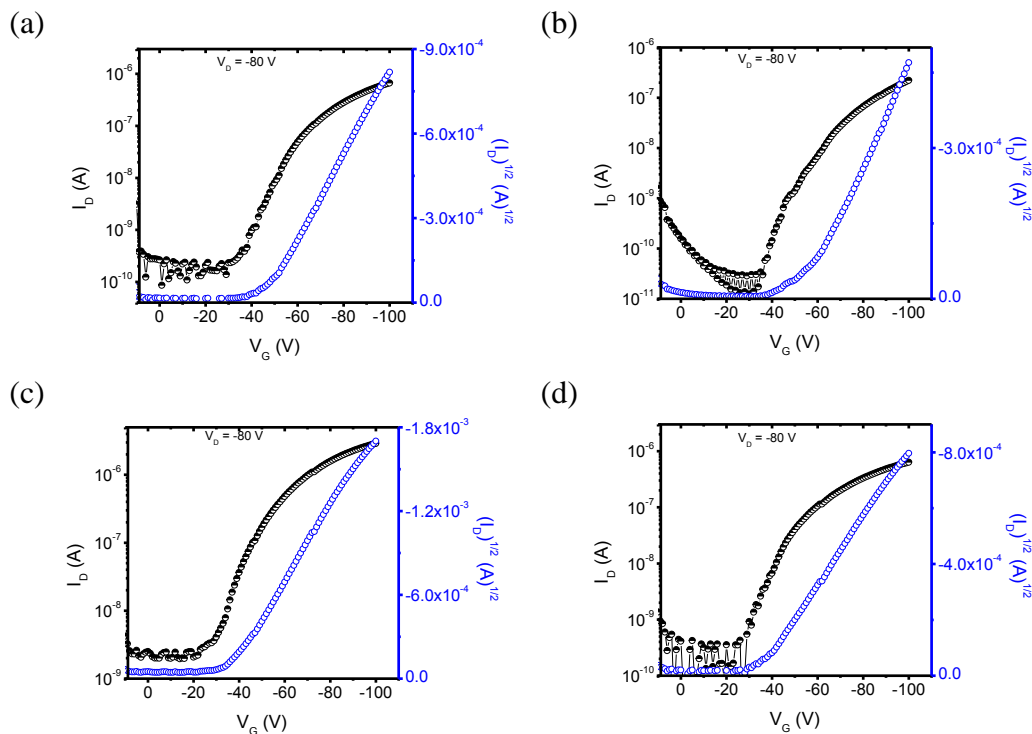


Figure II.12 Mass spectrum of compound (4).



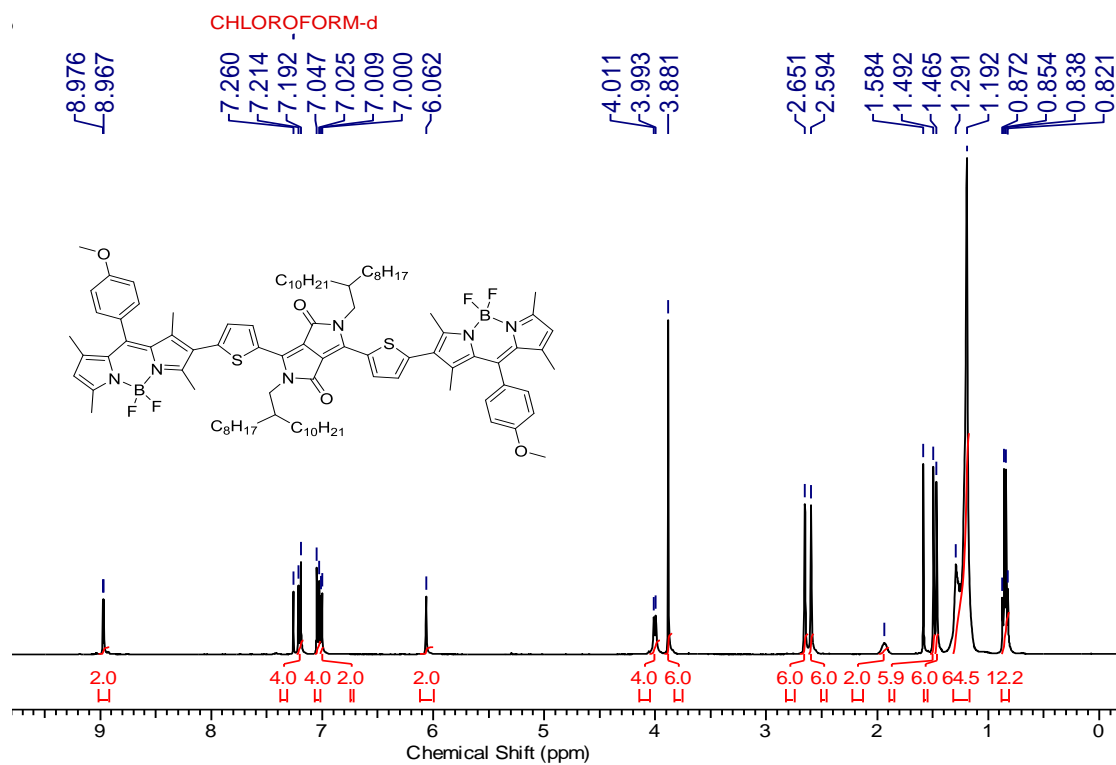
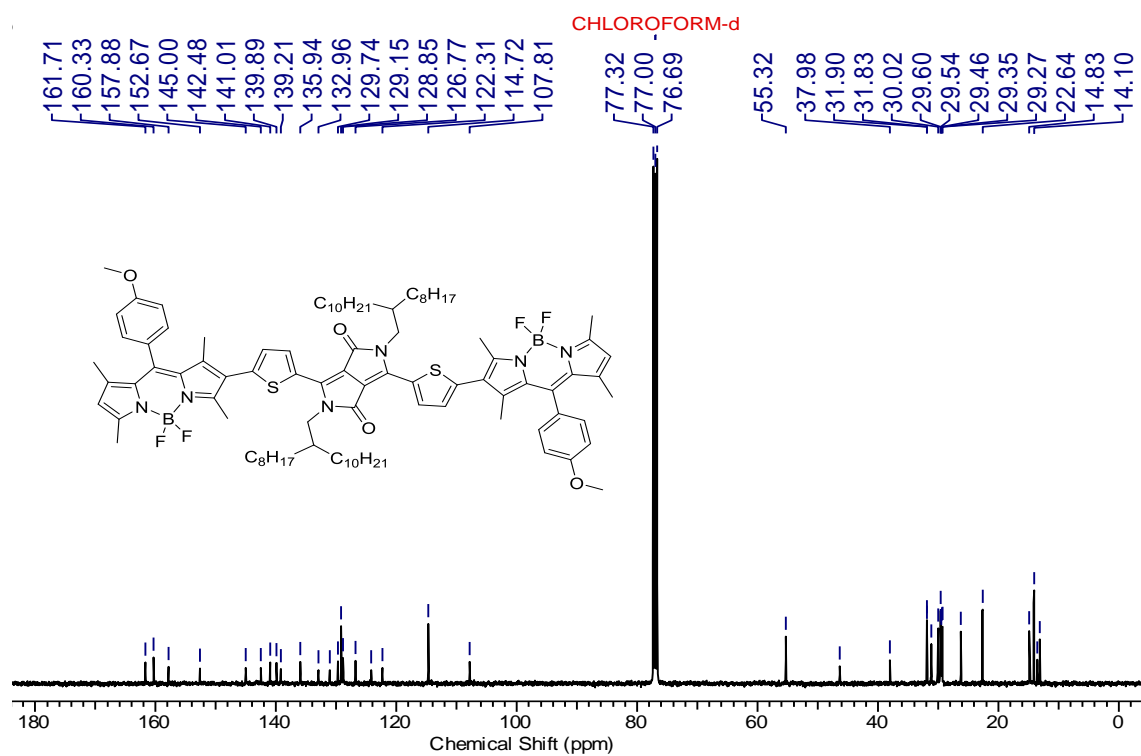
**Figure II.13** Output characteristic curves of 1(a), 2 (b), 3 (c), and 4(d) on HMDS modified FET substrate.



**Figure II.14** Transfer characteristic curves of 1(a), 2 (b), 3 (c), and 4(d) on HMDS modified FET substrate.

## Appendix III

## NMR and MALDI-TOF spectra for Chapter 4

Figure III.1 400 MHz  $^1\text{H}$  NMR spectrum of compound (1) in  $\text{CDCl}_3$ .Figure III.2 400 MHz  $^{13}\text{C}$  NMR spectrum of compound (1) in  $\text{CDCl}_3$ .

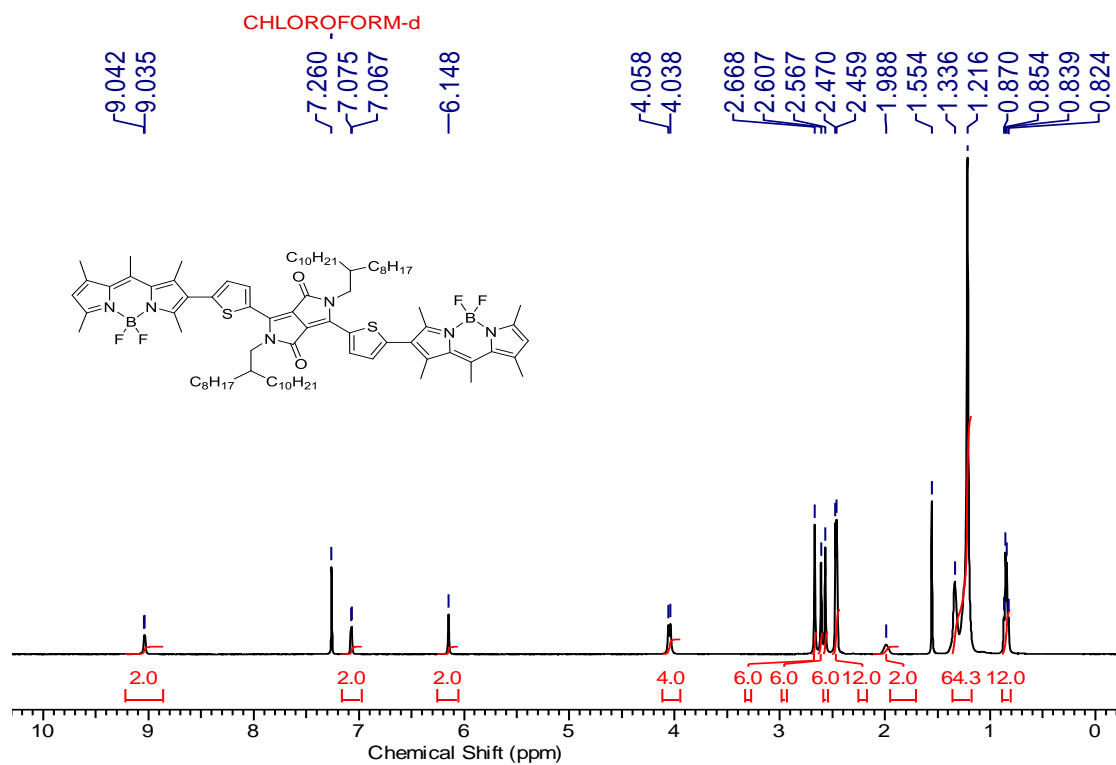


**Figure III.3** 400 MHz  $^1\text{H}$  NMR spectrum of compound (**2**) in  $\text{CDCl}_3$ .

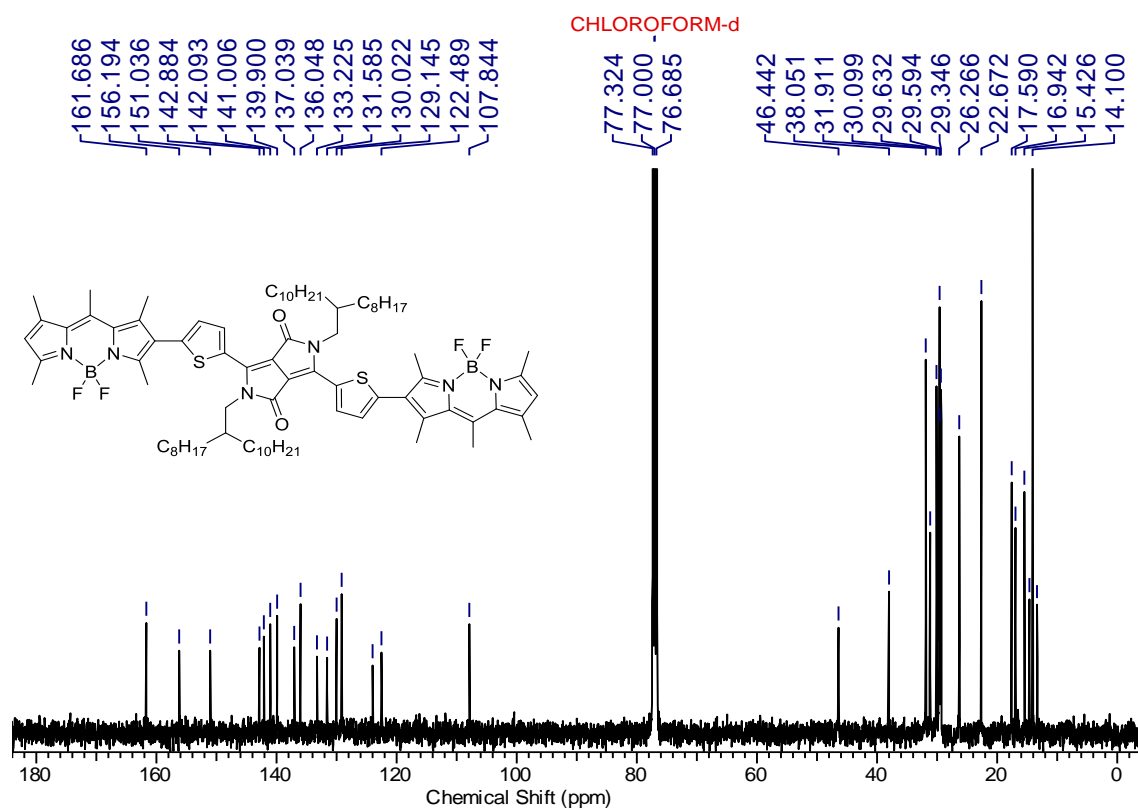


**Figure III.4** 400 MHz  $^{13}\text{C}$  NMR spectrum of compound (**2**) in  $\text{CDCl}_3$ .

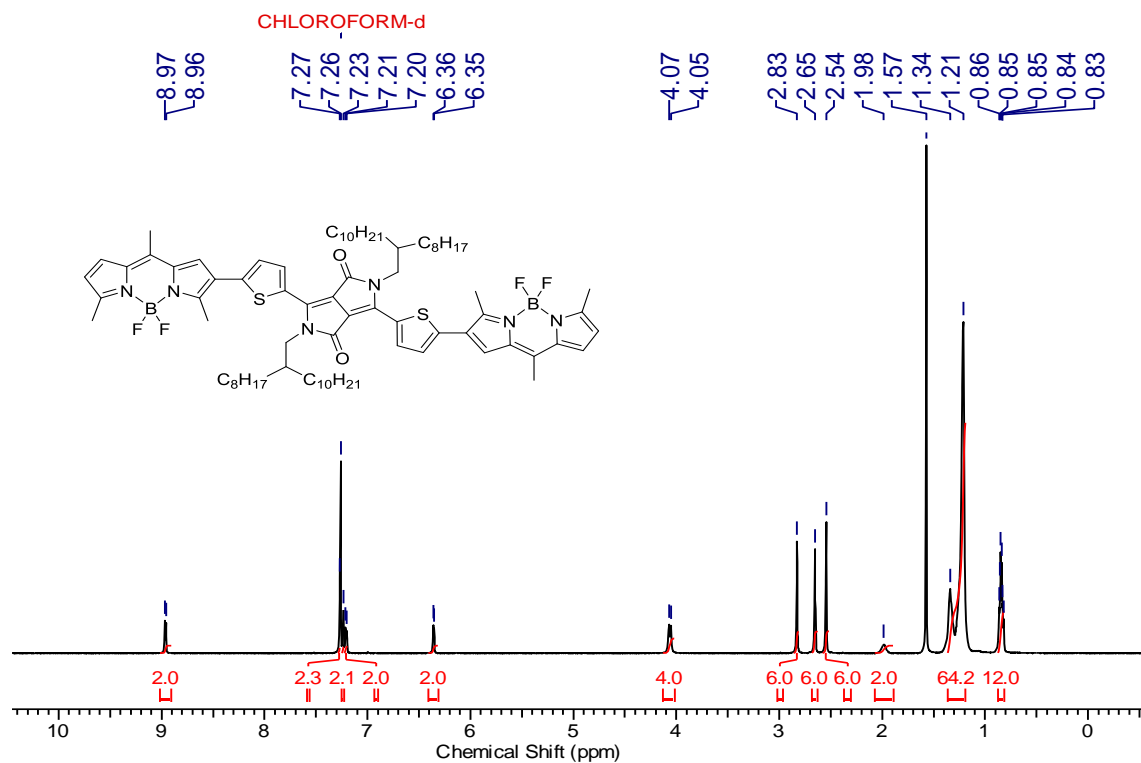


**Figure III.5** 400 MHz  $^1\text{H}$  NMR spectrum of compound (3) in  $\text{CDCl}_3$ .

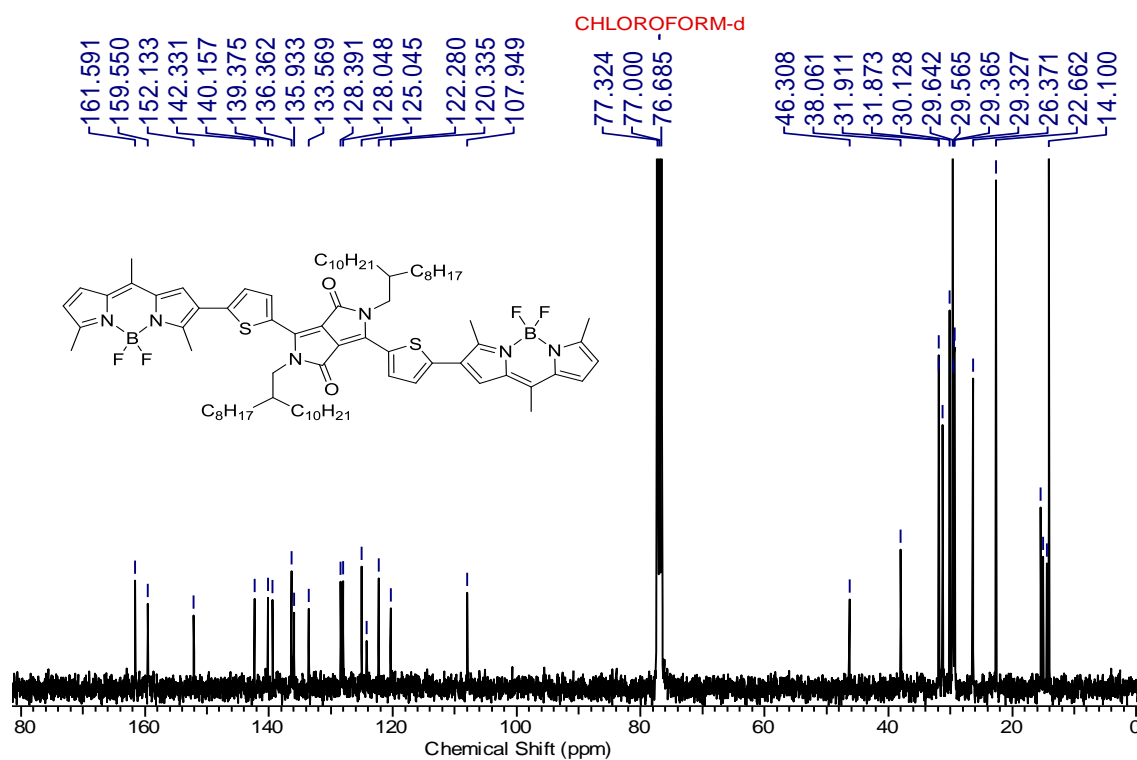


**Figure III.6** 400 MHz  $^{13}\text{C}$  NMR spectrum of compound (3) in  $\text{CDCl}_3$ .

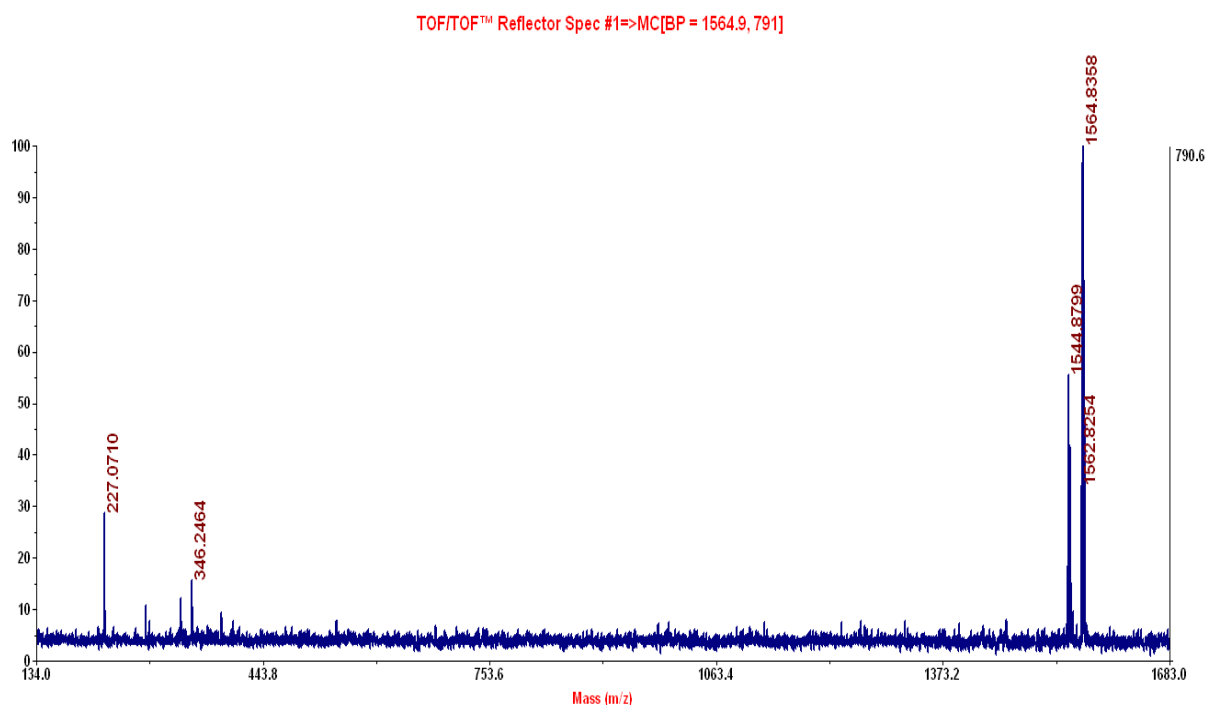


Figure III.7 Mass spectrum of compound (1).

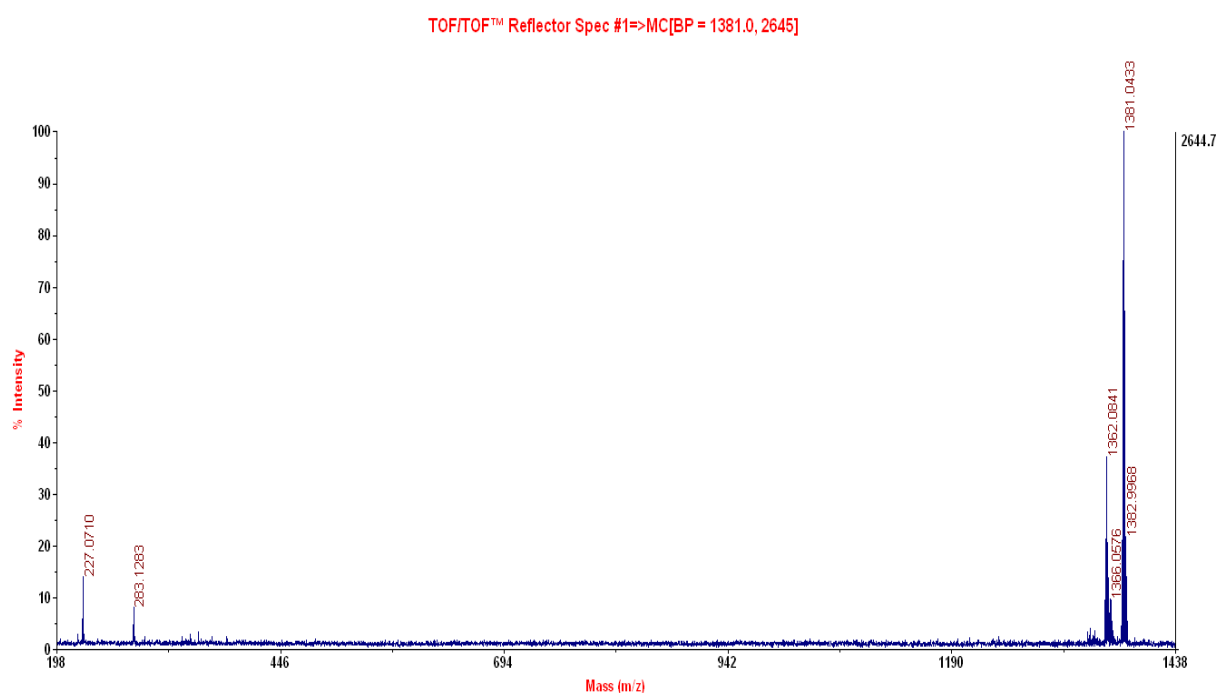
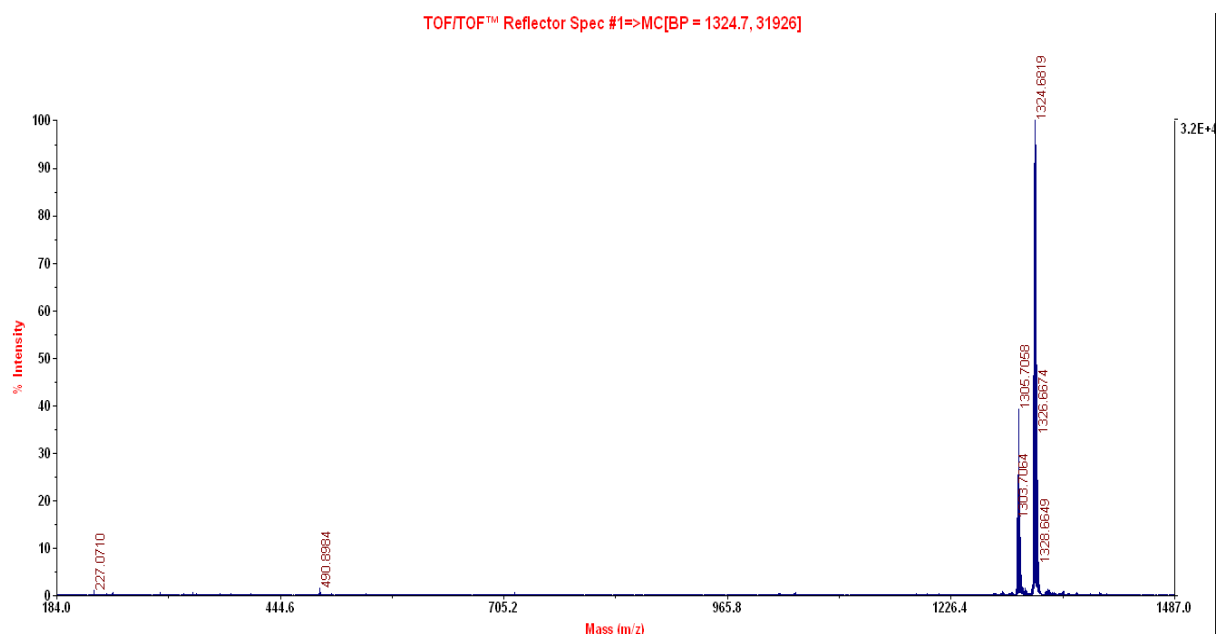


Figure III.8 Mass spectrum of compound (2).

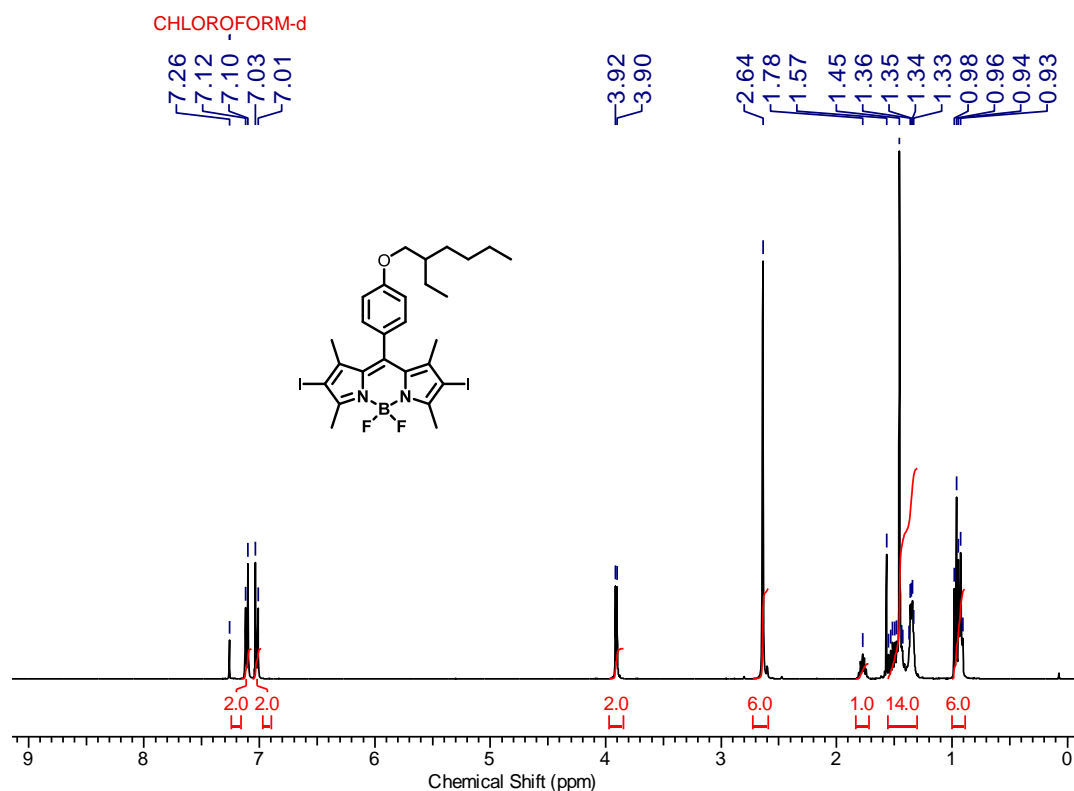
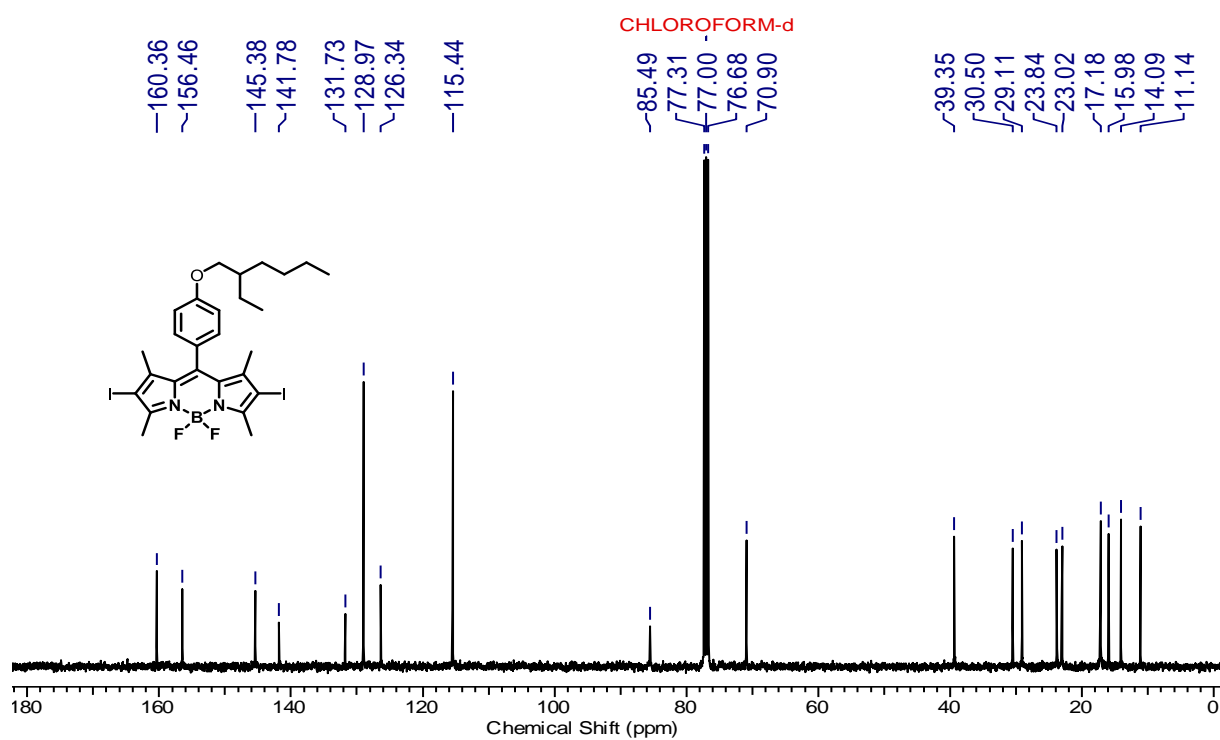


**Figure III.9** Mass spectrum of compound (3).



## Appendix IV

## NMR and MALDI-TOF spectra for Chapter 5

Figure IV.1  $^1\text{H}$  NMR (400 MHz,  $\text{CDCl}_3$ ) spectrum of compound (1a).Figure IV.2  $^{13}\text{C}$  NMR (100 MHz,  $\text{CDCl}_3$ ) spectrum of compound (1a).

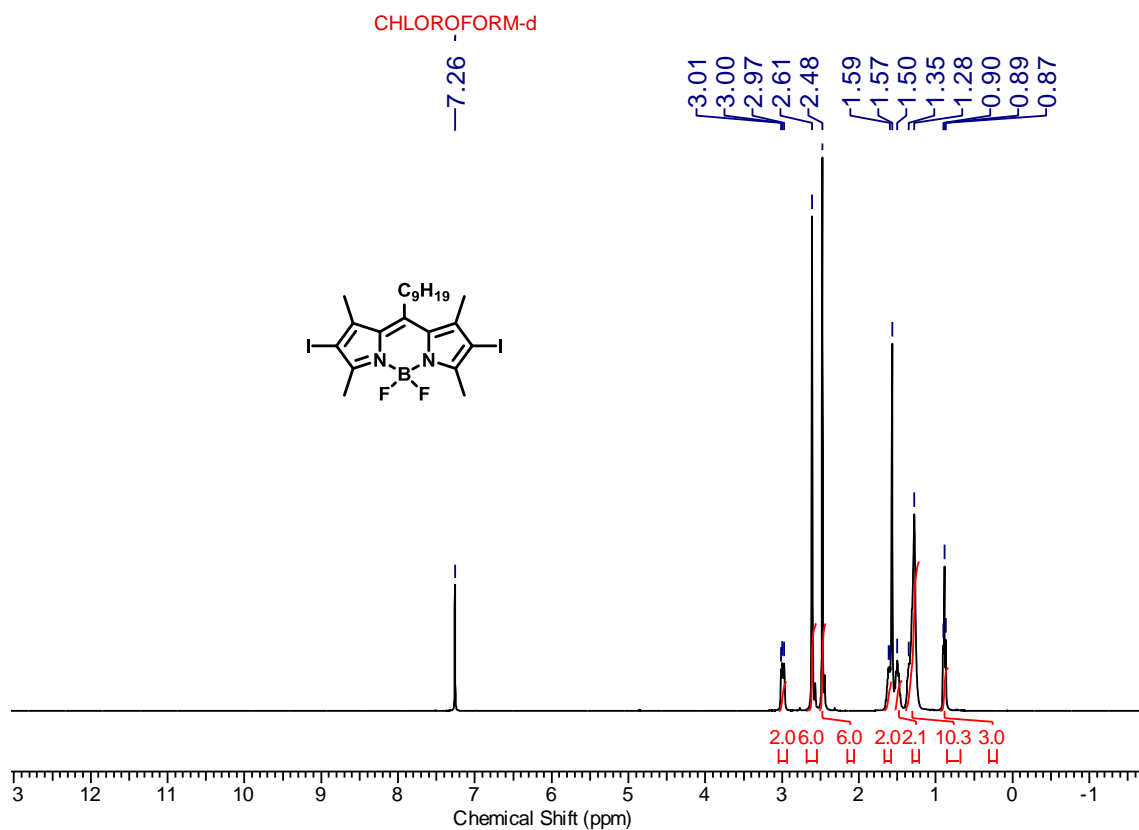


**Figure IV.3**  $^1\text{H}$  NMR (400 MHz,  $\text{CDCl}_3$ ) spectrum of compound (2a).

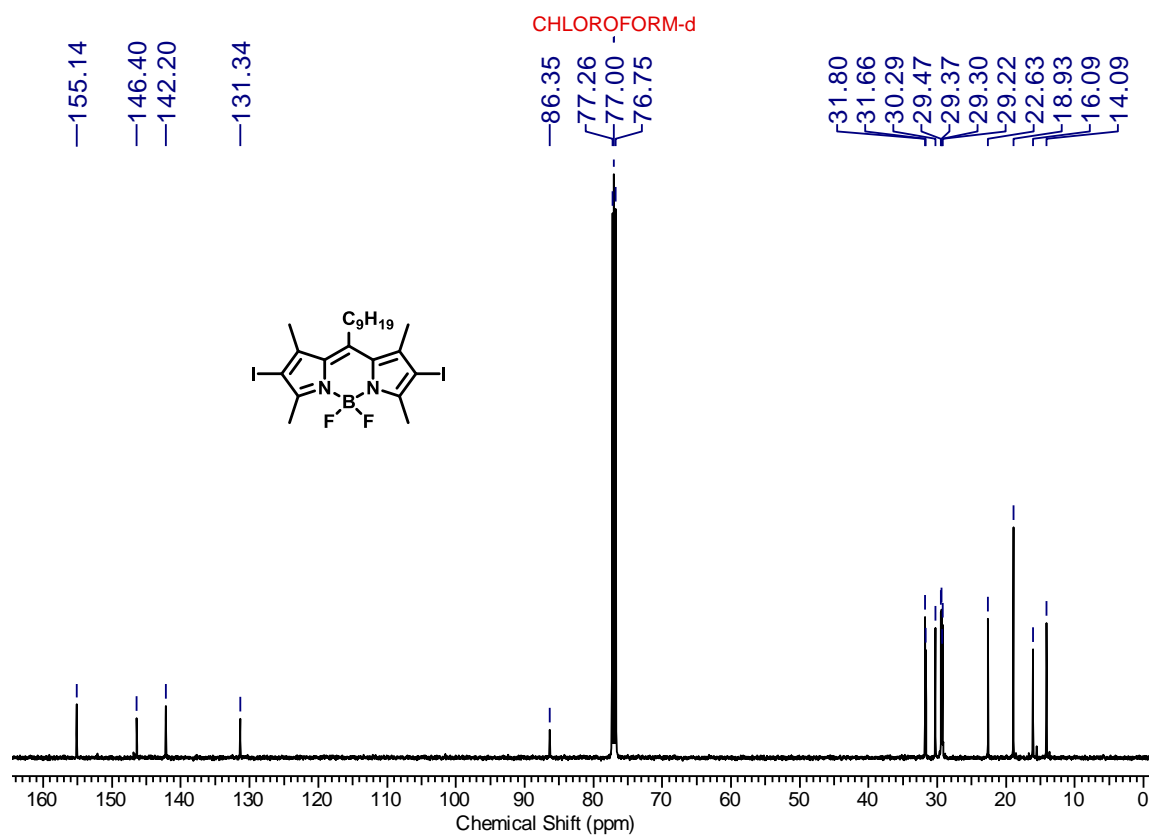


**Figure IV.4**  $^{13}\text{C}$  NMR (100 MHz,  $\text{CDCl}_3$ ) spectrum of compound (2a).

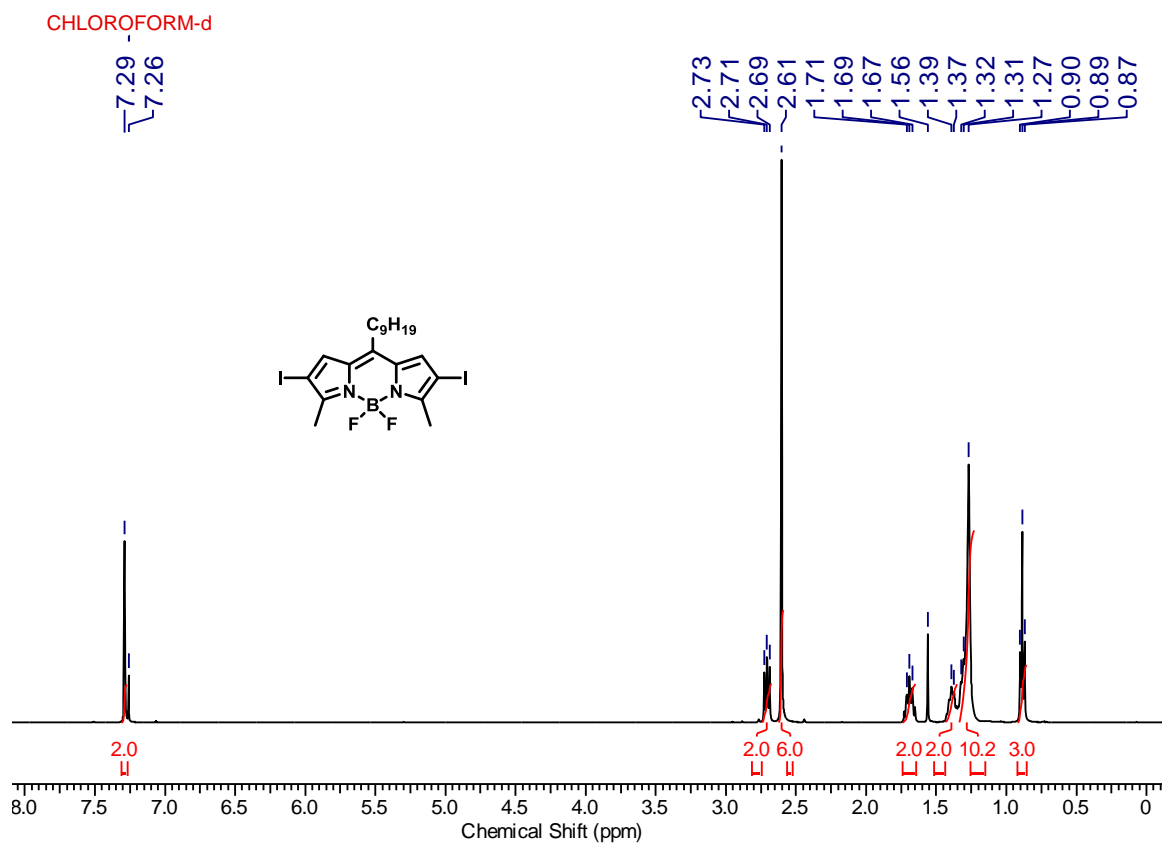


Figure IV.5  $^1\text{H}$  NMR (400 MHz,  $\text{CDCl}_3$ ) spectrum of compound (3a).

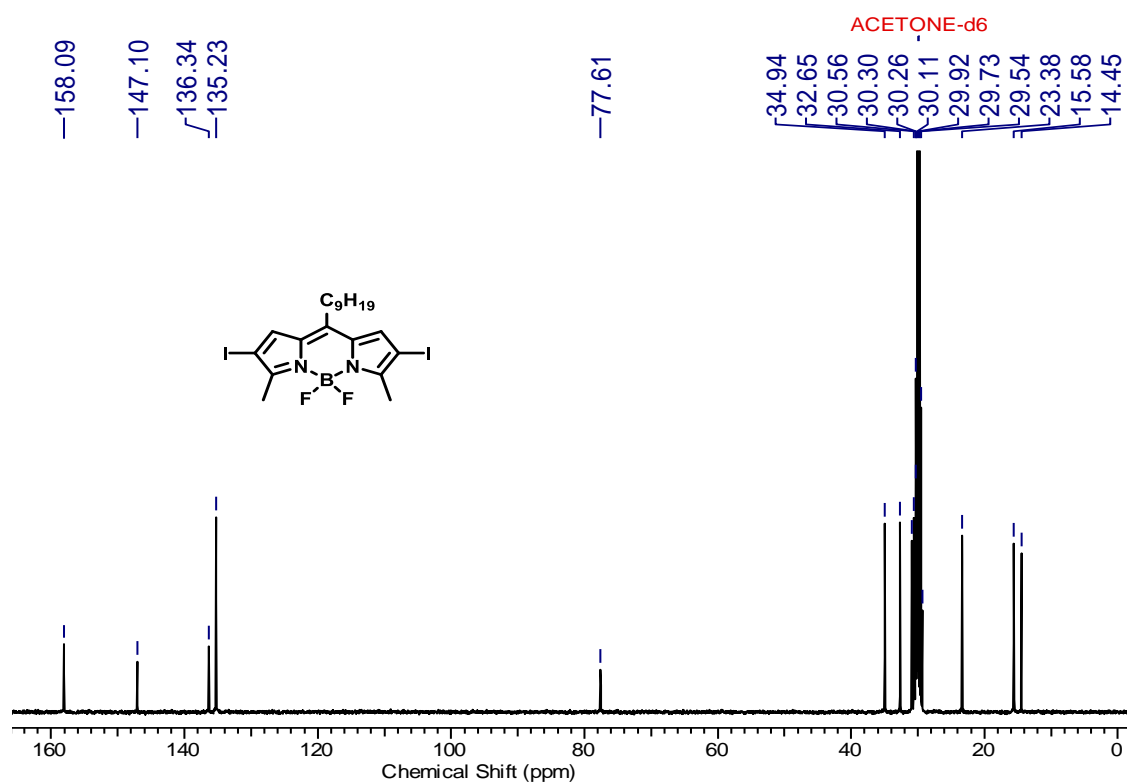
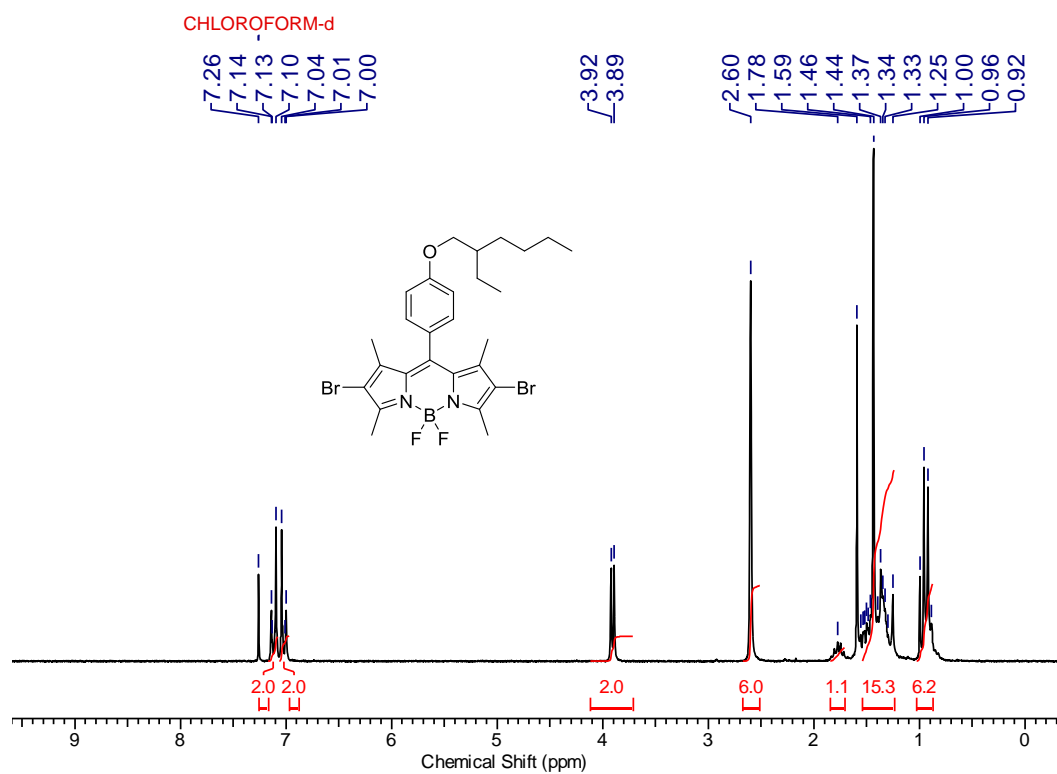
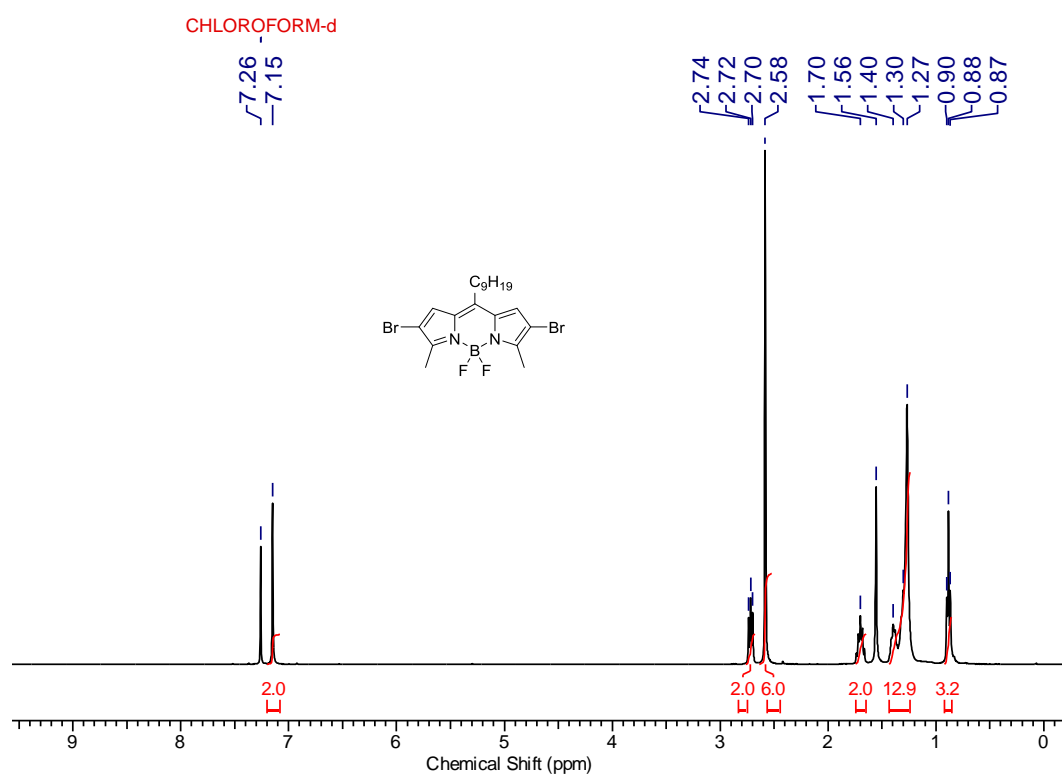


Figure IV.6  $^{13}\text{C}$  NMR (100 MHz, Acetone  $\text{D}_6$ ) spectrum of compound (3a).



**Figure IV.7**  $^1\text{H}$  NMR (400 MHz,  $\text{CDCl}_3$ ) spectrum of compound (b1).



**Figure IV.8**  $^1\text{H}$  NMR (400 MHz,  $\text{CDCl}_3$ ) spectrum of compound (b2).

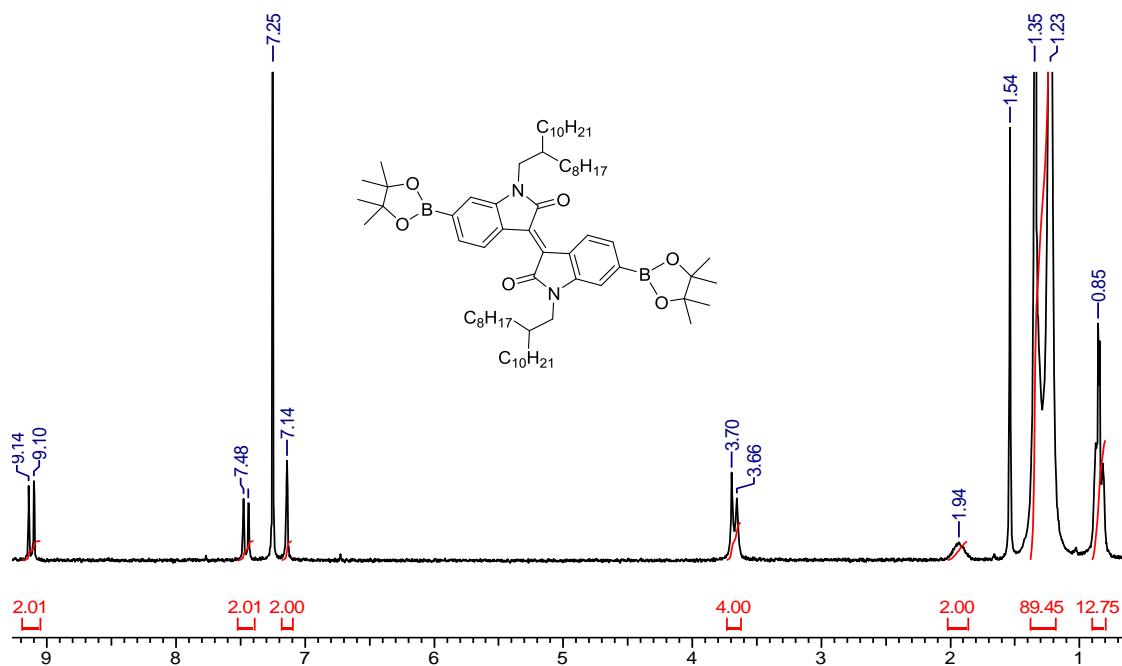


**Figure IV.9**  $^1H$  NMR (200 MHz,  $CDCl_3$ ) spectrum of compound (M1).

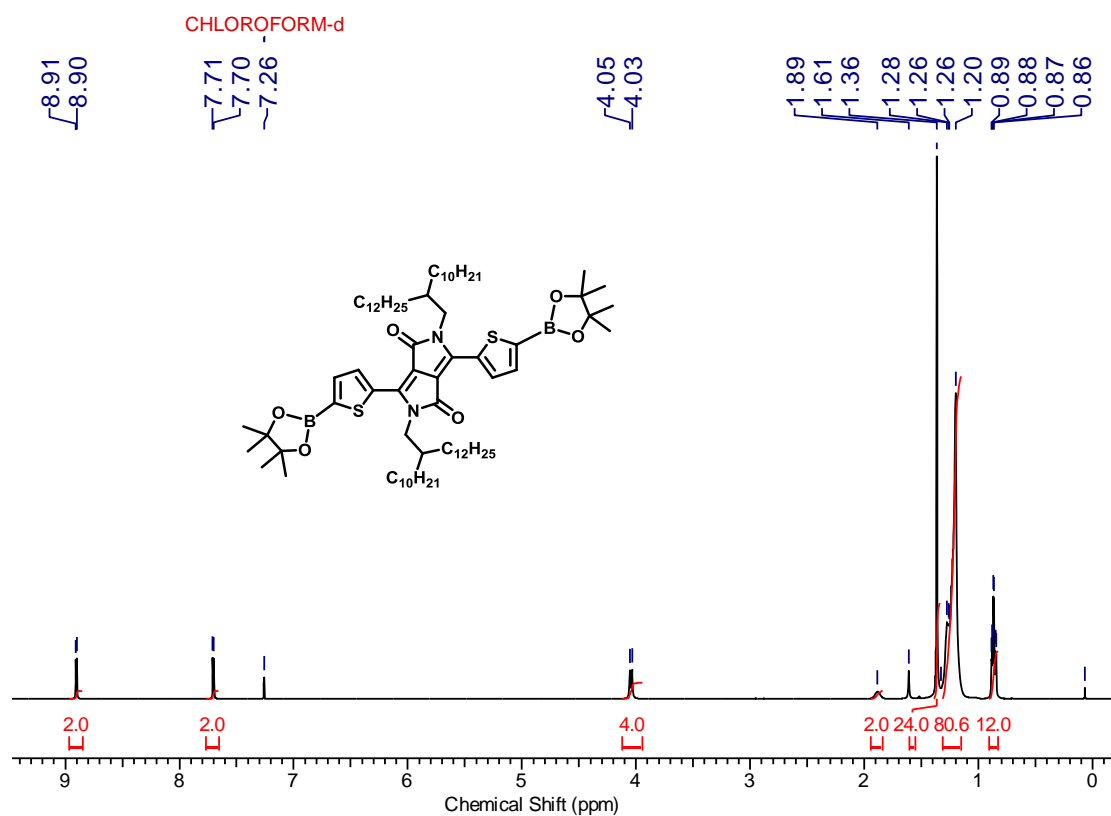


**Figure IV.10**  $^1H$  NMR (400 MHz,  $CDCl_3$ ) spectrum of compound (M2).

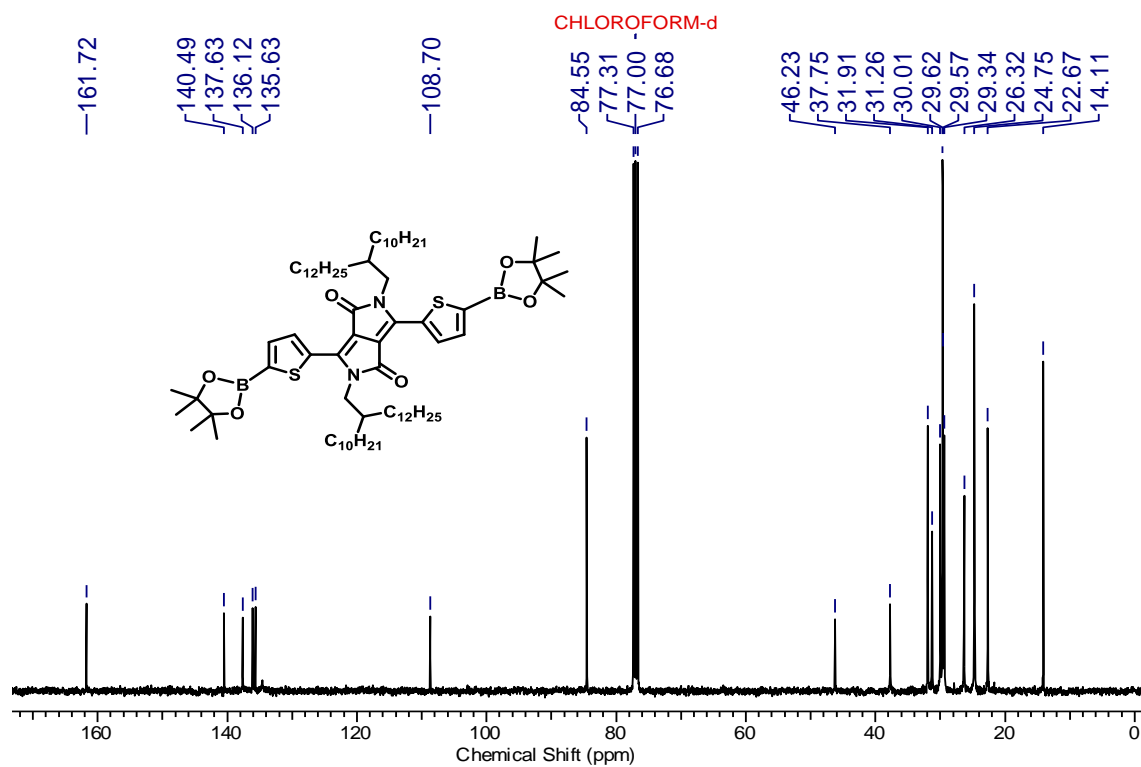


**Figure IV.11**  $^{13}\text{C}$  NMR (100 MHz,  $\text{CDCl}_3$ ) spectrum of compound (M2).

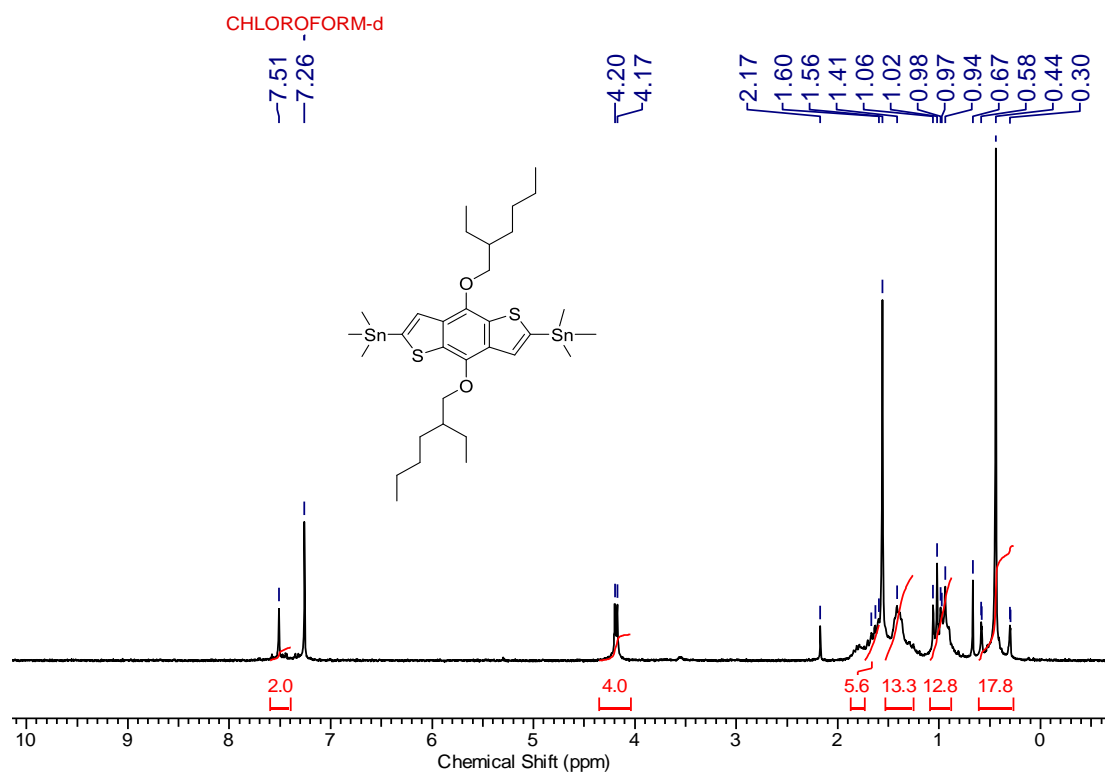


**Figure IV.12**  $^1\text{H}$  NMR (200 MHz,  $\text{CDCl}_3$ ) spectrum of compound (M3).

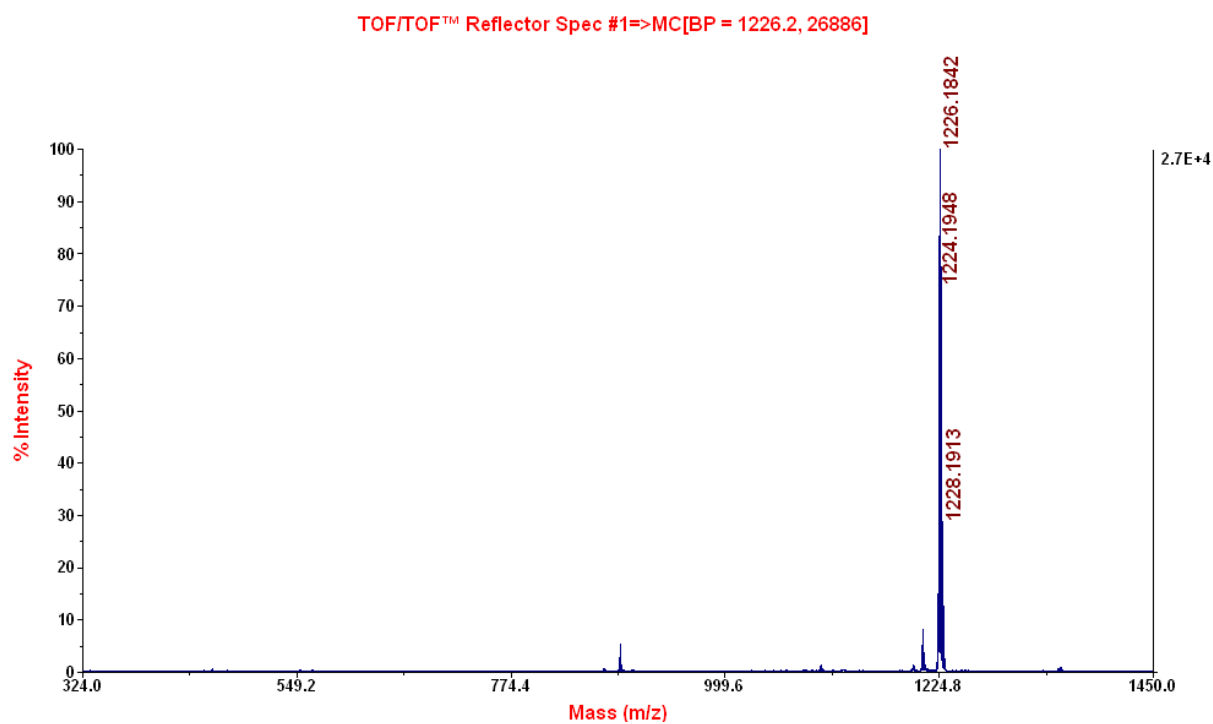


Figure IV.13 Mass spectrum of M2

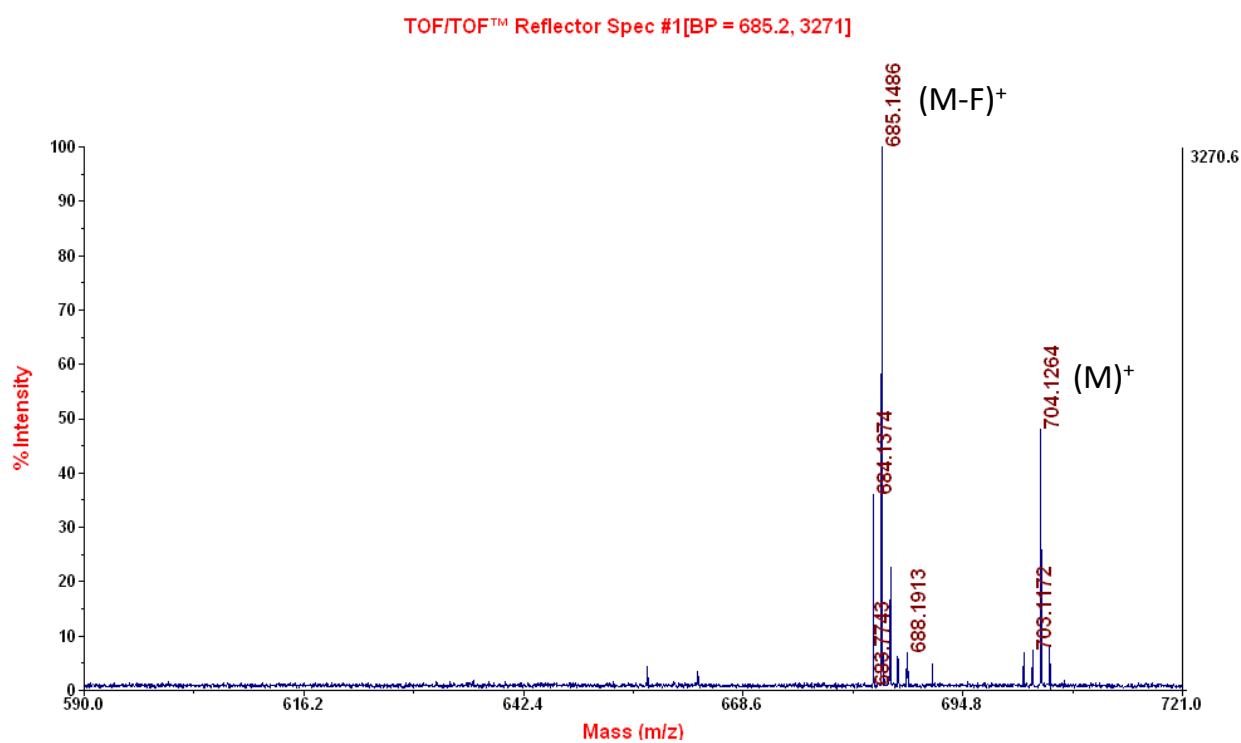


Figure IV.14 Mass spectrum of 1a

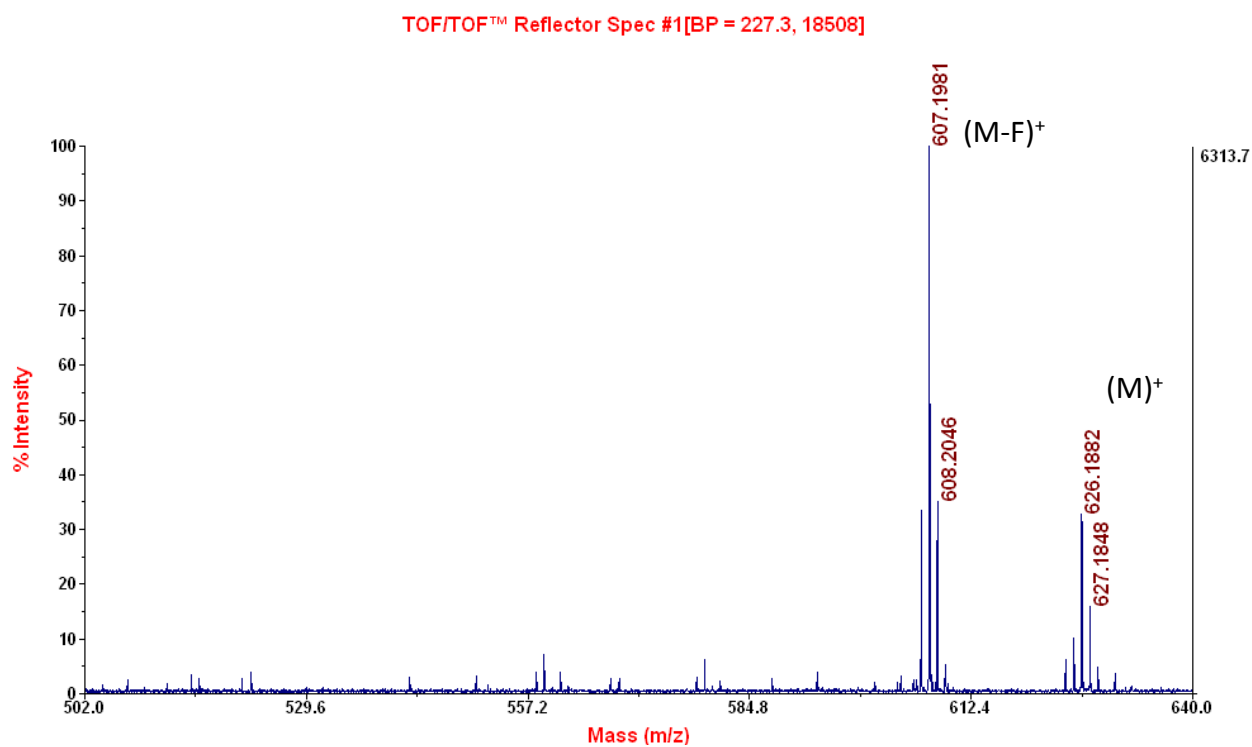


Figure IV.15 Mass spectrum of 2a

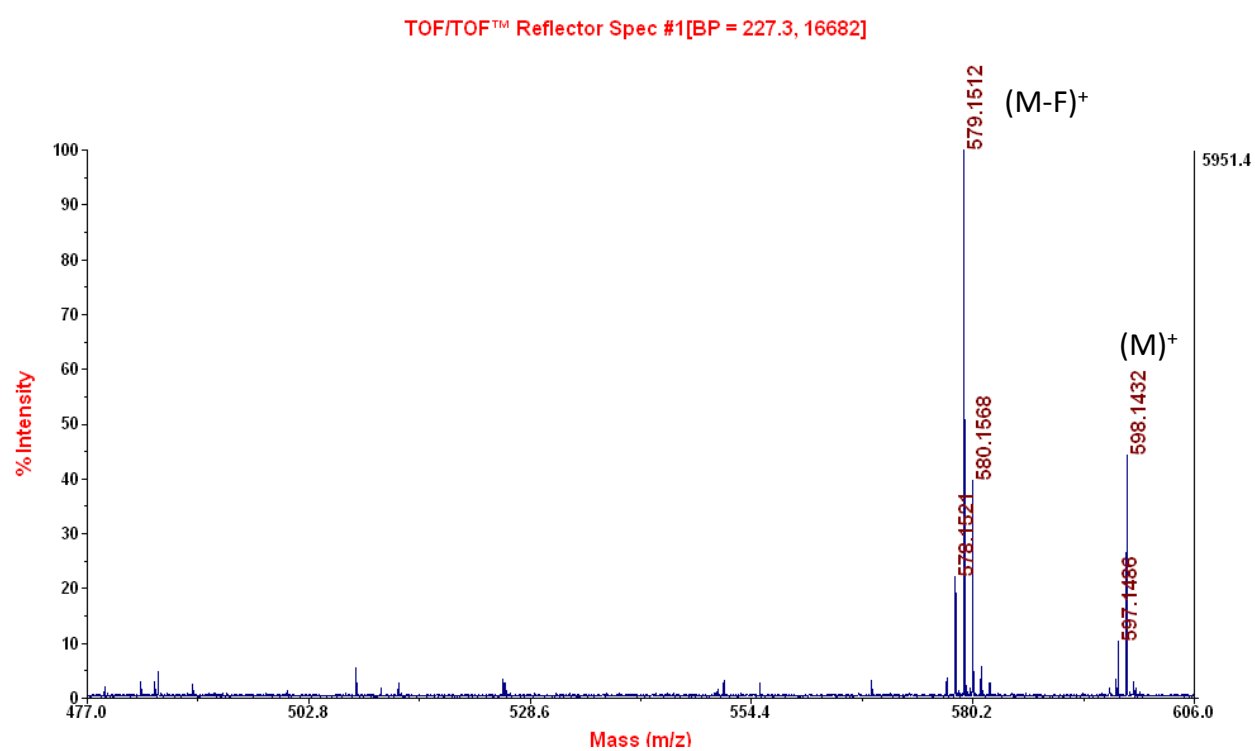


Figure IV.16 Mass spectrum of 3a



## List of Publications

1. **Saumya Singh**, Sundaresan Chithiravel and Kothandam Krishnamoorthy, “Copolymers Comprising Monomers with Various Dipoles and Quadrupole as Active Material in Organic Field Effect Transistors” *J. Phys. Chem. C*, **2016**, 120, 26199.
2. Sashi Debnath,<sup>#</sup> **Saumya Singh**,<sup>#</sup> Anjan Bedi, Kothandam Krishnamoorthy, and Sanjio S. Zade “Site-selective synthesis and characterization of BODIPY–acetylene copolymers and their transistor properties” *J. Polym. Sci. Part A: Polym. Chem.* **2016**, 54, 1978. (<sup>#</sup> These authors contributed equally to the work)
3. Sashi Debnath, <sup>#</sup> **Saumya Singh**, <sup>#</sup> Anjan Bedi, Kothandam Krishnamoorthy, and Sanjio S. Zade “Synthesis, Optoelectronic, and Transistor Properties of BODIPY- and Cyclopenta[c]thiophene-Containing  $\pi$ -Conjugated Copolymers” *J. Phys. Chem. C*, **2015**, 119, 15859. (<sup>#</sup> These authors contributed equally to the work)
4. **Saumya Singh**, Vijay Venugopalan and Kothandam Krishnamoorthy “Organic soluble and uniform film forming oligoethylene glycol substituted BODIPY small molecules with improved hole mobility” *Phys.Chem.Chem.Phys.*, **2014**, 16, 13376.
5. **Saumya Singh** and Kothandam Krishnamoorthy, “BODIPY in Conjugation with Diketopyrrolopyrrole (DPP) Core for Solution-Processable Small Molecule Organic Field Effect Transistors” (Manuscript under preparation).